Department of Engineering D-085 energy PhD course

Design and optimisation of innovative systems for hydrogen production using marine energy sources

PhD student:
Guercio Andrea
ID number. 0724758

Tutor:**Prof. Vincenzo Franzitta**

2022- 2023

Contents

Figures content

Tables content

Introduction

This thesis is focused on the exploitation of sea wave energy. However, this is just one of the several kinds of energy, related to the oceanic environment, thus a brief description of the main sea energy resources is necessary[1,2].

Oceans represent an enormous energy reserve that is distributed in different phenomena. Among these, the main kinds of energies related to the oceans are marine currents, osmotic salinity, OTEC (acronym of Ocean Thermal Energy Conversion), tide, and sea wave. Each oceanic energy source has a relevant potential for human applications; however, as shown in Table 1, sea waves and marine currents have the highest energy potentials[3].

Table 1. **Potential installable capacity and energy production from marine energy sources**

Ocean energy	Capacity [GW]	Potential generation [TWh/y]
Tide	90	800
Marine current	5000	50000
Osmotic salinity	20	2000
OTEC	1000	10000
Sea wave	1000-9000	8000-80000

All these oceanic energy sources are classified as renewable[4]. Indeed, tides are due to the Moon's orbit around the Earth, the orbit of this one around the sun, and the Earth's rotation. As consequence, a huge amount of seawater flows around the world's surface, modifying locally the sea level. The effects are locally different due to the irregular distribution of lands around the world. In any case, the tides are a regular phenomenon, whose effects can be accurately predicted. Thus, tides represent an interesting renewable energy source, allowing the exploitation of tidal streams or tidal ranges. The second one has few applications worldwide, since this phenomenon allows the installation of the power plant close to the coastline,

realizing a barrier equipped with low-head hydro turbines. The first one was the power plant in La Rance (France), installed in 1966 and still operating. Other plants are installed in Russia (Kislaya Guba, 1.7 MW), Canada (Annapolis Royal Generation Station, 20 MW), China (Jiangxia, 3.9 MW), and Korea (Lake Sihwa. 254 MW)[5]. The term ocean current is used to underline the different origin of marine currents in comparison to the tidal currents, previously described. Ocean currents are seawater circulations promoted by solar energy. Since the solar radiation varies with the latitude and considering the irregular distribution of the lands on the Earth's surface and the orography of seabed, the variation of water density produces water flows that are extended for thousands of kilometres. Superficial currents are, also, created by the wind interactions (that is also an effect of solar radiation) with the sea surface. Summing all these contributions, the thermohaline circulation is generated. The Gulf Stream is a famous ocean current (about 100 km wide and 800 m to 1200 m deep) that is originated from the Gulf of Mexico and flows up the North Pole with a speed of about 2.5 m/s[6]. Other famous currents are the Kuroshio Current (on the west side of Pacific Oceans)[7]. and the Agulhas Current (on the south-eastern part of the Indian Ocean, along the coastline of South Africa)[8].

About the Ocean Thermal Energy Conversion (OTEC), the idea is the installation of a thermal machine using the superficial seawater as a thermal source and the deep water as a thermal sink[9]. The main problem is the low energy efficiency of this system, also in the best cases. Considering the installation of an ideal Carnot heat engine to exploit the available thermal sources, the energy efficiency is no more than 7%. Consequently, introducing the irreversibility of a real system, the power plant requires huge dimensions (especially the heat exchangers) to obtain a significant power output; thence the required investments are high. Two layouts for a possible OTEC power plant have been proposed: open cycle and closed cycle[9,10]. In the first one, the warm water from the sea surface is flashed to produce steam and then condensed using the cold deep water. The main disadvantages are related to the operative conditions. Indeed, steam generation

requires a vacuum condition along with the entire plant, so air infiltration is possible. At the same time, the specific mass of steam is quite high (30–100 m^3/kg), hence the system requires large pipes for small power outputs. In the second solution, the warm superficial water is used to evaporate a working fluid, normally used in the chilling sector such as ammonia, propane, or chlorofluorocarbon. This vapor is used to run a turbine, then it is condensed using the deep water as a refrigerant. The advantage is that the system works under pressure, so air infiltration is avoided. As a disadvantage, large heat exchangers are required[11].

About the saline gradient energy source (called also Osmotic Power), the idea is the exploitation of chemical energy released when the freshwater from rivers is mixed with saltwater in the sea. Two solutions with different ions concentrations are characterized by different values of osmotic pressure. A solution, proposed in 1937, is the Pressure Retarded Osmosis, where the saltwater is pressurized before a semipermeable membrane. If the external pressure gradient is lower than the osmotic pressure, water flows from the diluted solution to the concentrated one. Brackish water is consequently produced, with the same pressure as the saline water but with a greater flow. Using a hydro turbine is possible to collect more energy than the pumping expenditure, producing an electrical output[12,13]. Finally, sea wave is a form of marine energy due to the several forces acting on the water surface, such as the friction generated by wind, the Coriolis force (related to the Earth rotation), the celestial bodies attraction (tidal), or other unpredictable phenomena as earthquake and volcanic eruptions (tsunami)[14].

Wave energy production, like other renewables, could be used to power electrolysers. Production from renewables is often not always accepted in the grid, especially on small islands. The simple electricity grid in these districts is still highly dependent on fossil fuel production. Precisely for this reason, feeding an electrolyser when the grid fails is a solution to avoid wasting precious energy. Hydrogen is the most abundant chemical element in the world. Its high presence on earth and the need to replace fossil fuels make it suitable for this purpose. Since the weight of hydrogen is less than that of air, its low density tends to cause it to rise in

the atmosphere, so it is rarely found in its pure H_2 form[15]. Hydrogen that is used as fuel in a fuel cell can be produced through an environmentally sustainable supply chain from the electrolysis of water in an electrolyser, producing "green hydrogen", precisely because it is produced from renewable energy.

Commercially available electrolysers are: alkaline, PEM electrolysers and solid oxide electrolysers. The following Figure 1 shows how the electrolysers can produce hydrogen from renewable energy sources to send fuel in transportation sector, in a storage or in industrial sector.
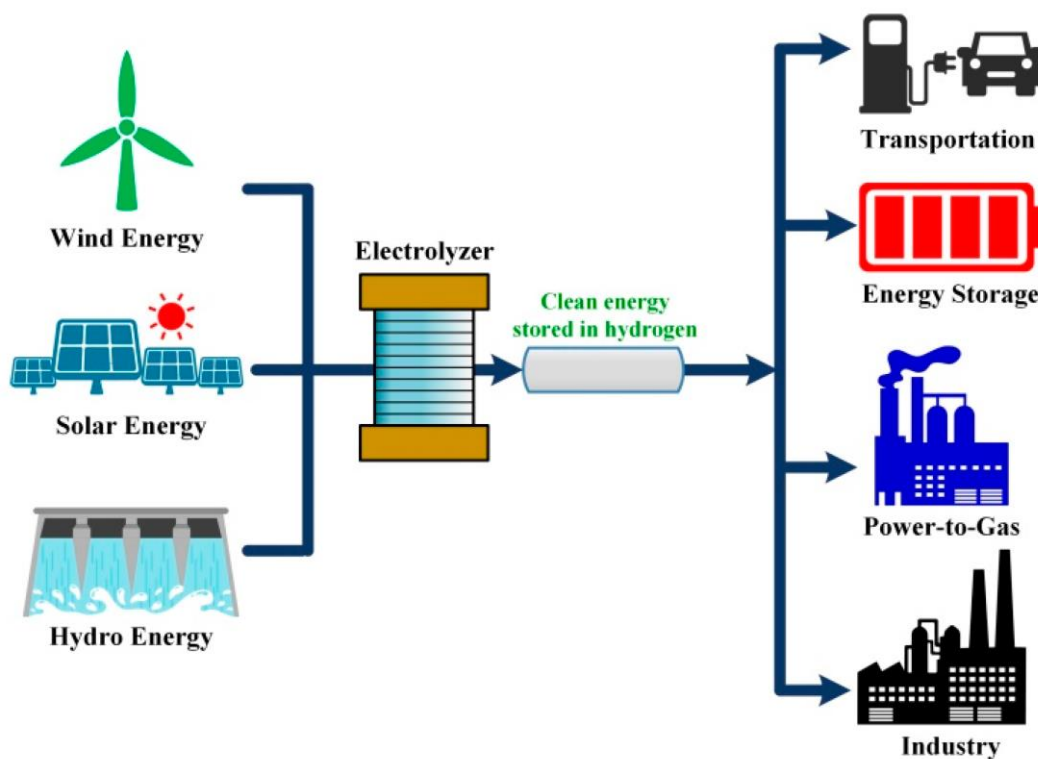
Figure 1. **The role of electrolyser in energy production**

The hydrogen production through electrolysers allows of storing and transporting it when and where required cleanly and sustainably. The following Figure 2 shows that the importance of green hydrogen production is related to electrolysers and how the green production is destinated to increase until 2050[16].
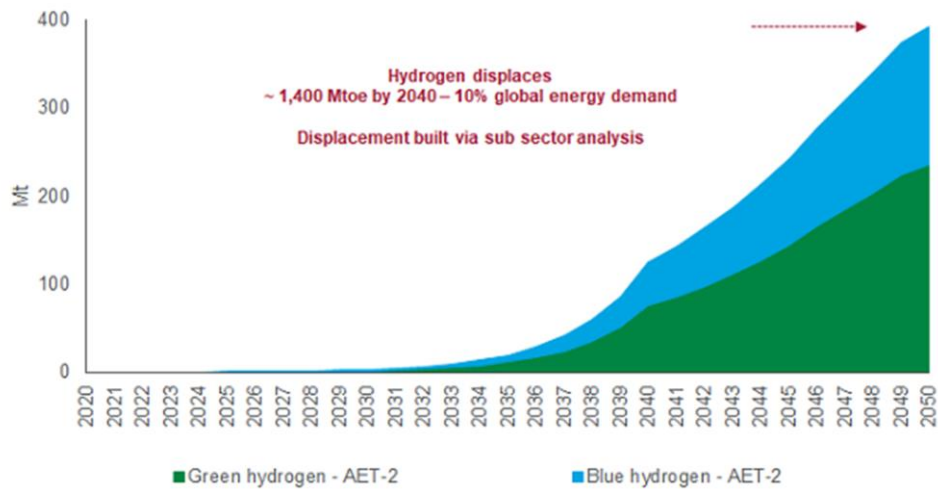
Figure 2. **Hydrogen deployment until 2050The overview of technologies**

The overview of hydrogen production technologies contains other kind of technical plant such as production from nuclear power (pink hydrogen), from solar power (yellow hydrogen) and the most environmental enemy production is related to fossil process (grey and black hydrogen).

The European commission (EC) puts emphasis on the hydrogen transport because this sector produces the 27% of greenhouse gas emission. To decarbonise this sector the EC affirms that need 30 million zero emission vehicles by 2030. The hydrogen will play a key role for this purpose and the European council is favourable of its deployment. Several manufacturers designing commercial, civil and heavy vehicles, but it is important that the politics help their diffusion. In the aviation sector, for example, Airbus has announced its intention to fly only zero-emission aircraft by 2035. As reported by the Environmental and Energy Study Institute, despite high efficiency improvements air transport is one of the most polluting. According to AirBus, the carbon footprint of the aviation sector can be reduced by more than 50%[17]. Their concept aircrafts "zeroe" are based on hybrid hydrogen technology in which liquid hydrogen is used as fuel for combustion with oxygen modifying gas turbine engine with more 3000 km of autonomy[18]. The following Figure 3 shows the fuel cell installed inside the aircraft fuselage.

Figure 3.   "Zeroe" Airbus project

The same approach is conducted in rail transport sector, where the manufacturers design train equipped by fuel cell engines. The Alstom company developed the "Coradia iLint", in commercial service in Germany today. This train is equipped by fuel cells and lithium-ion battery that guarantee 1000 km of autonomy[19]. The Figure 4 shows the technology of Coradia iLint project.
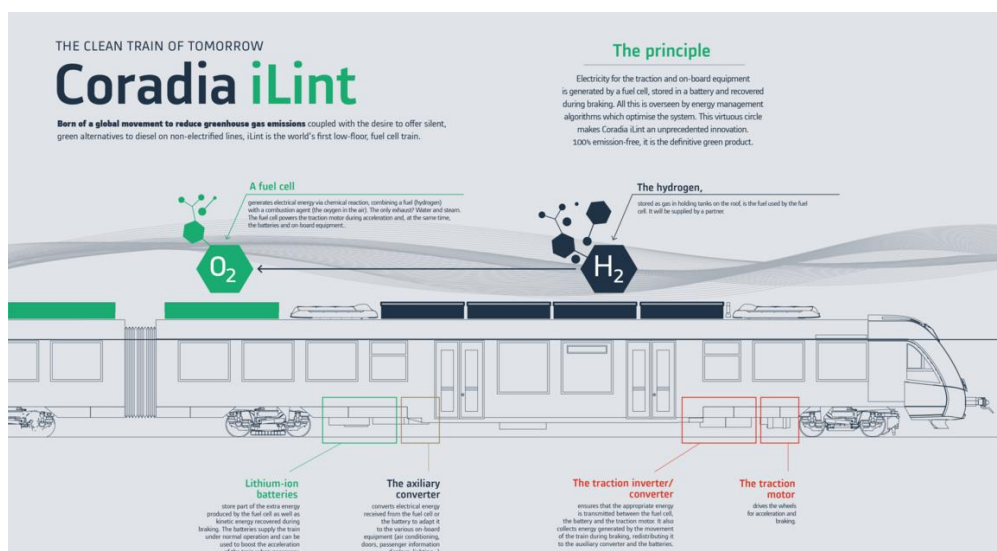
Figure 4.   "Coradia iLint" Alstom project

In road transport the most polluting vehicles are the heavy such as bus or truck. Some examples of commercial companies (DHL, French postal system) are adopting hydrogen vehicles. In a similar way, Toyota produces a hydrogen fuel powered car "Mirai" that is a family car with 650 km of autonomy[20]. The Figure 5 shows a typical configuration of a fuel cell powered truck.
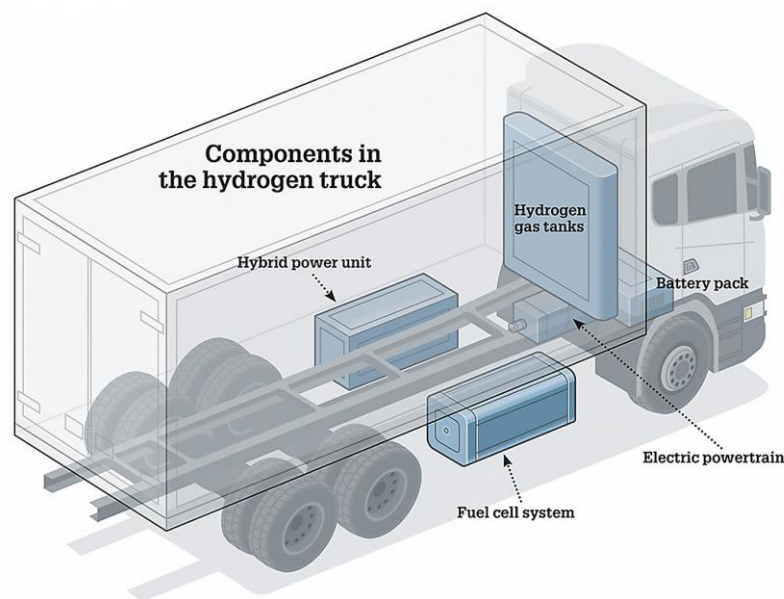
Figure 5. **Typical configuration of a fuel cell powered truck**

In all these 3 kinds of transport sector a similarity is repeated: the hydrogen fuel cell power generator and the battery pack ca be installed in the same position of fossil generator and fuel tank.

Naval sector from this point of view is less developed. However, Fincantieri launched a ship "ZEUS-zero emission ultimate ship" equipped with 130 kW fuel cell engine that guarantees 8 hours of navigation at the velocity of 7,5 knots. For safety navigation the power generator is a hybrid system composed from fuel cell coupled with a diesel engine. Fincantieri says that Zeus project will be of fundamental importance for the development of a new model of technologies for generating electricity and heat on board future cruise ships.

The goal of the research is to initially focus on the state of the art in the field of wave energy converters. Then optimize laboratory-built generators in order to characterize them and be able to simulate their operation. All of this provided results useful for future developments. The energy producibility, voltage, current, and efficiency values made it possible to hypothesize that these generators will be able to go into operation in pilot plants. The method followed was temporally discretized over the three years. The review of the initial state of the art refers to all technologies to date that have been designed and implemented even if only in pilot plants. Following the theory, the analysis on the three generators was performed in mechanical and electrical laboratory tests. These tests provided a way to validate the operation of the devices. In addition, the software simulations were performed to understand whether the devices could produce power in certain sea conditions. In order to get a general picture of the possible use of these devices, studies have been carried out on the power grids needed to understand how they might interface.

1. World energy scenario

The modern society needs a continuous energy demand to satisfy all its activities. The improvement in economic and social welfare has generated an increase in population, which has led to a progressive growth in demand for energy in the world. The following Figure 6 shows the increasing of world primary energy consumption from 1900 to 2021[21]. It is important to underline that during the 2020 there was a great decreasing due to the pandemic condition.
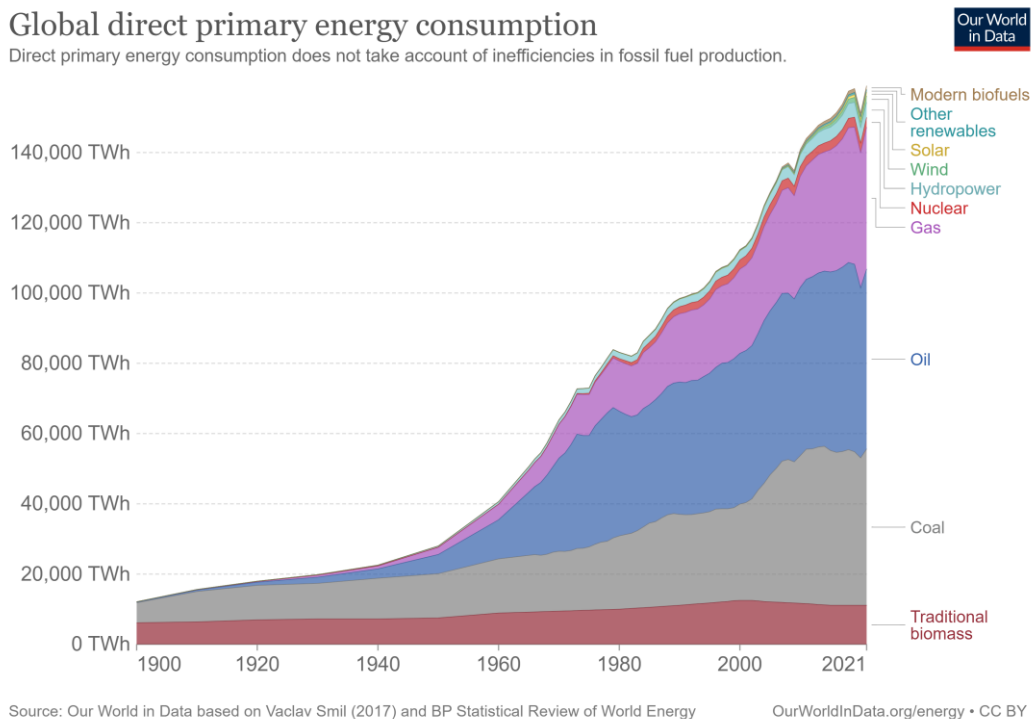
Figure 6. **The increasing of world primary energy consumption**

Primary energy consumption is related to all human needs, such as electricity production, transport, heating, industrial processes, etc.

Limiting the analysis to electricity alone, which is one of the most important sectors, Figure 7 shows how this has grown enormously on a global scale in recent years, in fact the production grows from 10000 TWh to more than 25000 TWh[22].
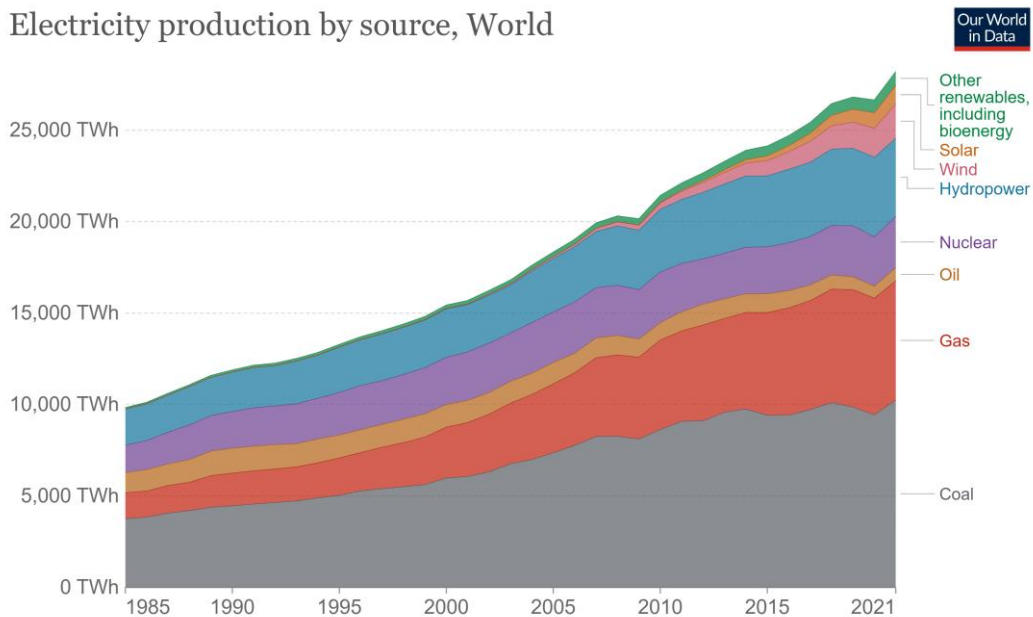
Electricity production by source, World

Figure 7.   Electricity production in the world by source

The graphs in the figures above show that the most exploited sources of electricity production are mainly based on fossil fuels such as coal, oil and gas, despite the great economic efforts made to spread renewable energy sources. A recent report by IRENA (International Renewable Energy Agency) shows the trend of additional power being installed worldwide year by year, broken down by energy source: Figure 8 shows that renewables are growing strongly. Despite this, IRENA also states that new fossil-based plants are still being installed, although the trend is declining slightly[23,24].
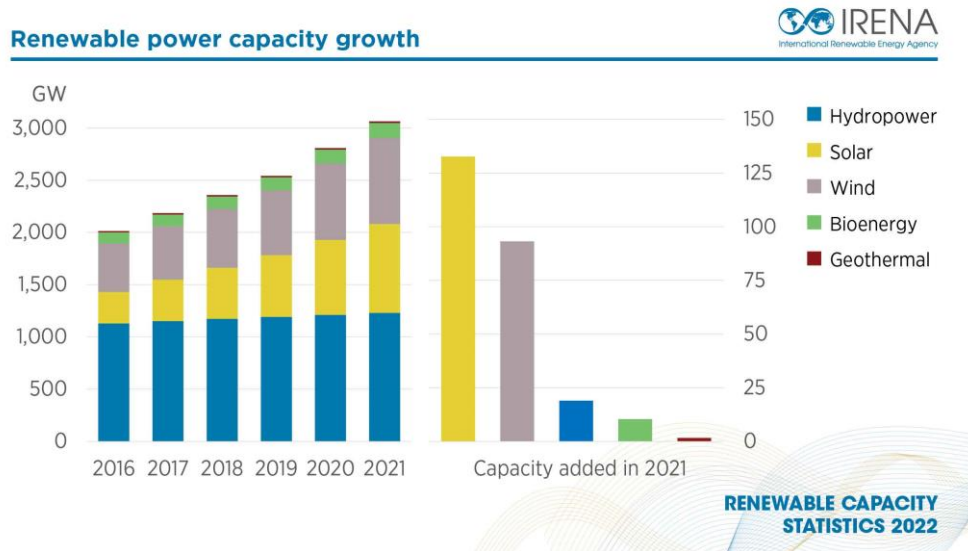
Figure 8.   Renewable power capacity growth, IRENA report

The energy transition will require considerable investments: Figure 9 shows the trend of annual investments applied to the development of the electricity sector worldwide[25]. A gradual increase in annual expenditure can be observed, from USD 1733 billion in 2010 to USD 1558 billion in 2018. Considering renewable energy sources alone, between 290 billion (in 2010) and 304 billion in 2018 are invested annually in the world.
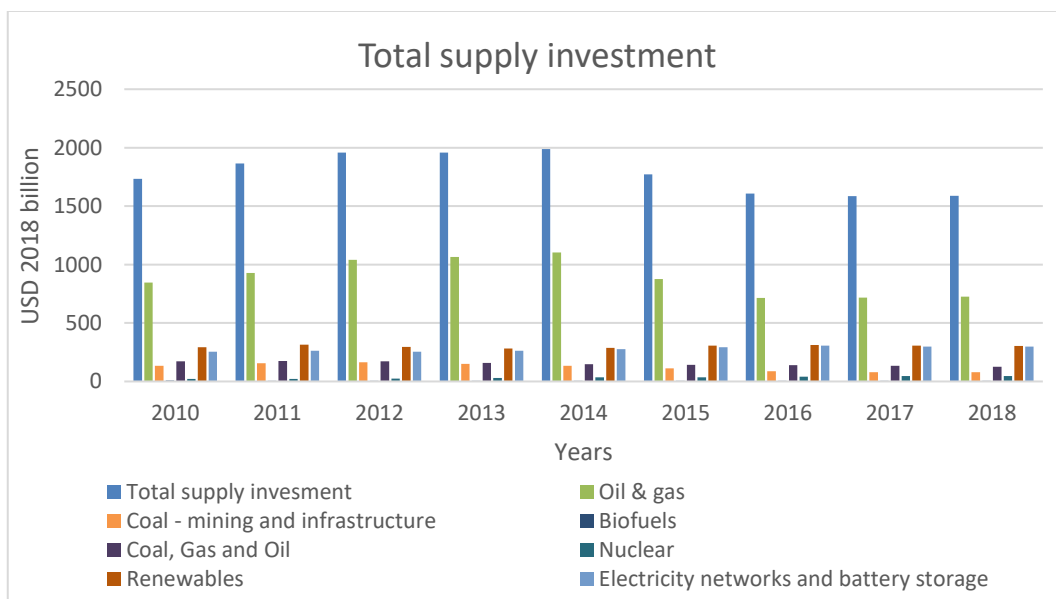
Figure 9.   Total supply investment in the world from 2010 to 2018

Despite, the investment in oil and gas sector decreased from 2010, how shown the Figure 9 and Figure 10, they take a large share of the total.
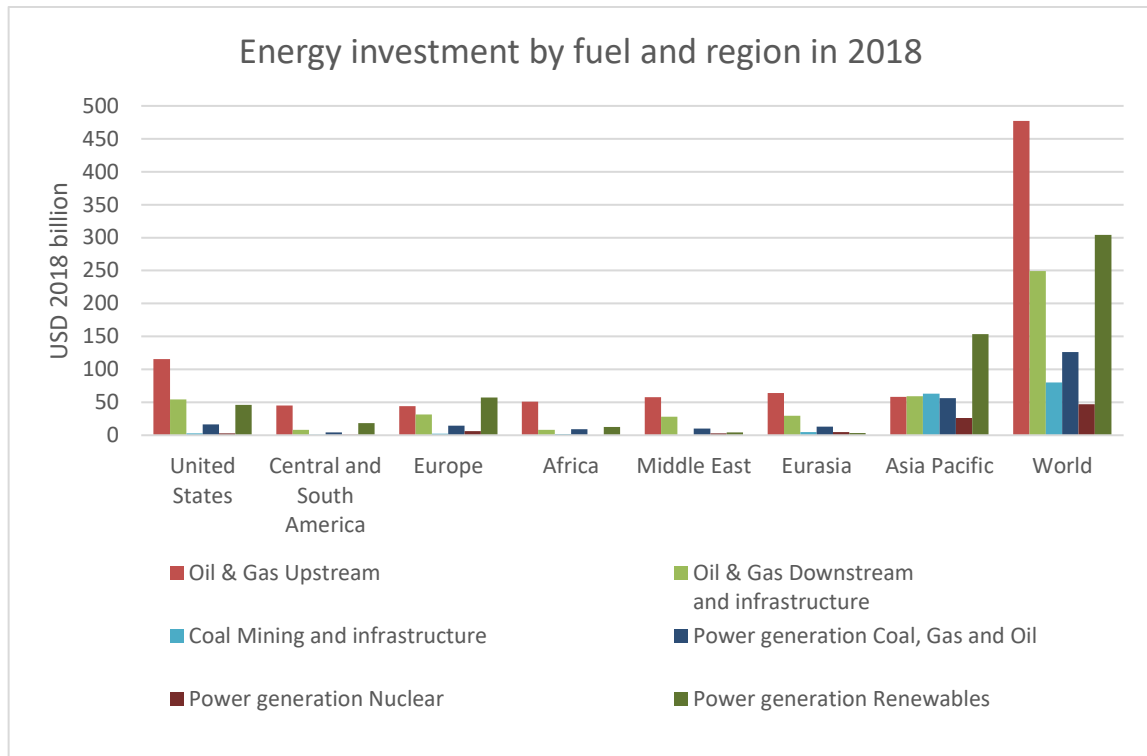
Figure 10.   Energy investment by fuel and region in 2018

This panorama describes the economic and political condition of the world during this century. The energetic transition process must be accelerated because:

- Fossil sources are running out; therefore, there is an urgent need to focus on alternative and renewable resources;

- Fossil fuels are highly polluting, are responsible for the emission of particulate matter, climate-altering gases (primarily CO_2) and the formation of acid rain[26]. In addition, accidents due to the spillage of these random fuels are not frequent but cause serious damage to the ecosystem[27];

- Fossil fuels are not evenly distributed around the globe: a few areas in the world (Latin America, the Middle East, Russia) hold the largest reserves of fossil fuels. This centralisation can lead to phenomena of strong energy dependency between states, with serious security of supply risks in the event

of political instability or the creation of conflicts in neighbouring states through which oil and gas pipelines pass.

Among the previous points, limiting CO_2 emissions has become a central issue, as this gas is identified as the main culprit in the global warming process. It is estimated that the energy sector accounts for at least two-thirds of the total anthropogenic CO_2 emissions[28]. In order to limit the consequences of global warming on the environment, early action must be taken before the process becomes irreversible. Recent studies indicate the need to achieve neutrality of anthropogenic CO_2 emissions by the middle of the 21st century[29,30]. To reduce the CO_2 emissions, it is mandatory replacing fossil fuels with renewable energy sources and reducing primary energy consumption in the various uses, improving management logic and preferring more efficient and durable technological solutions. Both strategies must be pursued in parallel if the objectives are to be achieved. Indeed, the first approach reduces impacts on the environment, without changing the energy requirements of end users. The second approach seeks to limit energy waste by reducing demand in the production chain. By following both approaches in the near future, we may therefore need less energy and be able to produce it in a more environmentally sustainable manner. At the international level, the promotion of renewables and energy efficiency measures benefited from the ratification of the Kyoto Protocol, and the subsequent Paris Agreement (2015), signed by 195 nations[31,32]. In this context, each state must adopt national policies aimed at reducing CO_2 emissions.

2. State of art

This section of the thesis studies the currently technology state of art related to wave energy converters sector, including power take off (PTO) and fuel cells sector as composed by fuel cells and electrolysers.

2.1 Wave energy converter state of art

Recent statistics indicate that the total theoretical wave-energy potential could achieve 30×10^6 GWh/year; however, this renewable source is irregularly distributed Worldwide[33]. As shown in Figure 11, there are, in the world, some hot spots, i.e., sites with the highest values of wave-energy potential. The most energetic area is the southern part of Australia, Africa, and America. Other relevant areas are located between North America and Japan in the Pacific Ocean and between Europe, Greenland, and North America in the Atlantic Ocean. Nevertheless, all these regions are exposed to extreme weather conditions, for this reason, sea wave harvesting is complicated[34].
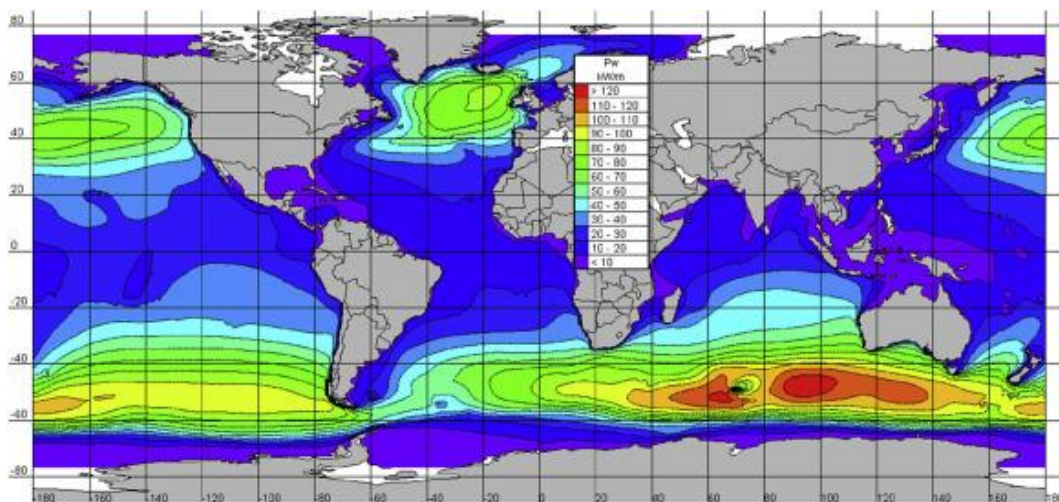
Figure 11.   Wave energy potential in the world

The device able to convert mechanical energy from the sea to electrical energy or other useful energy output is commonly defined WEC, Wave-Energy

Converters[35]. To classify these power plants, we can consider the distance from the coastline, the working principle and the orientation respect the wave direction. From distance from the coastline point of view three category are listed below and shown in Figure12[36]:

- Onshore, if the wec is installed on the mainland;
- Nearshore, if the wec is installed in water depths between 10 and 25 m;
- Offshore, if the wec is installed in seabeds deeper than 40 m.
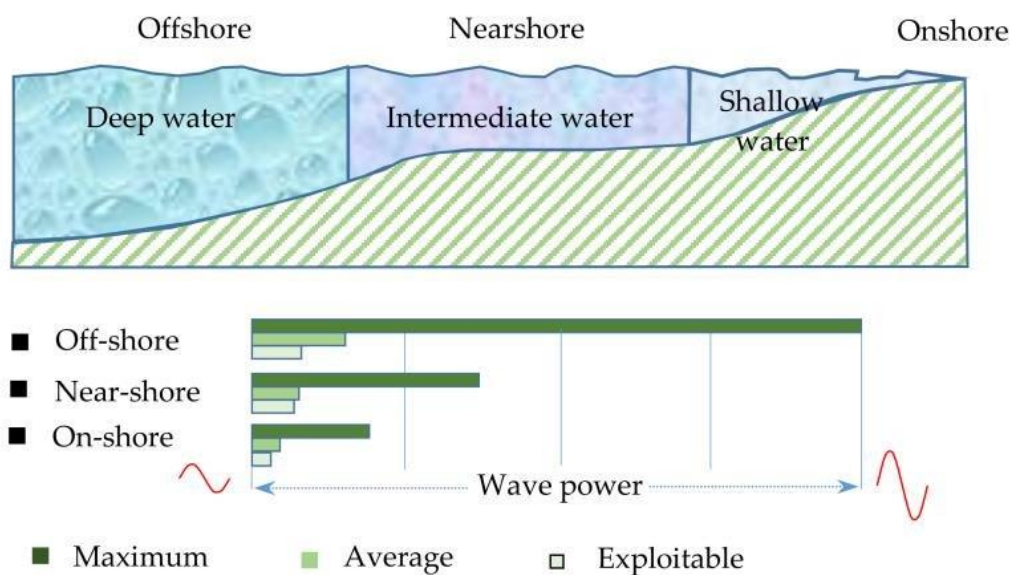
Figure 12. Classification for distance from the coastline

About orientation of the system to the direction of wave propagation, it is possible to define three kinds of technology, see Figure 13:

- Point absorber. The device is oriented independently to wave direction;
- Attenuator. The device is oriented parallel to wave direction;
- Terminator. The device is oriented perpendicular to wave direction.
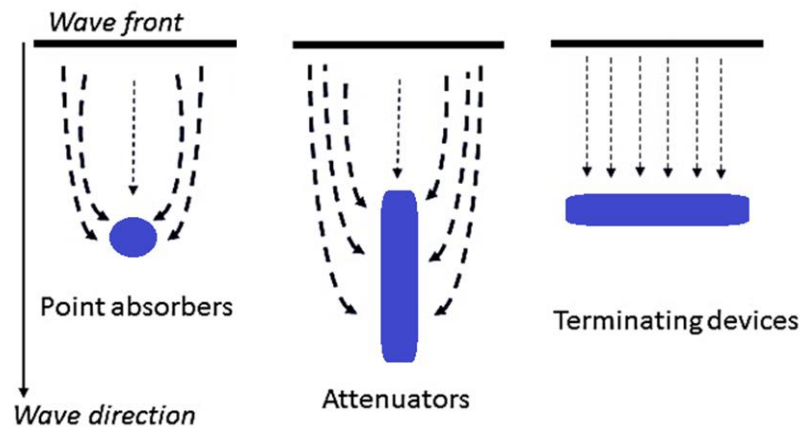
Figure 13.   Classification for orientation respect wave direction.

About the working principle it is possible to classify these three technologies[37]:

- Oscillating water column. In this case, the water of the sea enters in a chamber at the atmospheric condition. In this chamber sea wave produces a vertical water oscillation. The air inside the chamber is pressurized and depressurized by the water oscillation, producing a bidirectional air flow usable to run wind turbines. This device can be installed in onshore devices or into a floating device.

- Wave activated body. In this case, the sea wave produces relative motions on the system, running the energy converters. This device can be installed in an offshore system floating or submerged.

- Overtopping devices. The sea water is conveyed in a tank, converting kinetic energy of the wave in potential energy. Then this water is used to produce electrical energy through hydro turbine.

After these three classifications the different technologies are listed using example of really built power plant.

2.1.1   Oscillating water column

Several Oscillating Water Column (OWC) devices have been proposed in the past. According to the position of the system from the coastline, OWC devices can be classified as fixed or floating[38].

In the first case, the OWC plant is installed via a fixed structure on the shoreline or close to it, or in natural or artificial structures, such as breakwaters and rock cliffs. The installation of WEC directly on the shoreline has several benefits. The maintenance operations are simplified, reducing the relative costs. At the same time, the costs for the mooring system are minimized. Furthermore, the entire electrical equipment for the energy conversion is installed out of the water[35]. As mentioned before, the OWC devices are designed to produce a vertical oscillation of water inside a chamber to produce the alternative compression and expansion of the air inside the same chamber. Since the airflow changes continually its direction, the traditional horizontal-axis air turbines cannot be adopted. A solution is represented by the Wells turbine, developed in the mid-1970s by Alan Arthur Wells (in that period professor at Queen's University of Belfast)[35].

The Wells turbine is a low-pressure air turbine, characterized by the ability to rotate in one direction independently of the airflow direction. The blades are characterized by symmetrical air foils where the plane of the symmetry is the same as the plane of rotation and perpendicular to the airflow direction. The wells turbine is affected by a low or negative torque in the case of a small airflow rate, significant aerodynamic losses, and noise in comparison with other wind turbine. Thus, this turbine requires a greater section to achieve the same power output as other turbines. Nevertheless, the Wells turbine has been applied in several OWC plants.

As an example of full scale OWC system, the Kvaerner Brug's OWC plant was realized at Toftesfallen (Norway) in 1985[39], with 500 kW of electric power installation[40]. The lower part was realized in concrete, with a height of 3.5 m above sea level. As reported in Figure 14 this part of the system formed a chamber, communicating to the sea under the water level. The upper part, height 20 m, was equipped with a self-rectifying air turbine, with a 500 kW of electric power installation. This wave energy converter was destroyed by a storm during 1988. For this reason, the plant was decommissioned. It lived very short and produced only 29 MWh of electrical energy[41].
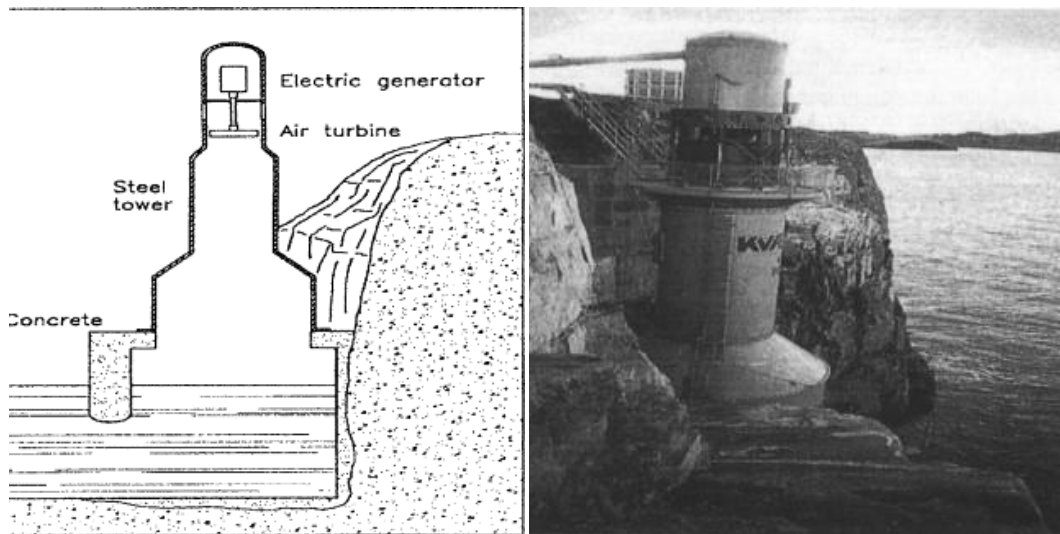
Figure 14. **Sectional drawing (left) and view (right) of the Kværner Brug's OWC plant**

In 1990 an OWC system was installed at Vizhinjam (Trivandrum, Kerala, India), composed by a concrete caisson and installed near the original breakeven structure. The project considered the installation of aWells turbine coupled with an induction generator (150 kW) in order to be directly coupled with the electrical grid[42].

In reality, the results were under the expectation: the output power was highly variable in the range 0–60 kW in a few seconds and the induction motor frequently was an electrical load instead of a generator, consuming more energy than the energy produced[43]. The plant was inactive for a long period. In 2004 the plant was investigated to supply a Reverse Osmosis desalination plant. This OWC device was finally decommissioned in 2011[44]. See figure 14.
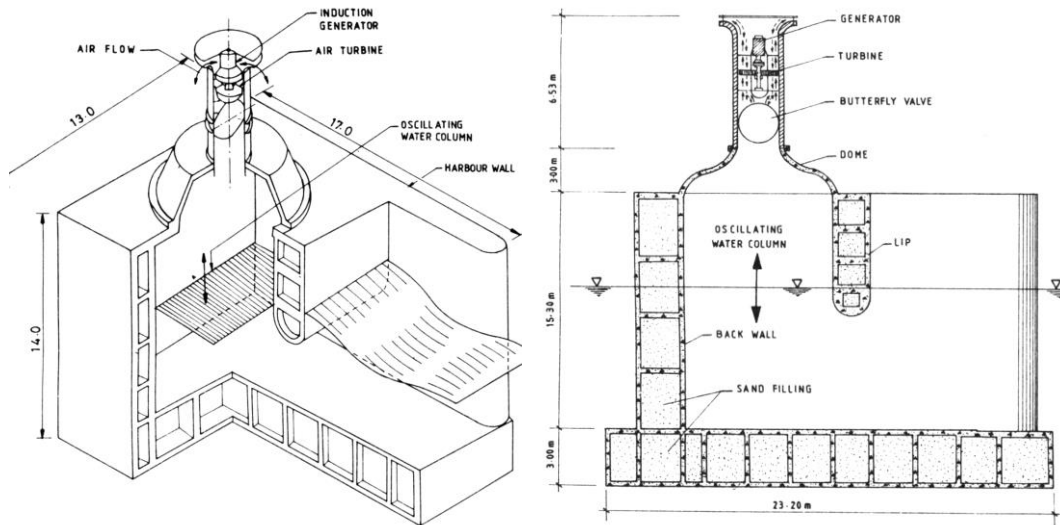
Figure 15. **Axonometric view (left) and section view (right) of the OWC device at Vizhinjam**

Based on the same principle, in 2000 the Islay LIMPET (Land Installed Marine Power Energy Transmitter) was installed on the Scottish island of Islay. This plant was realized and operated by Wavegen in cooperation with the Queen's University of Belfast. Islay LIMPET was the full-scale version of a previous prototype (75 kW) realized in 1991[45]. See the following figure 16.

Figure 16. **LIMPET OWC plant installed on the island of Islay (Scotland, UK)**

The envelope of LIMPET was entirely realized in concrete on the shoreline. It was equipped with two Wells turbines, each one with a rated power of 250 kW[3]. The plant was decommissioned in 2012 and today only the concrete building remains on the shoreline.

A similar technology was also developed in Portugal, under the supervision of Instituto Superior Técnico of Lisbon. In 1999 a full scale (400 kW) OWC plant was realized in Pico Island (Azores, Portugal). Some problems were due to malfunctions of Wells turbine and its support. The project was concluded on January 2018, demonstrating the feasibility of this technology[46]. The OWC system is reported in figure 17.
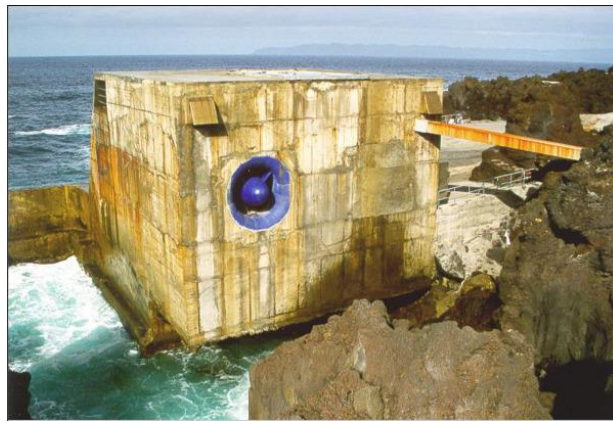
Figure 17.   Back view of the OWC plant installed on the island of Pico (Azores, Portugal)

In 2011, an OWC plant was inaugurated in the bay of Mutriku (Spain). The power plant is 100 m long and has an installed power of 296 kW. It is composed by 16 OWC chambers, each one equipped with a Wells turbine. The producer indicated a total electricity production equal to 1.6 GWh (updated to the end of June 2018)[47]. The OWC system is reported in figure 18.

Figure 18.   OWC plant installed in the bay of Mutriku (Spain)

An OWC system, called REWEC3 (REsonant Wave Energy Converter), has been developed in Italy, by the University of Reggio Calabria. This system is designed to be incorporated into a traditional vertical breaker in the harbour. In comparison with other OWC devices, the main difference is the U-shape connection between the internal chamber and the sea (see figure 19), that is chosen in order to adapt the resonance frequency of the system to sea wave. Thus, it is possible to maximize the energy extraction[48]. In the port of Civitavecchia, a full-scale plant has been installed, composed by 136 chambers and a rated power of 2.5 MW. In 2016 the system, with a length of 100 m, produced 500 MWh/y. After the optimization, the designers want to achieve an annual production of 800 MWh/y.
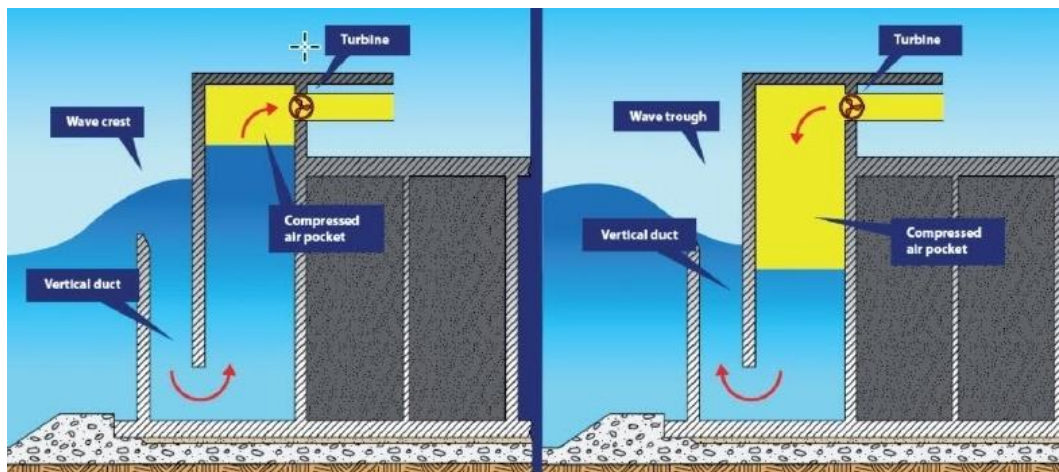
Figure 19.   Working principle of REWEC3

The Yongsoo plant (see figure 20) is another fixed OWC system, that was recently completed near to Jeju Island (Republic of Korea). The system is installed on seabed, at 1 km from the coastline. It is equipped with two horizontal axis impulse turbines, connected to different kinds of generators (a synchronous generator and an induction generator), both with a rated power of 250 kW. The plant has a length of 37 m and a width of 31 m.
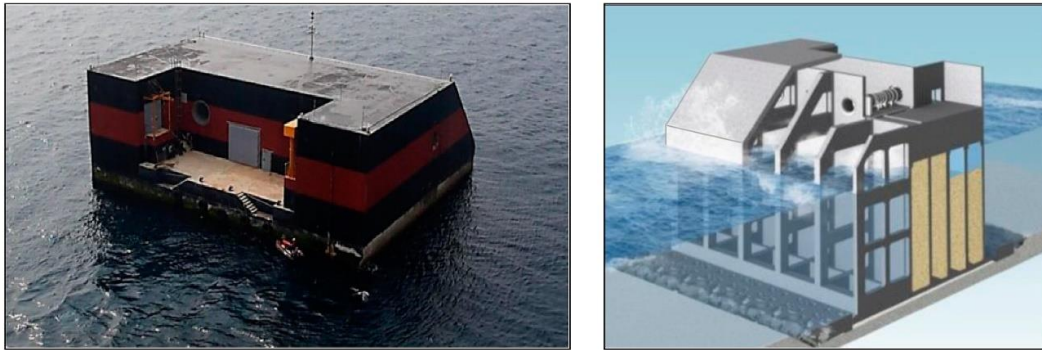
Figure 20.   Back (left) and perspective views (right) of OWC plant at Yongsoo

2.1.2   Wave activated body

The category of Wave-Activated Bodies (WAB) comprises several kinds of solutions for the sea wave exploitation. These systems are generally composed by two or more parts, arranged in order to produce a relative motion and run the energy converter[49].

These systems are generally designed for a nearshore or offshore installation, in order to exploit the more regular waves of the open sea, in comparison with the systems installed on the coastline. However, the installation far away from the coastline increases the number of problems. Indeed, long underwater cables or pipes are required to transfer the energy collected by the WEC to the mainland. These devices need also a mooring system, strong enough to resist to the extreme weather conditions[50].

Since there is a number of WAB, a classification is introduced by considering the working principle of the device as criterium[35]:

- Single body heaving buoys;
- Two-body heaving systems;
- Fully submerged heaving systems;
- Pitching devices;
- Bottom-hinged systems;
- Many-body systems.

2.1.2.1 Single body heaving buoys

An example is a system composed essentially by a buoy able to move along a metallic strut anchored to seabed by a universal joint. The idea was the exploitation of this vertical motion to pressurize an air reserve and consequently run an air turbine in a regular way. A prototype, having a buoy one meter diameter, was tested in 1983 in the Trondheim Fjord (Norway), replacing the air turbine with an orifice[35]. A solution of this technology (see figure 21) was developed at Uppsala University (Sweden), called Lysekil project[51]. This plant was enlarged with a second WEC and today is currently operating.
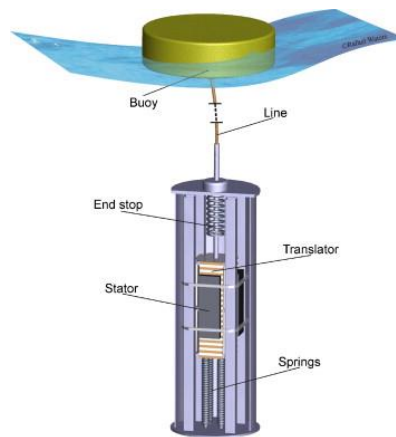
Figure 21.   Working principle of Lysekil project

2.1.2.2 Two body heaving buoys

The category "two body heaving systems" was introduced to solve the problem of the distance between the floating buoy and the fixed structure on seabed, where the energy production occurs. In this case, the WEC is composed by two floating buoys in order to produce a relative motion usable to extract energy. The shapes of two floaters are normally different in order to maximize the relative motion.

As shown in figure 22, Wavebob is an example of two body heaving system. To improve the relative motion between the two parts of the WEC, the central buoy is equipped with a big mass, increasing the inertia and limiting the vertical motion. The inferior buoy is designed to be submerged at depth enough to minimize the interference with sea wave. The vertical motion produced by the upper buoy (body

1) is used to run an oil pumping system. A small-scale (1:4) prototype was tested in the Galway Bay (Ireland)[52]. The prototype was installed in 1999 and decommissioned in 2015 because, during the 2013 the funding ended.
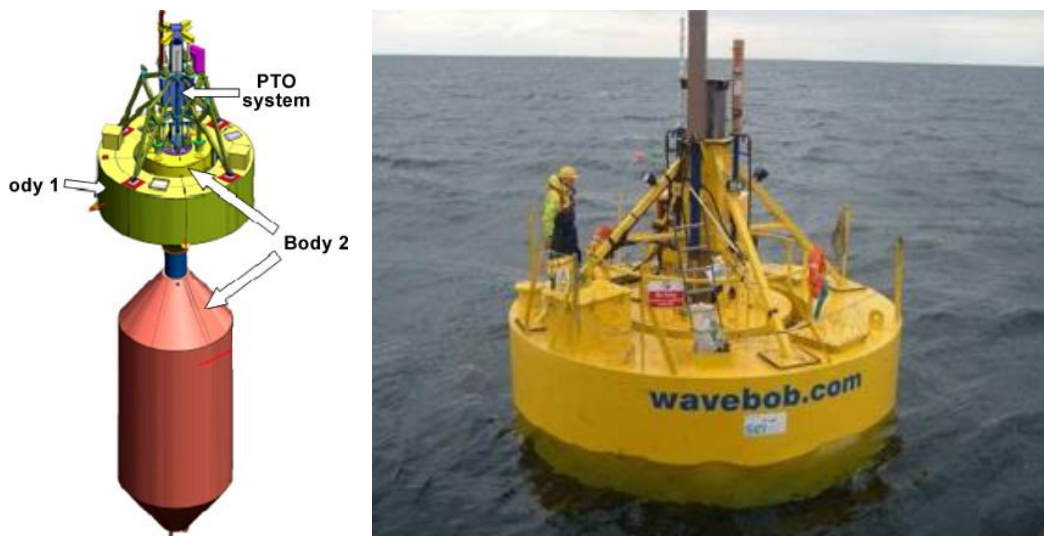
Figure 22.   Rendering view (left) and external view (right) of Wavebob

PowerBuoy is another example of two body heaving system, developed by the American company Ocean Power Technologies. As shown in figure 23, this WEC is composed by a floater, that is free to move up and down according to sea wave, and a submerged body, having a disk shape adopted to improve the inertia and hydrodynamic resistance of this part and maximize the relative motion between the two main parts of the device. The idea is the realization of a wave energy farm, installing several devices, each one producing electricity. To minimize the cost of the electrical connection with the mainland, an offshore substation could be realized. In 2005 a pilot plant (40 kW) was tested in an offshore site, close to Atlantic City (New Jersey, USA)[51]. In 2008, another plant of the same size was installed off the coast of Santoña.
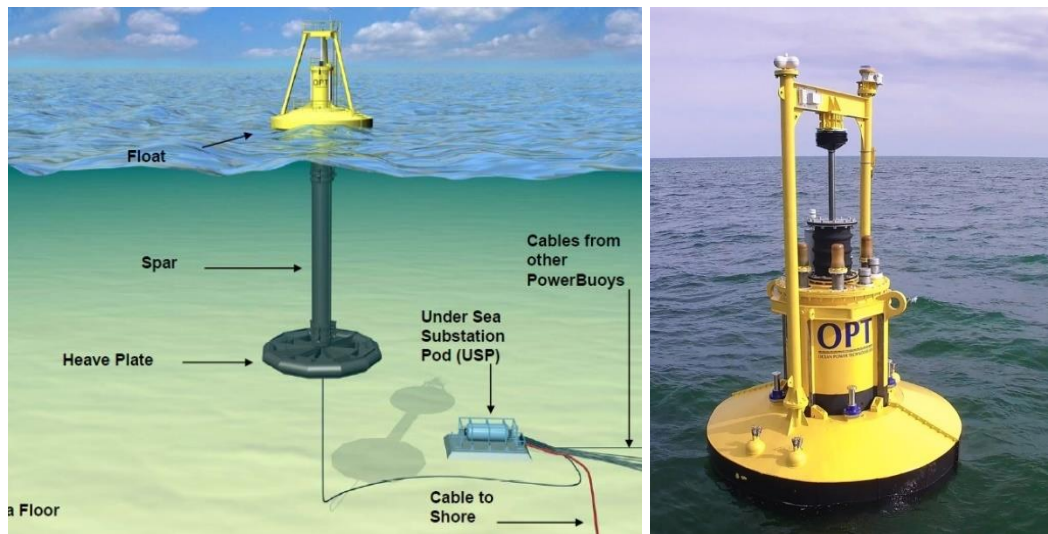
Figure 23.   Principle of operation and external view of PowerBuoy

2.1.2.3 Fully submerged heaving systems

About the fully submerged heaving systems, an example is the Archimedes Wave Swing, developed in Holland.

As shown in figure 24, the system is composed by two parts: a basement, that is anchored to seabed, and a floater. The device works by using the variation of the hydrostatic pressure applied to the floater, that pushes up and down a linear generator installed inside. In 2004, a pilot plant was tested with successfully in Portugal[35].
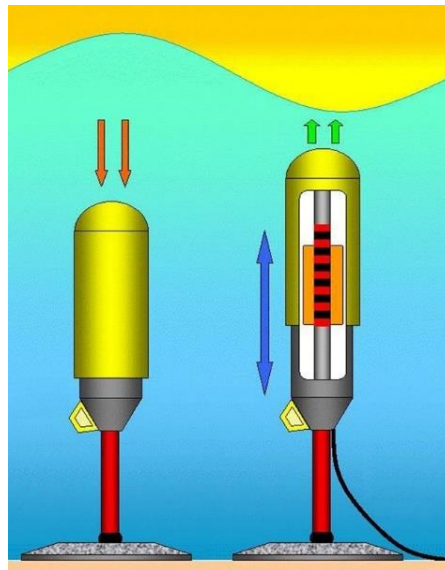
Figure 24.   Working principle of Archimedes Wave Swing[53]

CETO (name inspired by a Greek ocean goddess) is another full submerged device, proposed by Carnegie Clean Energy. This system is designed to be installed in the nearshore, a few meters below the sea level. The previous version (CETO 5) was designed to pump water for a station located on the coast where electricity and freshwater are produced, by using a Reverse Osmotic unit[54]. A new device (CETO 6) was installed in western Australia in 2014 to produce electricity directly on the WEC. The technology is shown in figure 25.
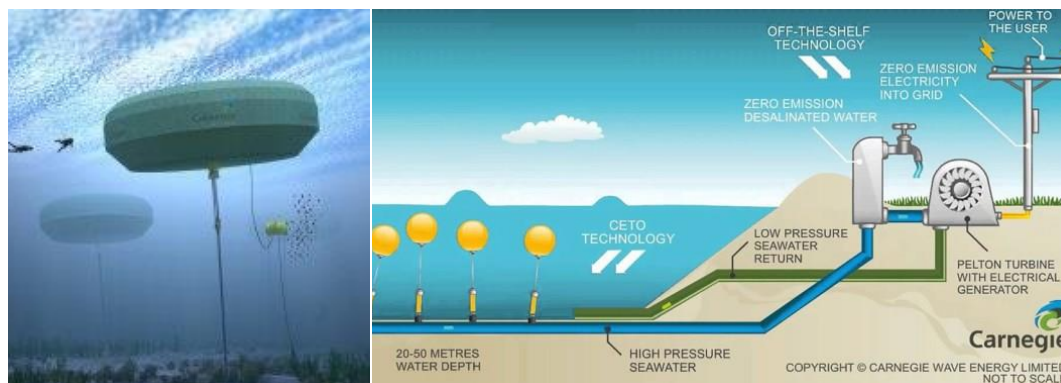
Figure 25.   CETO external view and working principle

2.1.2.4 Pitching devices

In the pitching devices, the main motion is a relative rotation (usually pitch) among the parts. Pelamis was a famous example of pitching device. It was developed in UK by Scottish company "Pelamis Wave Power Ltd". A first prototype, connected to the electrical grid, was tested in Orkney (Scotland) between 2004 and 2007. In 2008 a wave farm with three devices was installed at Aguçadoura (Portugal). Unluckily, the wave farm worked only for two months due to technical failures, causing financial problems to the company. The intellectual property was transferred to the Scottish government in November 2014. This WEC was composed by four cylindrical buoys, connected by three Power Conversion Modules (PCM), as depicted in figure 26[55–57].
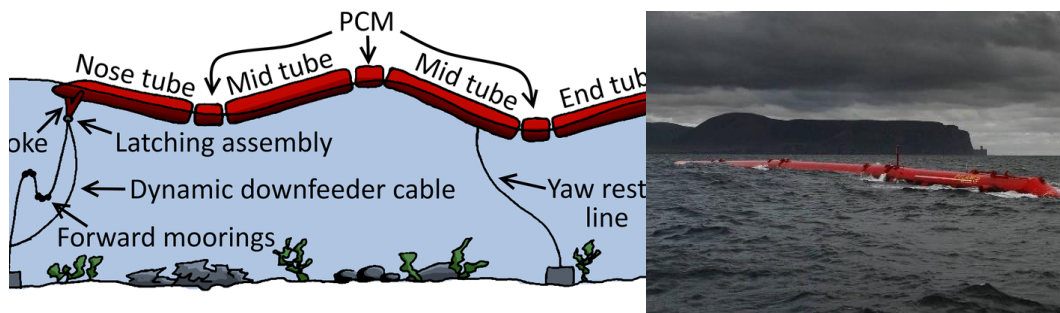
Figure 26.   Working principle and external view of pelamis

In detail, the system had a shape like a snake, oriented according to the wave direction, achieving a length of 120 m and a rated power of 750 kW. The working principle of Pelamis was based on the generation of a relative rotation on the PCM, equipped with hinged joints, in order to pump oil at high-pressure into accumulators and then run hydraulic motors coupled with induction generators.

2.1.2.5 Bottom hinged systems

The Bottom Hinged Systems are designed to exploit sea wave in shallow water (10 - 15m), where the sea motion is mainly horizontal. An example is Oyster, that is illustrated in figure 27[58,59].

Figure 27. Working principle of Oyster

This device consists essentially in a barrier, made by five cylinders horizontally stacked. Since the barrier is fixed by a horizontal hinge, the braking wave produces a rotation, activating a high-pressure pump. The pressurized water is conveyed along pipes to the coastline, where hydro turbines and alternators are installed to produce electricity. This kind of WEC was proposed by the team of Professor Trevor Whittaker, from the Queen's University of Belfast. The company Aquamarine Power developed and tested two full-scale plants at the European Marine Energy Centre's Billia Croo test site: Oyster 1 (315 kW) and Oyster 2 (800 kW). The second version was connected to grid in 2012 until 2015, when the company ceased trading[59].

AW energy (A Finnish company) proposed a similar system called Waveroller (see figure 28[60]). In 2007, a small scale (1:4) prototype was tested in Portugal.
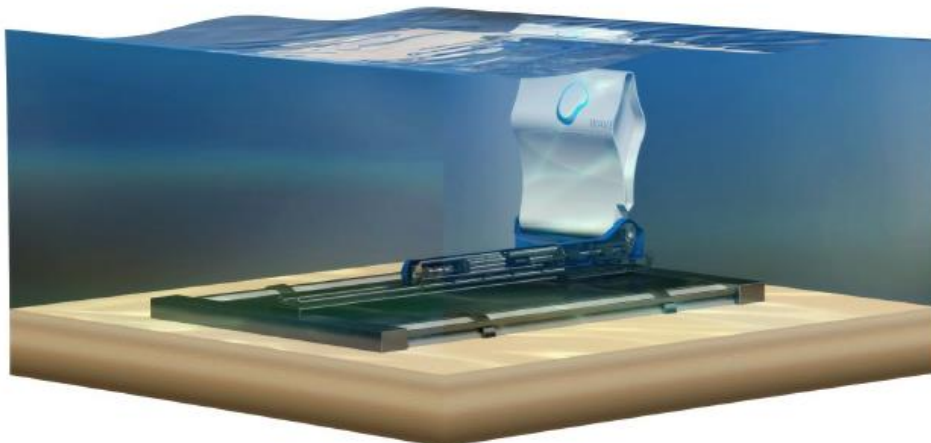
Figure 28. Rendering view of Waveroller

A full-scale prototype was installed in Järvenpää (Finland) in 2015, in order to optimize the technology. The device is designed to be installed at 0.3 – 2 km from the shoreline, where the sea depth is between 8 and 20 meters. The device has a rated power of 350 kW, equipped with a flap 18 m long and 10 m high. The company is currently working for new projects in Portugal, Mexico and Southeast Asia[60].

2.1.2.6 Many body system

Wavestar is an example of many-body systems. The first study on this device was started in 2000 by Niels and Keld Hansen in Denmark. A small-scale prototype (1:40) was tested in 2004 at the laboratory of Aalborg University. In 2005, a grid connected small scale (1:10) pilot plant was installed at Nissum Bredning. Finally, in 2009 a 1:2 scale prototype was connected to grid in Hanstholm. The plant was taken down in 2013[61]. Like other systems described above, Wavestar uses the relative rotation of the buoys to pump oil at high-pressure and runs hydraulic motors. The researchers are currently working on the full scale of the device. As shown in figure 29, Wavestar is composed, is composed by 20 buoys (10 m diameter), arranged in two lines, and able to extract until 6 MW according to the climatic conditions of the North Sea. The system could be also assembled with a star shape, using 60 buoys and achieving a total rated power of 18 MW[61,62]

Figure 29.   Rendering view of Wavestar

The same working principle can be applied along the coastline and the breakers of the harbours. An example is the EcoWave System, composed by several floaters,

which rise and fall according to the hydrodynamic interaction with sea wave. Using robust arms, the system pressurizes a fluid to run a generator installed on the coastline[63]. In 2016 a wave farm was opened at Gibraltar, located at the southern tip of the Iberian Peninsula. The plant has currently a rated power of 100 kW but it is planned to achieve 5 MW of installed power[3].

2.1.3 Overtopping devices

In the Overtopping Devices (OD), the exploitation of sea wave is based on the conversion of the kinetic energy of water into potential energy, usable by a low head hydro turbine.

An artificial water reserve should be created at a level superior than the sea level. To refill the system, a ramp is required to convey sea wave inside the water reserve. Historically, the first OD pilot plant was the Tapchan (Tapered Channel Wave Power Device), realized at Toftestallen (Norway) in 1985 (see figure 30)[64]. The collector was carved into a rocky cliff, realizing an entrance about 60 m wide and lifting water up into a reservoir 3 m above sea level and with a surface of 8500 m^2. To convert the potential energy into electricity, a low-head Kaplan-type hydro turbine was adopted, having a rated power of 350 kW. This plant was damaged by the storm in 1988. The plant was decommissioned in 1991.
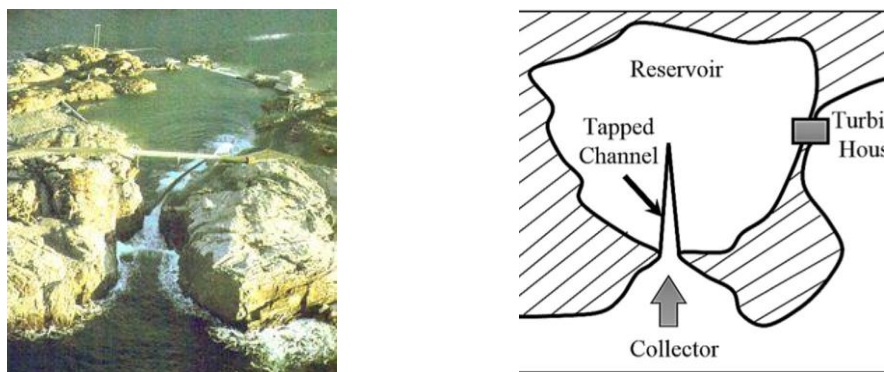
Figure 30.   View (left) and schematic plan view (right) of tapchan

It is also possible to realize an OD for an offshore application. As an example, the Wave Dragon was a floating slack moored WEC, developed by the Danish

company "Wave Dragon Aps". In March 2003 a 20 kW prototype (scale 1:4.5) was installed and tested in the Nissum Bredning fjord until January 2005[65]. In detail, Wave Dragon is composed by a floating water reserve, refilled with sea wave by using two reflectors (see figure 31)[66], and a ramp to convert the kinetic energy into potential energy through the increasing of water level[66]. This kind of energy can be used by Kaplan turbines to run permanent magnets rotary generators. To work properly, the system should be fixed to seabed by moorings and faced to the wave direction.

Figure 31. **Views of the small scale Wave dragon (left) and its working principle (right)**

The last OD project is called Seawave Slot-Cone Generator, depicted in figure 32[67]. This system is designed for an onshore installation.
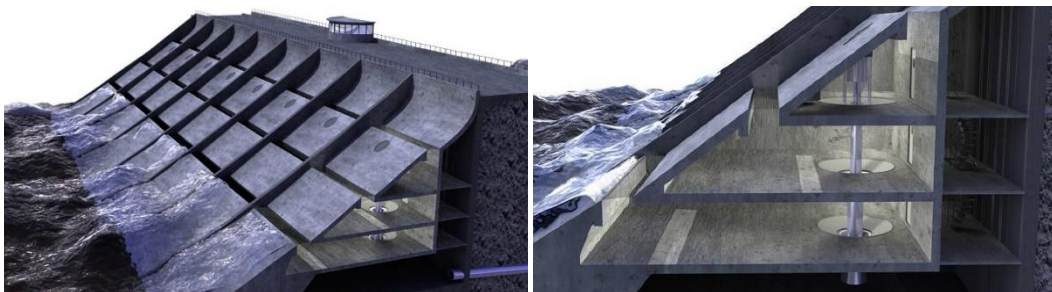
Figure 32. **External view (left) and section view (right) of Slot-Cone**

In detail the system is composed by three chambers, located at different heights. Each chamber has an opening, located at the superior point. The system has externally a ramp shape, in order to increase the water height and fill the internal chambers. A multistage low-head hydro turbine is adopted to transform the potential energy of water inside each chamber into electricity. Two pilot plants have been planned for the realization along the west Norwegian coasts, but have not been realized[67].

As shown in the list of various technologies, the exploitation of energy from the sea is an area of focus for university studies around the world. A summary table is provided to bring together all the installations mentioned, showing: project name, country of installation/design, technology, year of installation, years of operational life and notes.

Table 2.   Summary of the several WEC technologies

Project	Country	Technology	Year of installation	Years of operation	Note
Kværner Brug's	Norway	OWC	1985	3	
Vizhinjam OWC plant	Kerala, India	OWC	1991	20	Fragmented operation due to inefficiency of the system
LIMPET	Islay, Scotland	OWC	1991	21	
Pico island	Pico, Portugal	OWC	1999	19	
Mutriku wave power plant	Mutriku, spain	OWC	2011	10	Currently operating
REWEC	Port of Civitavecchia, Italy	OWC	2016	5	Currently operating
Yongsoo OWC Pilot Plant	Yongsoo South Korea	OWC	2016	5	Currently operating
Lysekil Project	Lysekil, sweden	WAB	2006	15	Currently operating and enlarged with 2 WEC
Wavebob	Galway Bay, Ireland	WAB	1999	14	In 2013 end of funding

PowerBuoy	Atlantic city, New Jersey	WAB	2005	16	Upgrade in 2020
Archimedes Wave Swing	Holland-portugal	WAB	2004		Pilot plant developed successfully
CETO 5	Australia	WAB	2015		Pilot plant developed successfully
CETO 6	Australia	WAB	2014	5	
Pelamis P1	Agucadoura, portugal	WAB	2008	Less 1	Technical and financial problem
Pelamis P2-001	Orkney, Scotland	WAB	2010	4	
Pelamis P2-002	Orkney, Scotland	WAB	2013		the council is studying how to use the device
Oyster	Orkney, Scotland	WAB	2012	3	the company ceased trading
Wave roller	Järvenpää (Finland)	WAB	2015	6	Currently operating
Wavestar	Hanstholm, Denmark	WAB	2009	4	
Eco Wave power	Gibraltar	WAB	2016	5	Currently operating
Eco Wave power	Jaffa port, Israel	WAB	2016	5	Currently operating
Tapchan	Toftestallen, Norway	OD	1985	6	Damaged by a storm

Wave Dragon	Nissum Bredning, Denmark	OD	2003	2
Seawave slot-cone generator	Norway	OD		Planned but not realized

As can be seen, some plants have been successful, producing electricity constantly, and others for various reasons have unfortunately been decommissioned.

As a result, the participation of governments becomes very important, in fact many governments have participated in the construction of energy production plants because it is in their interest to enable the development of renewable technologies, although some not very efficient plants have been decommissioned because funding has been cut off.

2.2 Power take off state of art

The power take off is the device that transform kinetic or potential energy from the sea wave in mechanical energy and then electrical energy or directly in this one.

The energy extraction system is of great importance as it affects the efficiency with which the absorbed wave power is converted into electricity, the mass, size and structural dynamics of the WEC. The PTO, similarly to the WEC, should be robust and reliable because these characteristics affect the availability of the device, operating and maintenance costs during its lifetime[68]. Generally, each type of WEC corresponds to its PTO. For example, the OWC device uses an air turbine coupled to the electric generator, while a point absorber may use several systems depending on their configuration and may require several cascading conversion mechanisms. In design, it is observed that PTOs are generally not scalable. The reason for this is that this system does not interact directly with the fluid, but with an interface system. Furthermore, on a small scale of a model of a WECs, the ratio of friction to other forces in the PTO is greater than in the actual model.

Furthermore, by further decreasing the scale, the mechanical power would become so small that it would be necessary to model, all over again, a PTO that could effectively convert that available mechanical energy into electrical energy.

As shown in figure 33, the technologies are essentially five:

- Hydraulic systems
- Air turbines
- Low head hydraulic turbines
- Direct linear generators
- Direct Mechanical Generators
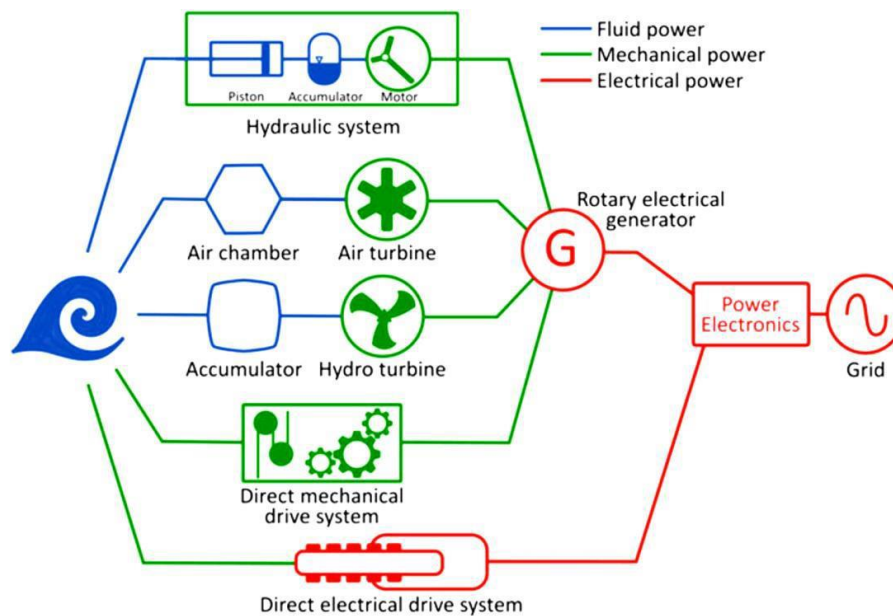
Figure 33.   Most common PTO devices

Each PTO has its own peculiarities, advantages, and disadvantages. As shown in the table, the most efficient extraction systems are those based on the linear generator and mechanical converter. In fact, they are currently the subject of research for this very reason[69]. In table 3 are shown the energy efficiency conversion of technologies.

Table 3. **Indicative average efficiency for different Power Take Off systems**

PTO system	Efficiency %
Hydraulic systems	65
Air turbines	85
Low head hydraulic turbines	55
Direct linear generators	95
Direct Mechanical Generators	90

2.2.1 Air turbines

Air turbines are mainly used in OWC systems. The turbine is driven by the pressure difference induced by the oscillation of the water level within the semi-submerged column. For this type of system, there are basically three types of turbines that can be used, as shown in the figure 34.

- Wells turbines
- Babinsten action turbine
- Denniss-Auld turbine
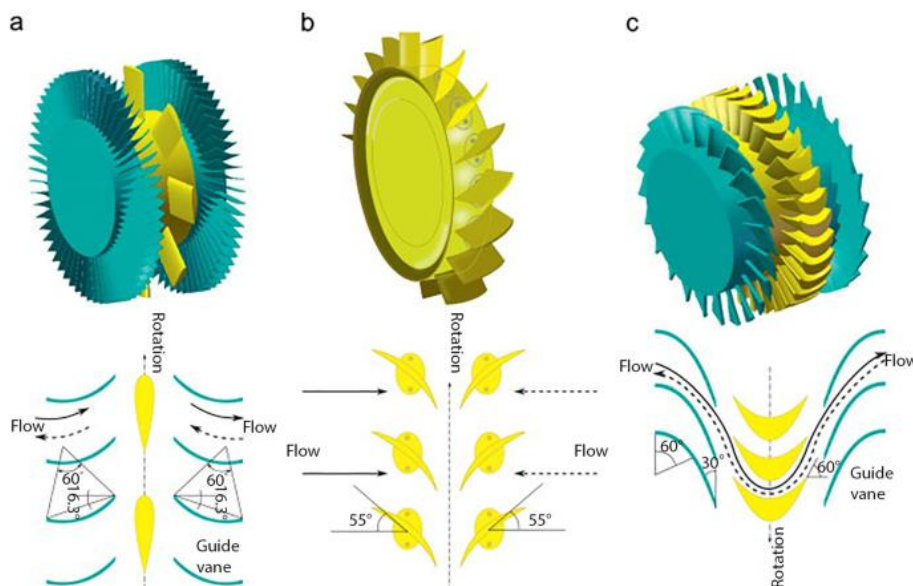
Figure 34. **The profiles of the different types of air turbines compared; a) Wells Turbine, b) Babisten Turbine, c) Action Turbine, Dennis-Auld**

The Wells Turbine is a self-rectifying axial-flow turbine, whose torque is not sensitive to the direction of airflow; this results in an alternating airflow in a unidirectional rotation[70]. For this reason, the Wells turbine is the widely used system in OWCs. However, a downside to be considered is that this type of turbine does not start automatically. To solve this drawback, it is necessary to accelerate the rotor through an external energy source at start-up. To overcome some of the limitations of the Wells turbine, the Babisten action turbine was developed. In this device, the diffusers are fitted with adjustable paddles to straighten the air flow, allowing it to be directed to the rotor. The paddles can be fixed or adjustable. In the latter case, there is a mechanism that adjusts the attachment of the paddles themselves, which can be self-controlled by the airflow or controlled by another active mechanism, such as a hydraulic actuator. Although adjusting the paddles results in a modest increase in turbine efficiency, it must be considered that increasing the moving parts of the turbine results in an increase in the complexity of the device and a decrease in reliability. This also leads to an increase in the cost of turbine operation and maintenance. The self-righting Denniss-Auld turbine is primarily based on the Wells turbine model. In this illustration, the air foil paddles can rotate around their neutral position, within a certain range, to achieve an optimal angle of incident airflow. The rotation of the paddles is modulated by measuring the pressure in the chamber.

2.2.2 Hydraulic system

Hydraulic systems are particularly used with point absorbers or attenuating devices. Such systems are well suited to the conversion of energy, very large forces, or moments, at low frequencies, applied by waves on oscillating bodies. In figure 35 is shown the system diagram of a hydraulic system.
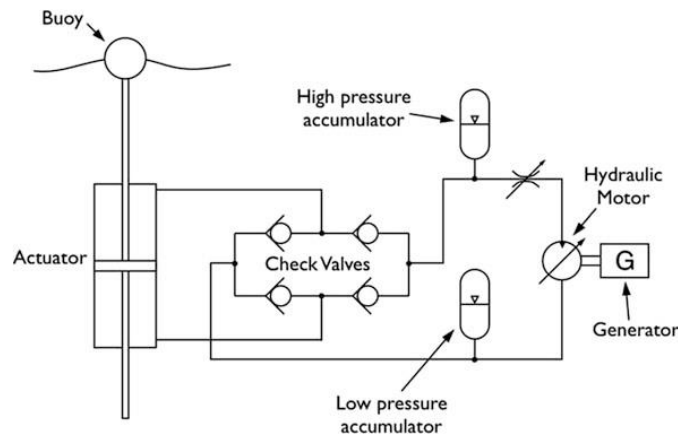
Figure 35. System diagram of a hydraulic system

The buoy is directly connected to a piston that is bound to move inside a cylinder, which contains the working fluid. The motion of the body drives the plunger, which pushes the working fluid, compressed, through a manifold that in turn feeds the hydraulic motor. A conventional electric generator is splined to the same shaft as the hydraulic motor, thus enabling the conversion of hydraulic energy into electrical energy[71]. The hydraulic circuit is also equipped with a gas storage system, high and low pressure, which allows for the accumulation or release of hydraulic energy and thus allows for the irregularity of the power absorbed by the waves[72].

2.2.3 Low head hydraulic turbines

These devices are exclusively used in overtopping systems. The potential energy of the water in the overtopping reservoirs is harnessed to drive low-head hydraulic turbines such as Kaplan, see figure36, which are widely used in such overflow systems. The turbines are coupled to a conventional electric generator. An advantage of water turbines is that they are a mature technology that has been used for many decades in hydroelectric power plants.
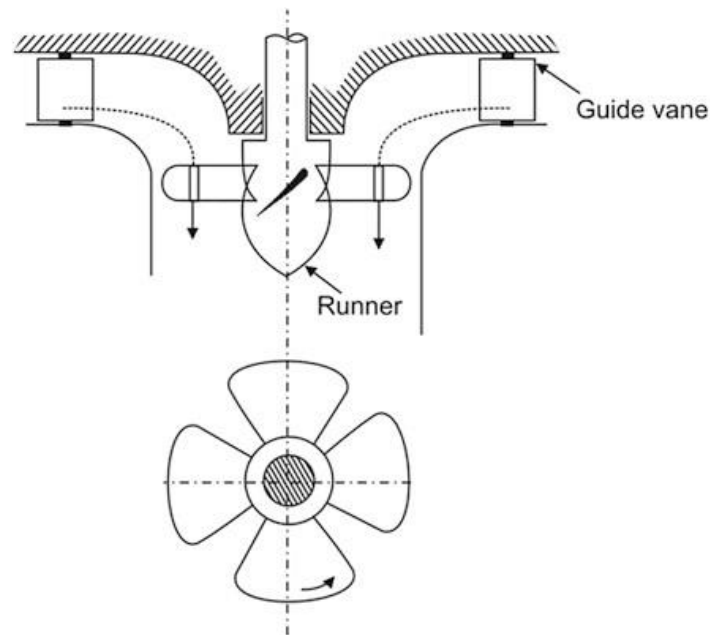
Figure 36. **Sectional view (top picture) and bottom view (bottom picture) of a Kaplan turbine**

The Kaplan is a jet turbine that includes a rotating element, called runner, completely immersed in water, and enclosed within a confined space that is under pressure. Adjustable paddles are installed on the diffuser; this allows management of the water flow sent to the turbine runner. In addition, the runner paddles are also adjustable, so that they have an almost flat profile for low flow conditions and a very inclined profile for high flow conditions.

2.2.4 Direct linear generators

Linear generators ensure the input conversion of linear motion into electrical energy. In this way, the energy conversion chain is drastically simplified by using a limited number of components. This allows for a higher overall system efficiency, as there are no intermediate energy conversions corresponding to an energy loss. Due to the direct-drive solution of directly coupling the speed and force of the floating buoy to the translator, linear generators are currently the subject of research. One of the most interesting configurations are linear generators with permanent magnets. Thus, the wave motion is converted directly into electrical

energy, however, this cannot be fed directly into the grid as it manifests a waveform and frequency not suitable for grid conditions. Therefore, a power electronic converter must be interposed in order to regularise the waveform and adjust the frequency before feeding energy into the grid. One of the great advantages conferred by the use of permanent magnets, in the moving part of the machine, is that the generation of the magnetic induction field takes place without the adoption of an excitation current, thus making it possible to abolish the entire excitation circuit, including conductors and sliding contacts[36][33].

The linear generators are composed by, see figure 37:

- Stator, the fixed iron part
- Translator, a movable element that is constrained to translate in only one direction
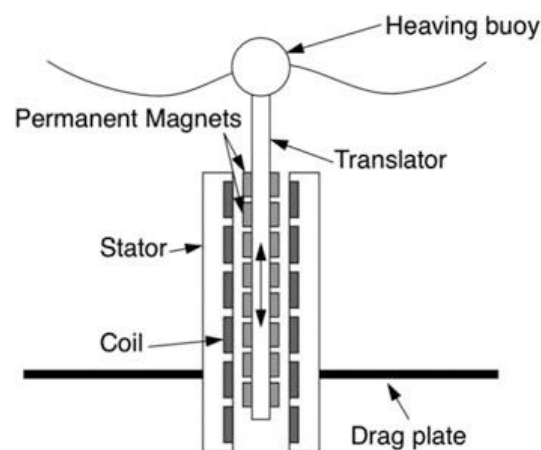
Figure 37.   Linear generator composition

2.2.5 Direct Mechanical Generators

A Power Take Off with direct mechanical drive converts the mechanical energy of an oscillating body, subjected to wave motion, into electrical energy using a mechanical conversion system that drives a rotating electric generator. The mechanical conversion system (gear box) comprises a whole series of elements whose ultimate purpose is to set the rotor of the electric generator in motion. In figure 38 is shown a block diagram of a mechanical PTO.
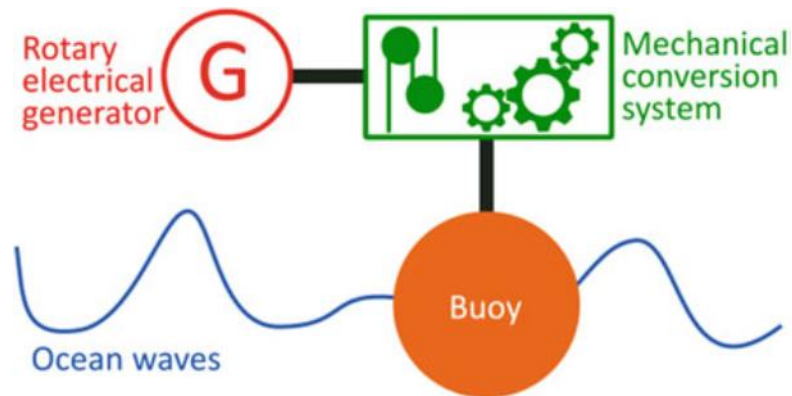
Figure 38.   Block diagram of a mechanical PTO

The latter two devices will be among the objects of study presented in this thesis work, as three prototypes were built in the University of Palermo's marine technology laboratories.

2.3 Electrochemical state of art

A fuel cell (FC) is a device that converts the chemical energy of a fuel, such as hydrogen, by an oxidising agent, such as oxygen, into electricity through a pair of redox reactions. Fuel cells differ from most batteries in that they require a continuous source of fuel and oxygen to sustain the chemical reaction[73]. The following figure 39 shows a typical fuel cell, composed by an anode negative pole, cathode positive pole, electrolyte allowing only ions to pass from the anode to the cathode or vice versa. The product of the chemical reactions is only water, see equation 1.

$$H_2 + \frac{1}{2}O_2 \rightarrow H_2O \tag{1}$$
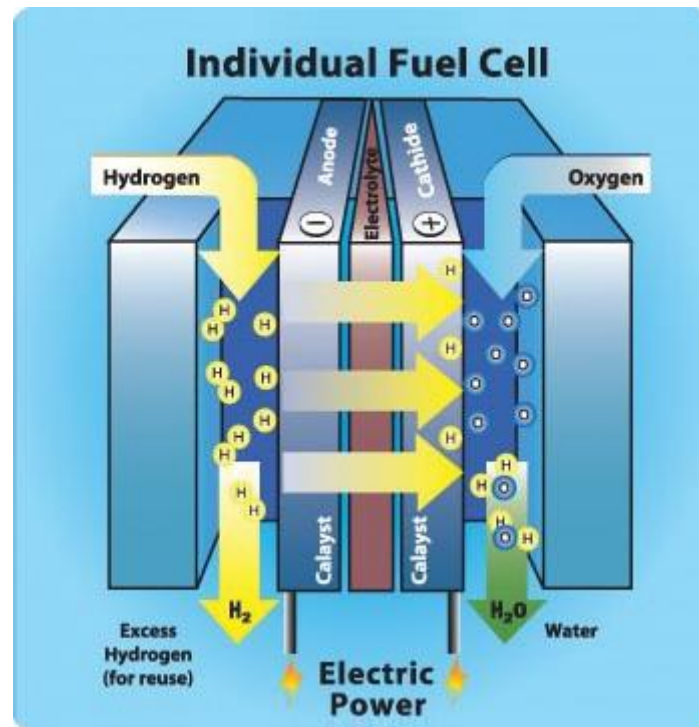
Figure 39.   Picture of a typical fuel cell

In literature there are many fuel cells technology, classified for different kinds of electrolyte: alkaline, phosphoric acid fuel cell, molten carbonate and solid oxides, polymeric electrolyte. The working temperatures are different from each technology. It is possible to distinguish low temperature FC, medium temperature FC and high temperature FC. Besides the type of electrolyte and operating temperature, the main characteristics of a fuel cell are:

- Cell voltage [Volt]
- Power density [kW/m^3]
- Energy density [kWh/m^3]
- Efficiency %
- Specific energy [kWh/kg]

As mentioned above, a FC uses hydrogen as fuel. Instead, hydrogen can be produced using the process of electrolysis of water, splitting it in gaseous hydrogen and oxygen[15]. The figure 40 shows a typical electrolyser, where the production of hydrogen takes place at the cathode according to a reduction reaction of water to

H_2 and that of oxygen at the anode according to an oxidation reaction of water to O_2.
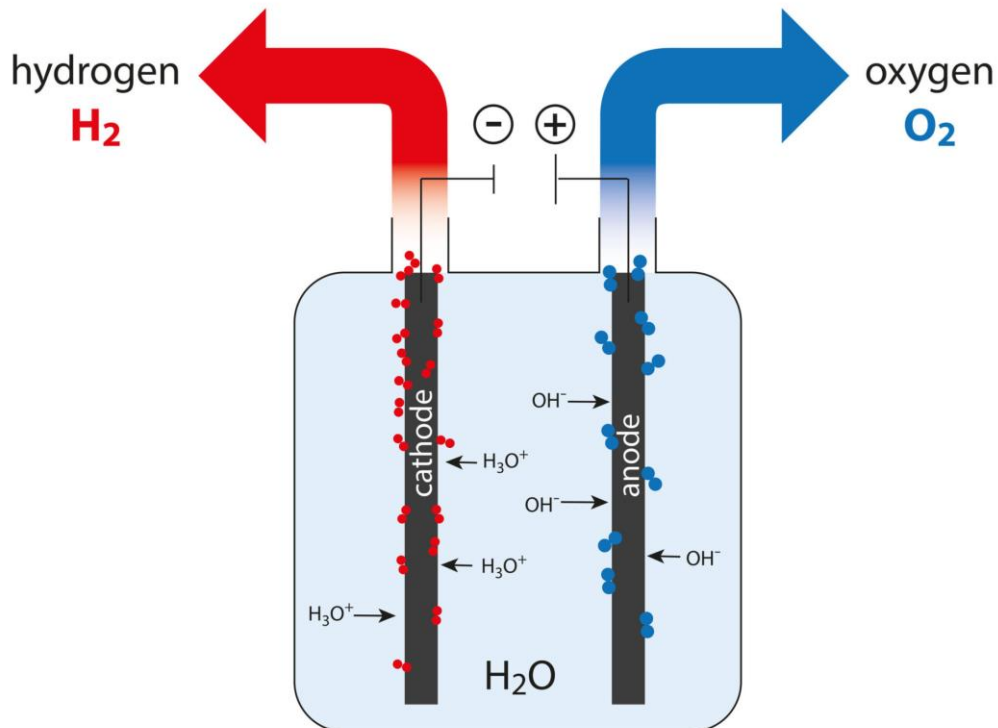
Figure 40.   Picture of a typical electrolyser

The global reaction is shown in equation 2.

$$2H_2O \rightarrow 2H_2 + O_2 \tag{2}$$

This is a non-spontaneous reaction, that requires electrical energy. From a technical point of view, they work like a FC but in a reverse way. Both FCs and electrolysers work with inert electrodes characterized by:

- Long lifetime
- High physical stability
- High electrical conductivity
- High chemical stability
- Non-polluting and non-contaminating
- Safe

- Low cost

In the same way the electrolyte that usually is characterized by liquid state or solid state in both technology it is a selective membrane. If they are cationic membranes allow only the cation pass and if they are anionic membranes allow only the anion pass. The main characteristics of the electrolytes are:

- Low solvent transport
- Impermeable to neutral molecules
- High chemical stability at operating temperature
- Mechanical stability
- Low voltage drops
- Low cost
- Long lifetime

In the following sections are listed the currently state of art of fuel cells[73] and electrolysers[15,74].

2.3.1 Alkaline fuel cell (AFC)

This technology works with potassium hydroxide (KOH) as a liquid electrolyte at the temperature of 60-120 °C. The fuel must be pure at 99% of hydrogen[73]. This implies that hydrogen, to have a good energy density, must be stored at around 300 bar. The scheme of an AFC fuel cell is shown in picture 41.
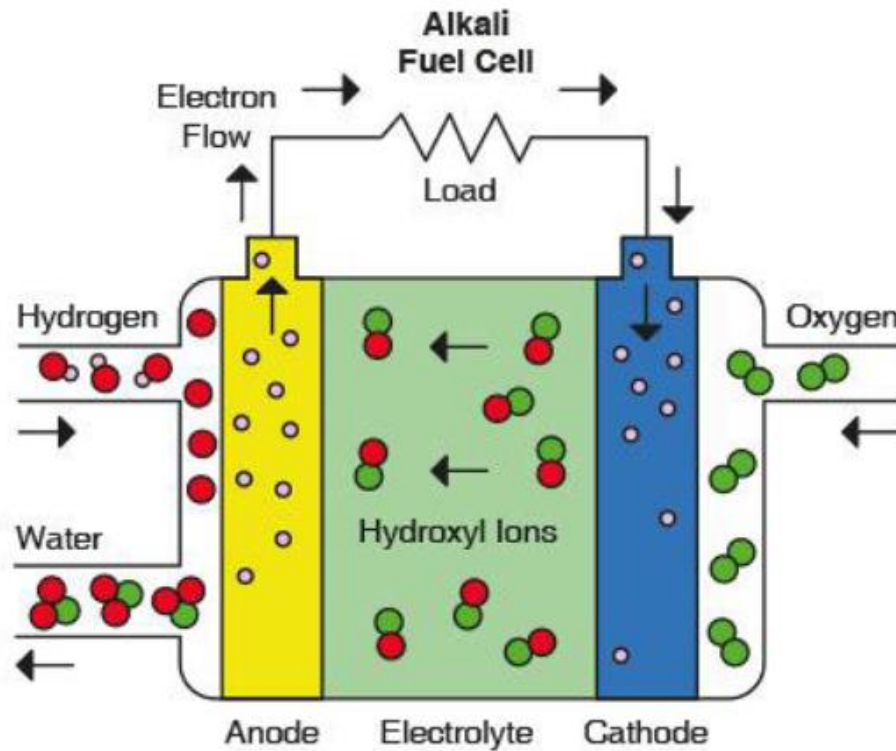
Figure 41.   A fuel cell

Electrons pass from the anode to the external load and then to the cathode via an external circuit. OH⁻ anions are produced at the cathode and pass to the anode through the electrolyte. The products of the FC are only thermal energy and:

- Anode side, unreacted fuel and water
- Cathode side, unreacted oxygen and water

The anode, cathode and global reactions inside the FC are shown in the following equations 3,4,5.

Anode reaction

$$2H_2 + 4OH^- \rightarrow 4H_2O + 4e^- \tag{3}$$

Cathode reaction

$$O_2 + 2H_2O + 4e^- \rightarrow 4OH^- \tag{4}$$

Global reaction

$$2H_2 + O_2 \rightarrow 2H_2O \tag{5}$$
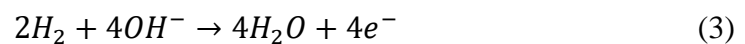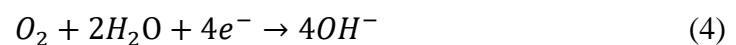
These devices find application in the military, submarine, and space sectors. It is used in these areas because one of the advantages is the high-power density, with electrical efficiency of 60%. Unfortunately, however, it is very sensitive to CO_2 and CO, which severely damage it.

2.3.2 Proton exchange membrane (PEMFC)

This technology uses a polymer membrane with high proton conductivity as electrolyte and operates at temperatures between 70 and 100 °C. The membrane must be humidified in order to function properly, otherwise it risks damage. The fuel must be pure hydrogen and only liquid water is produced. The electrical efficiency is around 40-60%. The small FC work at 1 bar pressure, instead the stacks that work over 10 kW exceed 1 bar operating pressure. The application PEM FC is essentially for automotive sector or energy production. The scheme of PEM FC is shown in figure 42.
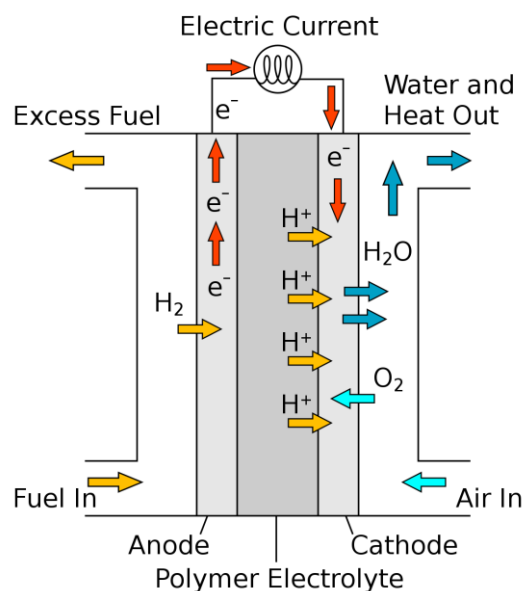
Figure 42.   PEM fuel cell

Between the two electrodes, an exchange of electrons takes place through the external circuit and an exchange of protons through the electrolyte with a flow from anode to cathode. The products of the FC are only:

- Anode side, unreacted fuel
- Cathode side, unreacted oxygen and water

The anode, cathode and global reactions inside the FC are shown in the following equations 6,7,8.

Anode reaction

$$2H_2 \rightarrow 4H^+ + 4e^- \tag{6}$$

Cathode reaction

$$O_2 + 4H^+ + 4e^- \rightarrow 2H_2O \tag{7}$$

Global reaction

$$2H_2 + O_2 \rightarrow 2H_2O \tag{8}$$

The advantages of this technology are low corrosion problems and CO_2 resistance and low start-up times. The disadvantages are low CO resistance and humidification, which must be very thorough.

2.3.3 Direct methanol (DMFC)

Methanol is used in this technology because it provides a high concentration efficiency in hydrogen and because it has a high energy density. Methanol does not have storage problems at high pressures like hydrogen, so it can be used as fuel from a normal tank. The FC works at temperatures between 70 and 120 °C. The electrolyte is a polymeric membrane. The efficiency of electrical production is around 20-25%. The scheme of a DMFC fuel cell is shown in picture 43.
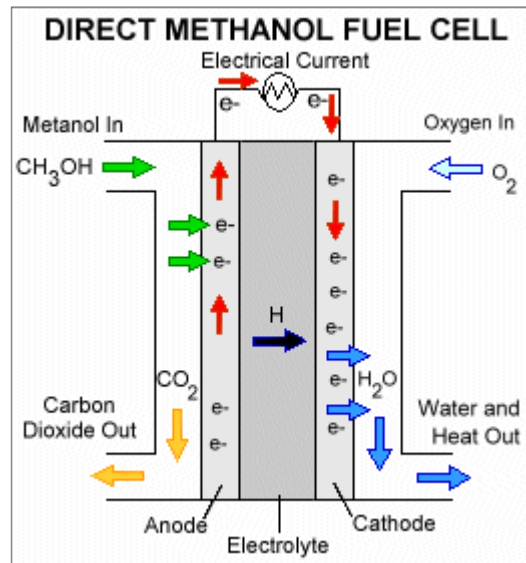
Figure 43.   DM fuel cell

Electrons pass from the anode to the external charge and then to the cathode. H^+ protons, produced at the anode, pass to the cathode through the electrolyte. The products of FC are:

- Anode side, non-reacted methanol and CO_2
- Cathode side, unreacted oxygen and water.

The anode, cathode and global reactions inside the FC are shown in the following equations 9,10,11.

Anode reaction

$$CH_3OH + H_2O \rightarrow 6H^+ + CO_2 + 6e^- \qquad (9)$$

Cathode reaction

$$\frac{3}{2}O_2 + 6H^+ + 6e^- \rightarrow 3H_2O \qquad (10)$$

Global reaction

$$CH_3OH + \frac{3}{2}O_2 \rightarrow H_2O + CO_2 \qquad (11)$$
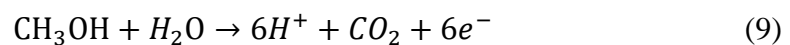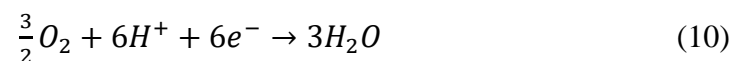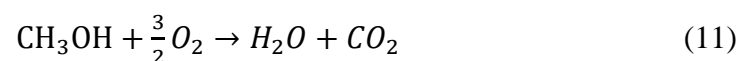
The principal application of this technology is related to portable devices.

2.3.4 Phosphoric acid (PAFC)

This FC family works at medium temperatures, i.e. between 200 and 250 °C. The electrolyte is a concentrated solution of phosphoric acid. They can work with pure fuel or with H mixed with CO or CO_2. The efficiency reaches good values between 40 and 50%. The scheme of PSFC is shown in figure 44.
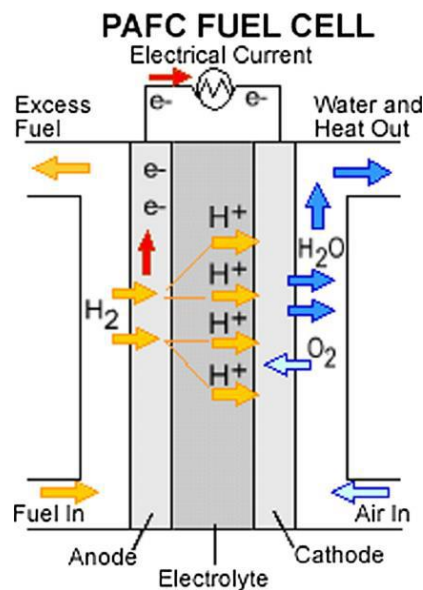
Figure 44.   PA fuel cell

These FCs allow the recovery of low-temperature heat from other systems in order to reuse it for domestic hot water production or heating. Here too, electrons pass from the anode to the outer circuit and then to the cathode, and H^+ from the anode passes to the cathode via the electrolyte. The products of Fc are:

- Anode side, non-reacted fuel
- Cathode side, unreacted oxygen and water.

The anode, cathode and global reactions inside the FC are shown in the following equations 12,13,14.

Anode reaction

$$2H_2 \rightarrow 4H^+ + 4e^- \tag{12}$$

Cathode reaction

$$O_2 + 4H^+ + 4e^- \rightarrow 2H_2O \tag{13}$$

Global reaction

$$2H_2 + O_2 \rightarrow 2H_2O \tag{14}$$

These devices are among the most widely used as they allow thermal waste to be recovered in power ratings between 50 and 200 kW.

2.3.5 Solid oxide (SOFC)

SOFC is a high temperature technology. They are completely solid-state cells and operate between 600 and 1000°C. The electrolyte is zirconium oxide doped with yttrium oxide. Pure hydrogen or natural gas can be used. The energy production efficiency is around 45-60%. The electrons pass from the anode to the outer circuit and then to the cathode, the anions O^{2-} produced at the cathode pass to the anode via the electrolyte. In the following figure 45 is shown the SOFC.
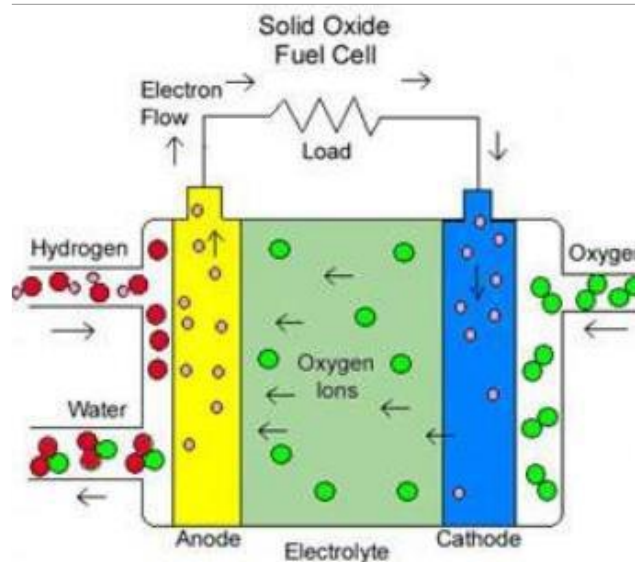
Figure 45.   SO fuel cell

The products of the Fc are:

- Anode side, unreacted fuel and water
- Cathode side, unreacted oxygen

The anode, cathode and global reactions inside the FC are shown in the following equations 15, 16, 17.

Anode reaction

$$2H_2 + 2O^{2-} \rightarrow 2H_2O^+ + 4e^-$$ (15)

Cathode reaction

$$O_2 + 4e^- \rightarrow 2O^{2-}$$ (16)

Global reaction

$$2H_2 + O_2 \rightarrow 2H_2O$$ (17)
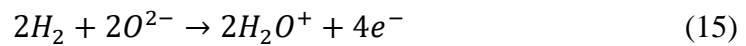
They are used for power generation and especially in cogeneration with high efficiencies. The disadvantages of working at high temperatures are the high costs of the materials that must be used.

2.3.6 Molten carbonate (MCFC)

This family of FCs also works at high temperatures, around 650°C. The electrolyte is a solution of alkaline carbonates such as Li, K, Na. The fuel used can be methane or synthetic gas. The efficiency is around 50%. The electrons pass from the anode to the outer circuit and then to the cathode, CO_3^{2-} carbonate anions produced at the cathode pass to the anode through the electrolyte. The scheme of this technology is shown in figure 46.
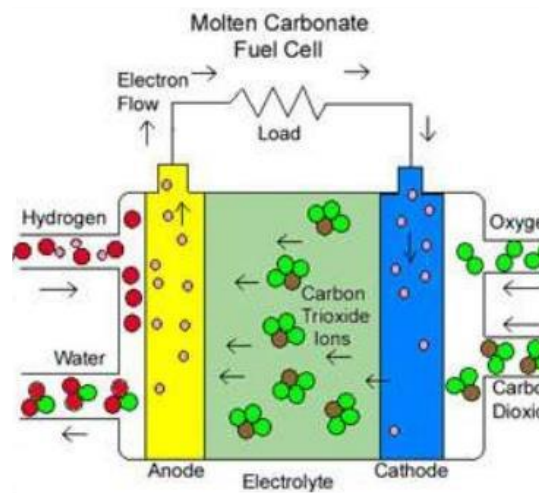
Figure 46.   MC fuel cell

The products of the Fc are:

- Anode side, unreacted fuel and water
- Cathode side, unreacted oxygen and CO$_2$

The anode, cathode and global reactions inside the FC are shown in the following equations 18, 19, 20.

Anode reaction

$$2H_2 + 2CO_3^{2-} \rightarrow 2H_2O + 2CO_2 + 4e^- \tag{18}$$

Cathode reaction

$$O_2 + 2CO_2 + 4e^- \rightarrow 2CO_3^{2-} \tag{19}$$

Global reaction

$$2H_2 + O_2 \rightarrow 2H_2O \tag{20}$$
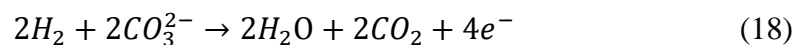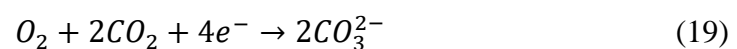
These FCs are used for combined heat and power generation. Here too, the disadvantages are related to the expensive and temperature-resistant materials.

In the following table 4 is shown a list of FCs most important peculiarities.

Table 4.   FCs peculiarities

	AFC	PEMFC	DMFC	PAFC	MCFC	SOFC
Electrolyte	Potassium hydroxide	Polymeric membrane	Polymeric membrane	Phosphoric acid	Lithium potassium carbonate	zirconium oxide
Ion Allowing Reaction	OH-	H+	H+	H+	CO_3^{2-}	O2-
T [°C]	60-120	70-100	70-120	200-250	650	600-1000
Fuel	Pure hydrogen	Hydrogen, reforming gas	Methanol	Hydrogen, reforming gas	Hydrogen, reforming gas	Hydrogen, reforming gas
Oxidation Agent	Pure oxygen	O2/air	O2/air	O2/air	O2/air	O2/air
Electrical Efficiency [%]	60	40-60	20-25	40-50	50	45-60
Applications	Military	Low power generation	Portable devices	Cogeneration	Industrial cogeneration	Industrial cogeneration
Advantages	High power density	High CO2 resistance, low stat-up time	No hydrogen storage	Thermal waste recover	High efficiency	High efficiency
Disadvantages	Low resistance to CO2	Low CO resistance, humidification required	Low efficiency	Low resistance to CO	High costs and thermal stress	High costs and thermal stress

2.3.7 Electrolysers

After analysing fuel cells, devices that generate electricity by consuming a fuel such as hydrogen, part of the scientific research developed during the PhD period focused on the study of electrolysers.

Currently, hydrogen production relies on technologies derived from fossil fuels. Methane (natural gas) processing is the most widely used technology for commercial hydrogen production[75]. Hydrogen gas can be produced from fossil fuels through the following techniques: steam reforming, partial oxidation and

autothermal reforming. These technologies produce a large amount of carbon monoxide.

The electrolyser technology involves splitting the water molecule using electricity and producing H_2 and O_2. The process of using electricity to produce hydrogen that will be used to produce electricity again may seem contradictory. In reality, this process has several advantages:

- It is possible to power a FC of a mobile device without having the storage and transport problems associated with hydrogen.

- When there is a surplus of energy in a power generation system, it can be diverted and fed to an electrolyser, for example at night when energy demand is lowest.

- The hydrogen produced is very pure, it is produced on site where it is needed, there are no emissions of pollutants.

In order not to run into the same problems as hydrogen production from hydrocarbons, it is necessary that the electricity that powers an electrolyser comes from a renewable source. Now the most common devices are Alkaline electrolysers, proton exchange membrane electrolysers and solid oxide electrolysers[15].

2.3.7.1 Alkaline electrolysers

This alkaline technology has potassium hydroxide (KOH) as its electrolyte. They work at a temperature between 65 and 100 °C and a pressure between 1 and 30 bar. In the following figure 47 the scheme is shown.
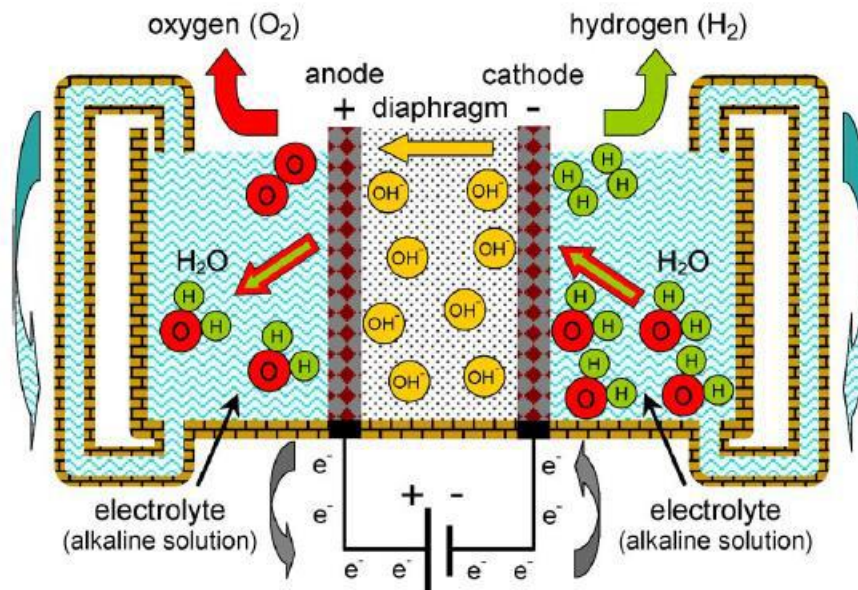
Figure 47.   Alkaline electrolysers scheme

The anode, cathode and global reactions are listed in equation 21, 22, 23.

Anode reaction

$$2OH^- \rightarrow \frac{1}{2}O_2 + 2e^- \tag{21}$$

Cathode reaction

$$2H_2O + 2e^- \rightarrow H_2 + 2OH^- \tag{22}$$

Global reaction

$$2H_2O \rightarrow 2H_2 + O_2 \tag{23}$$
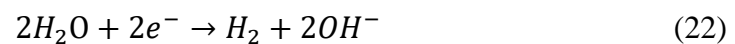
This technology is the most mature on the market and is characterised by long operating life and high efficiencies of up to 80%. The disadvantage is the high corrosiveness of the electrolyte. hydrogen production is around 500-760 Nm^3/h consuming around 3 kW of electrical energy.

2.3.7.2 Proton Exchange Membrane Electrolysers

As the PEMFC this electrolyser is composed by a polymeric membrane electrolyte. The working temperature must low 80°C and the pressure must low 85 bar[76]. In the following figure 48 the scheme is shown.
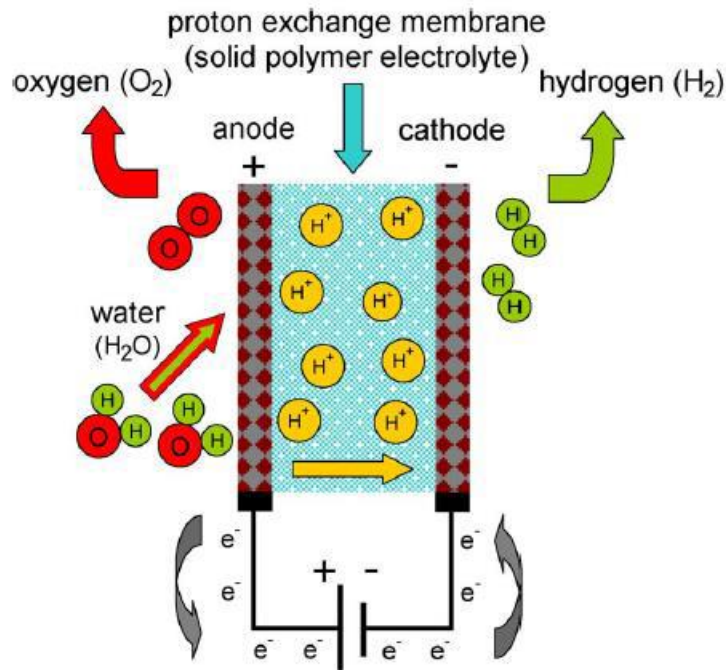
Figure 48.   PEM electrolyser scheme

The anode, cathode and global reactions are listed in equation 24, 25, 26.

Anode reaction

$$4H^+ + 4e^- \rightarrow 2H_2 \tag{24}$$

Cathode reaction

$$2H_2O \rightarrow O_2 + 4H^+ + 4e^- \tag{25}$$

Global reaction

$$2H_2O \rightarrow 2H_2 + O_2 \tag{26}$$

The efficiency is around 60% and the hydrogen production is pure over 99%. Their lifetime is less than alkaline technology.

2.3.7.3 Solid oxide electrolysers

This is a less established technology than the previous two and is under development. They work above 600 °C and electrical efficiency of 50%. The electrolyte is zirconia (ZrO_2) yttria-stabilised (Y_2O_3). All the device is composed by solid components. In the following figure 49 the scheme is shown.
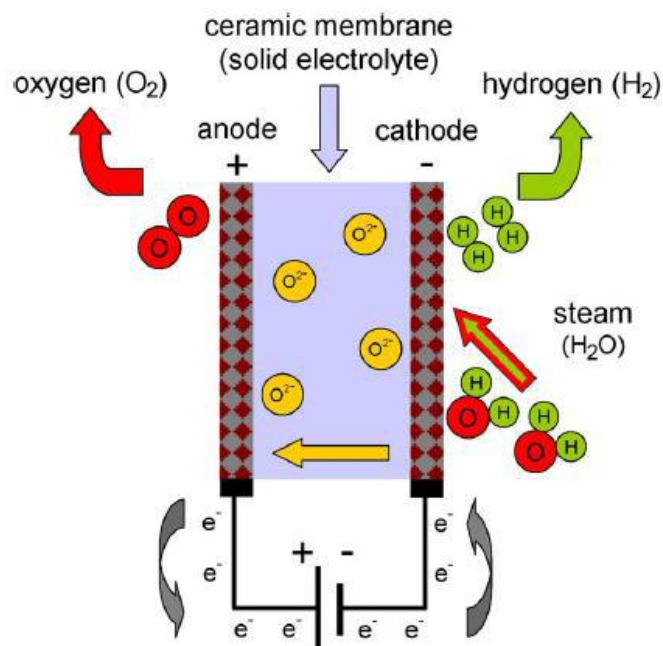
Figure 49.   SO electrolyser scheme

The anode, cathode and global reactions are listed in equation 27, 28, 29.

Anode reaction

$$O^{2-} \rightarrow \frac{1}{2}O_2 + 2e^-$$ (27)

Cathode reaction

$$H_2O + 2e^- \rightarrow H_2 + O^{2-}$$ (28)

Global reaction

$$2H_2O \rightarrow 2H_2 + O_2 \tag{29}$$

The high operating temperature reduces electricity consumption because reactions are faster. Therefore, both thermal and electrical energy are supplied. The disadvantage is that the hydrogen produced at the cathode contains a lot of vapour that must be condensed. The life of the cells is very short due to the working conditions.

In the following table 5 the main electrolyser characteristics are resumed.

Table 5.   Electrolyser characteristics

	Alkaline	**PEM**	**SO**
Electrolyte	KOH	Polimeric membrane	zirconia yttria-stabilised
Charge carriers	OH^-	H^+	O^{2-}
fuel	Electrical energy	Electrical energy	Electrical and thermal energy
T [°C]	65-100	<80	>600
Electrical efficiency %	<80	60	50
Advantages	Established technology, long lifetime	Pure hydrogen production	Low electrical consumption
Disadvantages	Corrosive electrolyte	Lower lifetime than alkaline	Low lifetime

3. Wave motion

Waves are a form of energy transport associated with an oscillation that propagates in space (so they do not necessarily involve an actual transport of matter but only the propagation of the oscillation). Some types of waves need a medium to propagate, such as water, air and solid; others, such as electromagnetic waves, have the characteristic of being able to propagate even in a vacuum. To define the characteristic elements of a wave, one considers the simple sine wave, which has a profile described by the sine function. This, representation is only a simplified approximation, used to describe the characteristics of most waves. It should be noted that waves have similar shapes but different characteristics to each other. The characteristic and essential elements of a sine wave are the following, see figure 50:

- Ridge (or apex): place of the points at which the sea surface rises most above sea level
- Valley: place of the points where there is the maximum lowering of the sea surface with respect to sea level
- Period (T): time between two consecutive rises of the surface (or between two consecutive subsidence) in the direction of wave propagation
- Wavelength (λ): distance between two successive crests or lines in the direction of propagation of the wave motion
- Height (H): vertical distance between a ridge and the next valley.
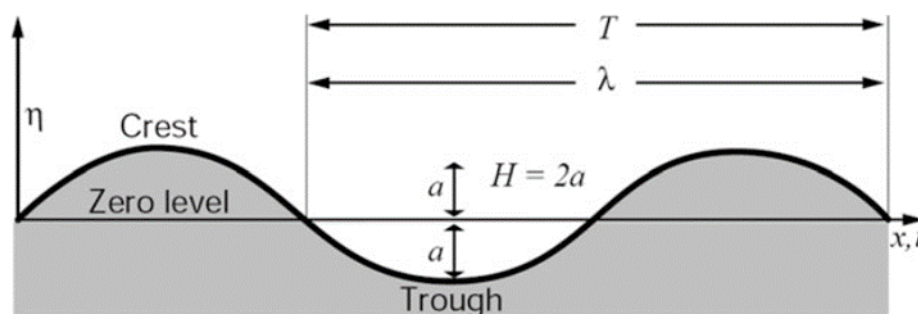
Figure 50.   Parameter definition of a sine wave

The elements that determine the strength of a sea wave are essentially three: wind speed, duration of interaction between wind and sea, wind distance. The relationship between the three causes and the size of the wave generated is directly proportional, i.e. the greater the intensity of the wind, the interaction between wind and sea in terms of time and the surface area affected, the greater the size of the wave produced. Figure 51 shows how waves propagate with wind interaction.
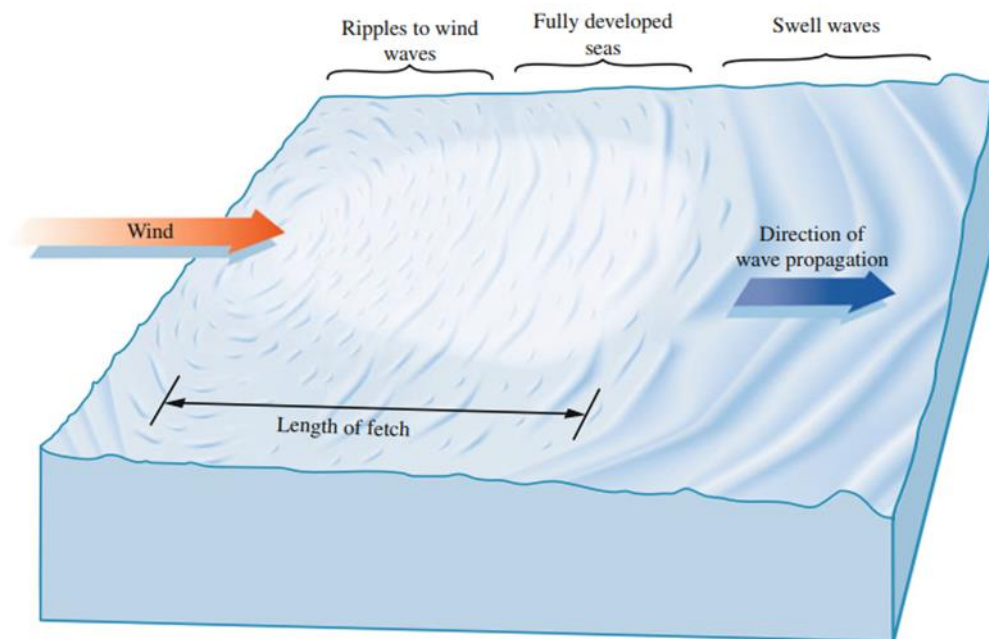
Figure 51.   Wind-sea interaction

A very important parameter that will be used to define the type and behaviour of the wave motion is the ratio between sea depth and wavelength, (z/λ), in fact one can make a subdivision, see figure 52:

- Deep water: when waves are not influenced by the presence of the seabed. This condition occurs when the ratio of sea depth to wavelength is greater than 1/2

- Shallow water: when the seabed significantly influences wave development. This condition occurs when the depth of the sea is less than about 1/20th of the wavelength[77].
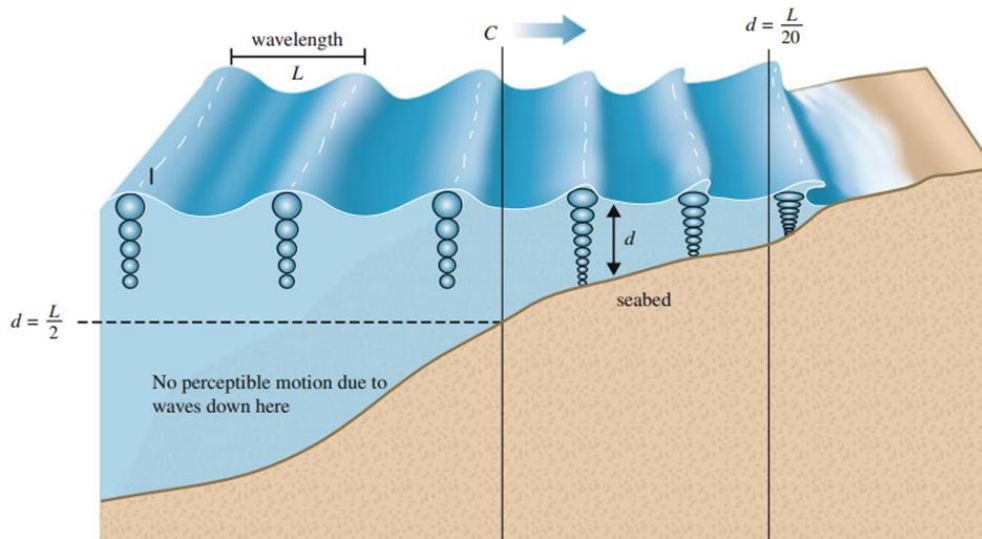
Figure 52.   Particles motion in deep and shallow water

Sea waves can be classified according to their height and wavelength λ, in fact by convention they are distinguished.

- Low waves with a height of less than 2m
- Medium waves with a height between 2 and 4m
- High waves with a height greater than 4m
- Short waves with λ < 100m
- Medium waves with 100m < λ < 200m
- Long waves with λ > 200m.

Two categories of sea state can be distinguished according to the type of waves that develop:

- Wind sea: characterised by a series of waves generated by the wind over a stretch of sea where they are detected. The length of the waves is generally small, and the wave motion presents a very irregular behaviour characterised by a disorderly succession of high and low waves. The formation of smaller waves propagating on the crests of the larger waves can also be observed. In the presence of the wind sea, the sea is rough, and sailing is not recommended

- Long sea: this is characterised by waves coming from even very distant areas. These waves no longer depend on the direct action of the local wind and can propagate for hundreds of kilometres through areas where the wind may even be absent. These types of waves are not dangerous to navigation, only if one is near shallow waters or harbours. It is appropriate to introduce a classification of sea state using the so-called Douglas Scale, shown below in table 6. It is a scale divided into ten degrees, from calm sea to stormy sea, and is often found associated with the scale that takes wind strength into account known as the Beaufort Scale, see table 7[77].

Table 6.   Douglas Scale

Douglas degree	Sea state	Average wave height [m]
0	Calm	0
1	Almost calm	0-0.1
2	Slightly rough	0.1-0.5
3	Rough	0.5-1.25
4	Very rough	1.25-2.5
5	Agitated	2.5-4
6	Very agitated	4-6
7	Coarse	6-9
8	Very coarse	9-14
9	Stormy	Over 14

Table 7.   Beaufort scale

Beaufort degree	Wind state	Wind velocity [km/h]
0	Calm	0
1	Very light wind	1-5
2	Light wind	6-11
3	Breeze	12-19
4	Moderate wind	20-28
5	Stiff wind	29-38

6	Fresh wind	39-49
7	Stronger wind	50-61
8	Moderate storm	62-74
9	Strong storm	75-88
10	Heavy storm	89-102
11	Very heavy storm	105-117
12	Hurricane	>118

The Beaufort Scale has considerable practical value, however it has the limitation that it can only be applied in the open sea, away from the coast, when fetch and wind persistence are not limited by the presence of the coast and land.

In deep water, water particles describe an orbital motion, where the size decreases exponentially with depth, i.e. at a depth that is half the wavelength. The displacements of water particles are about 4% of those at the surface. The orbits tend to decrease with the depth of the seabed (z), because the motion of the water particles will tend to decrease. The description of orbital motion as a function of depth is described in figure 53
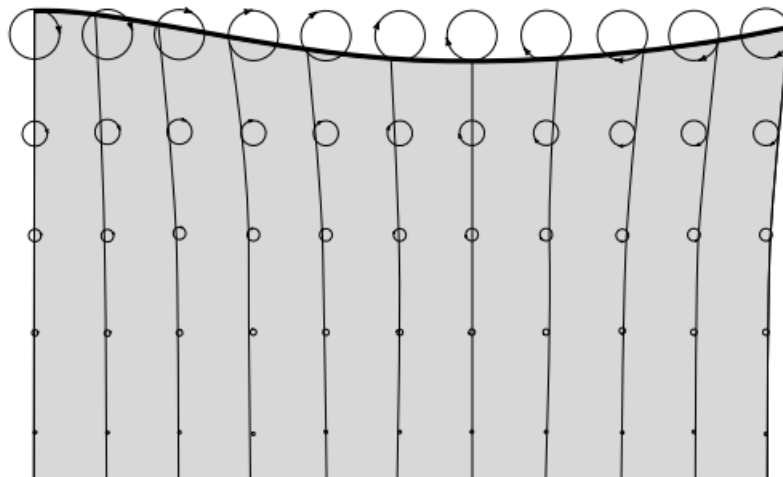
Figure 53.   The description of orbital motion as a function of depth

In shallow water, the seabed begins to make its effects felt, as the particles will feel the friction exerted by the seabed and the various circular trajectories described by

them will tend to flatten out, taking on increasingly elliptical shapes as one moves towards the bottom. This behaviour is described in figure 54.
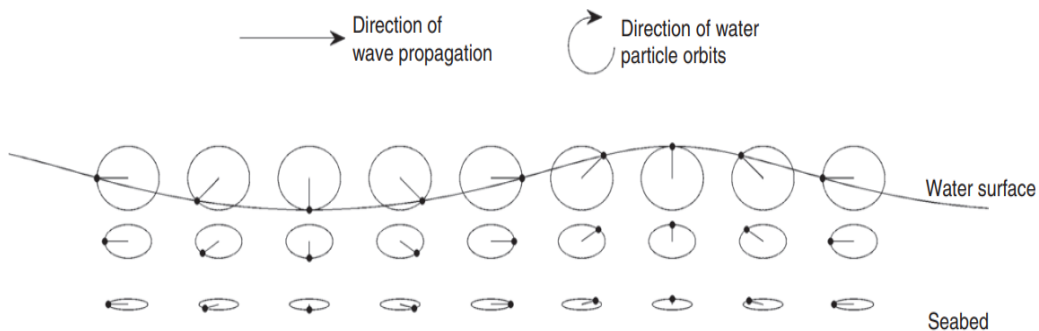
Figure 54.   Orbital motion of particles

Different approaches to studying sea motion exist in the literature. The theories that study this phenomenon are described below.

3.1 Classic theory

The classical theory proposes to find a mathematical model capable of describing the behaviour of a sea wave as it forms under certain assumptions or boundary conditions. The simplest of sea-wave theories is based on a series of approximations, the main one being that the height of sea waves is remarkably small. In calculations, the direct consequence is that this allows only quantities that depend on this height to be considered, neglecting all those terms that depend on, for example, the square or greater powers. For this reason, within the classical theory, we will then speak of linear theory or Airy's Theory[78]. This linear theory is the result of a series of considerable simplifications, but it gives a reliable and reasonable description of the main characteristics of wave motion.

As a direct consequence of the simplifications introduced, at the basis of the linear theory is the possibility of representing sea waves as purely sinusoidal waves, or rather, as a superposition of sinusoidal waves. There is no uniform motion of the sea, but considering the sine wave approximation reasonable, one can represent the

wave motion as a combination of different sinusoids. This can be studied with a periodic analysis by means of a Fourier series development, since it must also be considered that each wave is characterised by different periods and therefore different intervals of time and space.

Focusing on the analysis of the individual wave, in addition to the fundamental characteristics, three others can be identified that are of recurring use, namely:

- The amplitude, A: i.e. the maximum vertical displacement of the water with respect to the mean sea level (which coincides with the free surface). It is usually H/2, where H is the full height excursion between a crest and a belly

- The frequency f: represents the number of complete oscillations made by the wave in the unit of time. It is represented by the inverse of the period T

- The phase velocity c : given by the ratio of the wavelength to the period T.

The mathematical formula that best represents the single one-dimensional sine wave migrating forward according to the superposition trend is as follows, see equation 30.

$$\eta(x,t) = A\,sin\left(\frac{2\pi}{T}t - \frac{2\pi}{\lambda}x\right) \tag{30}$$

Where A represents the amplitude, t the instant of time at which the measurement takes place and x represents the measurement position.

The following equation 31 shows the dispersion equation derived from linearised equations of motion.

$$\omega^2 = gk\,tanh(kz_w) \tag{31}$$

Where ω is the angular frequency and k is the ratio of space to wavelength.

3.1.1 Airy's theory

Airy's theory is of fundamental importance as it describes wave behaviour in a simplified manner. It lends itself quite well to describing real wave behaviour under certain fundamental assumptions:

- Small wave height relative to wavelength and depth. This applies in practice for H/λ < 0.01

- Uniform sea depth (smooth, impermeable seabed), i.e. the seabed has no effect on motion

- Homogeneous, incompressible, and non-viscous fluid

- The Coriolis Force is neglected

- Surface tension is neglected

- The single wave is described by sinusoidal development

With these assumptions, the following equation 32 shows the phase velocity.

$$c = \sqrt{\frac{g \cdot \lambda}{2\pi} \cdot tanh\left(2\pi \cdot \frac{z}{\lambda}\right)} \tag{32}$$

The hyperbolic tangent can be expressed as the equation 33

$$tanh\, x = \frac{e^x - e^{-x}}{e^x + e^{-x}} \tag{33}$$

If the argument x of the hyperbolic tangent function goes to zero, then the function itself goes to the argument, the following remarkable limit being verified, see equation 34.

$$\lim_{x \to 0} \frac{tanh\, x}{x} = 1 \tag{34}$$

If the argument is greater than 1 then the function will tend to 1. If we are in deep water conditions with a z/λ ratio > 0.5 then the hyperbolic tangent will tend to 1 and thus the phase velocity will be equal to equation 35.

$$c = \sqrt{\frac{g \cdot \lambda}{2\pi}} \tag{35}$$

If we are in low water conditions (z < 1/20 λ), the phase velocity can be simplified appropriately and expressed as following equation 36.

$$c = \sqrt{g \cdot z} \tag{36}$$

Up to now, the set of waves in the sea has been schematised as a sine wave, made up of several waves, but examining the single wave that moves.

Another concept is introduced, namely the group speed v_g, understood as the speed resulting from the combination of all waves with a sinusoidal pattern but with slightly different period and characteristics. This group speed is shown in equation 37.

$$v_g = \frac{d\omega}{dk} \tag{37}$$

By explicating ω with the dispersion relation, one can express the angular frequency in shallow and deep water. In particular, it will be seen that from the solution of the dispersion equation (31) there are two possible solutions, see equation 38.

$$\omega^2 = \begin{cases} gk & se \ \frac{z_w}{\lambda} > \frac{1}{2} \ (deep \ water) \\ gk^2 z_w & se \ \frac{z_w}{\lambda} < \frac{1}{20} \ (shallow \ water) \end{cases} \tag{38}$$

Once the value of ω^2 has been identified, the general expression of the group velocity can be derived from relation (31) and is shown in equation 39.

$$v_g = \frac{1}{2} v_p \left(1 + \frac{2kz_w}{sinh \ 2kz_w}\right) \tag{39}$$

As in the previous case, two forms of group velocity can be distinguished, depending on whether one is in deep or shallow water, see equation 40.

$$v_g = \begin{cases} v_p & se \ \frac{z_w}{\lambda} < \frac{1}{20} \ (deep \ water) \\ \frac{1}{2} v_p & se \ \frac{z_w}{\lambda} > \frac{1}{2} \ (shallow \ water) \end{cases} \tag{40}$$

To better understand the characteristics of a group of waves, we will analyse the simplest case resulting from the superposition of two sine waves, characterised by the same amplitude and slightly different frequency and wave number, see figure 55.
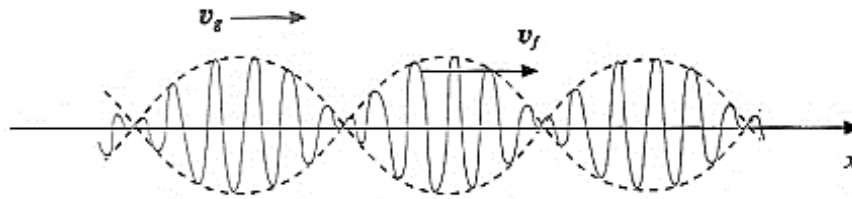
Figure 55.   Wave group profile

Starting from the knowledge of the phase velocity expressions, equating equation (35) with the definition of celerity, in high water conditions, knowing the period, the wavelength (λ) and phase velocity (c) can be determined using the following expressions 41, 42.

$$\lambda = 1.56\, T^2 \text{[m]} \tag{41}$$

$$\lambda = 1.56\, T \text{ [m/s]} \tag{42}$$

In deep water, the orbits of the particles will be perfectly circular along the entire water column, what varies will be the diameter of the orbits and will be decreasing starting from the surface of the water down to the bottom. The law that gives the radius of the orbit as a function of wavelength and depth is shown in equation 42a.

$$r = a \cdot e^{-\frac{2\pi}{\lambda}z} \tag{42a}$$

Where a = H/2 is the amplitude of the wave at the surface.

The consequence of this law is that the radius decreases with depth, but as the speed increases, the speed of the water masses also decreases. From the following figure 56, the direction of the wave is shown, the length of the wave and therefore also the interval in which the wave is to be reproduced in full.
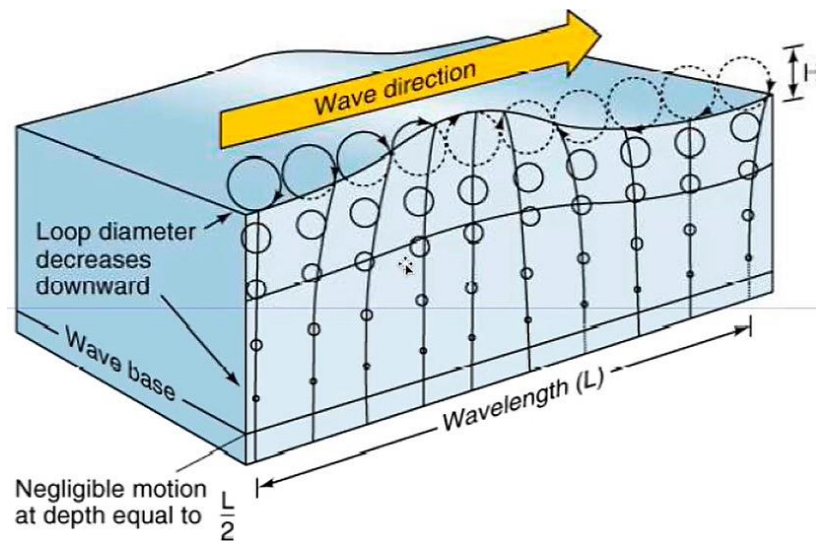
Figure 56.   Wave orbits in deep water

In conclusion, it is not possible to apply Airy's Theory in all real-life cases, although to a first approximation it gives useful information for describing and quantifying the phenomenon, except in the case of shallow water. In nature, we rarely observe a wave propagating in a regular manner, like a sine wave. What is actually observed is the superposition of a large number of waves, all with different characteristics in different directions. If one were to measure the displacements of a floating device placed on the surface of the sea, what could be observed would be a pattern like the one depicted in the figure 57.

Figure 57.   Example of a real waveform recording

Conceiving a sea state like the one in the figure above, understood as the superposition of several sinusoids, allows the use of spectral and Fourier analysis to describe the sea surface. Unfortunately, there is also an element of randomness and a statistical approach to the problem must also be introduced.

3.1.2 Stokes theory

In addition to the Airy approach, there are other far more complex models. Among these deserves attention the Stokes Theory according to which the wave profile is "trochoidal", this would be from the addition to the surface Airy wave, of a term with a period and wavelength halved and an amplitude related to the amplitude of the Airy wave and its wavelength. The following equation 43 describes the stokes theory.

$$\eta_{II} = a \cdot cos2\pi \cdot \left(\frac{x}{\lambda} - \frac{t}{T}\right) + \frac{2\pi}{\lambda} \cdot \frac{a^2}{2} \cdot cos4\pi \cdot \left(\frac{x}{\lambda} - \frac{t}{T}\right) \qquad (43)$$

The Stokes wave is a non-linear, periodic surface wave on a fluid layer of constant average depth. The theory has practical use for waves in intermediate and deep waters and is used in on-shore and off-shore constructions to determine wave kinematics.

3.2 Statistical Analysis

Wind-generated waves have a highly irregular behaviour and, according to linear theory, can be considered as the result of the superposition of many sine and trochoidal waves having heights, lengths, periods and directions that do not perfectly coincide with each other. To address the following problem, an average value of these quantities is usually found.

This approach has as its mathematical solution the use of a Fourier series development, according to which each function can be represented over a finite interval as the sum of an infinite series of sines and cosines, with different frequencies, multiplied by constant coefficients. For this reason, a particular record is assumed to represent a statistical sample (or statistical distribution) of the possible sea states in the area under consideration.

Under these conditions one is able to go and estimate, in probabilistic terms, the mean values of certain parameters such as, for example, mean wave height, significant wave height and mean wave period. Knowing these parameters, one

indirectly derives the speed and is thus able to go and determine how much the characteristic energy of the wave is worth. What is expected, then, is that the statistical properties of several successive recordings are similar assuming that the sea state is stationary, or rather that it statistically does not change over time. There are two possible approaches to estimating these values:

- Statistical temporal analysis: it directly estimates the mean values from statistical analysis of the signal seen as a temporal sequence of wave data.

- Spectral statistical analysis of the signal: a frequency analysis of the signals based on Fourier series development is followed.

3.2.1 Statistical temporal analysis

The characteristic parameters of the waves are listed below.

- Average wave height (H_m): can be calculated as the sum of the individual wave heights divided by the total number of waves recorded in a time interval, see equation 44

$$H_m = \frac{1}{N}\sum_{i=1}^{N} H_i \qquad (44)$$

- Significant height H_s (or H1/3): defined as the average of one third of the highest waves recorded during a given time interval. This parameter is of considerable practical importance in applications relating to the determination of energy potential, see equation 45. It is not possible to refer only to the average height, the height of the lowest waves would have too significant a weight leading to an underestimation of the wave height, at the same time if one were to refer to the highest waves one would have an overestimation of the wave height

$$H_{1/3} = \frac{1}{N/3}\sum_{j=1}^{N/3} H_j \qquad (45)$$

- The medium period is defined in following equation 46.

$$T_m = \frac{1}{N}\sum_{i=1}^{N} T_i \qquad (46)$$

- The significant wave period $T1/3$, in the same way as the significant height, is defined as the average period of one third of the highest waves and is expressed in equation 47.

$$T_{1/3} = \frac{1}{N/3}\sum_{j=1}^{N/3} T_j \tag{47}$$

In addition to the simple average value, it is also possible to calculate the probability that a wave of a given height will occur. In this case, the waves recorded within a given time are first divided according to their height into a number of regular intervals, then the number of waves belonging to each interval is counted and the sums obtained are divided by the total number of waves recorded during the time interval.

In this way, one is able to calculate the frequencies or probability densities for each wave category. Adding up the probabilities of the individual intervals, we obtain the cumulative probability function, which represents the probability that a wave of a height less than or equal to a certain value we have identified will occur.

Between characteristic height and significant height, the following empirical relationships called Cartwright (equation 48) and Nordenstrom (equation 49) respectively apply.

$$\overline{H}_{1/3} = 1.11 H_c \tag{48}$$

$$\overline{H}_{1/3} = 1.68 H_c^{0.75} \tag{49}$$

3.2.2 Spectral statistical analysis

Surface waves can be approximated with a Fourier series, i.e. as a sum of individual sinusoidal components each characterised by a different amplitude, wave number and frequency. The typical form of any record of the profile of an irregular wave system suggests representing the record of duration T by means of a Fourier series, as shown in equation 50.

$$\eta(t) \sum_{j=1}^{N} a_j \cos(\omega_j t - \delta_j) \tag{50}$$

Where:

- a_j is the amplitude of the j-th component
- ω_j is the angular frequency
- δ_j s the phase of the j-th wave in the observation section $x = 0$

It can be shown that the square of the standard deviation $\sigma\eta$ of the elevation is proportional to the sum of the squares of aj, see equation 51.

$$\sigma^2 = \frac{1}{2} \sum_{j=1}^{N} a_j^2 \tag{51}$$

The wave energy distribution, called the frequency spectrum, expressed as a function of frequency, can be defined by the following relationship, see equation 52.

$$E(\omega_j)(\Delta\omega_j) = \frac{1}{2} a_j^2 \tag{52}$$

Combining the two relationships results in the expression of the continuous energy spectrum, as shown in equation 53.

$$\sigma^2 = E(\omega) = \int_0^{\infty} E(\omega)d\omega \tag{53}$$

Consider two spectra relating to two different types of irregular sea. These are two particular processes that go by the name of narrow band process and wide band process, see figure 58.
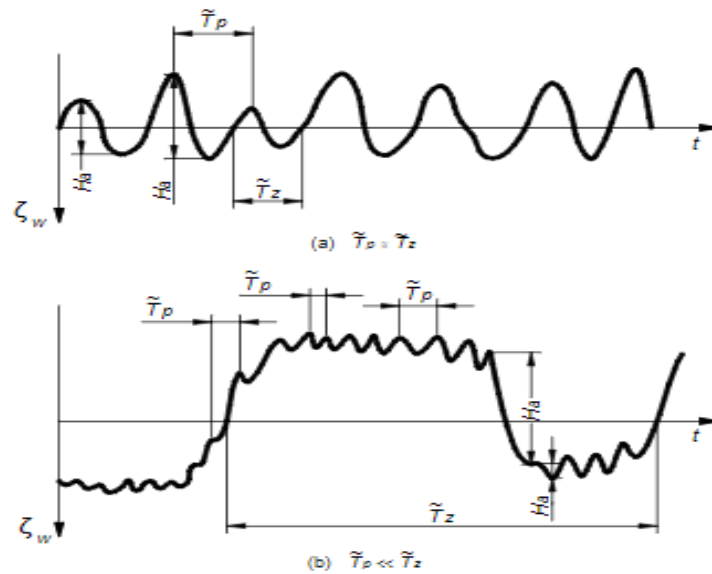
Figure 58. Particular time series: top narrowband process; bottom wideband process

The narrowband time series can be thought of as a harmonic component of variable amplitude. The characteristics of the spectrum show that the wave energy is concentrated only in a rather narrow band of frequencies, while little energy competes with the components at other frequencies. A characteristic property of this time series lies in the fact that each crest is almost always followed, in order, by a descending zero crossing, a leading zero crossing, an ascending zero crossing, another crest.

The broadband process contains energy over a wider band of frequencies. In this case, there can be many ridges and wires that are not immediately followed by a zero-crossing. The average period between peaks is therefore much shorter than the average zero-crossing period and there are many ridges below and many cables above the reference zero level.

ε is defined as bandwidth parameter and is defined by the following equation 54.

$$\varepsilon = \sqrt{1 - \frac{T_p^2}{T_z^2}} \tag{54}$$

The following figure 59 shows the different processes related to ε.
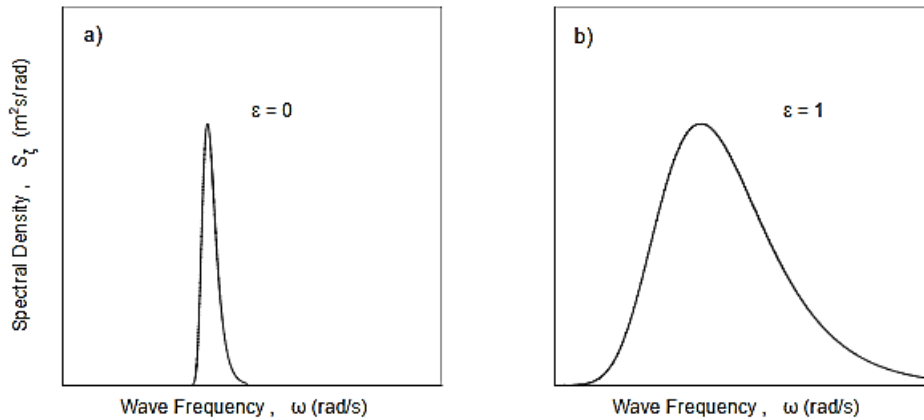
Figure 59.   **Comparison of a narrowband (a) and wideband process (b)**

It has been shown (Cartwright and Lounguet-Higgins, 1956) that the significant wave height of an irregular sea can be related to the area subtended by the energy spectrum, see equation 55:

$$H_{1/3} = 4{,}00 \cdot \sqrt{m_0 \cdot \left(1 - \frac{\varepsilon^2}{2}\right)} \tag{55}$$

For a narrow-band process (ε=0), equation 56 applies:

$$H_{1/3} = 4{,}00 \cdot \sqrt{m_0} \tag{56}$$

A broadband process, (ε=1) Equation 57 applies:

$$H_{1/3} = 2{,}83 \cdot \sqrt{m_0} \tag{57}$$

From an application point of view, for an ocean wave system it is often convenient to assume ε to be zero and then estimate the significant height with equation (56) after performing the integration of the energy spectrum.

3.3 Wave energy

Sea waves are associated with forms of energy transport. The total energy associated with the wave is partly kinetic energy, due to the motion of the water particles, and partly the potential difference or potential energy associated with the vertical displacement of the water particles in their gravitational field. In the case

of gravity waves, a displacement of water particles relative to the mean value of the sea generates a pull force due to the gravitational field that tends to bring them back to the so-called equilibrium position. It will be shown that the average kinetic energy per unit area, due to the motion of water particles, is equal to the average potential energy per unit area. Ultimately, we have that the average total energy per unit area associated with a sine wave of given amplitude is given by the resultant of the combination of these two forms of energy. Therefore, the total energy is given by equation 58:

$$E = E_c + E_p = \frac{1}{4}g\rho a^2\lambda + \frac{1}{4}g\rho a^2\lambda = \frac{1}{2}g\rho a^2\lambda \tag{58}$$

If a = H/2 and dividing by λ gives the average energy per unit area, see equation 59.

$$E = \frac{1}{8}g\rho H^2 \tag{59}$$

By finally integrating this expression, the total energy associated with the entire spectrum can be derived, see equation 60:

$$E = \int_0^\infty E(\lambda)d\lambda \tag{60}$$

The power that can be harnessed by a wave is calculated by considering W/m, i.e. the power produced by one metre of "captured" wave. At this point, to change from energy to power, equation 59 is multiplied by the group speed, see equation 61

$$P = \frac{1}{8}g\rho H^2 v_g \tag{61}$$

Explicitly the group speed in equation 62:

$$v_g = \frac{v_p}{2} = \frac{1}{2}\frac{\lambda}{T} = \frac{1}{2}\sqrt{\frac{g}{k}} = \frac{1}{2}\sqrt{\frac{g\lambda}{2\pi}} = \frac{1}{2}\frac{gT}{2\pi} \tag{62}$$

In order to know how much power is really worth, it is necessary, in addition to the value of the group speed, to specify the height, the expression for which is given in equation 63 for deep water:

$$H = H_{1/3}/\sqrt{2} \tag{63}$$

Substituting expression 61 gives the power relative to the significant wave height in deep water, see equation 64:

$$P = \frac{1}{64\pi} \rho g^2 H_s^2 T_e \tag{64}$$

It can be seen from this relationship that the power is directly related to the specific wave height and period.

In order to determine the energy potential of a stretch of sea, the various quantities must be grouped together in order to identify which phenomena are useful for this typology, i.e. to see how often a given event can occur in a given stretch of sea.

To calculate the maximum extractable energy, it is necessary to apply the following equation for all the waves characterising the motion of the sea and then introduce the various efficiencies, see equation 65:

$$E_{sw} = d_c \sum_{i=1}^{n} \sum_{j=1}^{m} \frac{\rho g^2}{64\pi} H_{s,i}^2 T_{e,j} \eta_{hy}(H_{s,i}, T_{e,j}) \eta_e(H_{s,i}, T_{e,j}) h_{i,j} \tag{65}$$

Where:

- η_{hy}, hydraulic efficiency
- η_e, electrical efficiency
- $H_{s,i}$, is the i-th significant height class
- $T_{e,j}$, is the j-th energy period class
- d_c, is the equivalent diameter of the system that exploits energy from the wave
- $h_{i,j}$, the number of hours in which the condition is measured ($H_{s,i}$, $T_{e,j}$).

An easy way to report data on measured sea states is the "Scatter Table", which reports the equivalent hours in which a specific condition is measured in terms of H_s and T_e or the corresponding annual energy availability. An example of a scatter table is shown in figure 60.
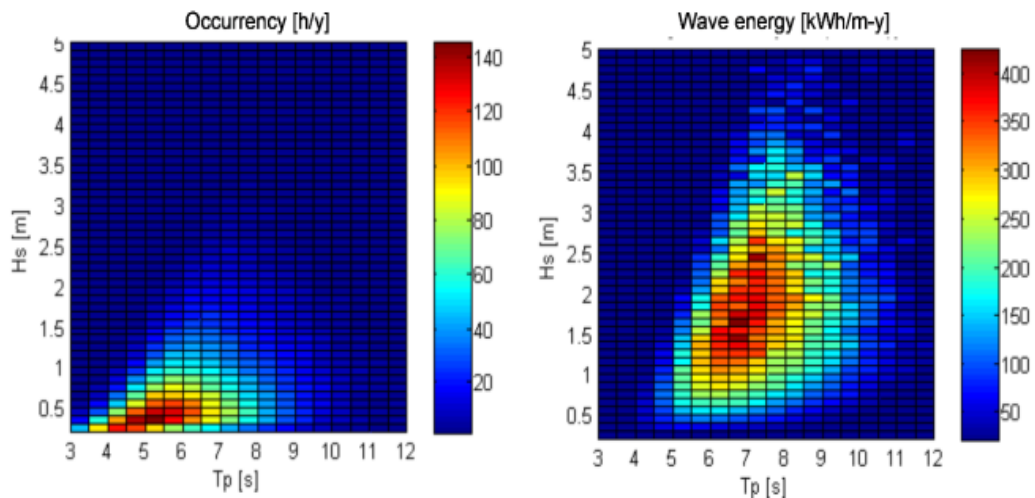
Figure 60. Scatter Table of the island of Lampedusa

3.4 Surf area

In shallow waters, a phenomenon known as sea wave refraction occurs, which leads to a change in the height and direction of propagation of the water mass, which will become substantially parallel to the shoreline bathymetry (regardless of offshore development). Another phenomenon is the possible breaking of the wave in the breakers or surf area, which may reach a greater height than it had in the open sea and disperse all its energy. The formation of breakers occurs when, at the same depth z_w of the sea, the valleys advance more slowly than the crests, then the wave deforms until it breaks as the depth decreases. The figure 61 shows the difference between the waves near the coastline and far the coastline.
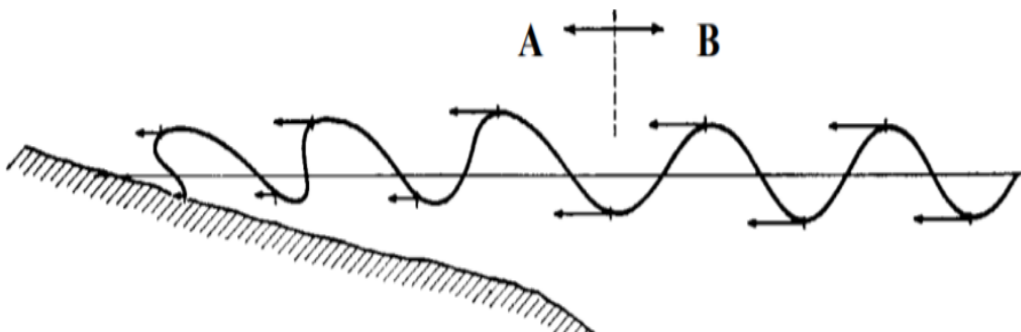
Figure 61. Wave evolution as it near the coast

The waves begin to change from the moment the depth z_w of the sea area becomes less than $\lambda/2$, it is at this moment that the waves begin to feel the effect of the bottom, until they lose their character of oscillatory motion. Bottom friction changes the geometry of the particles motion towards an elliptical trajectory, decreasing the vertical component as the bottom decreases; in shallow water, i.e. with $z_w < \lambda/20$, the particles follow practically straight and almost horizontal trajectories. The significant parameters of the wave change as follows:

- The period (T) does not change
- The velocity (c) decreases
- The length (λ) decreases
- The height (H) increases.

The limit value beyond which the wave breaks is $H/\lambda = 1/7$.

The orthogonals to the ridges, are equidistant on great depths and remain parallel, on shallower depths, due to refraction, they may curve and diverge or converge, moving away from or closer to each other. Since in general the energy contained in the section of a wave between two determined orthogonals can be considered constant during propagation, an increase in the distances between the orthogonals will correspond to a decrease in the average specific energy and therefore to a decrease in the wave height H. Instead, a decrease in the distance between the orthogonals will correspond to an increase in specific energy and thus an increase in the wave height H. The following figure 62 shows the developments of the orthogonals due to the seabed variation.
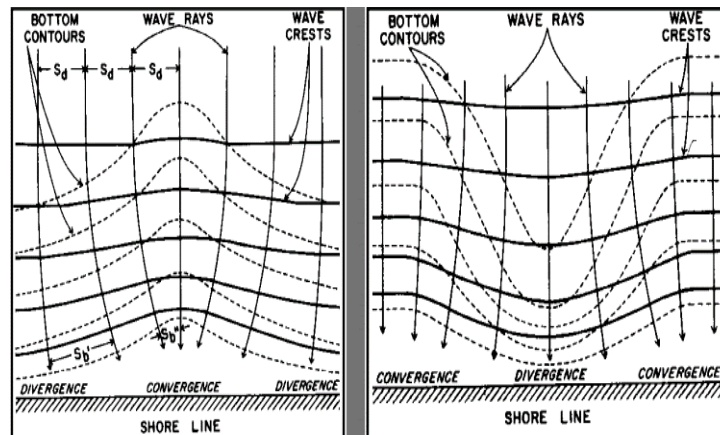
Figure 62.   Development of wave orthogonals as a function of seabed characteristics

4. Case studies

In this section of the thesis will be described the experimental tests carried out on the generators designed and built in marine technology laboratory of the engineering department of the university of Palermo. These are a power take-off for on-shore installation, a linear generator for off-shore installation and an ironless linear generator with the same characteristics as the previous one, but without metal components.

4.1 On shore Power take off

The case study is represented by a mechanical system consisting of a transmission to transmit a unidirectional rotational motion from a bidirectional motion controlled by a rod. The mechanical pilot project was developed in the Marine Technology Laboratory at the University of Palermo.

4.1.1 PTO working principle.

The main approach on which the PhD course was based was to perfect an existing prototype. The device prior to the technical improvement made is shown in figure 63.

Figure 63.   PTO before the technical improvements

The working conditions are shown in the following figure 64[79]
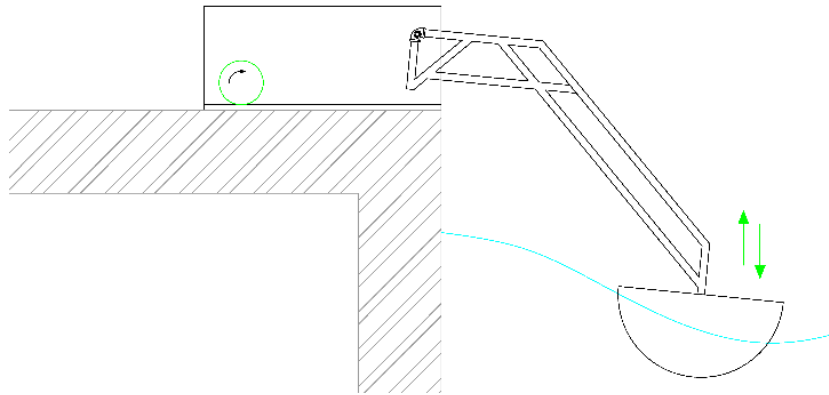
Figure 64. PTO idea of working conditions

The figure 64 shows a mechanical motion converter that could be installed in the harbours for the exploitation of sea wave in order to produce electrical energy and at the same time protect the piers. The idea is a floating buoy that is used to collect the mechanical energy of waves and produce a rotation around the main hinge of the device. The mechanical conversion is operated inside a gear box, that can be installed on the breakwaters. On the output axis, a commercial generator can be installed in order to produce electricity.

At an early stage, the PTO had a wooden frame and a sheet metal carriage. The lack of solidity resulted in low mechanical strength, especially in shear and torsion. The transmission system was unbalanced, and it was precisely this that led to the emergence of a system of tensions that levered on the axes of rotation. The forces unloaded on the frame, contributed to its torsion. The system consists in: a wooden support structure, a rod tied to a steel transmission carriage, a transmission system consisting of chains and pulleys, and finally a rotating generator. The carriage is constrained to move along its guides, so it has a start and an end stop. Holes were drilled in this structure to mechanically connect it to the connecting rod and drive chains. The bi-directional linear motion of the carriage is effectively transmitted through the chains to the connecting rods. This configuration is very efficient, compared to the one initially planned, because the chains are not the site of shear

forces that would put them under strain on the main rotating axles. The transmission carriage is shown in figure 65.
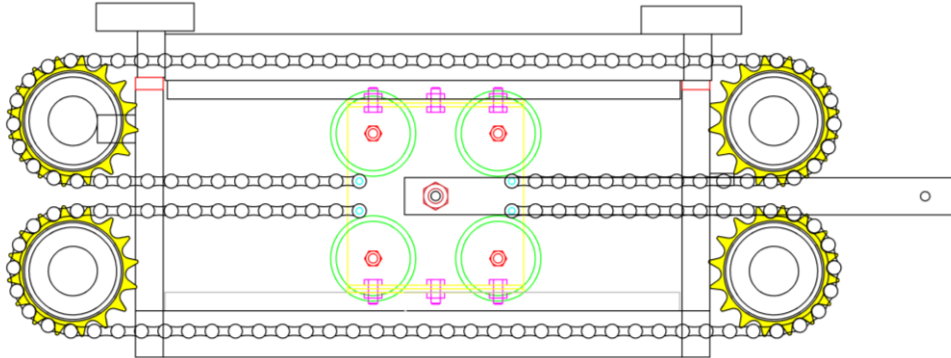
Figure 65. Transmission carriage

The chains are connected to four connecting rods whose rotating axes have been placed on four bearings, which in turn are installed inside the two panels containing the system. Despite the presence of four connecting rods, only two of them are responsible for transmitting torque. The connecting rod connected to the carriage is also connected to a rod, which is constrained to rotate around a hinge. As can be seen in Figure 66, by giving the bar input a certain rotation, around the hinge at B, the carriage moves, transferring torque to one of the four pulleys.
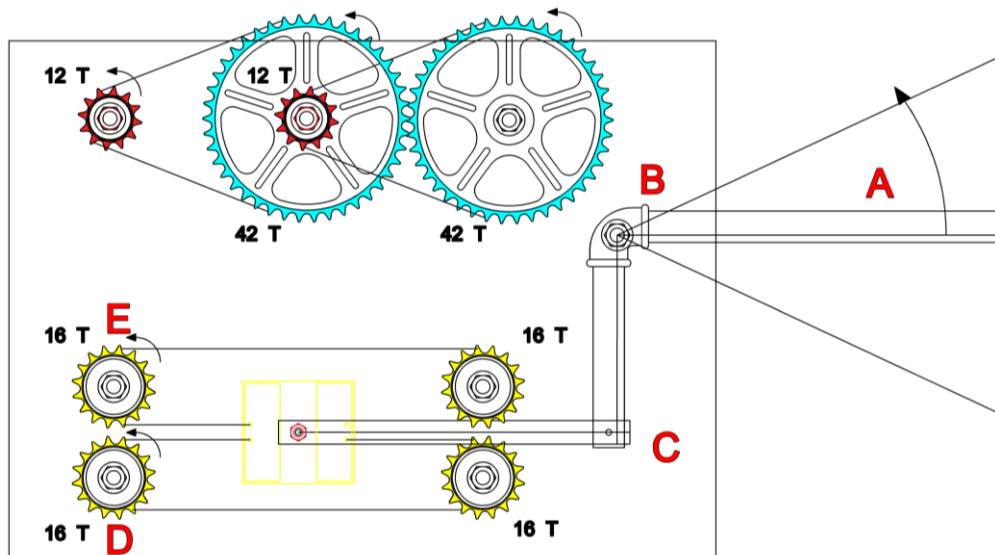
Figure 66. Internal view of the prototype of mechanical motion converter

Thus, the drive wheels are mounted, with the same direction of rotation, in such a way that torque is transferred during two periods of carriage movement. The pulley in D transfers torque when the rod rotates clockwise, the pulley in E transfers torque when the rod rotates counter clockwise. The torques generated by the two drive pulleys are transferred externally from two 28-tooth sprockets to two 12-tooth sprockets, which are installed on the same axis of rotation, via a chain connection. On the other axles, which also appear in the interior view of the prototype, a series of 42-tooth wheels and 12-tooth wheels are mounted with the aim of amplifying the angular speed to reach the optimum operating speed range for the generator. A flywheel has also been added before the alternator to stabilise the angular speed and at the same time regularise the power generation. See figures 67 and 68.
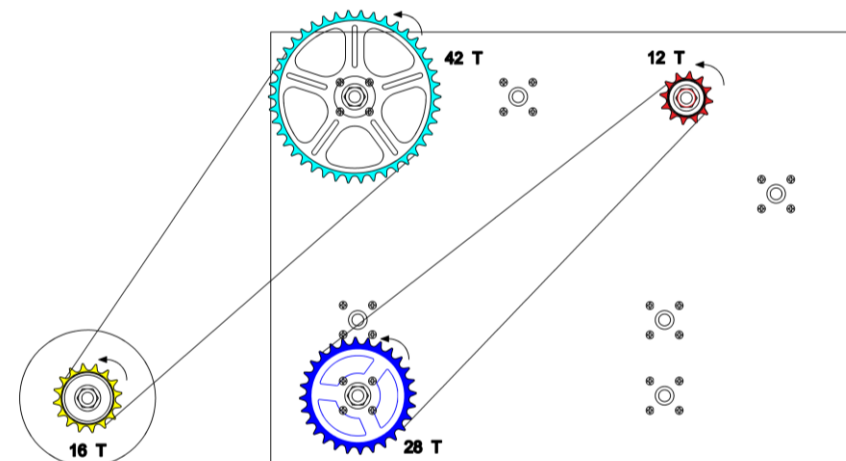
Figure 67.   Right view of the prototype
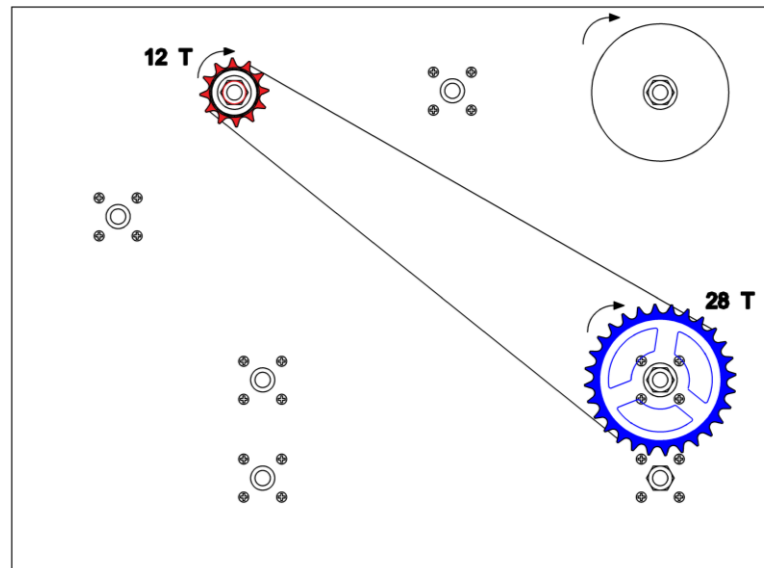
Figure 68.   Left view of the prototype

The heart of the PTO is the chassis and drive bogie. The latter is appropriately constrained to move only along the axis of the rails. The chassis body is made entirely of black steel with a 25 mm wide and 15 mm high, hollow, and rectangular section 2 mm thick. The rails are welded on the inside of the body, both upper and lower. The carriage is shown in figure 69.
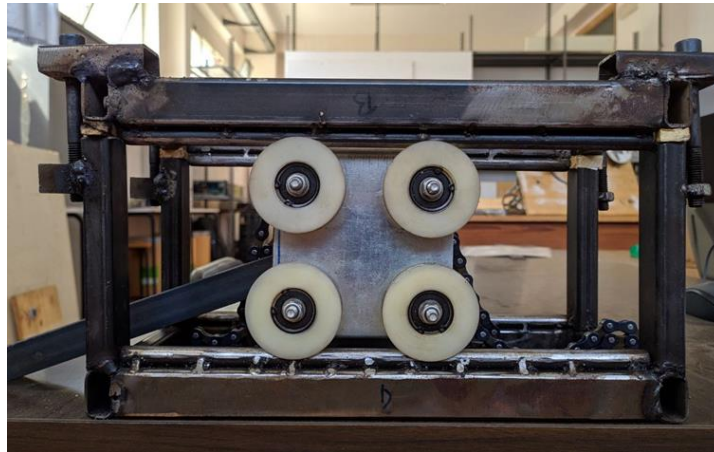
Figure 69.   Lateral view of the carriage

Analysing the kinematic mechanism, it is possible to derive the angular rotation exiting the system, following a series of steps which will be reported below.

The system was designed and set up in such a way that the horizontal connecting rod is parallel to the external movement rod and the carriage is arranged in the centreline of the frame within which it is constrained. In this discussion it is assumed that the x-axis originates at the centre of the hinge B, and the clockwise rotation of the manoeuvring rod will be considered positive.

It is possible to describe the position of the carriage as a function of the angle of rotation impressed ϑ_{in} by solving this system of equations from 66 to 68:

$$l' = \sqrt{l^2 - \Delta y^2} \tag{66}$$

$$\Delta y = b - b \, cos\vartheta_{in} \tag{67}$$

$$x(\vartheta_{in}) = l' + b \, sen\vartheta_{in} \tag{68}$$

Solving the system leads to equation 69.

$$x(\vartheta_{in}) = \sqrt{l^2 - b^2 (1 - cos\vartheta_{in})^2} + b \, sen\vartheta_{in} \tag{69}$$

Where the terms l and b are respectively the length of the horizontal connecting rod connected to the carriage and the length of the vertical section of the rod. Differentiating equation 69 gives equation 70.

$$\frac{dx}{d\vartheta_{in}} = -\frac{b^2 \, sen\vartheta_{in} \, (1 - cos\vartheta_{in})}{\sqrt{l^2 - b^2 (1 - cos\vartheta_{in})^2}} + b \, cos\vartheta_{in} \tag{70}$$

If ϑ_{in} is zero, the equation 70 is equal to b. With this approximation occur a 5% error. Under the assumption of small displacement variations, we can approximate Eq. 69 as equation 71:

$$x(\vartheta_{in}) \approx b \, \vartheta_{in} \tag{71}$$

It is possible to calculate the rotation of the first positioned pulley with equation 72:

$$\vartheta_1 \approx \vartheta_{in} \frac{b}{r_1} \tag{72}$$

with r_1 radius of the pulley positioned at D.

On the second axis, rotation is unidirectional since the two wheels in D and E transmit the same direction of rotation. The angle of rotation of this axis is shown in equation 73:

$$\vartheta_2 \approx |\vartheta_1| k_{2,1} \approx |\vartheta_{in}| \frac{b}{r_1} \, k_{2,1} \tag{73}$$

The term $k_{2,1}$ is the transmission ratio between axis 2 and axis 1.

As has already been expressed, the other sprockets are responsible for multiplying the number of revolutions per minute, hence the angular speed. On the last axis, output of the system, we obtain equation 74:

$$\vartheta_4 \approx |\vartheta_{in}| \frac{b}{r_1} \, k_{2,1} k_{3,2} k_{4,3} \tag{74}$$

In terms of angular velocity, the output axis collects kinetic energy by means of the flywheel, see equation 75.

$$\begin{cases} if \; \omega_3 \, k_{4,3} < \omega_4 \; \rightarrow \left(I_{vol} + I_a \frac{1}{k_a^2} \right) \frac{d\omega_4}{dt} = -\tau_e - \tau_f \\ \quad else \; \rightarrow \omega_4(t) = \omega_3 \, k_{4,3} \, (t) = \Upsilon_0 |\omega_{in}(t)| \end{cases} \tag{75}$$

In fact, thanks to the freewheel, the output axis rotates at the angular speed set by the mechanical converter. Vice versa, if the angular speed produced by the rotation of the input bar is lower than the instantaneous angular speed of output axis, the output wheel does not receive torque from the previous axis, and consequently reduces its regime removing kinetic energy from the flywheel.

In the following figure 70, is shown the PTO after improvements.

Figure 70.   PTO after improvements

4.1.2 Experimental tests

Mechanical tests performed in the marine technology laboratory were used to characterise the operation of the PTO under varying stresses. Tests in the laboratory were carried out by powering an alternator with a rated power of 250W (output), a rated voltage of 24V, direct current, and a rated current of 14A. The nominal operating speed is 2550 rpm. The control of the experiments was carried out using Ardunio cards. The wiring of the measuring system is shown in figure 71.
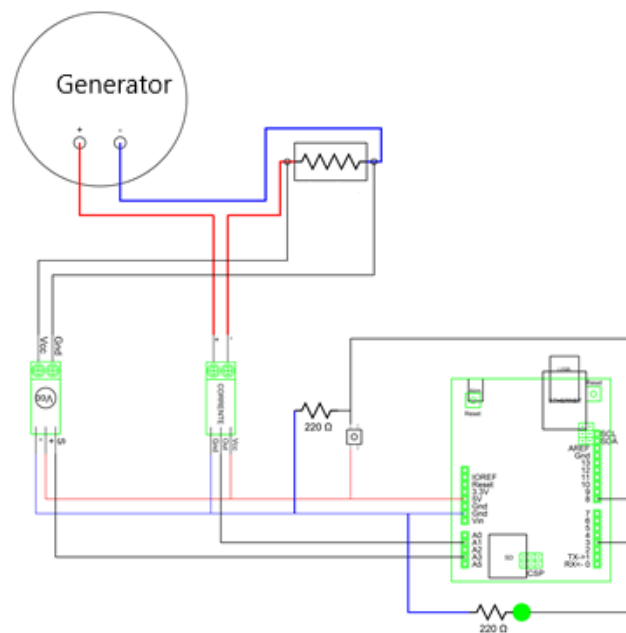
Figure 71.   Wiring of Arduino system

After wiring up the measurement system, the next step was to define the operating conditions for the tests. These were carried out for different values of the resistance of the bench rheostat, by varying the mechanical load supplied. There are three values of user resistance, 13 Ω, 8 Ω, 2 Ω, and for each condition the tests were carried out with weights, applied to the end of the bar, of 2.5 kg, 5 kg and 10 kg respectively. Another test carried out is the no-load test. In addition, each test was repeated three times in order to have a minimum of feedback with the measurements made, and therefore to understand if these were consistent.

4.1.2.1 No load-test

To perform the no-load test, the generator and rheostat terminals were disconnected and connected to the Arduino's voltage reading sensor. The voltages obtained, for given weight load test, will be the maximum because there is not active power generation, so there is no resistant torque opposing the driving torque. The equation 76 shows the drive torque.

$$C_{in} = mg\ l_b \cos \vartheta \tag{76}$$

Where:

- mg is the weight force.
- l_b is the distance between the centre of mass and the point of application of the force.
- ϑ is the angle between the rod and the direction of the force.

The graph shown in figure 72 shows the trend in voltages in the three measurements carried out with no load and with a weight of 5 kg.
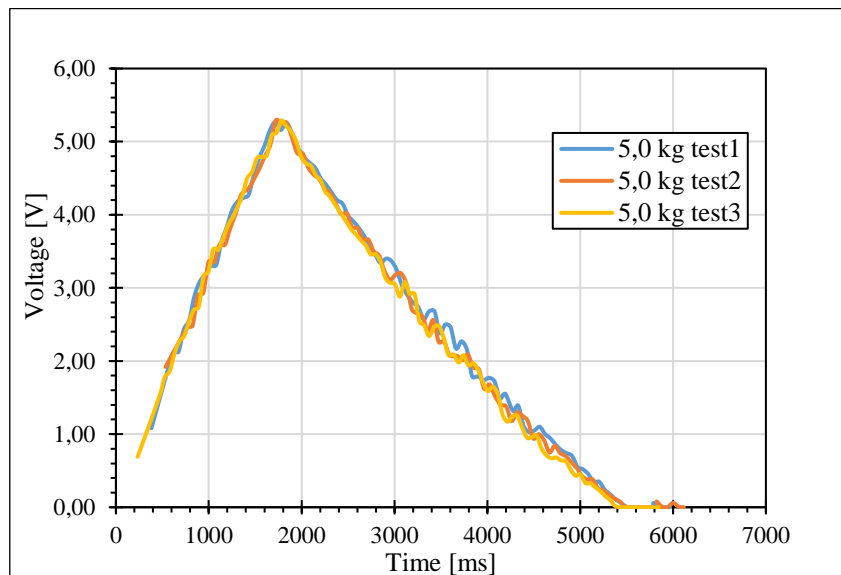
Figure 72. Voltage: no load test with 5kg weight

4.1.2.2 Load test with 13 Ω resistance

Load tests were carried out by connecting the rheostat to the measuring system. The graphs shown in the following figures referred to the tests carried out varying the weight with the rheostat locked to 13 Ω.
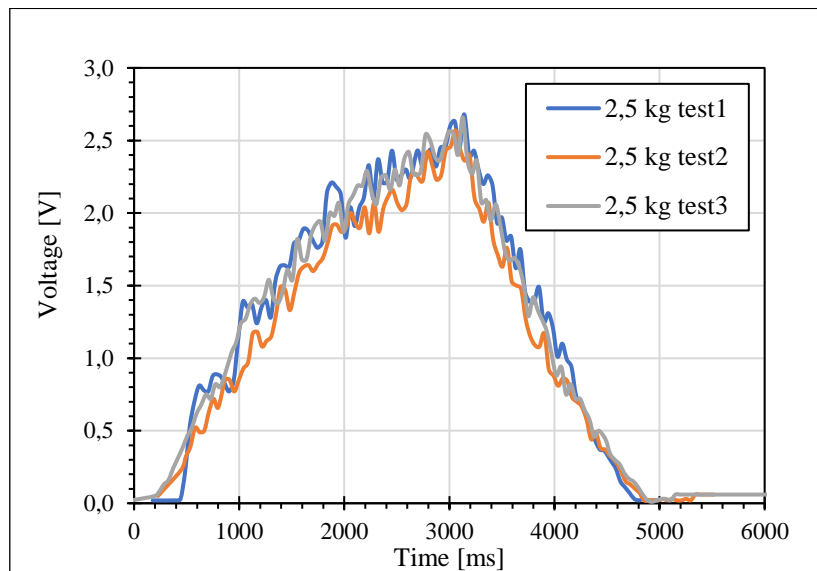
Figure 73.   Voltage: 13 Ω load test with 2,5 kg weight

Figure 74.   Current: 13 Ω load test with 2,5 kg weight

Figure 75.   Voltage: 13 Ω load test with 5 kg weight
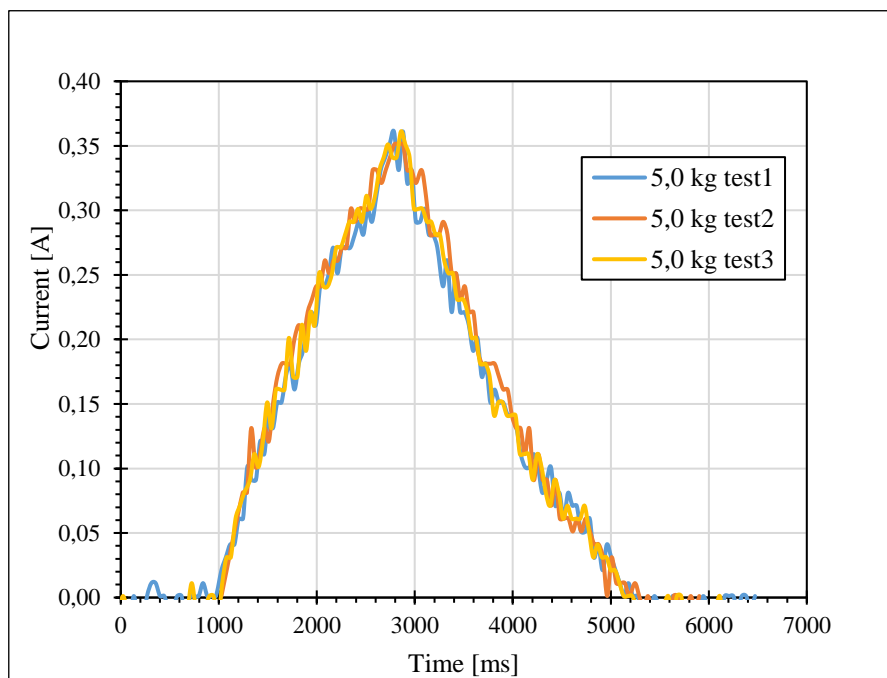
Figure 76.   Current: 13 Ω load test with 5 kg weight
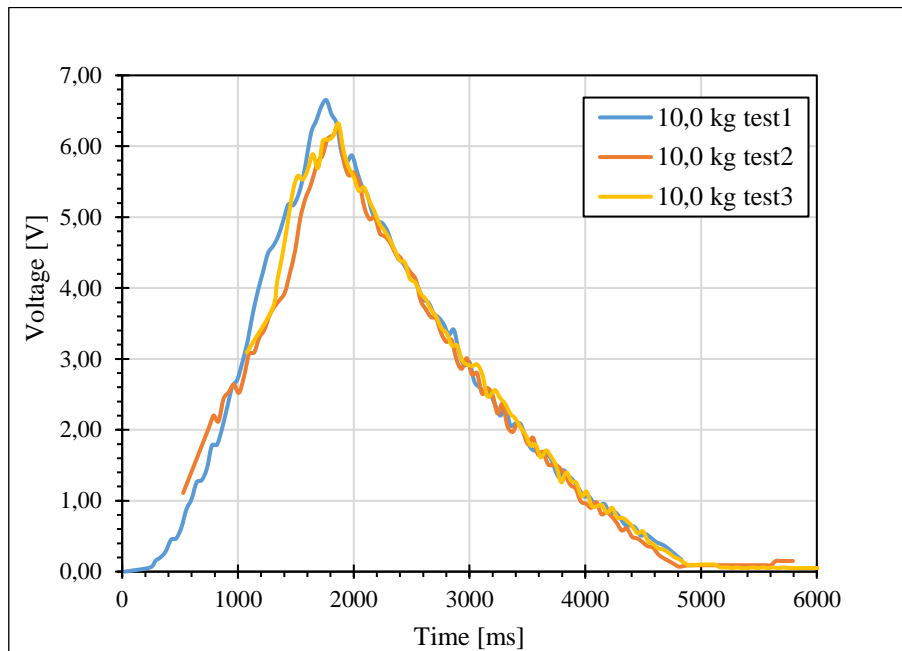
Figure 77. **Voltage: 13 Ω load test with 10 kg weight**
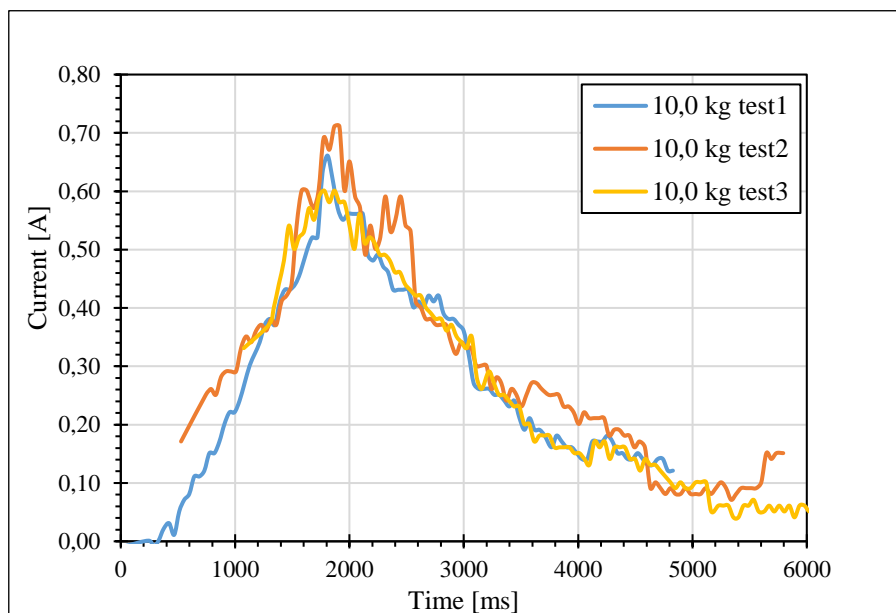
Figure 78. **Current: 13 Ω load test with 10 kg weight**

4.1.2.3 Load test with 8 Ω resistance

Load tests were carried out in the same way by connecting the rheostat to the measuring system. The graphs shown in the following figures referred to the tests carried out varying the weight with the rheostat locked to 8 Ω
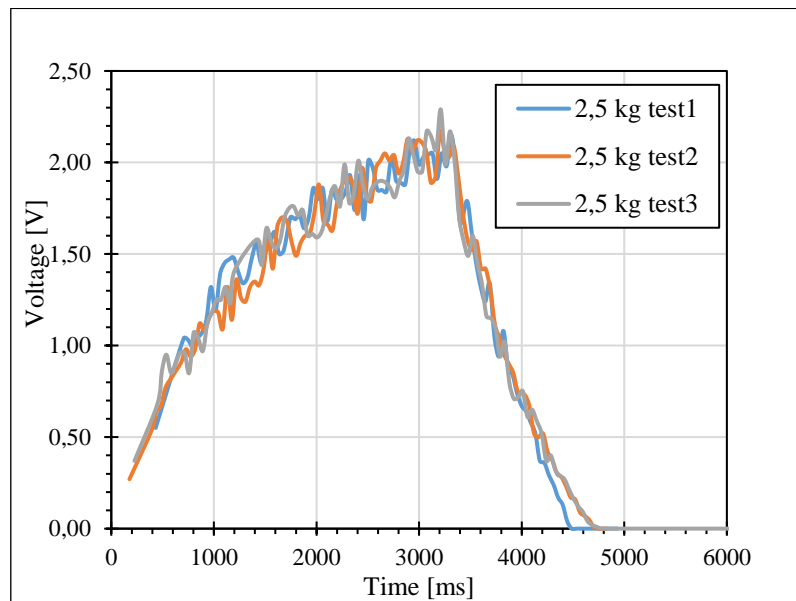
Figure 79.   Voltage: 8 Ω load test with 2,5 kg weight
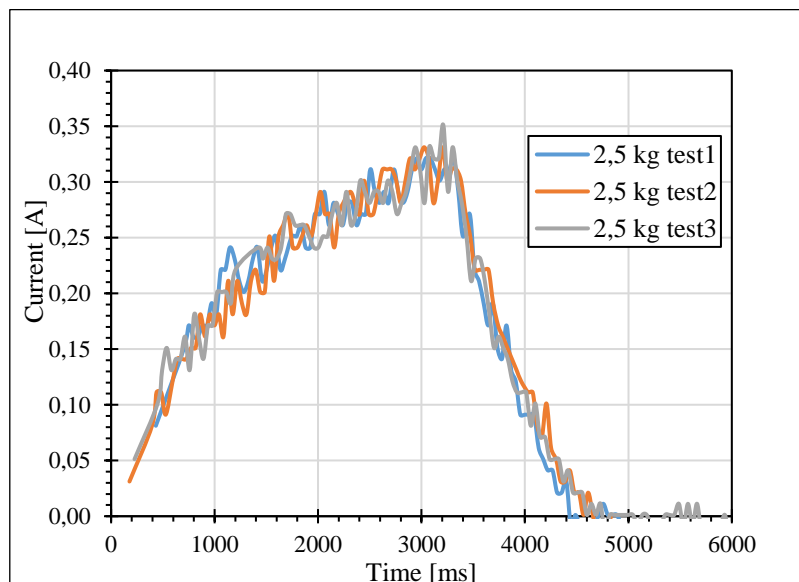
Figure 80.   Current: 8 Ω load test with 2,5 kg weight
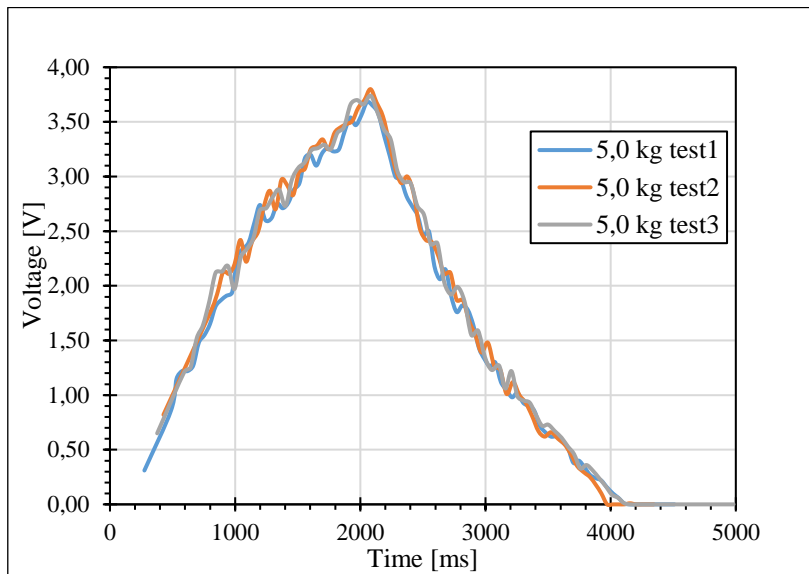
Figure 81.   Voltage: 8 Ω load test with 5 kg weight
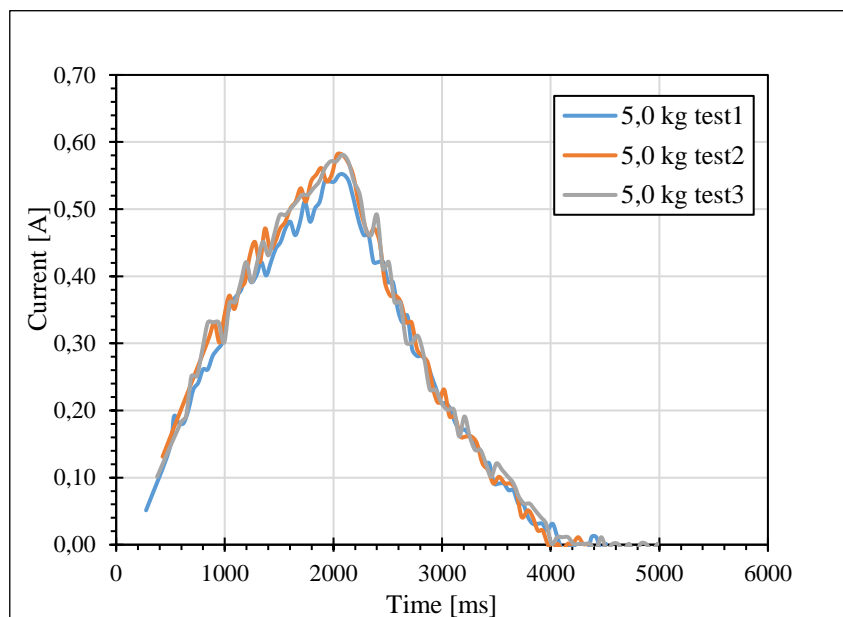
Figure 82.   Current: 8 Ω load test with 5 kg weight
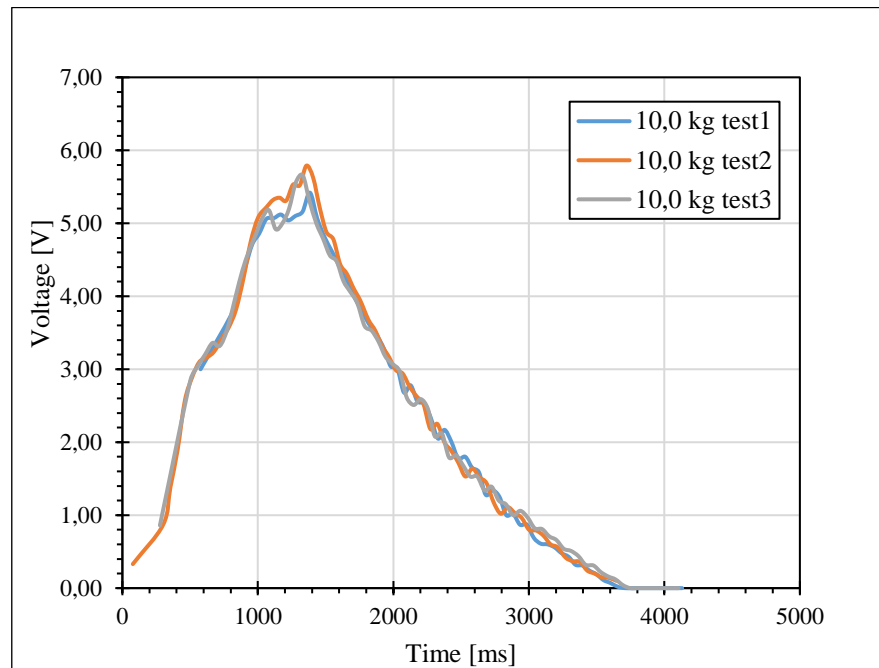
Figure 83.   Voltage: 8 Ω load test with 10 kg weight
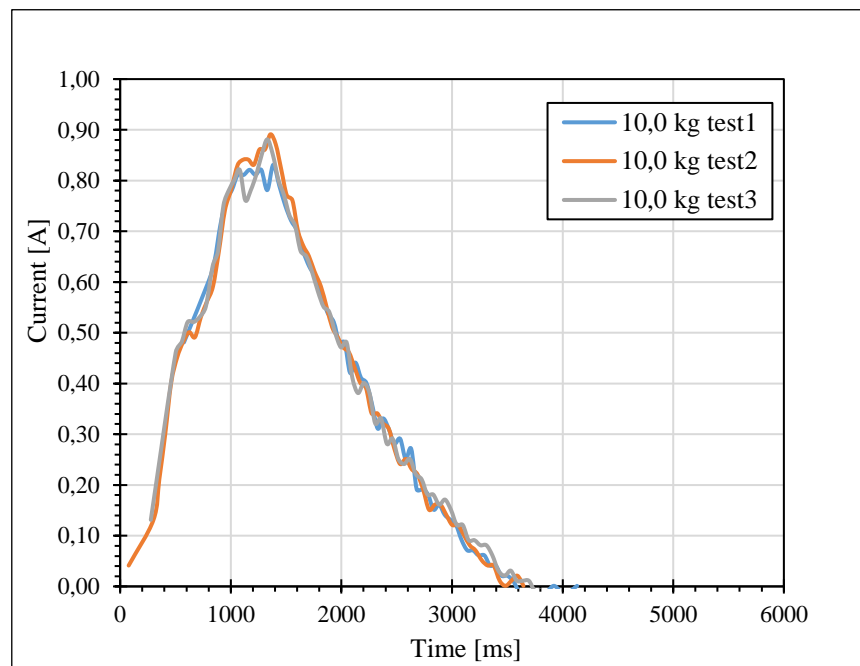
Figure 84.   Current: 8 Ω load test with 10 kg weight

4.1.2.4 Load test with 2 Ω resistance

Load tests were carried out in the same way by connecting the rheostat to the measuring system. The graphs shown in the following figures referred to the tests carried out varying the weight with the rheostat locked to 2 Ω
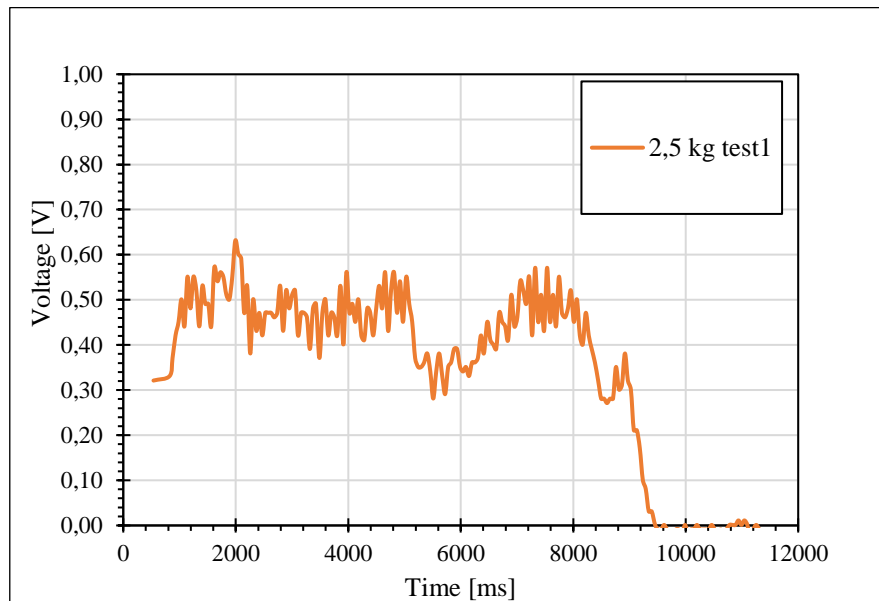
Figure 85.   Voltage: 2 Ω load test with 2,5 kg weight
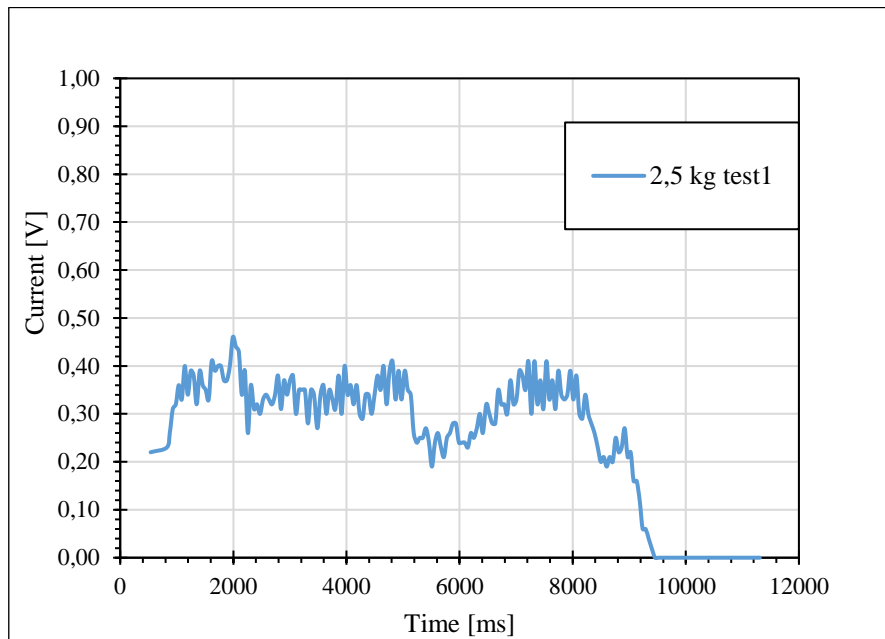
Figure 86.   Current: 2 Ω load test with 2,5 kg weight
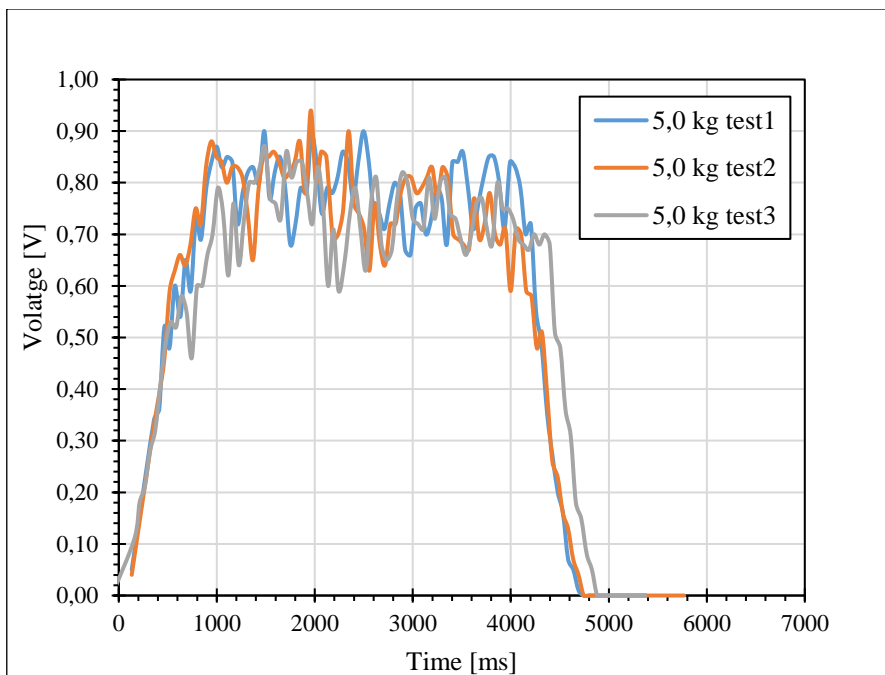
Figure 87.   Voltage: 2 Ω load test with 5 kg weight
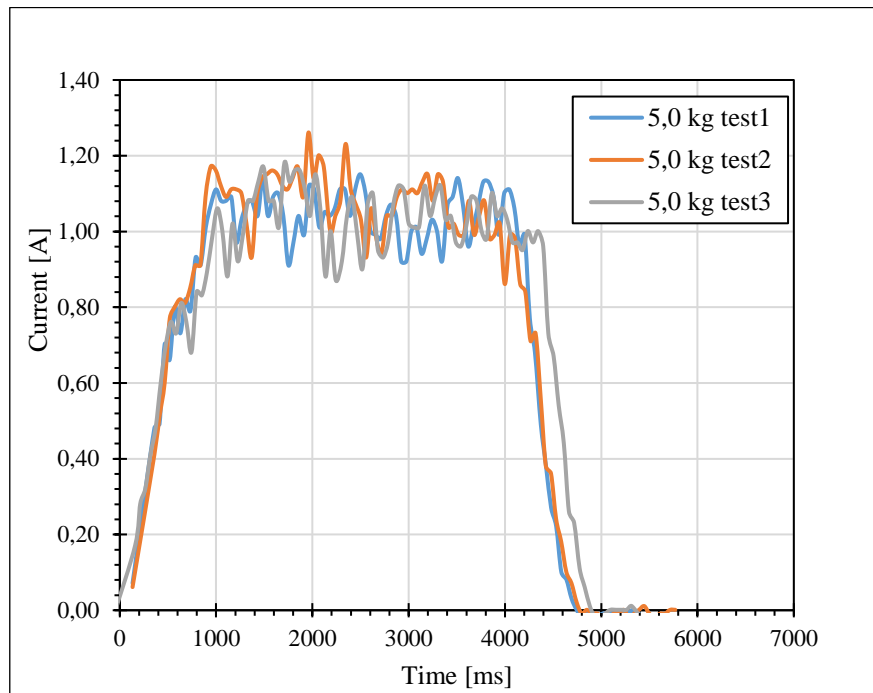
Figure 88.   Current: 2 Ω load test with 5 kg weight
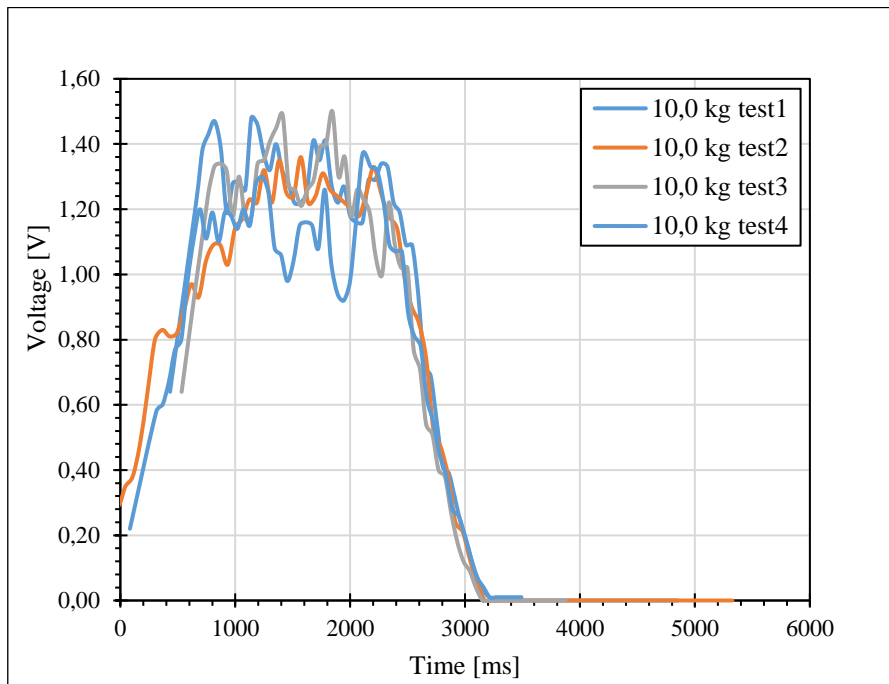
Figure 89.   Voltage: 2 Ω load test with 10 kg weight
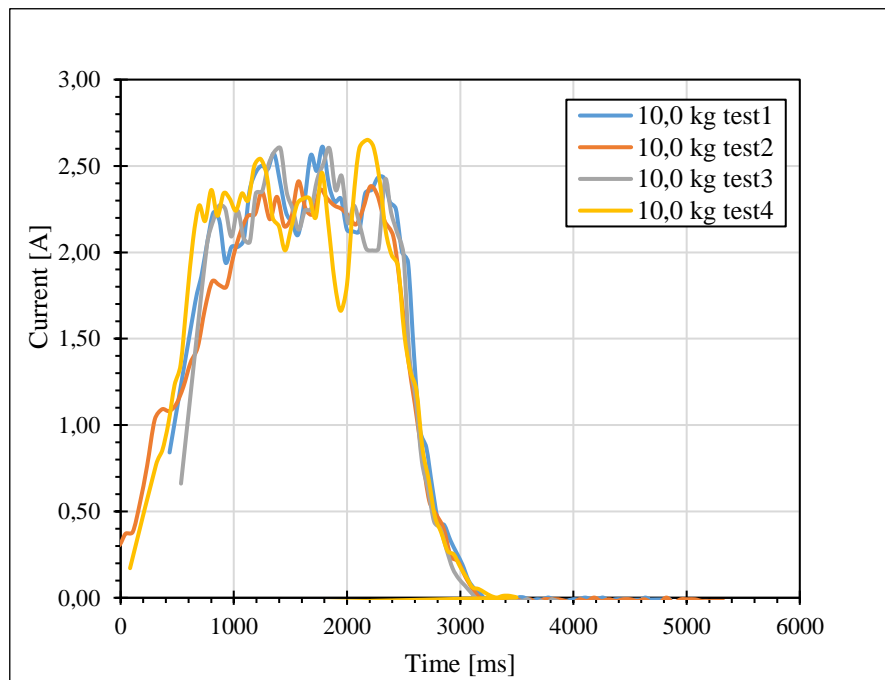
Figure 90.   Current: 2 Ω load test with 10 kg weight

After all tests have been performed, the average energy delivered to the load in each test is calculated. The set of equations, which allows this assessment to be made, is shown in equations 77, 78, 79:

$$P_i = V_i \, I_i \tag{77}$$

$$P_{i-1} = V_{i-1} \, I_{i-1} \tag{78}$$

$$E = \int_{t=0}^{T} V(t)I(t)dt = \sum_{i=0}^{n} \left(\frac{P_1 + P_{i-1}}{2}\right)(t_i + t_{i-1}) \tag{79}$$

Where:

- P is the power [W]
- V is the voltage [V]
- I is the current [A]
- Terms with subscript "i" are those evaluated at the i-th instant
- The terms with subscript "i-1" are those preceding the i-th instant
- E is the energy [J].

The results obtained from the tests carried out are summarised in Table. 8, which shows the values of gross energy production and net energy delivered to the load for each weight-load value pair.

Table 8.   On shore PTO characteristics

Weight [kg]	Electric load [Ω]	Gross energy production [J]	Net Energy production [J]
2.5	13	24.83	1.26
2.5	8	24.83	1.38
2.5	2	24.83	1.22
5	13	43.21	2.11
5	8	43.21	2.84
5	2	43.21	3.05
10	13	79.96	5.04
10	8	79.96	5.14
10	2	79.96	5.47

After measuring the producibility of the system, it was decided to characterise the device by calculating the efficiency using the following equation 80.

$$\eta_{PTO} = \frac{E_a}{E_p} \tag{80}$$

Where:

- E_n is the net energy production [J]

- E_g is the gross energy production [J]

The next diagram, figure 74, shows how the mechanical efficiency varies with respect to the total resistance value measured in the electrical circuit. There is a maximum, which corresponds to the minimum resistance value. This is also an expected result, because at that value the maximum electrical energy is produced. So, the active power gives rise to a braking torque, the generator slows down its rotation. This results in a reduction of mechanical energy lost through friction. Conversely, as the resistance of the circuit increases, the opposite occurs, and the efficiency decreases with a steep slope to a value of 10 %.
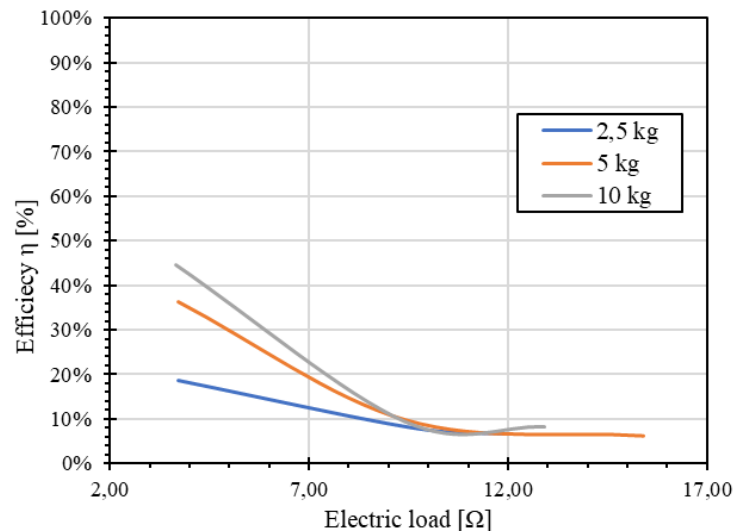
Figure 91.   PTO efficiency

4.2 Linear generator

Linear generator is a machine composed by two main parts: the fixed one (stator) is equipped with coils where the power output is produced. The movable part, called translator, is equipped with permanent magnets, necessary for the excitation of coils[80,81]. In literature, there are linear generators with different characteristics. They differ according to the interaction characteristics between the magnetic field lines and the direction of motion of the translator. The magnetic field is generated with permanent magnets or exciter coils. But given the small power involved in the device under study, it was decided to use the first solution. There are two types of classification according to the relationship between the magnetic flux field lines and the direction of motion of the moving part:

- Generators with longitudinal flux
- Generators with transverse flux

The first generator works with magnetic field lines parallel to the translator movement, for this reason the coils are installed in such a way as to have their perpendicular parallel to the motion field of the moving part. The second generator works with magnetic field lines perpendicular to the movement of the translator[82,83]. The following figure 92 shows the linear generator and his translator designed by the engineering department of the university of Palermo, during the experimental tests.

Figure 92.   Linear generator experimental tests

In sea technology laboratory of the department of engineering of Palermo the producibility has been tested varying weights and resistance applied. The experimentation was performed fixing the stator to the workbench, connecting the translator to the load with rigid cable, and using a pulley to allow the weight to pull the load. The aim of the tests was carried out values of Voltage, current, power production and electrical efficiency. The need to have as much data as possible was met by using 2 different weights (5, 7 kg) and 4 different resistances (0, 5, 10, 20 ohm) applied. The following section lists the main test graphs, considering only one of them for each load.

4.2.1   No load tests.

In this section are shown the results of no-load tests.
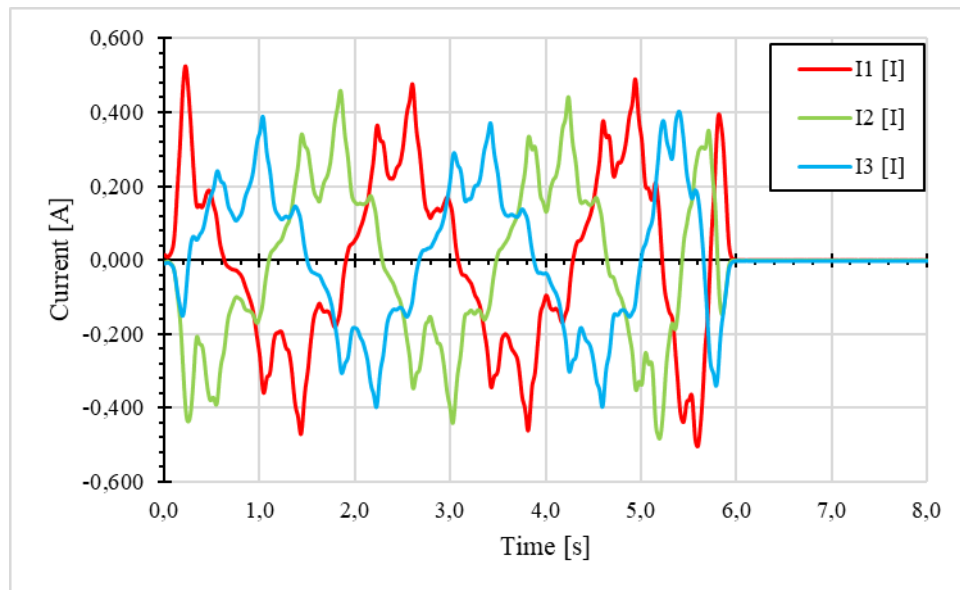
Figure 93.   Current: no load test with 5 kg weight
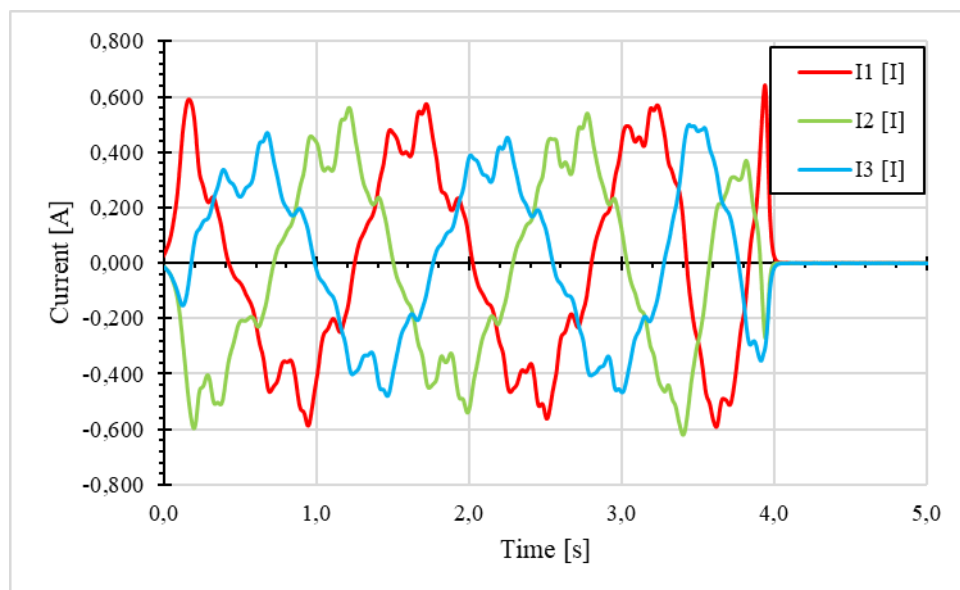
Figure 94.   Current: no load test with 7 kg weight

4.2.2 *Load test with 5 Ω resistance.*
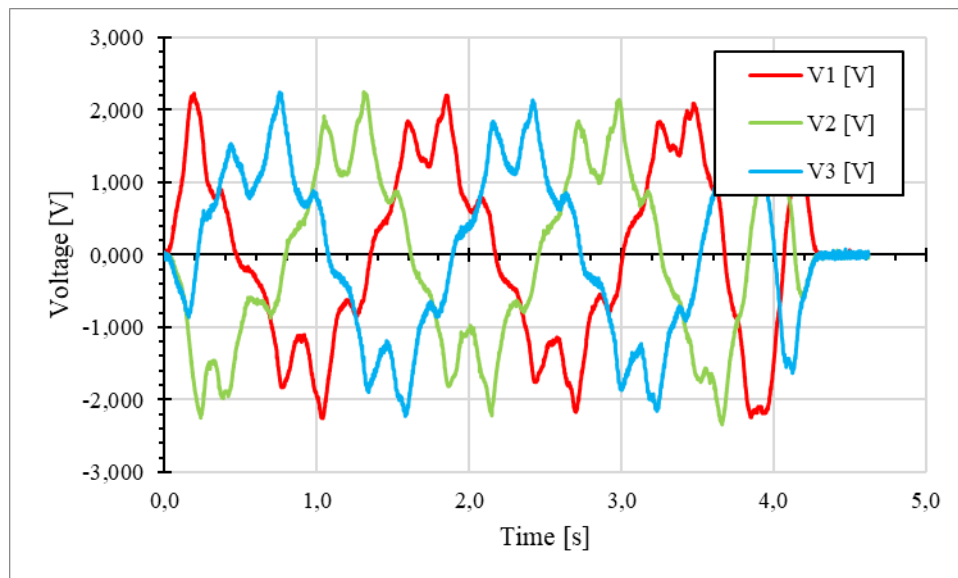
Figure 95. **Voltage: 5 Ω load test with 5 kg weight**
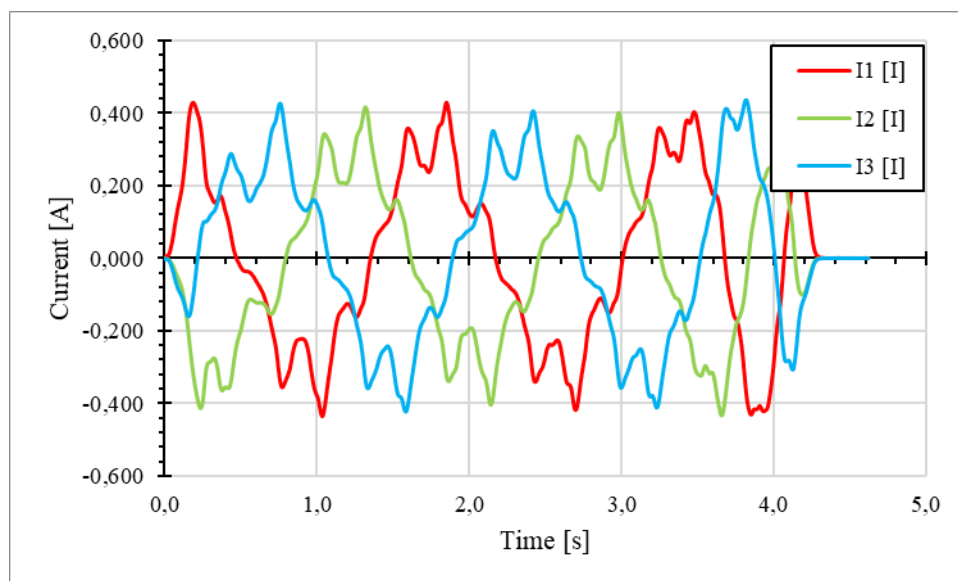
Figure 96. **Current: 5 Ω load test with 5 kg weight**
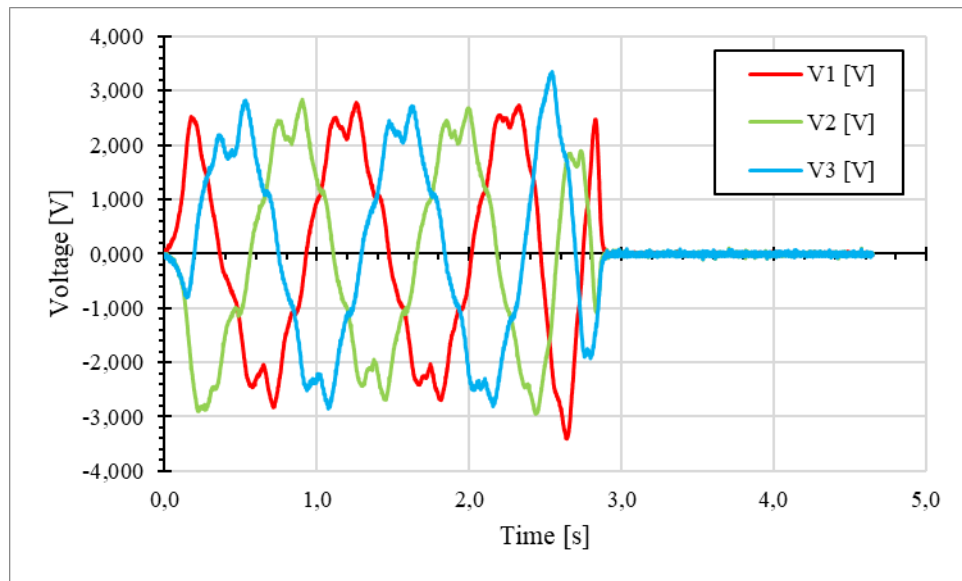
Figure 97.   Voltage: 5 Ω load test with 7 kg weight
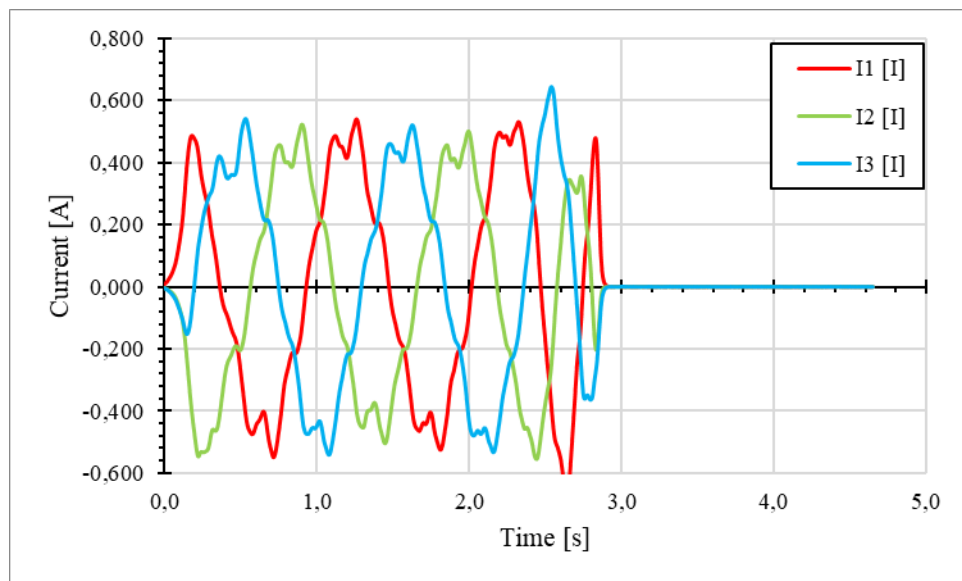
Figure 98.   Current: 5 Ω load test with 7 kg weight

4.2.3   Load test with 10 Ω resistance.
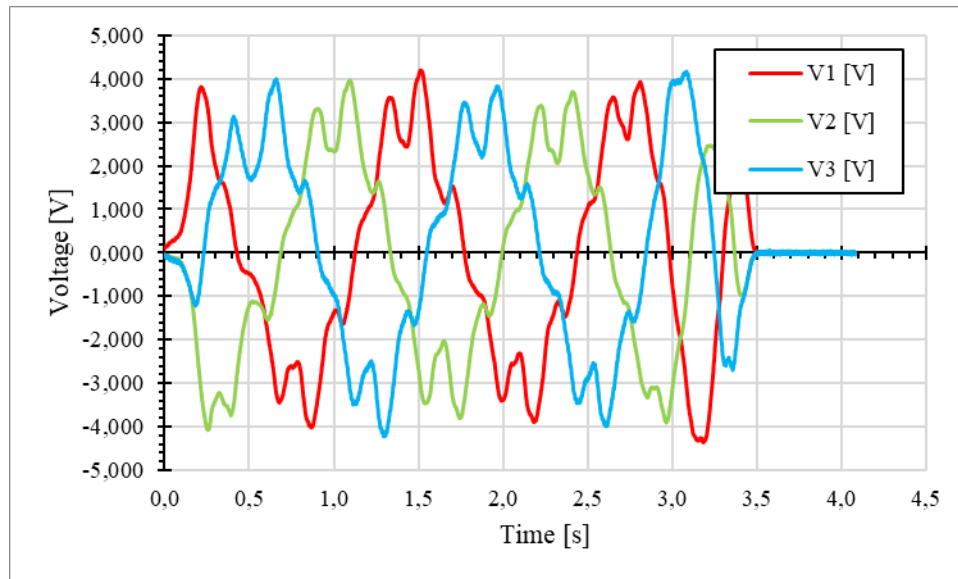
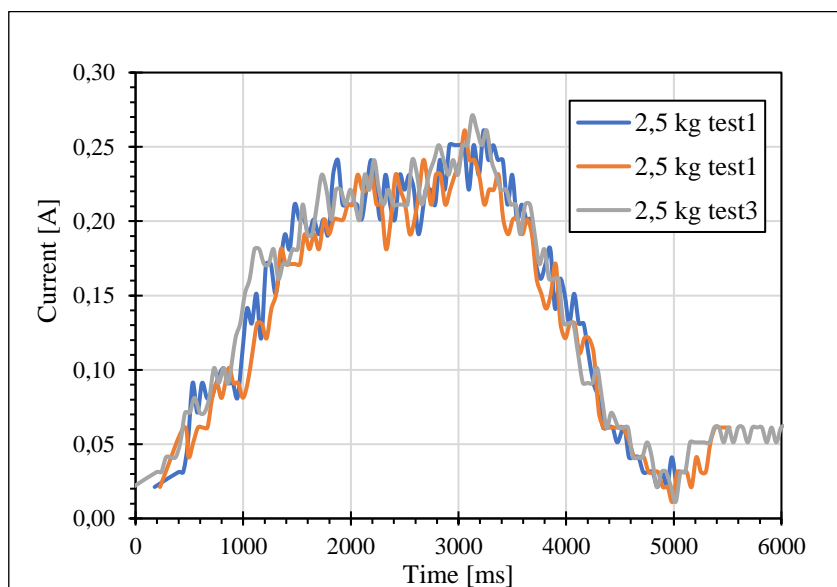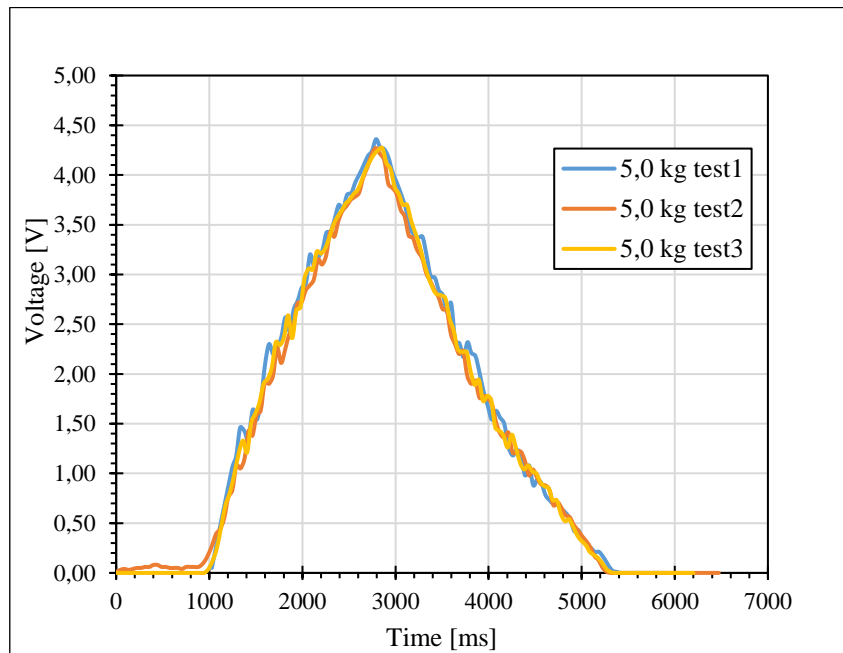**Figure 99.   Voltage: 10 Ω load test with 5 kg weight**
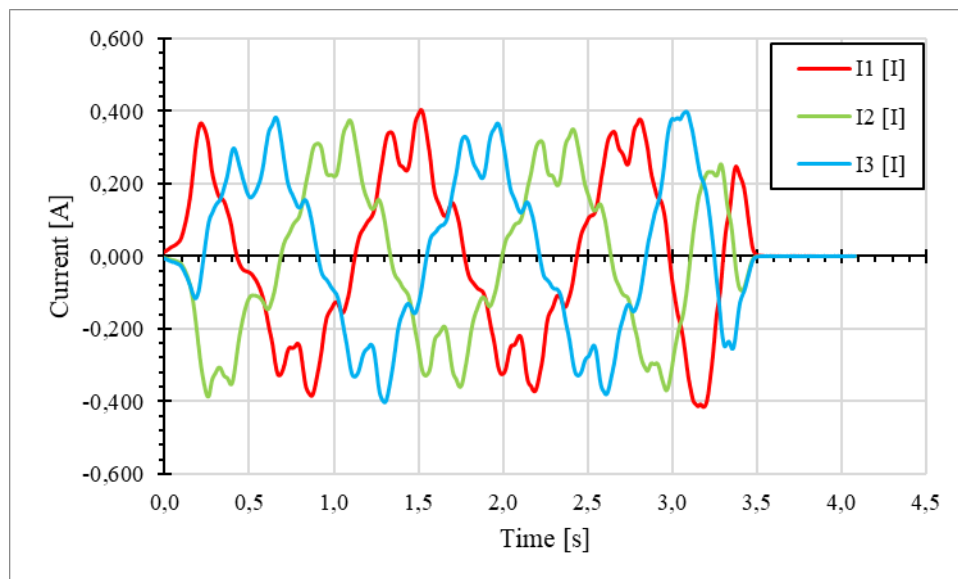
Figure 100. Current: 10 Ω load test with 5 kg weight
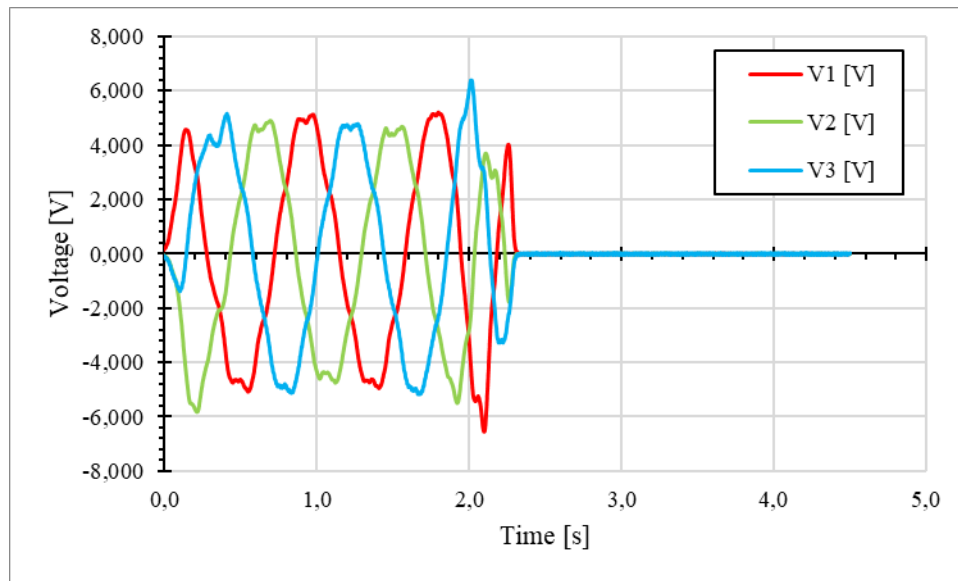
Figure 101. Voltage: 10 Ω load test with 7 kg weight
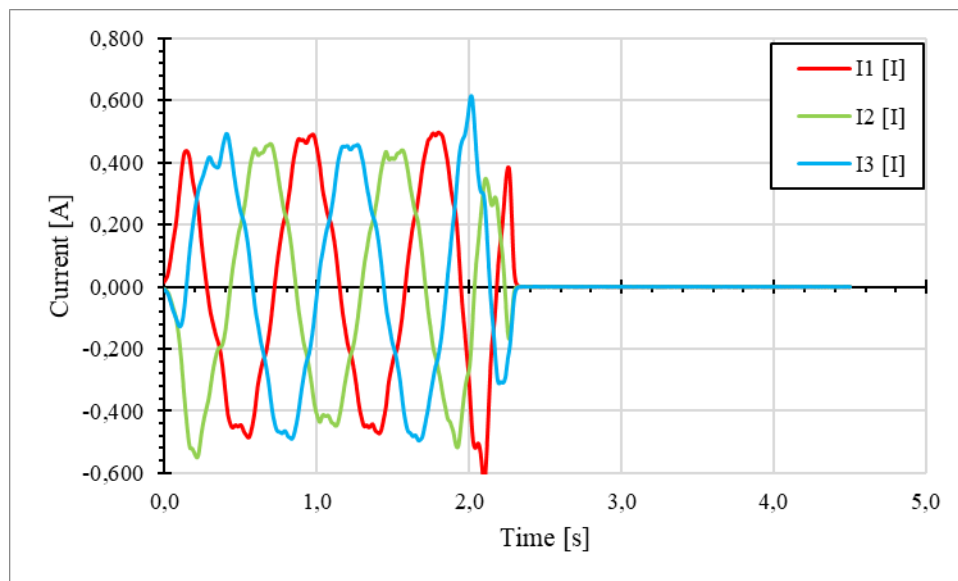
Figure 102. Current: 10 Ω load test with 7 kg weight

4.2.4 Load test with 20 Ω resistance.
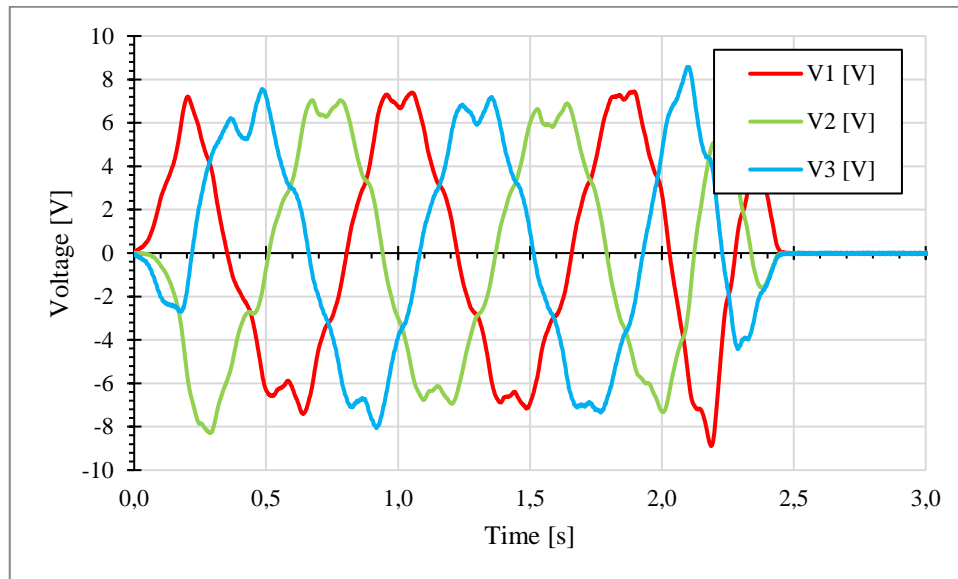
Figure 103. Voltage: 20 Ω load test with 5 kg weight
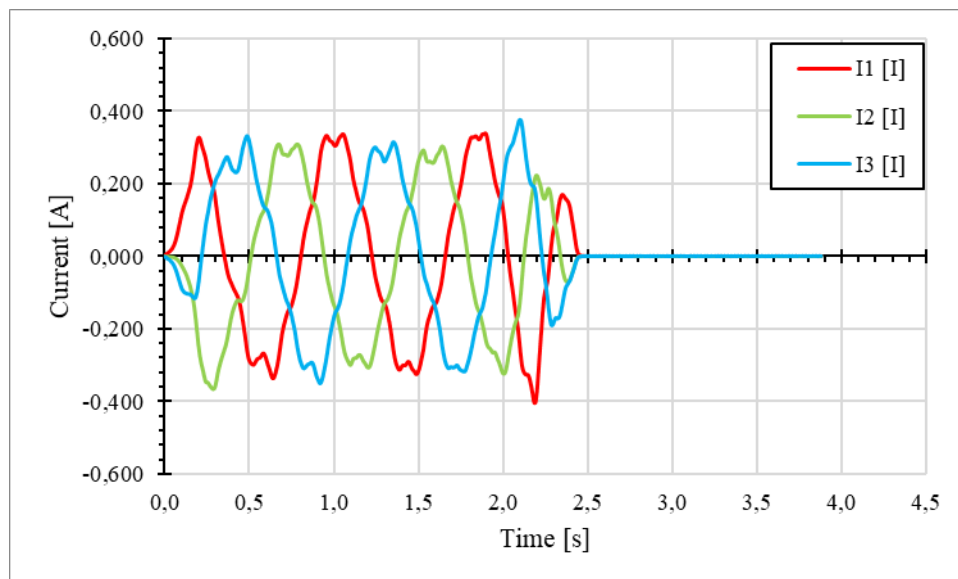
Figure 104. Current: 20 Ω load test with 5 kg weight
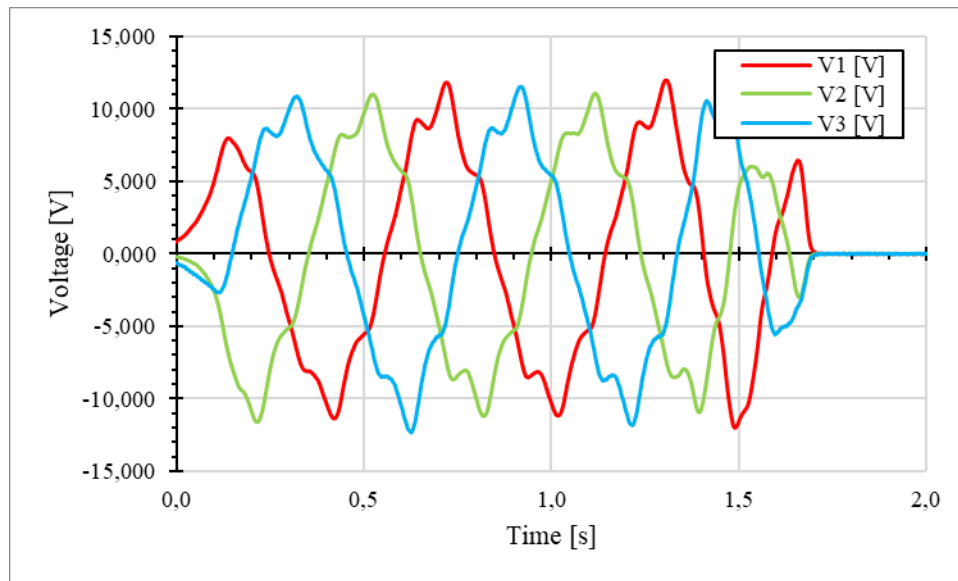
**Figure 105. Voltage: 20 Ω load test with 7 kg weight**
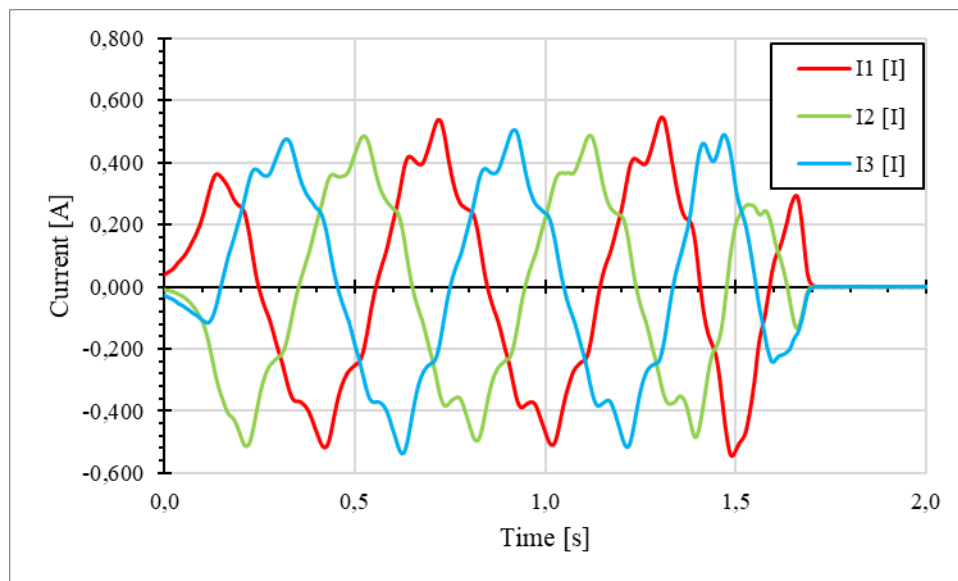

Figure 106. Current: 20 Ω load test with 7 kg weight

After all tests have been performed, the average energy delivered to the load in each test is calculated with the same approach of 4.1.2.4 paragraph.

Table 9. **Linear generator characteristics**

Weight [kg]	Electric load [Ω]	Gross energy production [J]	Net energy production [J]	Efficiency
5	0	26,46	/	/
5	5	26,46	4,13	15,6
5	10	26,46	5,88	22,22
5	20	26,46	7,83	29,60
7	0	37,04	/	/
7	5	37,04	5,86	15,83
7	10	37,04	8,63	23,29
7	20	37,04	7,83	21,14

The efficiency of the system varying weights and electric loads is shown in figure 107.
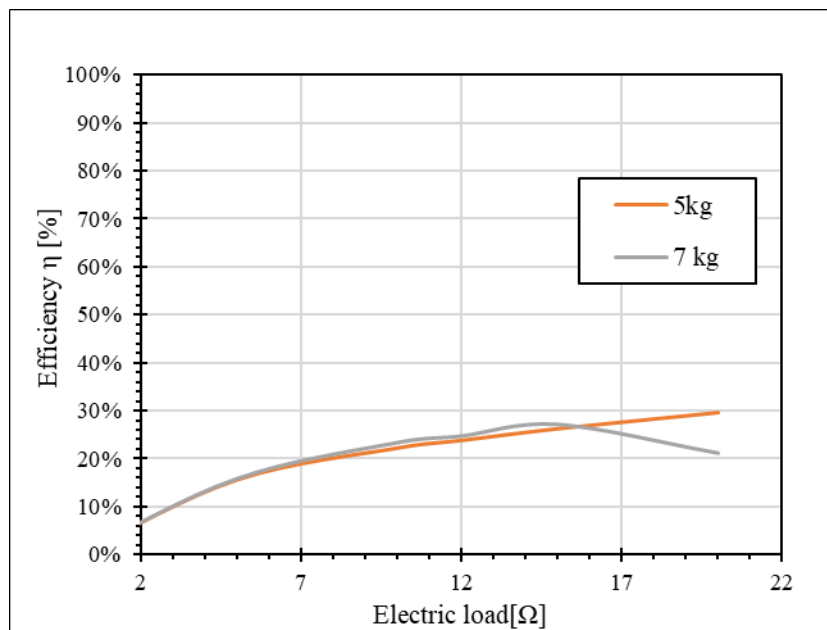
Figure 107. Iron linear generator efficiency

4.3 Ironless linear generator

The ironless generator is a kind of linear generator designed and built by the Engineering Department of University of Palermo. The generator is composed by a fixed part, stator, comprising the coils where the power output is produced. The movable part, called translator, is equipped with permanent magnets, necessary for the excitation of coils. The main innovation of this device is related to the adoption of an ironless stator. This solution is introduced in order to remove the disturbing phenomenon of cogging force. Indeed, in the classical iron stator the alternance of teeth and slots produces a pulsating variation of the magnetic flux in the entire stator. As consequence, vibrations are produced. Also, the activation of the machine could require greater value of force; thence, if the device is adopted in a sea wave harvesting, the energy extraction is reduced. As secondary effect, the removal of iron from the stator also reduces the internal loss of generator, eliminating the eddy currents inside the stator and reducing the total weight of the system for a fixed geometry. The device is a three-phase machine. The step between two adjacent coils is equal to one sixth of the step between two magnets with the same magnetic pole. This geometrical configuration allows with a block of six adjacent coils, and by selecting one of them, to always have one that produces a voltage in phase opposition. The phenomenon of cogging force, caused by the passage of the translator magnets alternately in front of the teeth and in front of the stator slots. This difference of cogging force has been measured and quantified in laboratory. The following figure 108 shows the cogging force values of iron and ironless generators. The cogging force in the iron generator reaches 45 N whereas in the iron less machine it is almost negligible.
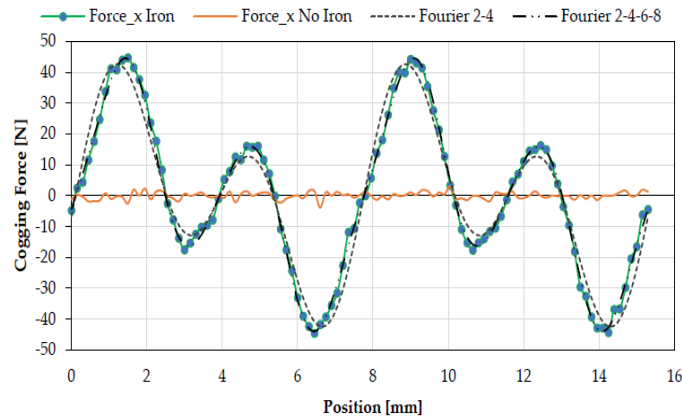
Figure 108. Cogging force difference between iron and ironless generator

In sea technology laboratory of the department of engineering of Palermo the producibility has been tested varying weights and resistance applied. The experimentation was performed fixing the stator to the workbench, connecting the translator to the load with rigid cable, and using a pulley to allow the weight to pull the load. The aim of the tests was carried out values of Voltage, current, power products and electrical efficiency. The equipment required was an oscilloscope, three rheostats and probes capable of providing instantaneous monitoring of electrical quantities. The following figure 109 shows all devices employed.

Figure 109. Ironless linear generator experimental tests

The need to have as much data as possible was met by using 3 different weights (2.5, 5, 7 kg) and 4 different resistances (0, 5, 10, 20 ohm) applied. In this way it was possible to characterize the linear generator. The measurements were carried

out by testing the generator at all resistance levels for each weight repeated 3 times each. The following section lists the main test graphs, considering only one of them for each load.

4.3.1   No load tests.

In this section are shown the results of no-load tests.
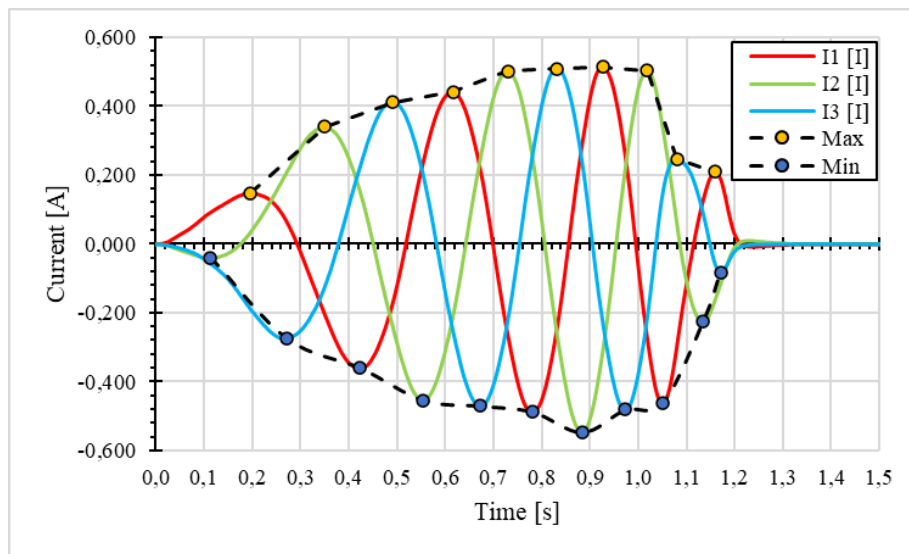
Figure 110. Current: no load test with 2,5 kg weight
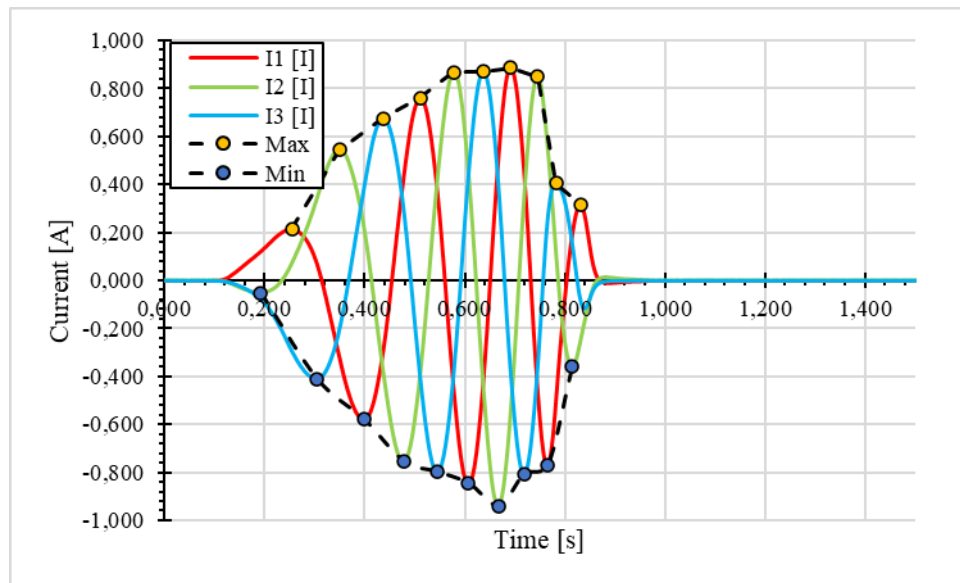
Figure 111. Current: no load test with 5 kg weight
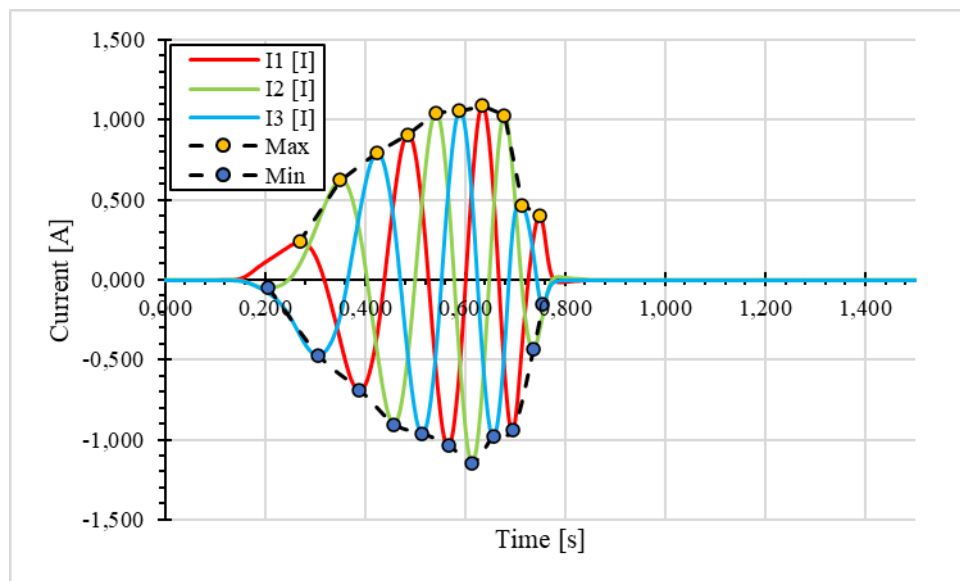
Figure 112. Current: no load test with 7 kg weight

4.3.2 Load test with 5 Ω resistence.
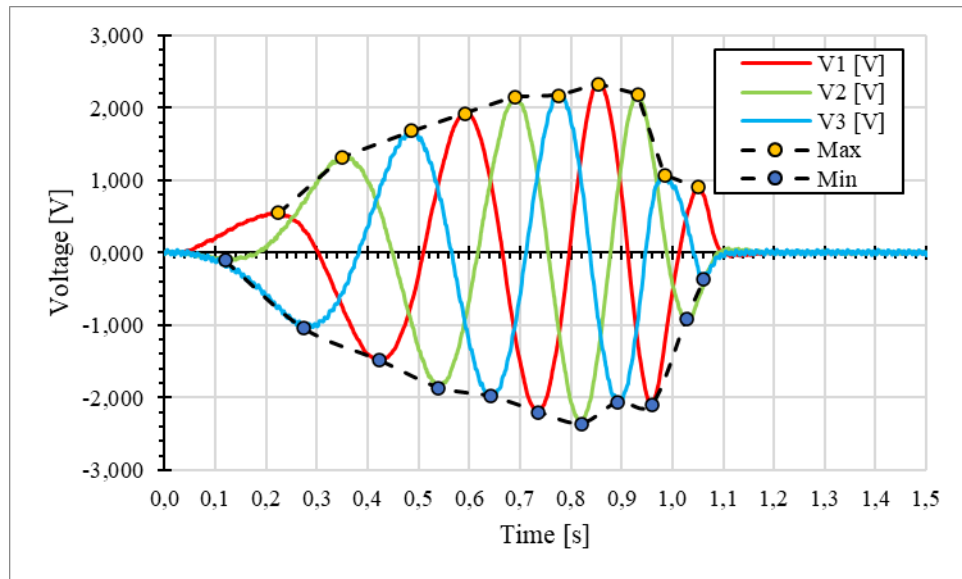
Figure 113. Voltage: 5 Ω load test with 2,5 kg weight
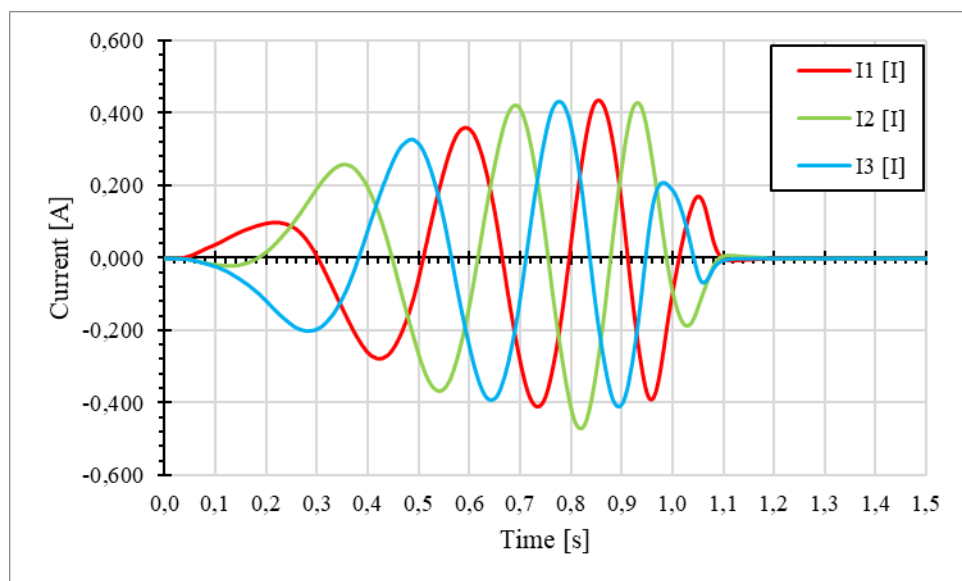
Figure 114. Current: 5 Ω load test with 2,5 kg weight
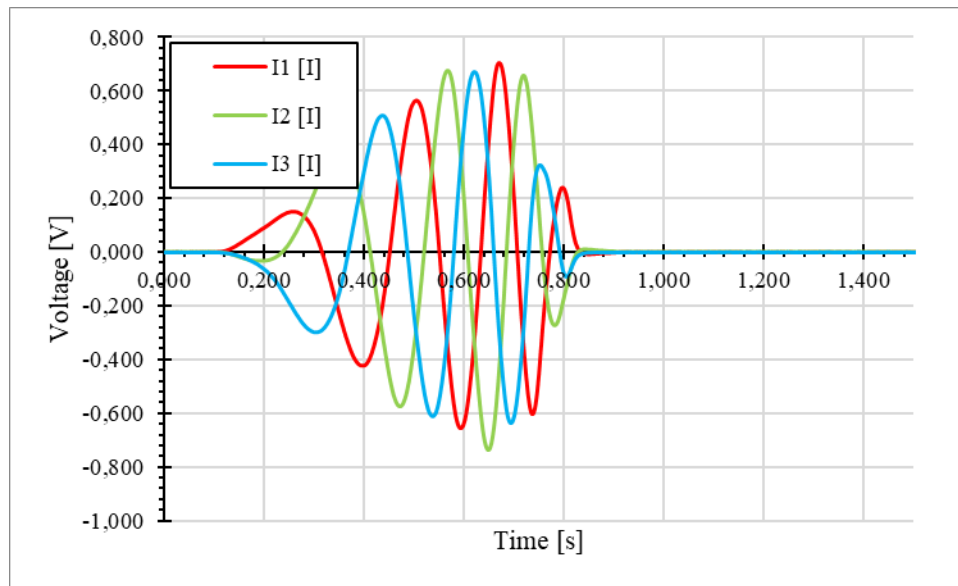
Figure 115. Voltage: 5 Ω load test with 5 kg weight
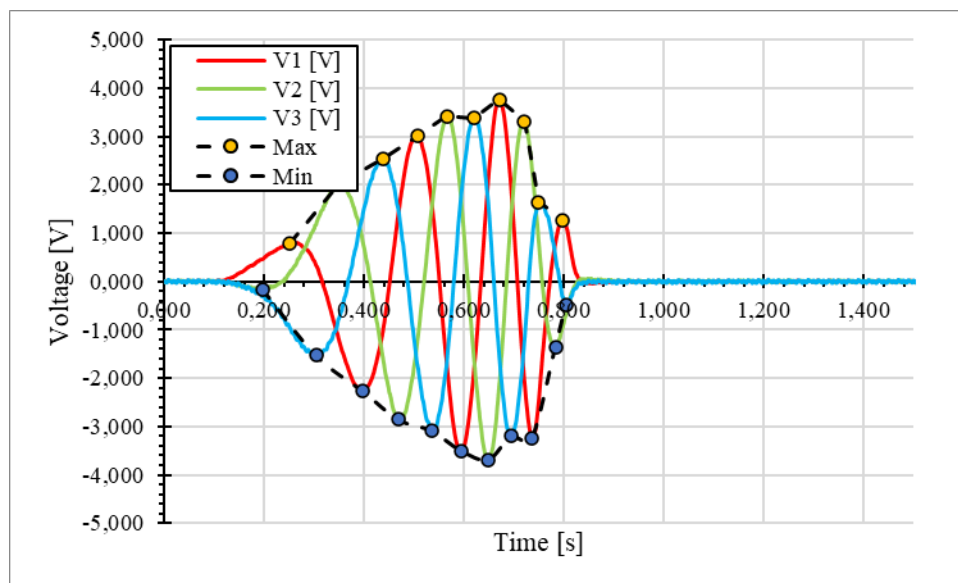
Figure 116. Current: 5 Ω load test with 5 kg weight
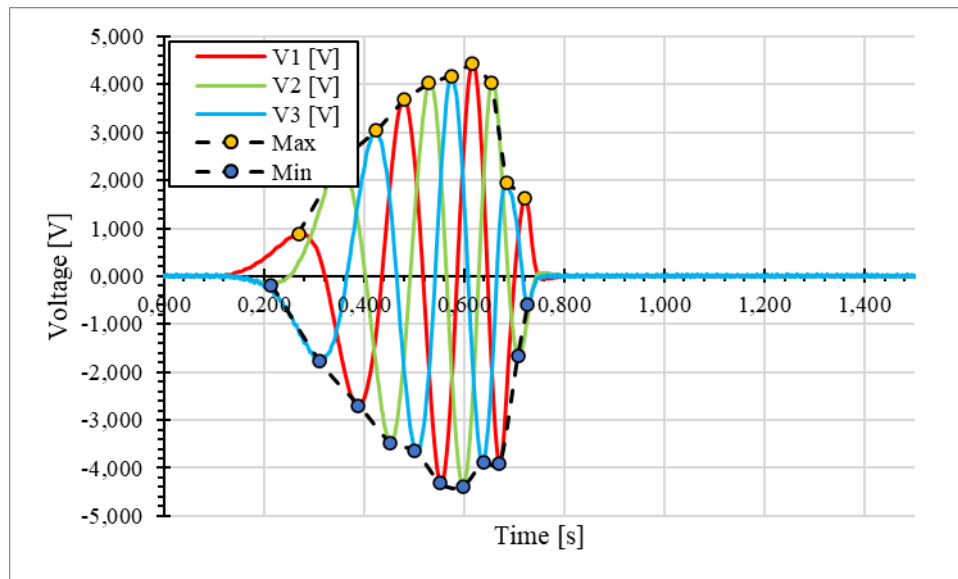
Figure 117. Voltage: 5 Ω load test with 7 kg weight
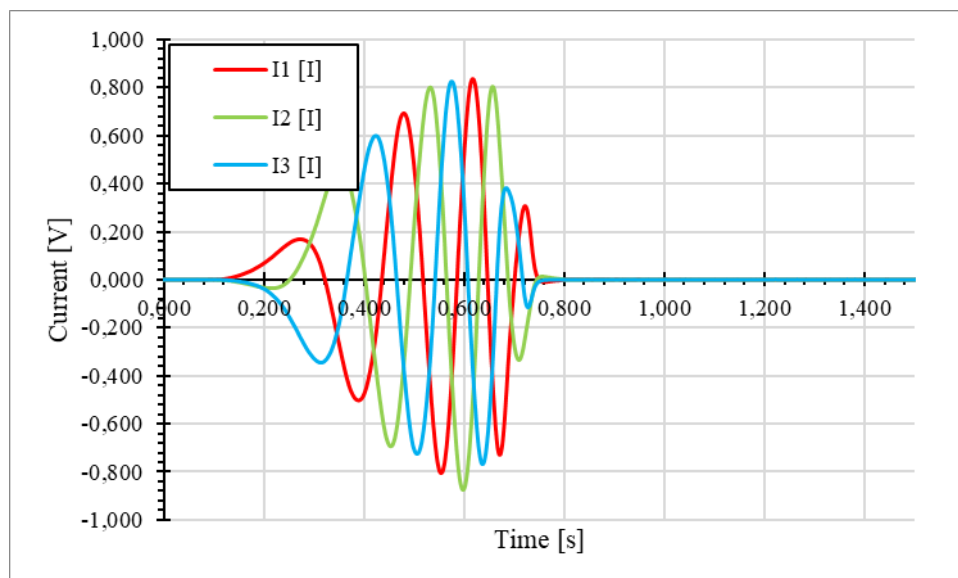
Figure 118. Current: 5 Ω load test with 7 kg weight

4.3.3   *Load test with 10 Ω resistence.*
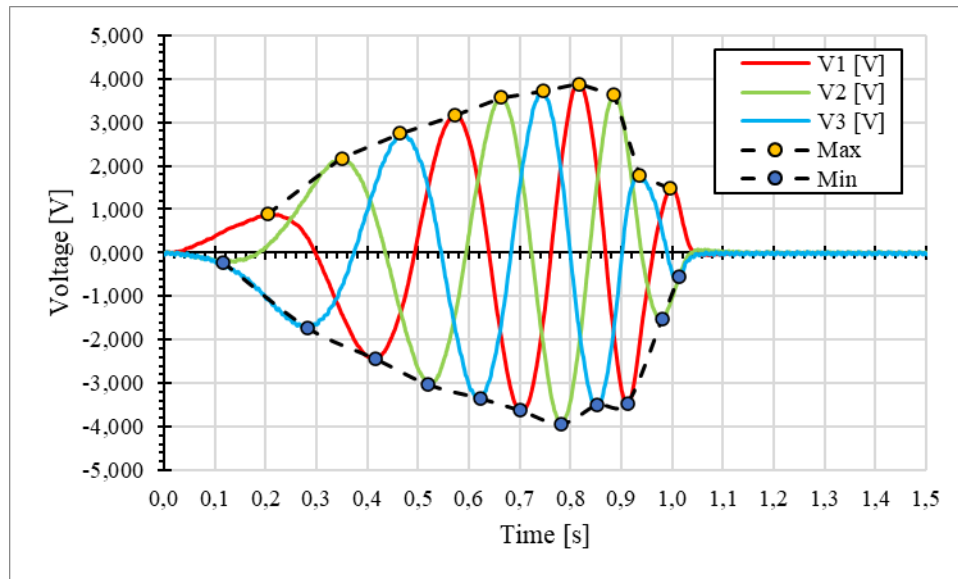
Figure 119. Voltage: 10 Ω load test with 2,5 kg weight
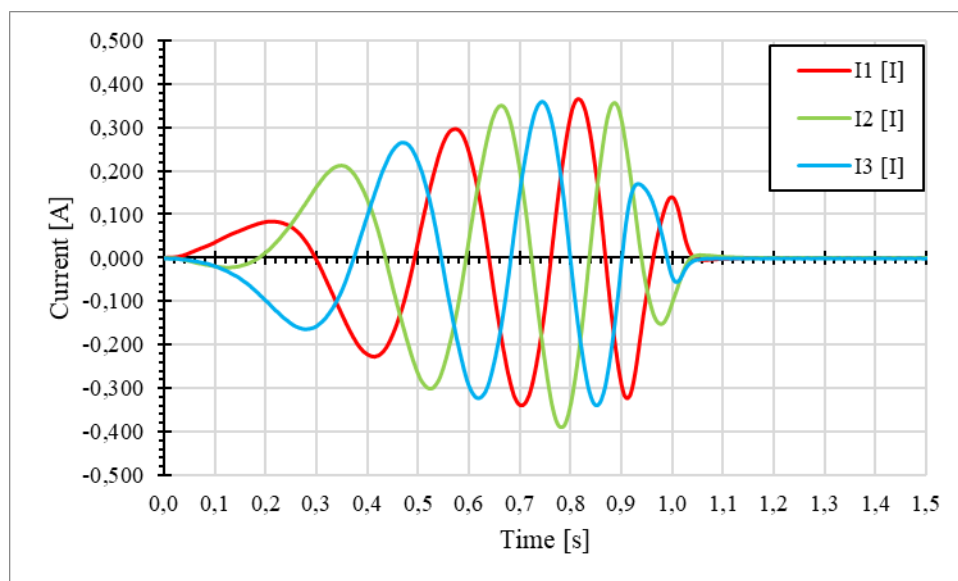
Figure 120. Current: 10 Ω load test with 2,5 kg weight
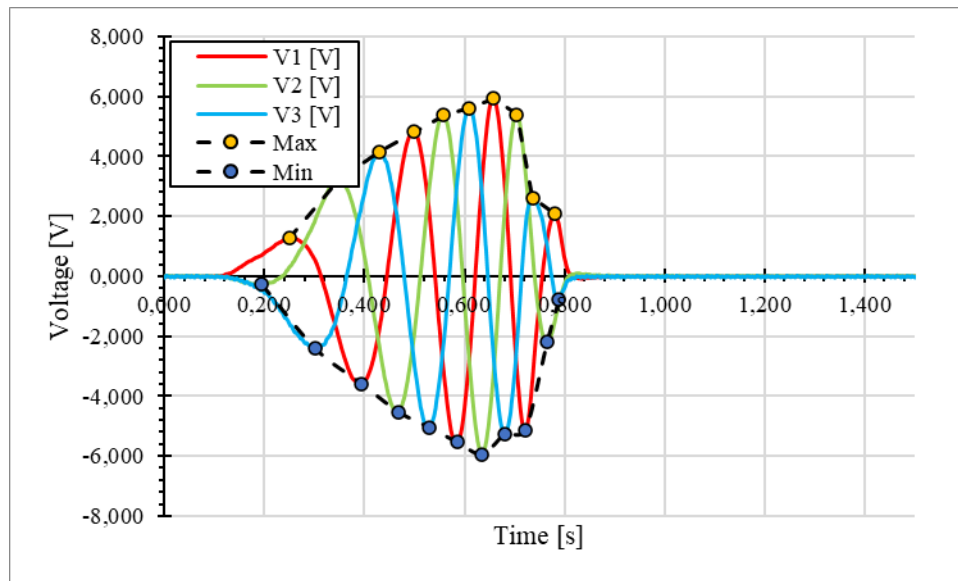
Figure 121. Voltage: 10 Ω load test with 5 kg weight
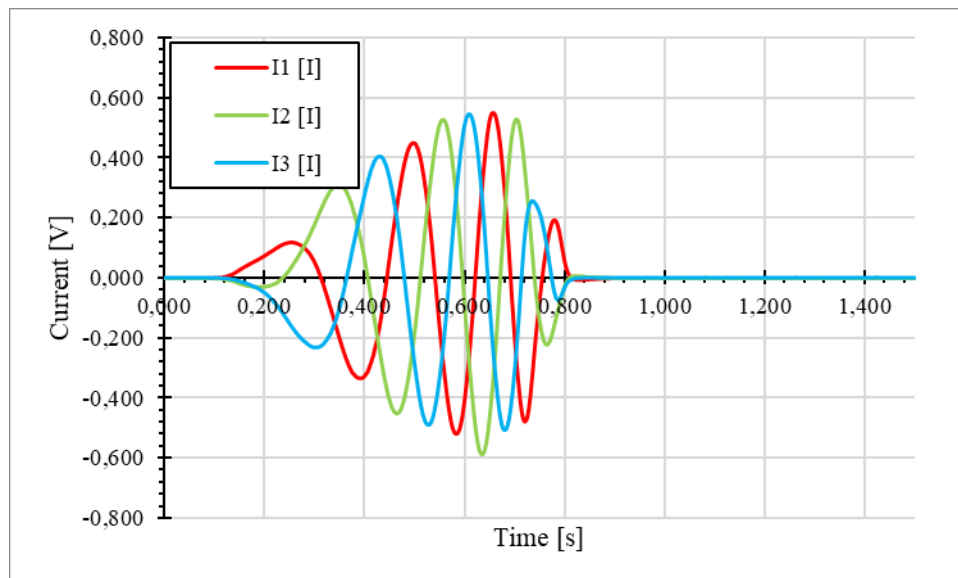
Figure 122. Current: 10 Ω load test with 5 kg weight
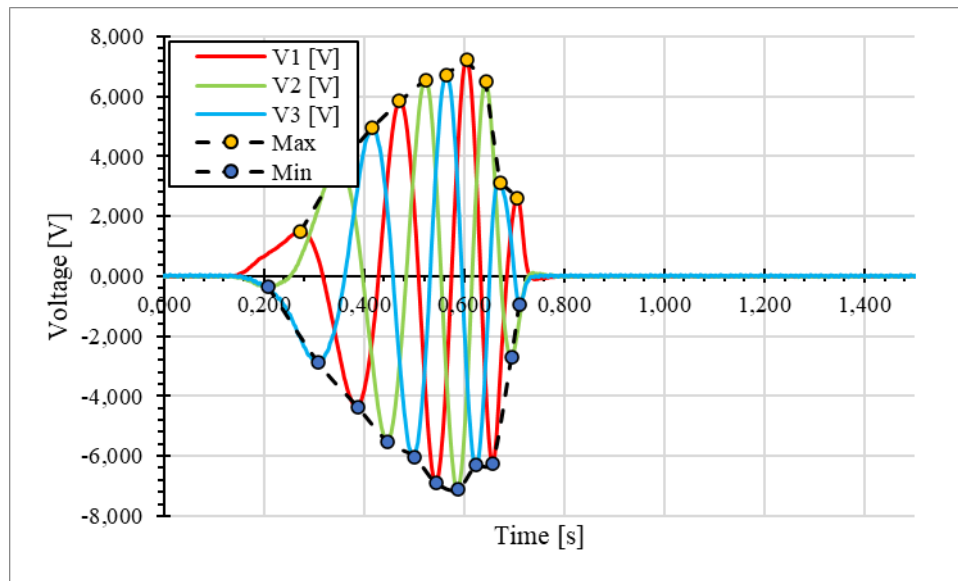
Figure 123. Voltage: 10 Ω load test with 7 kg weight
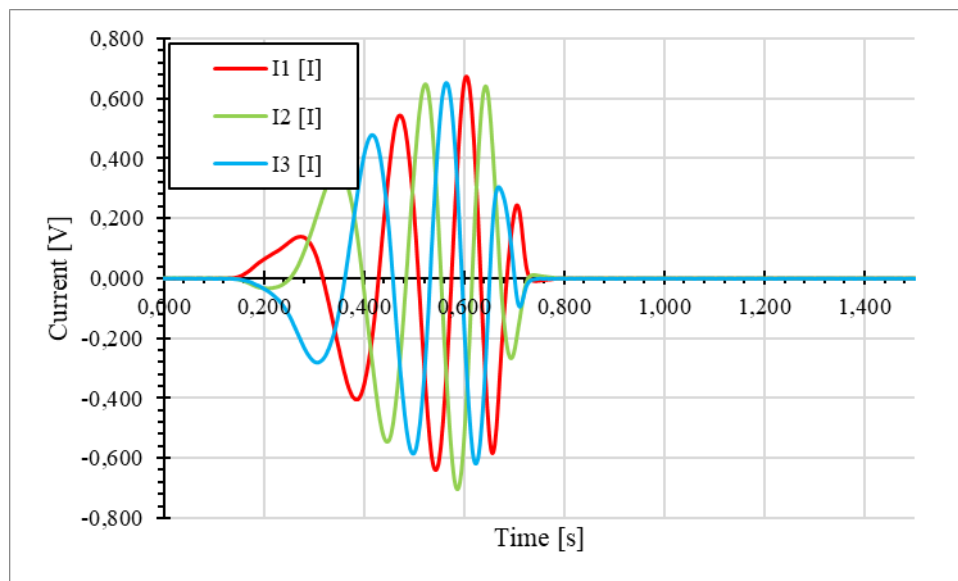
Figure 124. Current: 10 Ω load test with 7 kg weight

4.3.4   Load test with 20 Ω resistence.
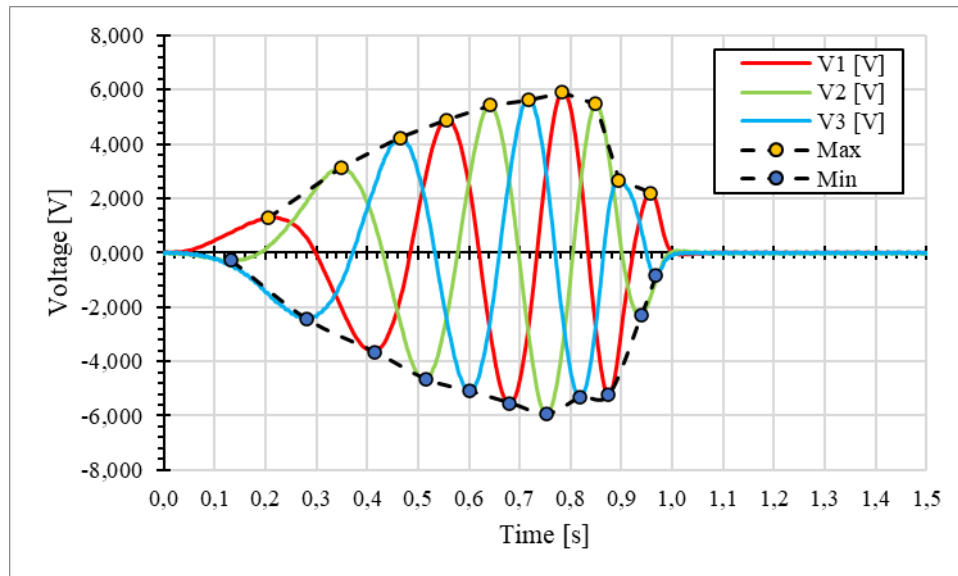
Figure 125. Voltage: 20 Ω load test with 2,5 kg weight
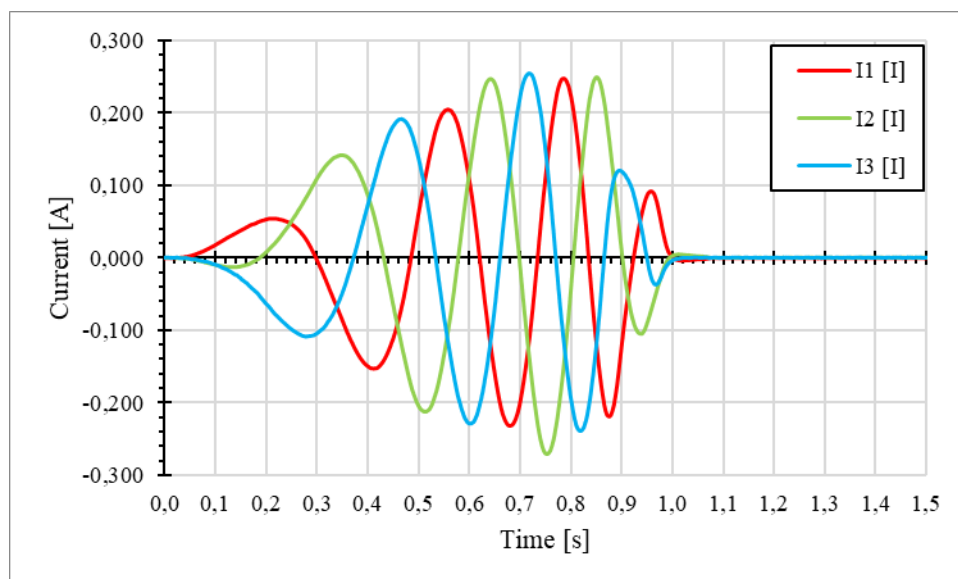
Figure 126. Current: 20 Ω load test with 2,5 kg weight
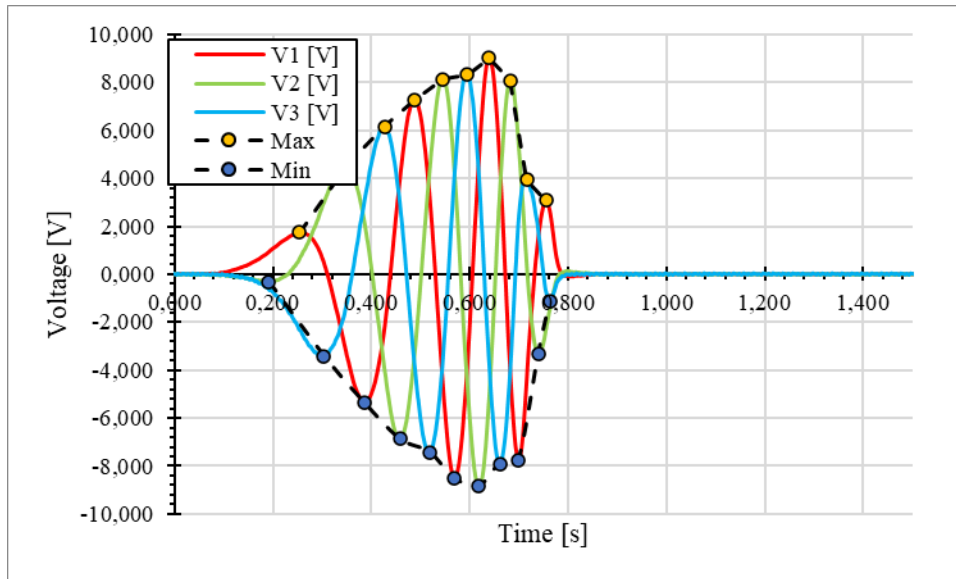
Figure 127. Voltage: 20 Ω load test with 5 kg weight
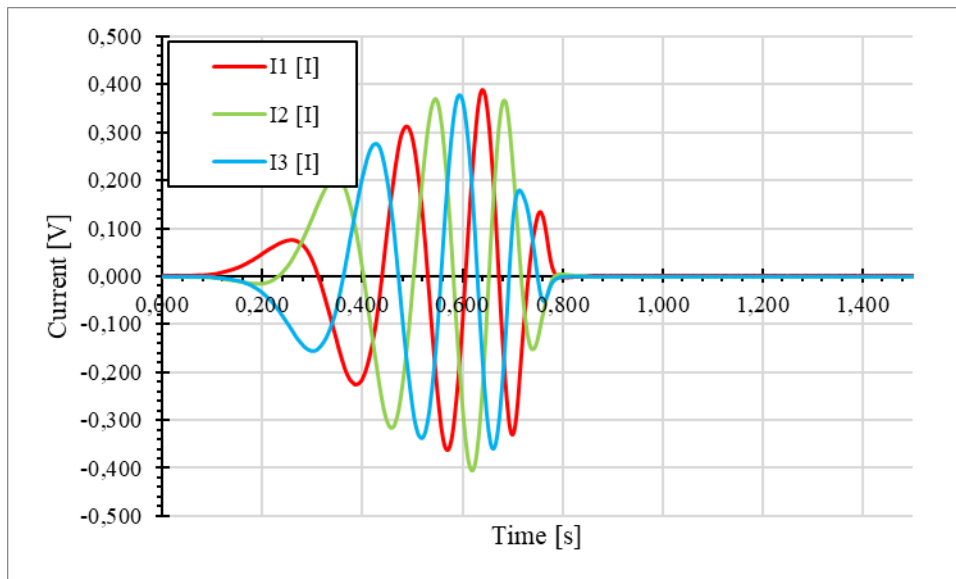
Figure 128. Current: 20 Ω load test with 5 kg weight
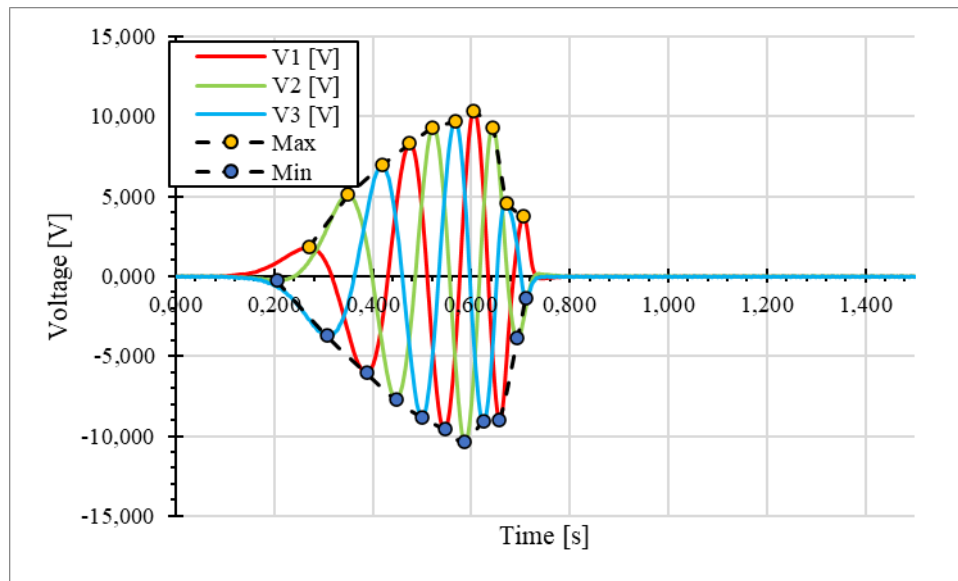
Figure 129. Voltage: 20 Ω load test with 7 kg weight
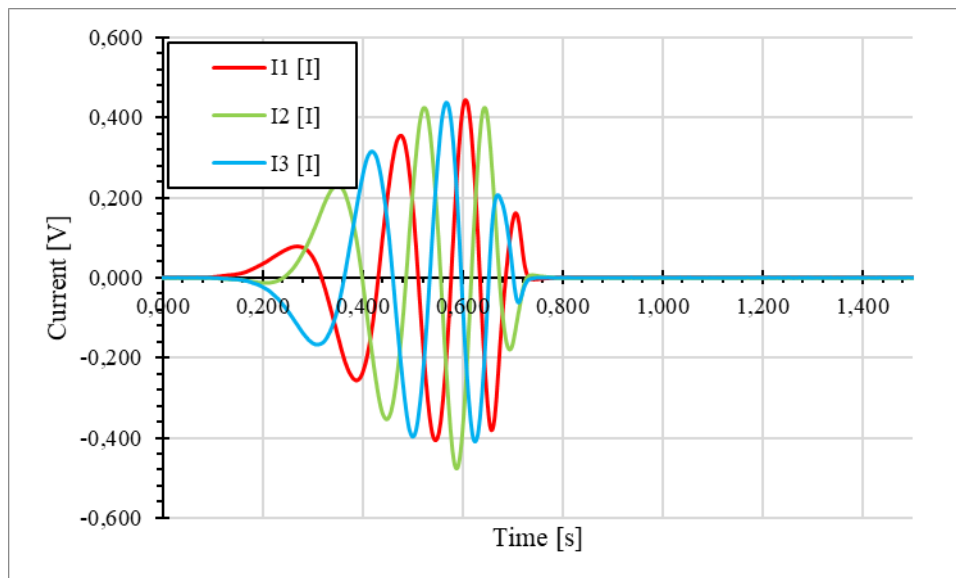
Figure 130. Current: 20 Ω load test with 7 kg weight

After all tests have been performed, the average energy delivered to the load in each test is calculated with the same approach of 4.1.2.4 paragraph, see table 10.

Table 10.   Ironless linear generator characteristics

Weight [kg]	Electric load [Ω]	Gross energy production [J]	Net energy production [J]	Efficiency
2,5	0	13,23	/	/
2,5	5	13,23	0,80	6,02
2,5	10	13,23	1	7,59
2,5	20	13,23	0,99	7,52
5	0	26,46	/	/
5	5	26,46	1,23	4,64
5	10	26,46	1,53	5,77
5	20	26,46	1,48	5,59
7	0	37,04	/	/
7	5	37,04	1,46	3,95
7	10	37,04	1,82	4,92
7	20	37,04	1,69	4,57

The efficiency of the system varying weights and electric loads is shown in figure 131.
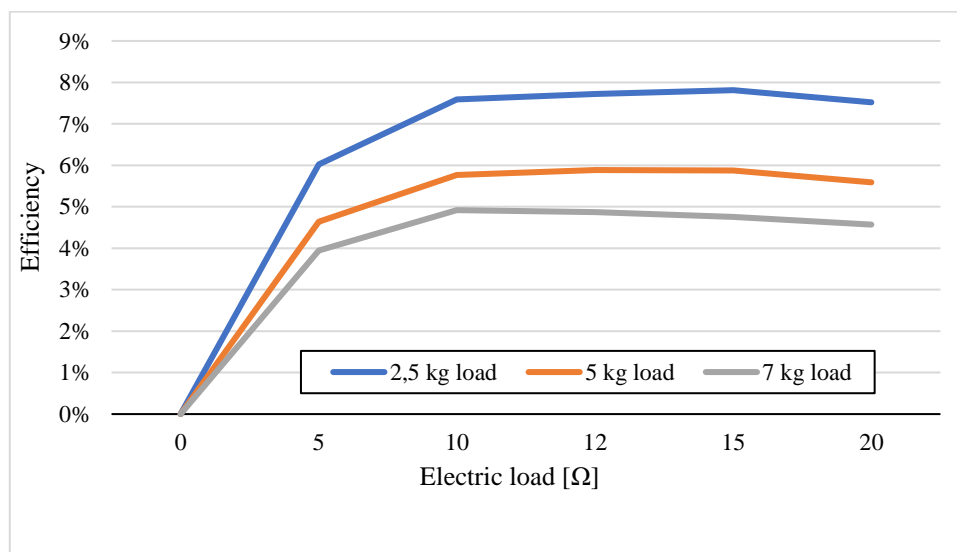
Figure 131. Ironless linear generator efficiency

4.4 Energy production simulation software

In the preceding paragraphs, the values of the tests carried out in the laboratory have been reported. The values obtained were used to characterise the PTOs designed and built in the University of Palermo's marine technology laboratory. The values obtained showed that the proposed technologies could be exploitable in wave energy pilot plants, especially the linear generator in offshore plants and the PTO with carriage and rod for onshore plants. In addition to the characterisation in the laboratory, two modelling was carried out with the "Ansys Aqwa" software.

The first model considers the WEC under consideration as a point absorber, whose PTO is the linear generator. It is a special system that enables the direct conversion of wave energy into electrical energy, without the need for intermediate systems. The pilot plant is suitable for offshore operation, i.e. far from the coast and with a depth of more than 50 meters, so that its behavior can be studied using linear theories, see paragraph 3.1. The Ansys Aqwa software, was used for the study and optimization of the experimental WEC, which allows the modelling of the system by entering in input all the data relating to the state of the sea, the forces acting on the various bodies, the reference points and everything that allows a description, as detailed as possible, of the physical phenomena affecting the model. Initially, a study was carried out on the state of the sea in Palermo, as the chosen site, and then the geometry was constructed, optimizing the parameters, in order to analyze the results obtained and choose the model that best suited our purposes. The model presented in this study is composed by two system:

- The cylinder-ballast system.
- The floating buoy.

The model simulated in the software is positioned in the sea in front of the city of Palermo, see figure 132. The data characteristics of this site have been carried out from the Italian wave network. From the time series of elevation, slope and displacement of the buoys, the following synthetic parameters are obtained:

- Spectral significant wave height

- Mean wave period

- Peak wave period

- Mean direction of wave origin

- Monthly maximum of significant wave height

- Direction associated with monthly maximum of significant wave height.
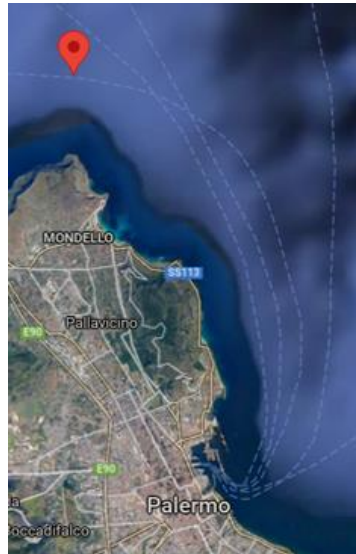
Figure 132. Italian wave network: site of the buoy of Palermo (Capo Gallo)

This data listed above are necessary to size the WEC. For this reason, are carried out especially significant wave height, figure 133, mean wave period, figure 134, mean direction of wave origin, figure 135.
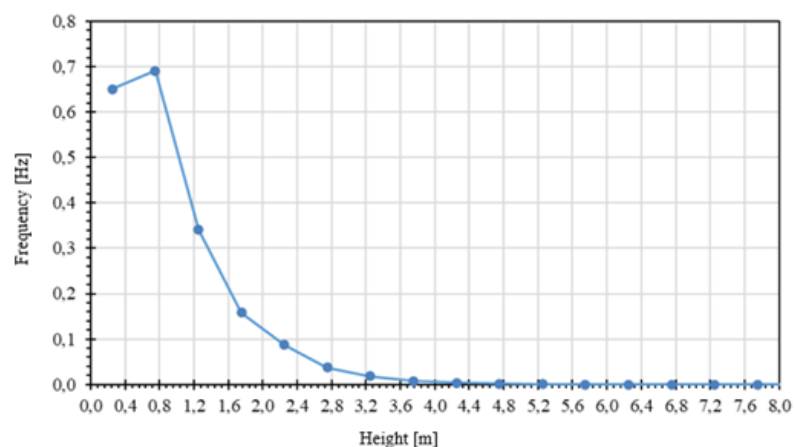
Figure 133. Significant wave height, Capo Gallo
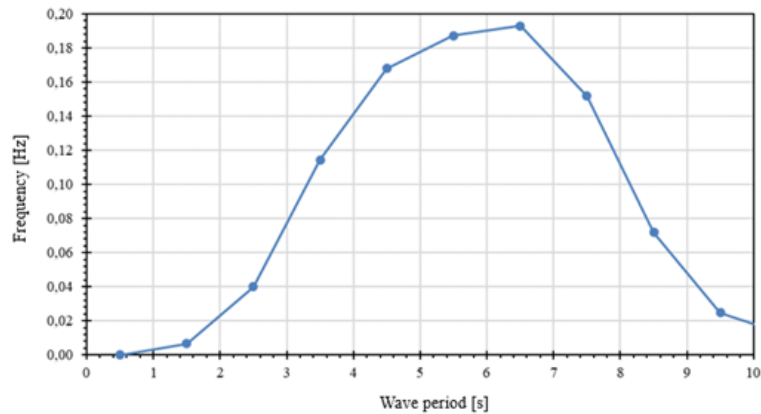
Figure 134. Mean wave period, Capo Gallo
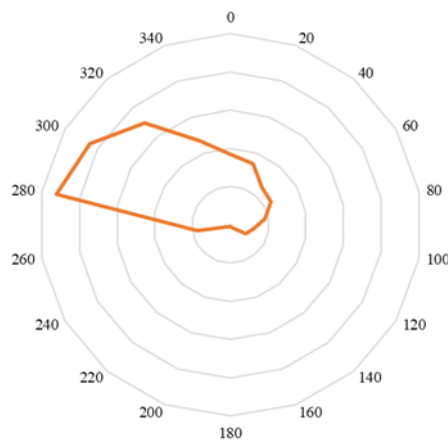
Figure 135. Mean direction of wave origin, capo Gallo

From the study of the database available for Palermo, it was possible to explore the following data:

- Significant height of 0,8 m.
- Wave period of 5,5 m.
- Origin of the wave from north-west with an angle of 300° from the north approximately.

After studying the characteristics of the sea, it was possible to start modelling work, building the geometry on Ansys. The coupled system is composed by a partially submerged central part, the cylinder, in which the linear generator could be inserted, and a totally submerged part, the ballast, which, appropriately sized, will serve to stabilise the entire system and keep it in an optimal position for energy extraction.

Since the cylinder-ballast system must be as stationary as possible, the geometry is optimised to minimise all translation and rotation movements. The optimum configuration for the system to be stable and not sink is shown in table 11.

Table 11.   Geometric parameters

	Value
Total mass [kg]	257761
Cylinder mass (kg)	2000
Ballast mass (kg)	23761
Thickness (m)	0,2800
Ray (m)	4
ZG (m)	-3,36
Izz (kg m2)	191088
Iyy (kg m2)	32774
Ixx (kg m2)	32774

Where ZG is the centre of mass and I the moment of inertia.

The simulations were based on Airy theory, see chapter 3.1.1, under the following conditions:

- Negligible wave height relative to wavelength and depth
- Uniform depth, smooth, and impermeable bottom
- Homogeneous, incompressible, and non-viscous fluid
- Coriolis force is neglected
- Surface tension is neglected
- Harmonic motion is assumed.

The field of validity of Airy's theory is, therefore, that of deep waters in which the entire water column is composed of circular orbits of decreasing diameter until they assume infinitesimal dimensions. The 3D geometry modelled of the coupled system is shown in figure 136, where the ballast is coloured in grey and the buoy in red.
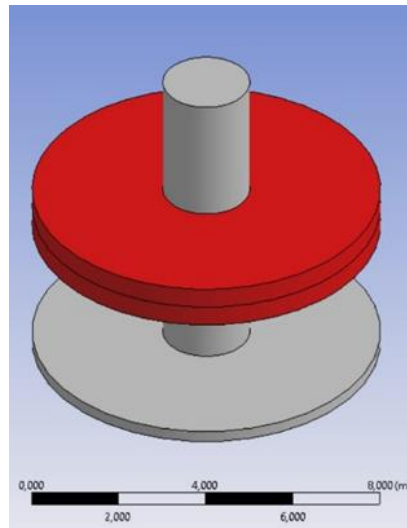
Figure 136. Coupled system object of simulation.

The goal of the simulations is to optimize the energy production. Despite in the table 11 are shown the optimal values to flotation of the system, in this phase, have been modified varying the geometry in scale. This approach shows the different value of energy producibility up to a limit value of buoy thickness beyond which it is not convenient to go. In tab 12 are listed the simulations.

Table 12.   Parametrized simulations

Thickness [m]	Mass [kg]
1	24151
0,9	21736
0,8	19321
0,7	16906
0,6	14491
0,5	12075
0,4	9660
0,3	7245

The mass-spring-damper system is the physical model with which it is possible to study the movement of a body with a certain mass, connected to a fixed point by means of a spring and a damper placed in parallel. A time-varying external force

(otherwise known as the external force) is applied to the mass, the course of which is a function of time. This model is the base of the power calculation in output. By analysing the output data, it was possible carried out the instantaneous power generated, for the simulation period of 60s and time-step of 0.1s, for the different configurations under consideration. The power can be calculated as in equation 81.

$$P_g = Fv \tag{81}$$

The force F will be that of the spring-damper system, while the velocity v is the relative velocity between the ballast and the buoy. By evaluating the average and maximum power, the maximum convenient thickness value can be seen in tab 13.

Table 13.   Output power during simulations

Buoy thickness [m]	Power [W]	
	Average	*Max*
1	3164,7	11901,6
0,9	3083,7	11917,1
0,8	2970,3	11703,0
0,7	2898,3	11554,5
0,6	2845,5	12067,1
0,5	2747,7	11711,2
0,4	2462,0	11405,0
0,3	2344,5	9995,4

Analyzing the data and the results obtained from the simulations, it can be seen that the configurations are all acceptable for the final purpose of the project, but the configurations with thicknesses varying from 0.8m to 1m are too massive, while those with thicknesses of 0.3m and 0.4m are not too heavy. Of the remaining options, the configuration with a thickness of 0.6m is the one that has stable behavior in all areas of analysis.

The simulations are carried out using the data of Italian wave network, in particular significant wave height from 0,5 m to 2 m and Peak wave period from 3 s and 9 s. the results have been parametrized forming a matrix in which is shown the average power related every couple of significant wave height and peak wave period. The

results are shown in table 14. Particularly interesting is the medium energy that the generator can produce, see table 15.

Table 14.   **Average power matrix [W]**

Significant wave height [m]	Peak wave period [s]						
	3	**4**	**5**	**6**	**7**	**8**	**9**
2	21186,8	15383,1	16224,8	12884,6	9687,7	9588,5	8318,4
1,5	9469,5	10992,4	7760,9	6340,1	5810,8	4778,9	3243
1	4824,4	5547,7	4102,8	3861,3	3036,8	1861,5	1368
0,5	1196,4	1489,8	1274,6	757,3	472,9	351,9	290,7

Table 15.   **Average energy matrix [kWh]**

Significant wave height [m]	Peak wave period [s]						
	3	**4**	**5**	**6**	**7**	**8**	**9**
2	11424,2	16628,2	19660,8	8043,4	7152,6	2114,9	486,2
1,5	126,4	2262,7	3135,7	4099,1	3555,8	816,2	260,6
1	0	29,1	308,2	706,6	1498,8	336,4	62,3
0,5	0	0	6,5	26,8	102,9	57,6	13,4

Analysing the results obtained, the potential of this type of system is very important, considering that a single WEC of this type can produce a large amount of energy. Despite the simplifications and approximations of the linear theory, it was possible to model a theoretically functioning system, ready for further study and optimisation for definitive implementation. From this data, it is possible to optimise an array of such generators in order to create a real energy production plant.

In the same way another study, carried out using the Ansys Aqwa software, was performed. The system object of the study is shown in figure. 137 and it is composed by:

- Wave energy captor is a cylindrical buoy tall 1 m and diameter 2.5 m.

- Power take-off (PTO) is composed by 3 linear generators.

- Connection between WEC and PTO through pulley and rope.
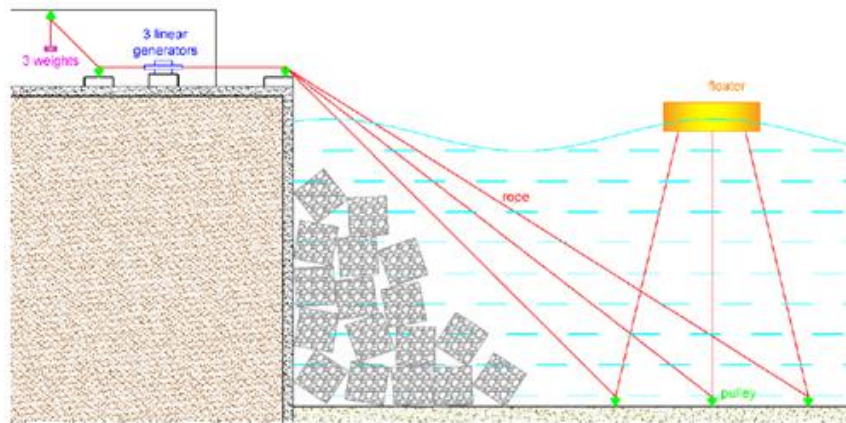
Figure 137. Working principle for the nearshore application of the WEC

As shown in the picture, a floater is used to collect the mechanical energy of wave. The movement of the buoy pulls three ropes, connected to the mainland through pulleys. In this way, the movement of the buoy is used to activate three linear generators (one per each rope). The buoyancy of the floater is compensated by weights installed in the opposite side of the rope, inside the machine room. This solution allows the reduction of the weight of the floater. At the same time, the proposed layout allows the possibility of completely submerging the buoy, in case of bad weather conditions, as a solution to make the system safe. As introduced above, the electrical energy is directly produced by linear generators[84]. The device was planned to be installed off the coast of Pantelleria, 110 km southwest of Sicily and 65 km northeast of Tunisia, see figure 138.

Figure 138. Island of Pantelleria

The characteristic sea data for this site were obtained from the Italian wave network buoy sited in Mazzara del Vallo, the closest survey site to the island. The significant wave eight and the peak wave period are shown in figures 139 and 140.
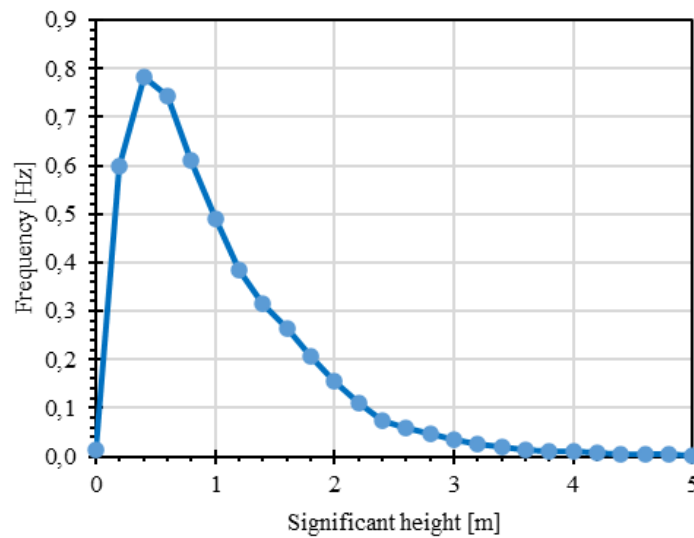
Figure 139. Significant wave height, Mazzara del Vallo
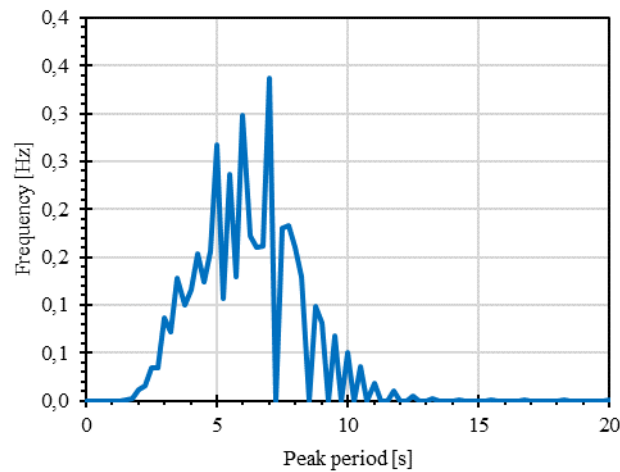
Figure 140. Peak wave period, Mazzara del Vallo

To choose an optimal orientation for the installation of the device in order to exploit the wave as much as possible and determine the stresses to which it would be subjected during its operation, the main wave direction is west and west-northwest shown in figure 141.
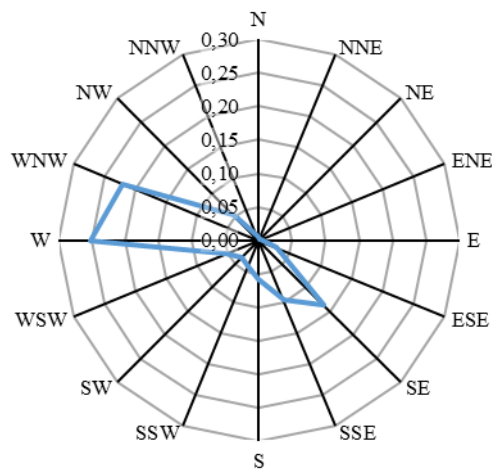
Figure 141. Main wave direction, Mazzara del Vallo

As in the first simulation, here the Airy's theory was implemented. The first step is the three-dimensional construction of the geometry under examination, which is carried out using the Design Modeler tool. The geometry consists of a cylinder generated by the extrusion of a circumference. The mean sea level is represented

by the section plane that divides the cylinder into two parts of equal height. The floater is shown in figure 142.
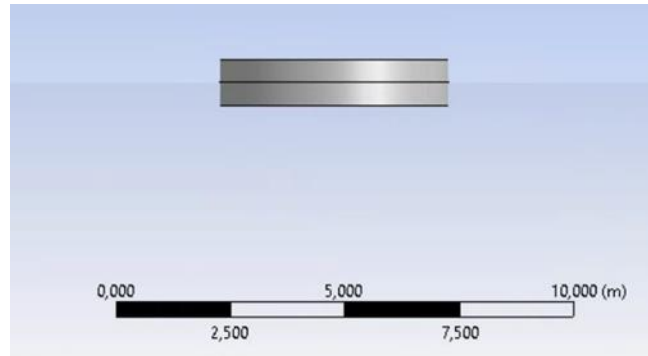
Figure 142. 3D floater model

To complete the WEC, the counterweight on the shore and the base on the seabed were added. Fig 143 describes the mechanical connection between the float, rope, pulleys, and PTO on land.
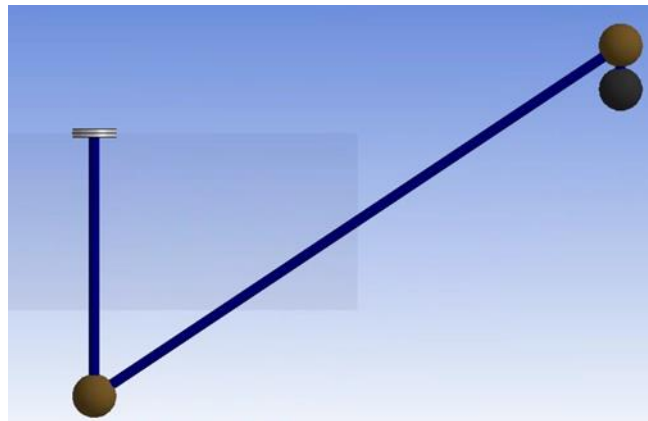
Figure 143. 3D connection between the WEC components

The database was analyzed by processing the data and then constructing the recurrence matrix, representative of the frequency with which waves with certain heights and periods were recorded. The most frequent condition occurs for a peak period of 5 s and a significant height of 0.5 m. The recurrence matrix indicating the number of occurrences can be transformed into a matrix indicating the annual equivalent hours in which a given sea state occurs. This makes it possible to calculate the normalized recurrence matrix, figure 144.

Significant height [m]	Peak period [s] - Equivalent hours per year [h/y]											
	1	2	3	4	5	6	7	8	9	10	11	12
0.5	0.0	75.1	538.7	772.6	805.2	684.7	363.2	213.4	70.4	18.8	0.0	0.0
1.0	0.0	0.0	29.9	362.1	459.4	723.7	412.3	209.2	122.9	52.9	0.0	0.0
1.5	0.0	0.0	0.0	18.4	166.4	408.7	417.3	224.3	104.5	40.8	0.0	0.0
2.0	0.0	0.0	0.0	0.0	17.6	157.1	251.2	216.7	77.0	20.2	0.0	0.0
2.5	0.0	0.0	0.0	0.0	0.0	22.8	82.7	125.2	78.7	0.0	0.0	0.0
3.0	0.0	0.0	0.0	0.0	0.0	0.0	24.0	61.7	66.4	0.0	0.0	0.0
3.5	0.0	0.0	0.0	0.0	0.0	0.0	0.0	20.2	37.3	0.0	0.0	0.0
4.0	0.0	0.0	0.0	0.0	0.0	0.0	0.0	0.0	0.0	0.0	0.0	0.0
4.5	0.0	0.0	0.0	0.0	0.0	0.0	0.0	0.0	0.0	0.0	0.0	0.0
5.0	0.0	0.0	0.0	0.0	0.0	0.0	0.0	0.0	0.0	0.0	0.0	0.0
5.5	0.0	0.0	0.0	0.0	0.0	0.0	0.0	0.0	0.0	0.0	0.0	0.0
6.0	0.0	0.0	0.0	0.0	0.0	0.0	0.0	0.0	0.0	0.0	0.0	0.0

Figure 144. Equivalent hours per year for each sea state

For each sea state shown in the recurrence matrix, simulations were performed in order to derive the damping coefficient that maximizes the average power output. The device was then optimized. The average power output was derived for different damping coefficients until the maximum attainable value was found. The annual producible energy was then derived, as shown in figure 145.

Significant height [m]	Peak period [s] - Annual energy production [kWh/y]											
	1	2	3	4	5	6	7	8	9	10	11	12
0.5	0.0	12.5	388.7	559.6	489.5	357.9	165.6	87.1	25.8	6.5	0.0	0.0
1.0	0.0	0.0	58.0	681.2	629.9	808.9	405.5	282.7	93.8	38.2	0.0	0.0
1.5	0.0	0.0	0.0	52.4	366.2	710.5	645.6	301.2	122.3	45.6	0.0	0.0
2.0	0.0	0.0	0.0	0.0	52.6	365.0	528.6	397.8	120.1	30.3	0.0	0.0
2.5	0.0	0.0	0.0	0.0	0.0	64.2	211.6	280.7	156.0	0.0	0.0	0.0
3.0	0.0	0.0	0.0	0.0	0.0	0.0	74.6	168.5	161.4	0.0	0.0	0.0
3.5	0.0	0.0	0.0	0.0	0.0	0.0	0.0	63.7	100.9	0.0	0.0	0.0
4.0	0.0	0.0	0.0	0.0	0.0	0.0	0.0	0.0	0.0	0.0	0.0	0.0
4.5	0.0	0.0	0.0	0.0	0.0	0.0	0.0	0.0	0.0	0.0	0.0	0.0
5.0	0.0	0.0	0.0	0.0	0.0	0.0	0.0	0.0	0.0	0.0	0.0	0.0
5.5	0.0	0.0	0.0	0.0	0.0	0.0	0.0	0.0	0.0	0.0	0.0	0.0
6.0	0.0	0.0	0.0	0.0	0.0	0.0	0.0	0.0	0.0	0.0	0.0	0.0

Figure 145. Annual energy production for each sea state

The following figure 146 shows the energy production for one year.
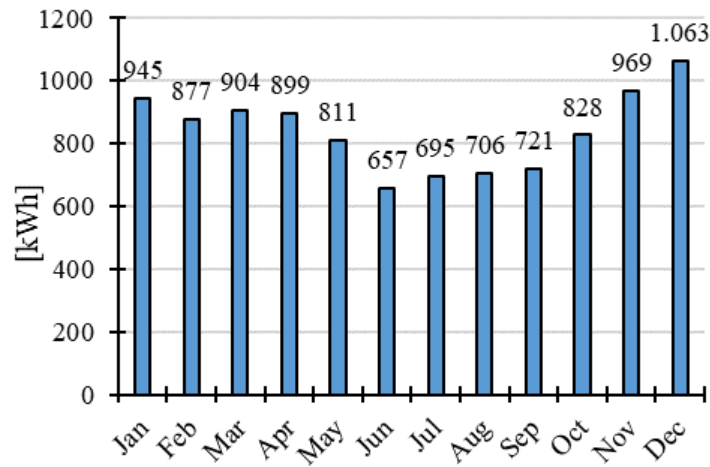
Figure 146. WEC energy production for 1 year

Thus, the devices can produce about 10 MWh/y in the test site of Pantelleria. In conclusion, the size of the WEC device is strongly influenced by the characteristics of the incident wave at the site where such a structure is to be built. The ideal installation for a system of this type is on small islands, where the energy demand is low compared to the energy availability of the marine source, which would make these contexts more sustainable without visually impacting them, which are often subject to stringent architectural and landscape constraints.

4.5 Economic analysis and impact evaluation

4.5.1 Economic analysis

The economic feasibility was carried out simulating a WEC farm composed by the second technology presented in the 4.4 paragraph. The aim is to produce about the 10 MWh/y calculated near shoreline in Pantelleria island. To study economic feasibility, the Discounted Cash Flow is calculated for a scenario with a linear generator as PTO and a system that is anchored in sandy seabed. The discounted cash flow is calculated using the following equation 82[85]:

$$DCF = -I_0 - \sum_{i=1}^{n} \frac{I_i}{(1+\tau)^i} + R \sum_{i=1}^{n} \left(\frac{1+\varepsilon}{1+\tau}\right)^i \qquad (82)$$

Where:

- I_o is the initial investment cost.

- I_i are the annual operating and maintenance costs.

- τ is the interest rate.

- ε is the interest rate in the energy sector.

- n represents the number of years elapsed up to the year under consideration.

- R, the loss of expenditure on electricity if it were produced by the power plant.

The investment costs are shown in the table 16, while the operation and maintenance costs of the farm are shown in the table17.

Table 16.   Investment costs

	Unitary cost		Quantity	Total cost
Buoy	1,2	€/kg	9557,8	137.632,32 €
Mooring (pulley, ropes)	125	€/kW	5	7.500,00 €
underwater foundation	300	€/m3	0,75	2.700,00 €
ballasts	1,5	€/kg	500	9.000,00 €
Linear generator	2200	€/kW	5	132.000,00 €
Installation costs	35	€/kW	5	2.100,00 €
Electrical grid connection	71,32	€/kW	5	4.589,20 €
Electric control panels	18	€/kW	5	1.080,00 €
Engine room	2350	€/cad.	12,5	29.375,00 €
Total investment				**325.976,52 €**

Table 17.   Operation and management costs

	Unitary cost		Quantity	Total cost
Maintenance	55	€/(kW-year)	5	3.300,00 €/y

To complete the DCF has been considered:

- Electrical energy production 10111 [kWh/y].

- Interest rate τ 1%

- Energy rate ε 3%

- Discount rate Currency 0,99

- Discount rate Energy 1,02

The lost electricity cost is derived by multiplying the total sales cost by the energy produced annually by the farm. As far as the cost of electricity is concerned, reference is made to the Single National Price (PUN in Italy - Prezzo unico Nazionale), which to date is an extremely aleatory parameter, and one that is constantly rising. The PUN has reached values of 450-550 €/MWh and to show the effects this value has on the investment, a sensitivity analysis was carried out, which shows how the breakeven time varies as the value of the PUN varies. The payback Time is the time required for the discounted cash flows generated by a project to equal its initial cost. The useful lifetime for wave energy plants is not yet well known but has been assumed to be 15 years. The payback time has been calculated varying PUN from 150 to 450 €/MWh, see the following table 18 and figure 147.

Table 18.   Payback time table

PUN [€/MWh]	Payback time [y]
150	17,32
250	10,54
350	7,57
450	5,9
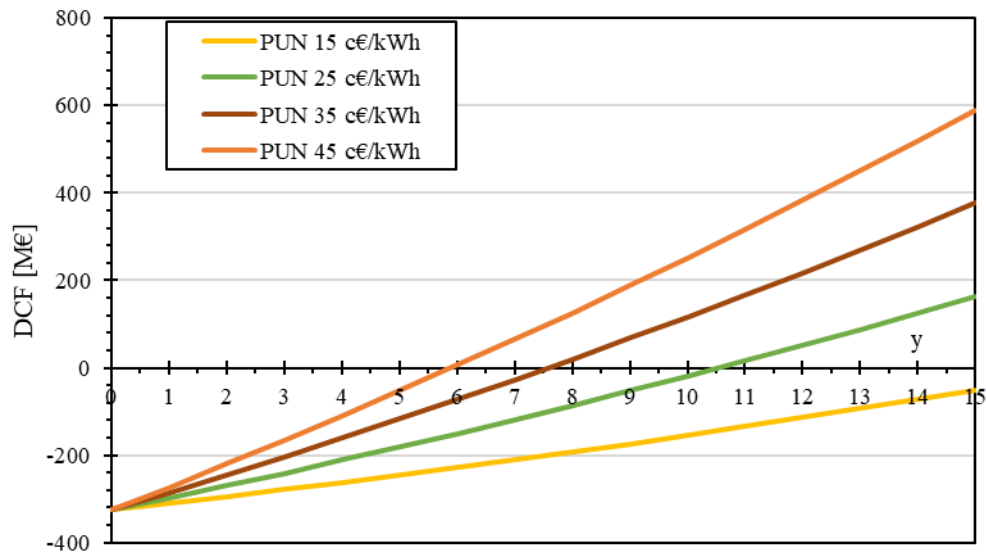
Figure 147. Payback time figure

From the economic analysis, we can deduce that for the assumed lifetime, the investment is not profitable for a PUN of 150 €/MWh and consequently for values lower than this. In the case of a price of 250 €/MWh, there would only be a gain for a few years, which leads us to consider the investment profitable only if supported by possible incentives proposed for developing technologies.

If the single national price reaches values of 350-450 €/MWh or higher, the investment can be made without the need for further incentives.

Considering the same parameters as above, it is possible to calculate the LCOE parameter, levelized cost of energy. This parameter represents the average revenue per unit of electricity generated needed to recover the construction and operating costs of a generation plant over an assumed operating life. The LCOE is often cited as a summary measure of the overall competitiveness of different generation technologies. Key inputs for calculating the LCOE include capital costs, fuel costs, fixed and variable operation and maintenance costs, financing costs and an assumed utilisation rate for each type of plant. The LCOE can be calculated according to equation 83.

$$LCOE = \frac{\frac{I_0}{\Sigma(1+\tau)^i} + M}{E} \tag{83}$$

The obtained value around 280 €/MWh it is an high value compared with photovoltaic (48 €/MWh) in 2021[86]. The development of the proposed technology could reduce the costs for the realization of all components, improving the LCOE up to achieve the values of other renewable energy sources.

4.5.2 Environmental impact

Not much information can be found in the literature on the impacts of WEC exploitation. The lack of data lies in the fact that these devices are still in the development phase and not many installations have been realised so far, as shown in state of art section almost only power pilot power plants have been built. However, with the growth in the number of projects and the increase in the number of prototypes, the environmental impact aspect has begun to attract interest. Since all forms of power generation have consequences for the environment, the perceived environmental effect of converting energy from the waves of the sea is small compared to other energy sources, especially about air emissions. In fact, WECs do not emit gas, liquid or solid into the atmosphere under normal operating conditions and are therefore virtually no sources of pollution. This type of device can still cause environmental impacts. The main consequences vary depending on the type of resource and technology[87]. Long-term studies are needed because the impact of human activities on the ecology of an area occurs slowly, and it is not easy to make predictions. Furthermore, studies of marine environments, especially in the open sea and deep water, are usually very expensive and require advanced underwater technologies. Potential environmental impacts are listed:

- Against animals, underwater noise emission, collisions against devices, vibrations, electromagnetic fields, could create danger.
- Underwater environments, seabed modification.
- Coastline modification.

- Visual impact.
- Oil and lubricant leakage risk.

The use of fixed or mobile wave energy conversion devices can change the size and frequency of waves, as well as affect tides and drift currents. In particular, fixed devices alter the wave regime more significantly than mobile devices; the consequence is a change in coastal composition and sedimentation. The nature of coastlines and shallow water areas is affected by the reduction of wave energy, affecting aquatic flora and fauna.

Once installed, the devices can become substrates for biological systems, on which a variety of algae and invertebrates can attach themselves. This phenomenon is called biofuling. If the biological aspect is considered, this could be a positive as it contributes to species richness and diversity but could become a negative aspect if it reduces device durability and efficiency. There is certainly an additional burden from a maintenance point of view, especially for those devices placed in the open sea. Efficiency problems could affect devices such as buoys more as organisms can alter the weight and shape. Studies conducted within the Lysekil project in Sweden show that for a 3 m diameter buoy, 150 kg of fouling can be created[88]. The most economical solution would seem to be to size the buoy with this phenomenon in mind and thus avoid the use of substances capable of inhibiting it, i.e. to ensure that biofuling does not affect the buoy's lifting force.

Noise impact can occur both above and below sea level. Each converter emits noise caused by different factors, such as mechanical components (turbines, generators, pumps, cylinders, etc.), cavities, vibrations, and the fact that water and waves hit the device. It is necessary to identify the frequency spectrum of noise because the effects are different depending on the frequency at which they occur. The problem of noise pollution has an impact especially on marine mammals because it interferes with the communication system of these animals and in that of perceiving danger or obstacles. For plants working above the sea surface, noise pollution is due to the expulsion of air from the turbine or when it is pumped inside the turbine, as in

OWCs. The sound wave can propagate over long distances, disturbing the communication systems of some mammals, such as dolphins, whales, and seals, but also various species of fish. Certainly, the fauna's acoustic system is accentuated during the installation phases if these involve, for example, drilling and laying cables; while for the long-term effects, there is still no certain data on the consequences caused to marine populations. Noise mitigation can be achieved by varying the anchoring cables of the devices so that they do not produce synchronous noise at low frequencies, or by including internal noise-absorbing systems such as sound-absorbing panels in the design of the device.

The problem of the electromagnetic field produced, can be solved by burying them. But it increases the cost and creates destruction and modification of the seabed, producing a considerable environmental impact. The worst limitations of tidal power plants are in the high environmental impact, in terms of building large infrastructures and coastal erosion risks. A less impactful way of using tidal energy is to exploit the underwater currents caused by the tides. In this way, it is possible to build plants partially or totally submerged in water and without dams. The absence of dams and impactful infrastructure, thanks to the partial or total immersion of the turbines in the water, minimises the environmental impact of these plants. The arrangement of structures and foundations can affect the speed of flow by modifying erosion or sediment deposition, which can reduce or increase this phenomenon by creating shoals or alterations to the morphology of the coastline.

The visual impact is greater for installations installed at the coast or for installations which, although offshore, have a considerable share of the emerged part. A further visual impact is related to navigation signalling devices: lights, sound signals, radar reflectors.

Pipe fouling generated by seawater at coastal power stations is controlled by electrolytic injection of chlorine. Adverse effects may occur if chlorine is reacted to form chlorinated organic compounds that tend to accumulate and persist in the environment, although this seems unlikely to happen in open water.

Further impacts may occur during the installation phase of the devices, especially during the placement of foundations, during which particles of solid material may be released. These affect the feeding behaviour of fish; moreover, living creatures living on the seabed may be buried as a result of the placement of structures on the seabed.

Devices characterised by moving parts (such as paddles) could collide with marine fauna. Rotation at low speed can be predicted by fish both acoustically and visually; it is a different case when fish, during migratory phases, get carried away by ocean currents. It is important that devices do not impede the migratory paths of different species. Large areas covered by buoys, for example, can become barriers for migrating species. The problem lies in the fact that the paths followed by fish and marine mammals are unpredictable as they are susceptible to currents, season, regional and local climate, and the arrangement of food resources.

Cables for electrical transmission are usually made of overhead lines to avoid excessive installation and maintenance costs. In addition to causing visual impact, overhead lines can be an obstacle for birds, especially those following migratory routes, or they can obstruct nesting sites.

Installations may also obstruct other activities at sea, such as fishing, farming, tourist or industrial navigation, and oil platforms. For this reason, these kinds of devices should be appropriately signalled, not only with buoys or signalling devices, but by marking them in digital and paper maps.

The device under consideration has minimal environmental impact. It produces no emissions of climate-changing gases, solids, or liquids in any way, also due to the absence of hydraulic devices requiring oil. The absence of underwater connection cables avoids erosion of the seabed or the generation of electromagnetic effects that disturb fauna. In the case of Pantelleria, there is a minimal alteration of the seabed necessary to anchor the pulleys, but there is no need for a base that could cover the existing flora on the site. The shoreline device may cause a slight visual impact, especially due to the presence of the PTOs placed on the shoreline; the buoys have a reduced emerged height, but the farm may be intrusive. The Pantelleria diesel

plant consists of 8 diesel generators, with a total installed capacity of about 23 MW[89].

In 2018, the thermal power plant consumed around 8000000 kg of diesel and produced 39000000 kWh[89]. Comparing these two values gives an average unit consumption of 0.2 kg/kWh. Considering the farm energy producibility of 10000 kWh the diesel consumption saving is around 2000 kg/year. This result, added to green energy production from PV, and wind technology could save in the future more diesel consumption.

The use of wave devices does not produce any greenhouse gases or air pollutants. For a correct comparison with other technologies that produce energy from renewable sources, and therefore for a correct LCA study (Life Cycle Assessment), the emissions produced in the production and installation phases of the device should be considered.

5. Energy storage

The term energy storage refers to a storage system consisting of a set of devices, management, and control equipment functional for the absorption and release of electrical energy. These energy storage systems can be installed on different types of plants powered by renewable sources. The different types of energy storage can be classified into the following categories [90]:

- Thermal storage, involve the storage and release of heat or cold, in a liquid or solid to give energy on demand. A Thermal Energy Storage System usually consists of a series of tanks, thermally insulated, that contain a heat transfer fluid, which is a substance that can transfer heat from one source to another. This fluid is heated by a renewable or not energy source, such as a solar panel or gas boiler, and then stored in the tanks until it is used. Thanks to this mechanism, it is possible to store the thermal energy produced during the peak production hours and use it when there is less availability of the source. In the same way cold storage systems are devices used to store cold thermal energy, that is, to store cold produced by refrigeration sources or air conditioning systems. These systems are used in various sectors, such as the food or pharmaceutical industry.

- Mechanical storage uses kinetic or gravitational energy to store electricity. Mechanical systems include some key technologies in managing the non-programmability of RES: pumped hydro systems (PHS), compressed air systems (CAES) and flywheel energy storage (FES).

- Hydrogen storage, in this family the electrical energy can be used to fuel an electrolyser to produce hydrogen. As shown in 2.3 paragraph of this thesis.

- Electrical storage.

In recent years, the concept of energy storage has developed greatly. Storage systems in the recent past were used mainly for small mobile devices. Since renewables technology have taken a large share of the electricity market, it has

become necessary to manage the feed in. Storage systems play a key role in this field. They can improve the stability of the electric grid by balancing the generation of energy from nonprogrammable renewable sources and the much-distributed generation due to domestic systems. The classic balancing system between power fed into the grid and consumed involves the use of active systems that control grid frequency and voltage. The use of batteries, on the other hand, involves the possibility of regulation with static systems. In general, this approach could be a solution for balancing demand and production in small islands or all those stand-alone utilities. One application in which storage systems potentially can generate benefits is with residential users who own a home photovoltaic system. The benefits that can result from increasing of so-called "self-consumption" or "prosumer" that is, the fraction of energy generated and consumed/stored instantaneously by the same user, can be high. In this way if the produced energy is instantaneous consumed the electric grid is not overcharged. Many storage technologies are studied. One classification frequently adopted in the literature refers to the specific form of energy and distinguishes storage systems into:

- Electrochemical storage
- Mechanical storage (pumping hydroelectric reservoirs)
- Electrostatic storage (supercapacitors)
- Chemical storage (hydrogen)
- Electromagnetic storage (superconductive magnetic energy storage).

All these technologies have in common the following parameters:

- Capacity [Ah]: amount of electrical charge that can be extracted from the system during discharge
- Energy [Wh]: energy that the system provides during discharge, starting from a fully charged condition to a fully discharged condition, given by the product of the capacity for the voltage of the accumulator
- Energy efficiency: ratio of energy discharged to energy expended to return the storage system to its initial state of charge

- Lifespan: operating time of the accumulator, which ends when system performance degrades below operational limits. This parameter can be expressed in years or in charge-discharge cycles

- State of charge (SOC) [%]: amount of charge present in the accumulator, related to a reference value most often coinciding with the rated capacity

- Depth of discharge (DOD) [%]: amount of charge in Ah delivered by a fully charged accumulator, related to its rated capacity

- Cost: considerable in €/kWh or €/kW.

Another key role played by storage is to serve special electrical systems. Under the condition of a grid failure connection, storage comes into action, replacing it. For example, commercial activities where the tills are all connected to the central server would crash if a power failure occurred. Or if the grid connection is lost in a utility where emergency lighting is present it is supplied by an appropriately installed and sized storage. These categories of storage are classified in this way:

- Very short duration storage applications, Uninterruptible power supply (UPS): include storage systems capable of intervening in a very short time, albeit with limited power levels, to support the voltage quality of privileged utilities, see the following figures

Figure 148. UPS systems

- Grid transient support applications for load/production shifting and subsequent increase in self-consumption. The storage system installed in a renewable energy plant enables self-consumption of the energy produced and stored, during the hours when the source is available, in hours when that source is not available, but the load is present

- Grid support applications. Fall into this category, large power installations supporting voltage and frequency regulation of the grid. They thus play a role similar to that offered by conventional thermoelectric plants.

5.1 Electrochemical accumulators

Electrochemical accumulators are the most widely used technology capable of directly converting chemical energy into electrical energy. The operation of these devices is based on the processes of oxidation-reduction and electrolysis that result in reversible conversion of chemical energy into electrical energy. They consist of a structure composed of two half-cells separated by a porous septum, each of which contains a metal electrode (anode and cathode) immersed in electrolyte solution.

Through oxidation-reduction reactions, the anode oxidizes and gives up electrons to the cathode, which reduces; the generated electron flow is subsequently captured by a conductor. The many types of accumulators differ in the electrochemical species between which the reaction takes place, the type of electrolyte, and the construction characteristics. Their great advantage is the modularity. The main types of electrochemical accumulators are:

- The accumulators with aqueous electrolyte, which include the lead acid accumulator. Lead-acid accumulators consist of a lead electrode and a lead dioxide electrode immersed in an aqueous solution of sulfuric acid. Lead-acid accumulators can be open or hermetic. The formers are characterized by the presence of openings that allow gases produced during charging to escape and are widely used in stationary and traction applications. Hermetic accumulators are popular due to the fact that they require less maintenance, less space, and don't emit gas

- Electrolyte circulation batteries. This category involves the use of a graphite anode and a cathode composed of lithiated metal. They can store electrical energy in electrolyte solutions using coupled oxidation-reduction reactions in which both reactants and reaction products are dissolved in solution. Flow batteries are composed of a core called a stack, consisting of a number of elementary cells connected in series

- The high temperature batteries (sodium/sulphur). This storage family include the ZEBRA Zero Emission Battery Research Activities. Such batteries operate at a temperature of about 300°C, which is necessary to keep the electrodes in a molten state and to increase the conductivity of the electrolyte. The average life of this type of device is longer than that of lead-acid batteries, but because of the high operating temperature, appropriate safety systems must be provided;

- Lithium-ion batteries. Lithium/ion batteries have many variations and are characterized by high specific power, which is why they are also widely

used in electric traction, and in all portable electronics components. Their great disadvantage is the risk of explosion in case of overheating. There is a great deal of research in the field of lithium cells, with goals such as improving and developing new materials, increasing performance, expected life, and reliability. Among the aims pursued in research and development activities is that of increasing cell capacities. At moment, most lithium battery production is absorbed by the consumer electronics market, so the cells produced are small. However, the prospect of using the cells for electric vehicle propulsion and in the electric system has led some manufacturers to develop cells of medium to large size. Lithium-ion batteries have a specific energy of up to 180 Wh/kg, corresponding to an energy density of 270 to 380 Wh/l (the highest among all electrochemical storage systems).

The level of technological maturity of electrochemical accumulators varies according to the specific battery type. In general, electrochemical accumulators, given the wide range of sizes in which they are available and their considerable flexibility, occupy a significant space within the global market for storage systems. Although they have reached a good maturity both technologically and commercially, they are still the subject of research activities aimed at improving their performance. In particular, efforts are being made to increase battery lifetime by studying new types of electrodes, on the estimation of battery state of charge, and on the development of management systems. Lead-acid batteries are heavy and bulky and, for that reason, are about to be surpassed by lithium-ion. The latter, albeit with a slightly lower level of technological maturity, are rapidly gaining popularity in energy applications. Given their better performance in terms of durability, efficiency, and energy density, in fact, lithium-ion batteries are now the most popular storage system for residential PV and electric vehicle-related applications. The environmental impact of batteries related to the end of life of storage systems, depends on the technology. Disposal of electrochemical accumulators is mandatory and the responsibility of the manufacturer; the cost of disposal affects the selling

price of the product and changes depending on the specific technology. Lead-acid batteries have a very low cost of disposal, and at the end of their life they must be handed in almost entirely recycled (more than 90 % of the constituent material of the battery can be recovered, which can be reused to make more).

Nickel/cadmium technology has the worst environmental impact, as cadmium is a highly polluting material.

For lithium-ion batteries, procedures for recycling the materials of which they are made, such as rare earths, metals, and lithium itself, have been developed, but these are not yet widely applied given the lack of economic viability associated with recovery. In general, one of the weak points for electrochemical storage systems, is the speed of charge and discharge, in fact batteries cannot be charged or discharged at any power, but precise current parameters must be respected (especially for lithium batteries), beyond which the cells would suffer irreversible damage up to the danger of explosion. A second problem is degradation over time, regardless of hours of use. Another less impactful but still binding problem is the working temperature; lithium batteries, for example, cannot work at temperatures below 0°C.

5.2 Mechanical accumulators

This kind of storage is divided essentially into three categories[91]:

- Compressed air energy storage
- Flywheel
- Pumping water storage.

Pumped water storage systems find large-scale application for balancing the national power grid. These systems normally consist of two reservoirs placed at different elevations, a pump that lifts water to the higher elevation reservoir in such a way as to accumulate electrical energy in the form of hydraulic potential energy when there is no peak energy demand, a turbine that generates electricity when the water returns to the lower elevation reservoir, converting the potential energy into

electrical energy during peak hours. The amount of energy that can be stored is proportional to the difference in elevation between the two reservoirs and the volume of water stored[92]. A typical power plant is shown in the following figure.
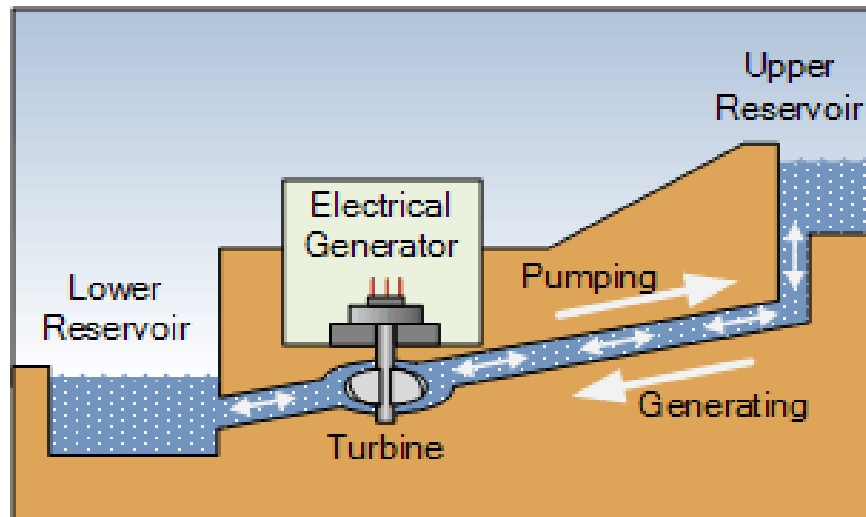
Figure 149. Pumped storage power plant

Water storage by pumping is a mature technology, thanks to decades of operational experience. Therefore, no major technological improvements in terms of cost, structure, or processing efficiency are expected in the coming years. Such storage technologies make use of all the experience gained in hydropower plants. However, it should be considered that the implementation of storage systems by large-scale pumped storage, requires large spaces and special land morphologies, both in terms of altitude and soil type, although easier to implement than hydroelectric plants. From the point of view of environmental and landscape impacts, water storage by pumping, involves strong attention and study of impacts on the surrounding flora and fauna. The reservoirs involve high engineering work necessary to create large volume dams and barrages.

5.3 Electrostatic storage

Supercapacitors, known as electrochemical capacitors, have been developed mainly in recent years and belong to the category of electrostatic-type accumulators. Their physical structure is characterized by the presence of two electrodes immersed in

an electrolyte solution and separated by a permeable membrane. Unlike electrochemical accumulators they are characterized by porous-type electrodes, which have a larger useful surface area. Unlike ordinary capacitors, their structure allows high energy storage[93,94].

Classic batteries are characterized by high energy density and low power density and are, suitable for slow charge and discharge processes (duration of hours). Instead, conventional capacitors, have low energy density and high-power density and can be used in extremely fast charge and discharge processes (duration of fractions of a second). Supercapacitors, because of their intermediate characteristics of energy density and power density, are suitable for charge-discharge processes of durations around one minute. Supercapacitors can be classified according to the materials used to make up the electrodes, (carbon, metal oxides, polymers) or by the type of electrolyte used (organic, aqueous). The most widely used electrodes are carbon-based electrodes, which are characterized by low cost, high surface area, wide availability, high polarizability, and finally made with a well-established production technology process. Carbon electrodes can be divided into two types, those based on activated carbons, powders, and fabrics, and those based on nanostructured carbons such as nanotubes.

The most common and commercialized are those based on activated carbon, which are relatively inexpensive and have high surface areas. Nanostructured ones are characterized by higher porosity with pore sizes as small as 2 nm but are more expensive and with capacities ranging from a few farads up to thousands of farads per cell.

Metal oxides are an advantageous alternative to carbon because of their low resistivity and high specific capacitance such that capacitors with high energy density and high-power density can be constructed. Metal oxide electrodes, however, suffer from high production costs and low cell voltage ratings (1 V). Some studies have suggested the use of conducting polymers to make electrodes. Polymers accumulate or release electrical charge by oxidation-reduction reactions. In the oxidation reaction, ions are transferred into the polymer matrix, while in the

reduction reaction, ions are released into the solution. With conducting polymers, charge accumulation occurs in the entire volume of the electrode and not only on the surface as with carbon. This characteristic allows high values of specific capacitance to be achieved. Rather high values of power density and energy density have been reported for supercapacitors with polymer electrodes. However, contraction and expansion of the polymer during charge-discharge operations can lead to structural deterioration. The energy density of supercapacitors is very low compared with that of electrochemical accumulators, but their specific power output is very high. This, combined with the rapidity with which they can be charged and discharged over a large number of cycles, makes the components particularly suitable for applications that require the delivery of high power for short periods, from a fraction of a second to a few minutes. In the following table are shown the main differences between electrochemical and supercapacitors technologies.

Table 19.   Comparison between electrochemical and supercapacitors

Technical features	Electrochemical accumulators	supercapacitors
Specific power [W/kg]	6-300	5000
Specific energy [Wh/kg]	30-45	4-5
Lifespan [cycles]	500	500000-1000000
Charging time	Hours	Seconds
Self-discharge time	Months	Days
Efficiency	0.7-0.9	0.95

Specifications provided by the manufacturers indicate that the accumulator allows full depth of discharge (up to 99%), rapid charge/discharge cycles, and functionality at low and high temperatures (-30°C to 85°C) all without compromising capacitor performance and lifetime. The absence of electrochemical processes, typical of classical batteries, safeguards supercapacitors from rapid aging and ensures 500,000 charge-discharge cycles with a minimum lifespan of 10 years, with no change in capacity as a function of time. The disadvantages of this technology are

the low specific energy values of 40÷60 Wh/Kg, where instead lithium batteries easily reach 100÷250 Wh/Kg. These technologies are currently used in the field of electric or hybrid traction, coupled with battery or fuel cell systems, for the purpose of providing peak power at startup or during sudden acceleration and for energy recovery during braking. In addition, supercapacitors can be coupled to renewable source generation systems, with the aim of compensating for fluctuations in generated power due to the randomness of the primary source, improving the quality of generation[93]. They are particularly suitable for power quality applications, where storage systems are used to improve the quality of supply and ensure the goodness of the supply voltage waveform, and for supplying loads that are particularly sensitive to even slight anomalies in the supply voltage. Applications of supercapacitors in the transportation sector are very promising. Numerous studies are underway for applications in electric or internal combustion vehicles, trains, and subways[95]. The goal is to recover energy dissipated during braking. Supercapacitors, in this case, are the most suitable technology because of their specific power characteristic. Storage systems using this technology are often used in pilot projects, with the aim of evaluating their ability to provide ancillary services to the power grid. The development of this technology is highly dependent on the research that goes into the materials used for the electrodes and electrolyte. These devices have a low level of deployment due to their very low autonomy. The environmental impact potential of the technology is mainly related to the production of systems and the eventual disposal of the solvents contained in the organic electrolytes, which have a level of toxicity comparable to that of the solvents in Lithium/ion batteries.

5.4 Chemical storage

As discussed in section 2.3 of this thesis paper, hydrogen is the most abundant element in the universe, and its use as an energy carrier has gained interest in recent decades. The hydrogen molecule (H_2) is endowed with high stability at environment temperature, however, in its atomic state (H), hydrogen is characterized by high

reactivity and therefore must be used appropriately. The low energy content of hydrogen per unit volume makes its storage particularly complex. Several physical and chemical methods are being investigated for hydrogen storage: pressurization at high pressures (700 bar), liquefaction and storage in cryogenic tanks (-252°C), adsorption on materials with high surface area (T<700°C), adsorption in interstitial sites (ambient temperatures and atmospheric pressure), formation of chemical compounds in which hydrogen participates in ionic and covalent bonds (atmospheric pressure), and oxidation of reactive metals with water. Although a system was already developed in the 1980s that intended to push into research and development, in the following years due to little funding the technology did not spread.

5.5 Case Study in island of Pantelleria

The use of storage systems finds application in the very current research area of small islands. In this case study first, the optimal renewable energy mix that can minimize the levelized cost of energy (LCOE) for the island's generation system was evaluated. After this characterization the inertial response of diesel generators is calculated for one year to characterize his intervention varying the optimum renewable energy mix. Finally, the rated power and capacity of a battery energy storage system (BESS)[96] is calculated to compensate the reduction of the inertial response in the power system thanks to a suitable synthetic inertia control. Pantelleria is an Italian island sited at west of Sicily and north-west of Tunisia in the Mediterranean Sea, see the following figure.

Figure 150. Pantelleria island site

In this context, the present research proposes a methodology for sizing battery energy storage systems (BESS) able to provide synthetic inertia, in replacement of the missing rotational inertia of the diesel generators. The provision of synthetic inertia is a specific control of power converters characterized by a rapid absorption or injection of electrical power proportional to the frequency derivative, in a way which emulates the natural behaviour (inertial response) of rotating mass in synchronous generators.

First step was evaluating the minimum LCOE considering the energy mix scenario composed by solar, wind, sea wave and geothermal energy sources. The exploitation of the solar source can be performed by using commercial silicon photovoltaic panels with the following characteristics:

Table 20.   PV panels features

Number of cells per panel	96
Maximum power rating	330 Wp
Max. Power at NOCT	251.9 W
NOCT	44 °C
Open circuit voltage	69.7 V
Short circuit current	6.07 A
Module efficiency	19.70 %
Temperature Coefficient (Pmax)	0.258 %/°C

Temperature Coefficient (Voc)	0.164 V/°C
Temperature Coefficient (lsc)	3.34 mA/°C
Dimensions	1590x1053x40 mm
Weight	19 kg

The wind turbine commercial technology is used with these characteristics:

Table 21. **Wind turbine features**

Nominal power	250 kW
Cut-in wind velocity	2.5 m/s
Nominal wind velocity	9 m/s
Cut-off wind velocity	32 m/s
Rotor diameter	42.5 m
Generator	Synchronous permanent 400V/50Hz
High	28 m

The technology used to exploit sea wave energy was a point absorber device composed by floated buoy and linear generator and mooring system.
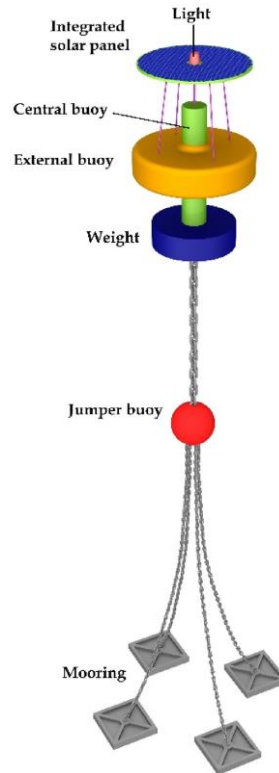
Figure 151. WEC device

To evaluate the energy production from each natural source, the following equations are introduced. In detail, the specific annual energy production from photovoltaic panels e_{pv} is calculated by summing all the corresponding monthly energy productions, according to Equation 84.

$$e_{pv} = \sum_{i=1}^{12} e_{pv,i} = \frac{1}{P_{pv,rated}} \sum_{i=1}^{12} I_{T,i} S_{pv} \eta_{pv} t_{d,i} \tag{84}$$

Where $I_{T,I}$ is the monthly average daily solar radiation, S_{pv} is the surface of the PV plant, η_{pv} is the average efficiency and $t_{d,I}$ represents the number of days per month. Finally, $P_{pv;rated}$ is the rated power of the photovoltaic plant.

To evaluate the annual specific energy production from wind turbines e_w was used the equation 85. The number of hours $t_{j,I}$ was evaluated when a discretized value of wind speed v_j was measured. This equation can be used if the power output function of wind speed for the chosen wind turbine $\psi <v_j>$ is known.

$$e_w = \sum_{i=1}^{12} e_{w,i} = \frac{1}{P_{w,rated}} \sum_{i=1}^{12} \sum_{j=1}^{n} \psi \langle v_j \rangle t_{j,i} \tag{85}$$

To evaluate the energy production of WEC can be used the formula depending significant wave eight H_s, energy period T_e, ρ_w is seawater density. The following equation 86 shows the energy production of wave energy converter.

$$\varphi_i = \frac{\rho_w g^2}{64\pi} H_s^2 T_e \tag{86}$$

The electrical energy production can be calculated with equation 87, where $P_{sw,\,rated}$ is the rated power of the Wave Energy Converter, φ_i the monthly average sea wave energy flux, d_c the diameter of the WEC, η_{sw} the average electrical energy efficiency, η_{hy} the hydraulic efficiency of the power take off and $t_{h,i}$ the number of hours in the i-th month.

$$e_{sw} = \sum_{i=1}^{12} e_{sw,i} = \frac{1}{P_{sw,rated}} \sum_{i=1}^{12} \varphi_i d_C \eta_{sw} \eta_{hy} t_{h,i} \tag{87}$$

The ultimate technology, geothermal plant, can be considered a programmable and the monthly energy production is calculated using equation 88.

$$e_g = \sum_{i=1}^{12} e_{g,i} = \frac{1}{P_{g,rated}} \sum_{i=1}^{12} \sum_{j=1}^{24} P_{g,avg} \langle t_{i,j} \rangle \Delta t_i \tag{88}$$

In electrical network with high share of aleatory renewable production, thus, the production from geothermal energy can be managed to give a contribution for the balance between load and generation from the unprogrammable RES (sea wave, wind, and solar energies). In this way, geothermal energy represents an effective replacement of the local diesel generators. Consequently, the energy contribution from geothermal must be evaluate by considering the hourly trend of the energy demand, and the expected hourly energy production from aleatory sources.

The following equation 89 show the minimization problem that shows the better energy mix.

$$\begin{aligned} P_{sw} &= n_{sw,Z} P_{sw,rated} \\ P_{pv} &= \left(n_{pv,X} + n_{pv,Y} + n_{pv,Z}\right) P_{pv,rated} \end{aligned} \tag{89}$$

$$P_w = (n_{w,X} + n_{w,Y})P_{w,rated}$$

$$P_g = n_{g,Y}P_{g,rated}$$

The parameters $\eta_{hy,Z}, \eta_{pv,X}, \eta_{pv,Y}, \eta_{pv,Z}, \eta_{w,X}, \eta_{w,Y}, \eta_{g,Y}$, represent the unknown variables for the LCOE optimisation problem, see equation 90. The value was calculated in the X, Y, Z sites show in the figure 152. The colour green and blue represent the reserved areas, and yellow the airport area.

$$LCOE = \frac{\sum_{i=1}^{20} E_f c_f \left(\frac{1+\varepsilon}{1+\tau}\right)^i + C_{r,0} + \sum_{i=1}^{20} \frac{C_{r,A} + C_{f,A}}{(1+\tau)^i}}{\sum_{i=1}^{20} \frac{E_d}{(1+\tau)^i}} \tag{90}$$
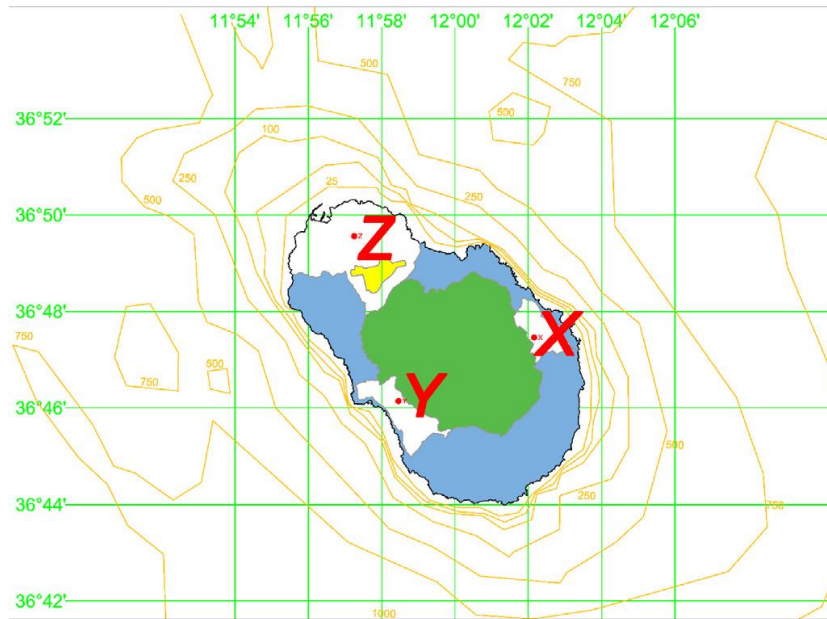
Figure 152. GIS map of Pantelleria

The optimization problem was considered a linear constrained optimization problem. The constraints are:

- The annual electricity production from the proposed RES mix should cover the desired share a $\alpha = E_{RES}/E_d$ of the local energy demand. Since the

installed powers from each source assume only discretized values, a tolerance ($\pm 0.05\%$) is introduced in the evaluation of the RES share.

- Each source must produce at least 5% of the total annual production from RES, to justify the introduction of this technology in the energy blend. This threshold is imposed in order to assure the presence of all assessed RES in the proposed energy mix, since more expensive technologies could be excluded by the solver trying to minimize the LCOE. The energy production from aleatory energy sources is based on the adoption of monthly data, in order to improve the accuracy of the estimation of LCOE. The preliminary sizing of energy storage systems (batteries and inverters) and the evaluation energy production from geothermal energy consider a more complex approach. Considering the climatic data for several years (12 in the case study), for each reference day per month, three different profiles of energy production from sea wave, wind, and solar sources, are evaluated:

- Maximal unprogrammable RES production (subscription "max"), considering that each source produces as much as possible, according to the climatic data.

- Average unprogrammable RES production (subscription "avg"), considering the average condition of climatic data.

- Minimal unprogrammable RES production (subscription "min"), in which each source produces a minimal contribution, according to the worst condition reported in the climatic data.

The three different profiles were used to model the operative conditions to which the local grid could be exposed. Indeed, if the maximal unprogrammable RES contribution, diesel engines and geothermal plant give their lowest contribution.

The average unprogrammable RES scenario represents the normal operative condition of the grid. Finally, the minimal unprogrammable RES profile was used to model the case in which plants are stopped for maintenance, or the energy sources were missing.

Finally, the BESS must be sized. In this phase, the BESS size was chosen independently on its usage for providing synthetic inertia but in order to reduce curtailment of RES production when the generation from renewables exceeds the load demand. Considering the energy scenario with the maximal contribution from RES, the rated power of the BESS (equal to the rated power of the inverter) was given by Equation 91.

$$P_{inv} = \max\left[P_{sw}\langle t_{i,j}\rangle + P_{pv}\langle t_{i,j}\rangle + P_w\langle t_{i,j}\rangle + P_g\langle t_{i,j}\rangle - P_d\langle t_{i,j}\rangle\right] \quad (91)$$

About the sizing of the energy storage, the day with the maximal energy unbalance between the unprogrammable RES production and local demand was considered, see equation 92.

$$Q_{batt} = \max\Big[\ 1hour * \sum_{j=1}^{24} P_{sw}\langle t_{i,j}\rangle + P_{pv}\langle t_{i,j}\rangle + P_w\langle t_{i,j}\rangle + P_g\langle t_{i,j}\rangle - P_d\langle t_{i,j}\rangle\Big] \quad (92)$$

After having evaluated the optimal RES mix, the system inertia must be calculated for each hour of each day considered in the analysis, starting from the hourly production both of diesel generators and RES plants. Due to the electricity production from nonprogrammable RES interfaced to the grid by static converters, the natural inertial response of the isolated power system decreases. Higher the power produced by RES, lower the power produced by diesel generators[97], lower the system inertia according to the following equation 93[98,99].

$$H_{sys} = \frac{\sum_1^n H_i * S_{n,SG,i}}{\sum_1^n S_{n,SG,i} + \sum_1^n S_{n,RES,i}} \quad (93)$$

Where $S_{n,SG,I}$ is the rated apparent power of the i-th diesel generator in the considered hour, H_i is the inertia of the same generator and $S_{n,RES,I}$ is the rated apparent power of the i-th RES generator at the same hour. The minimum, average and maximum system inertia is calculated for three different conditions of generation from RES (minimum, average and maximum production from the installed mix).

The values of the system inertia were used for the sizing of the storage for providing synthetic inertia according to the following procedure. The H_{target} was calculated assuming that the system inertia with the support of the synthetic inertia from BESS is equal to the average inertia of the system in the absence of RES-based static generators. As an alternative, the target inertia is evaluated by imposing that for a maximum imbalance $\Delta P_{imbalance}$ occurring in the grid, the maximum frequency deviation ΔF_{max} is contained into a given limit, according to the following equation 94.

$$H_{target} = \frac{DTd}{2\ln(\frac{\Delta f_{max} D}{\Delta P_{imbalance}}+1)} \tag{94}$$

Where T_d is the response time of the diesel generators and D represents the load frequency dependence. Consequently, the value of the synthetic inertia H_{bess} provided by the BESS is imposed, in this two ways:

- analysing the dynamic response of the converters for interfacing the batteries to the grid in order to obtain a stable response with few oscillations
- imposing a maximum allowed value for the Rate of Change of Frequency (RoCoF) and using the expression[100].

The H_{bess} is calculated following equation 95.

$$H_{bess=\frac{f_0}{2RoCoFmax}} \tag{95}$$

Where f_0 is the frequency at 50 Hz.

Finally, the rated power of the BESS is assessed by the following equation considering the worst operating condition in terms of inertia of the isolated power system, see equation 96.

$$H_{bess} * H_{bess,0,N} + H_{sys,min} * (\sum_1^n S_{n,SG,i} + \sum_1^n S_{n,RES,i} = H_{target} *$$
$$(P_{bess,0,N} + \sum_1^n S_{n,SG,i} + \sum_1^n S_{n,RES,i} \tag{96}$$

From this ultimate equation $P_{bess,0}$ can be calculated and then the effective power exchanged P_{eff} by the storage can be evaluated dividing for the discharging efficiency η_d. If the energy storage discharges P_{eff} is >0 and viceversa.

After methodology explanation the data collected for the case study will show. The island of Pantelleria is just over 80 km² in size and lies 110 km south-west of Sicily and 65 km north-east of Tunisia. The stable population is around 7400 inhabitants, and the climate is warm and windy, making the Pantelleria an ideal place for the installation of solar and wind power plants. Pantelleria's power system is not connected to the Italian electric power grid. The supply is provided by eight diesel synchronous generators (SG) with a total rated power 24.5 MVA. The distribution system has two voltage levels: 10 kV for Medium Voltage (MV) and 0.4 kV for Low Voltage (LV). The electrical load profile is shown in the figure 153.
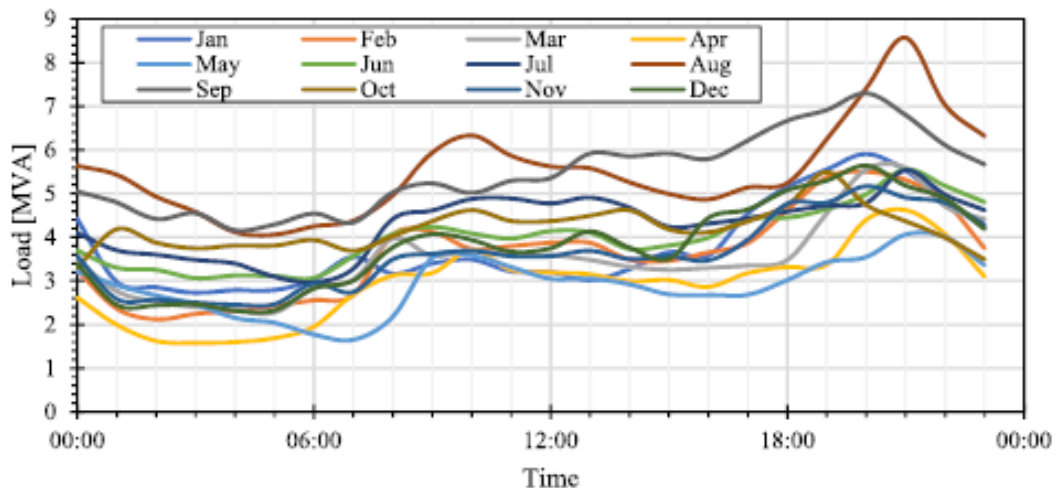
Figure 153. Daily power profile of Pantelleria island in 2017

Analysing the GIS map the RES plant can be divided in these different areas:

- wind turbines can be installed only in X and Y reference points, avoiding any interference with the airport
- PV plants can be installed in a distributed way in the entire territory
- sea wave can be installed only in the northern area, where the sea depth is limited

- geothermal energy can be exploited only in Y reference point, where the source is located.

The algorithm was implemented using the excel non-linear solver considering as variables the numbers of installed devices for each reference points, 7, and 16 inequalities. For each technology was considered implementation in multiple rated power: 3.3 kW for PV plant, 80 kW for sea wave plant, 250 kW for wind turbine and geothermal plants.

The value considered related to investment and O&M are listed in the following table 22.

<div align="center">

Table 22.   Wind turbine features

</div>

Technology	Investment [€/kW]	O&M costs [€/kWy]
Wind turbine	1212.57	42.12
PV	980.10	12.15
WEC	5020	75
Geothermal	4353	115
Inverter	100	10
Battery	200	20

The inflation rate for the energy sector was fixed to 2.993%, by considering the trend of diesel price in Italy[101]. The interest rate was set equal to 1.14%[102].

The simulations carried out from excel spreadsheet show a contribution of renewable energies at different RES share from 5% to 70%, figure 154. The LCOE varying from 0.45 €/kWh to 0.19 €/kWh, figure 155. The levelized cost follow an inversely proportional linear trend respect the RES share. The increase the renewable energy production decreases the LCOE.
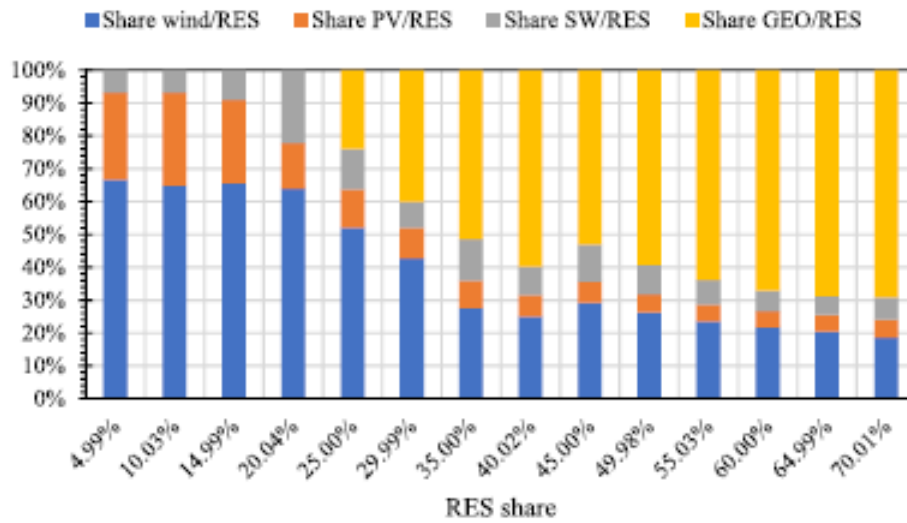
Figure 154. Contribution of renewable energy sources at different RES share
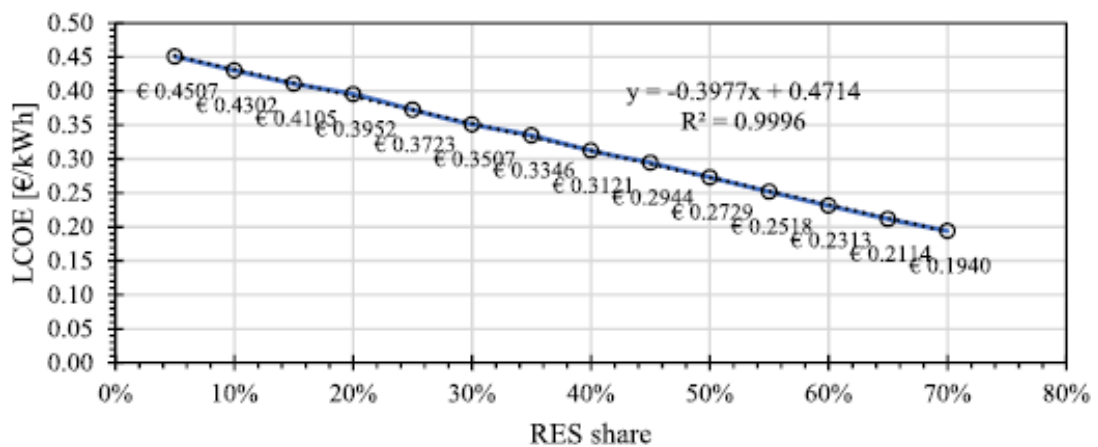
Figure 155. LCOE variation

The results of the energy production considering RES share from 50 to 70% in April (minimum and average production) and august (maximum production) are shown in the following figures 156 and 157.
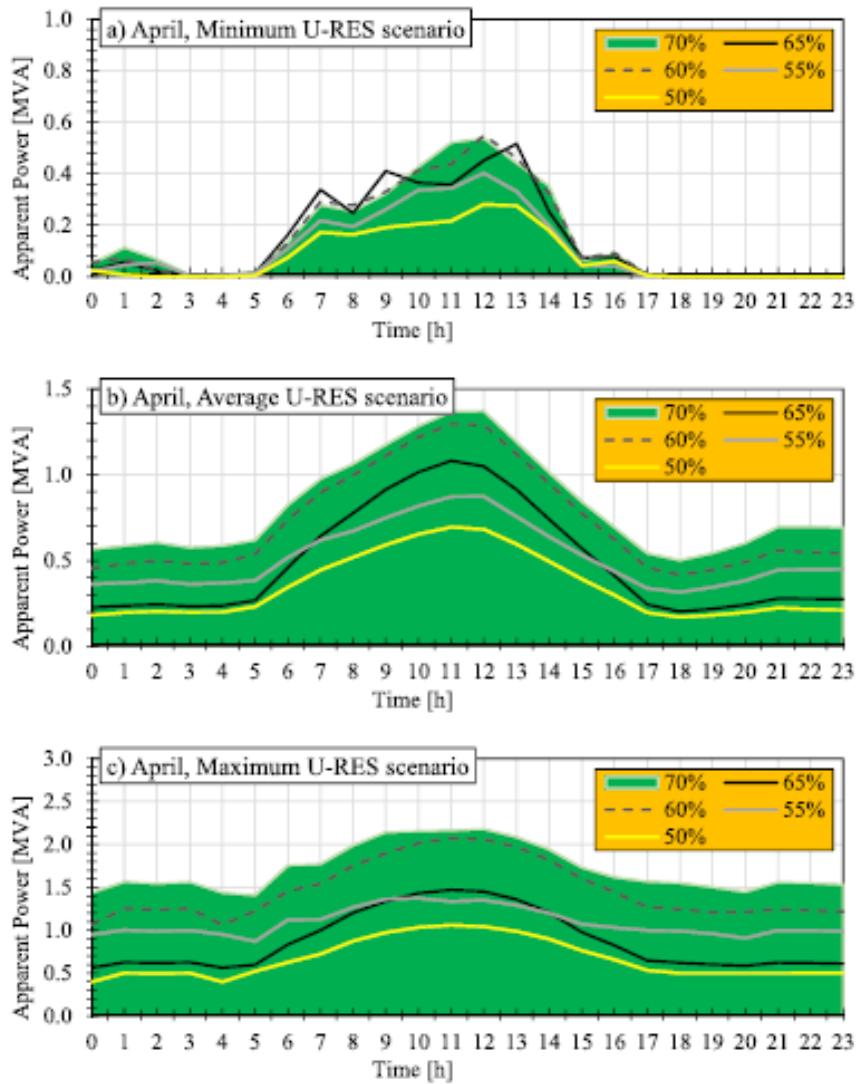
Figure 156. RES production in April considering three different daily contributions of RES (maximum, average, and low profiles)
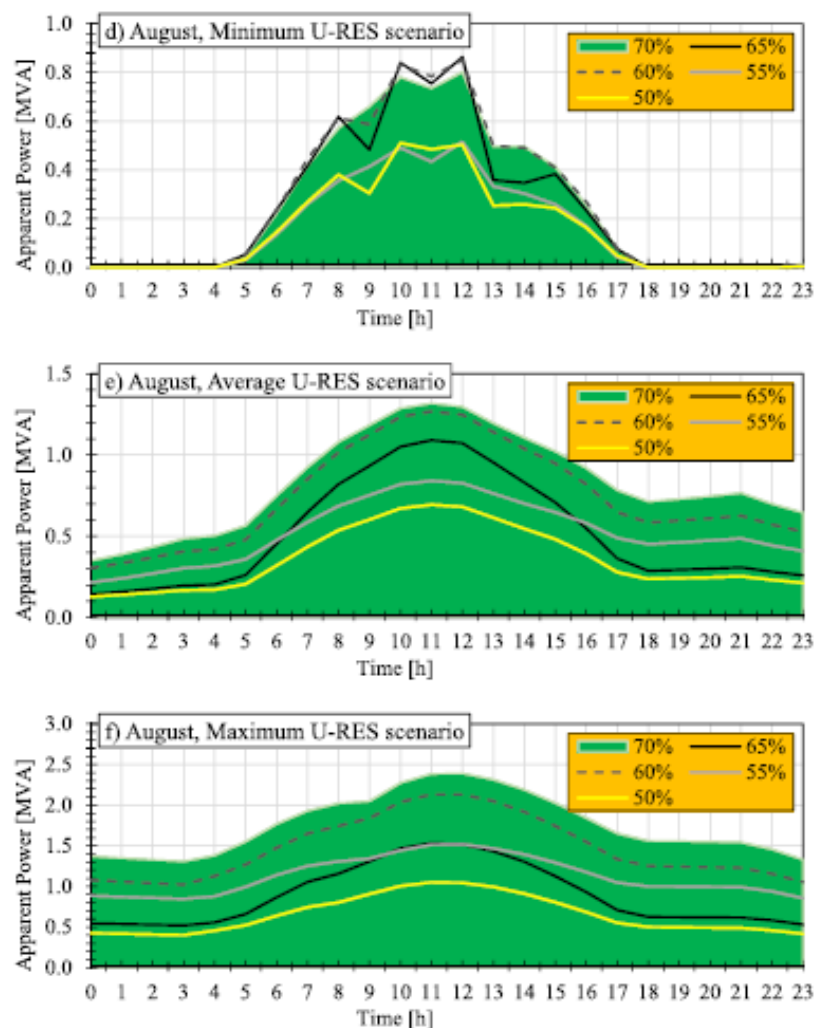
Figure 157. RES production in August considering three different daily contributions of RES (maximum, average, and low profiles)

The scenarios with 65% and 70% of RES production have final costs that differ only around 3%, while in the other scenarios (60%, 55% and 50%), the differences are between 17% and 19%. In this way, 60%, 55% and 50% scenarios are discarded because the production is approximately one half than in the 70% scenario. The best energy mix from a techno-economic point of view is the 70% RES, composed by:

- 792 kW of photovoltaic panels (divided into 240 roof-integrated plants, each one with a rated power of 3.3 kW). The energy production is 1386.87 MWh/y

- 1000 kW of wind turbines (4 wind plants, each one with a rated power of 250 kW). The energy production is 4736.89 MWh/y
- 1120 kW of wave energy converters (14 devices, each one 80 kW). The energy production is 1743.61 MWh/y
- 2250 kW geothermal turbines (9 steam turbines, each one with a rated power of 250 kW). The energy production is 17664.2 MWh/y
- 92 kW of BESS.

The total investment for RES mix installation, including the energy storage is around 17 M€.

Considering the listed power plants the inertia of the electrical grid was estimated. The following figure 158 refers to months from January to June considering the minimum (graph a), average (graph b) and maximum (graph c). Instead, from graph d to f the months from July to December are depicted.
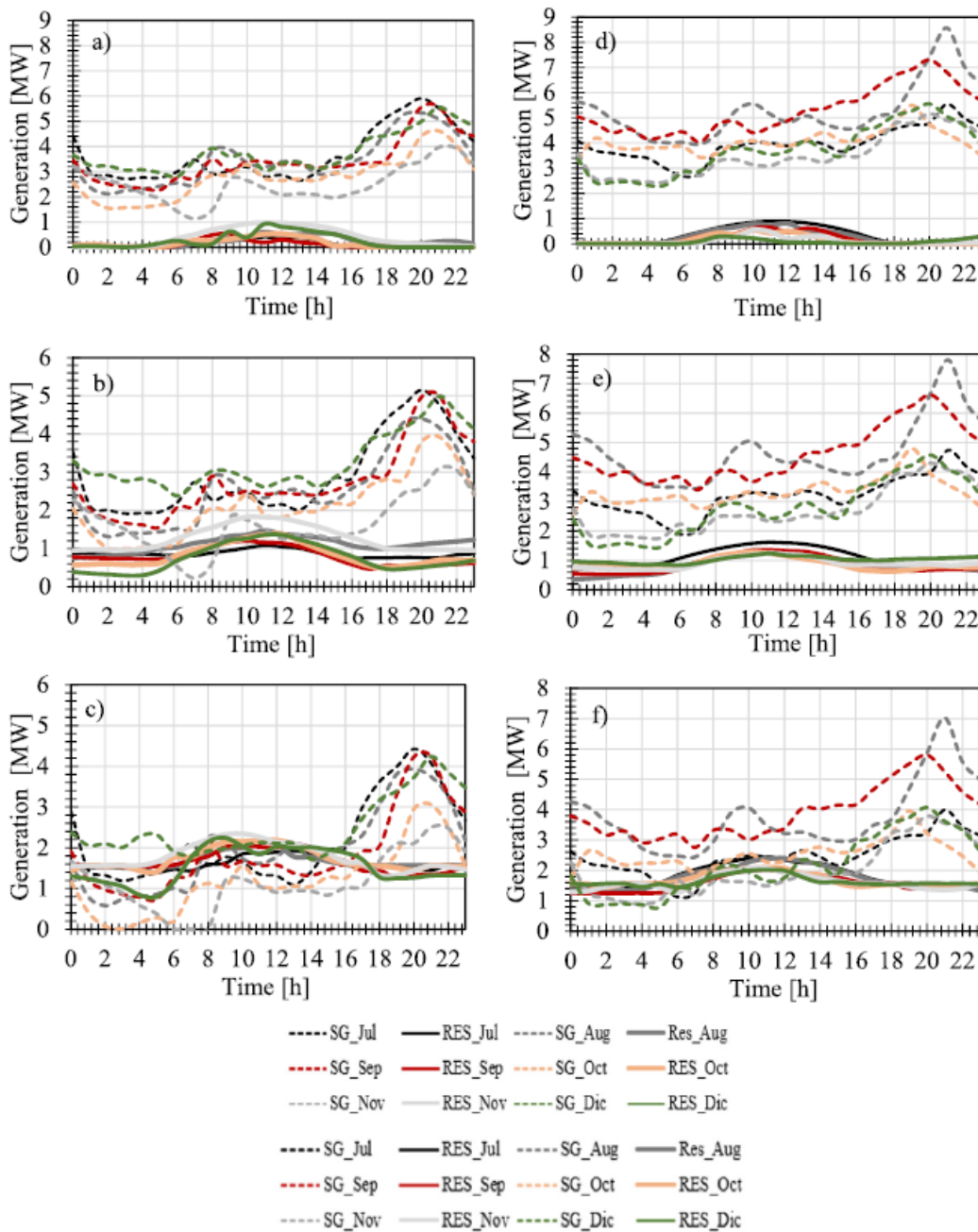
Figure 158. Electrical energy generation

When the RES plants produce at their maximum and the traditional power plants generate the missing electricity production for compensating the load demand, the RES inclusion automatically causes the disconnection, on average, of 2/3 of synchronous generators production with respect the case without RES plants.

The comparison of the hourly electricity productions shows that:

- RES trends of both groups reveal peaks between 6 a.m. and 6 p.m. due to the presence of the PV plants

- The decrease in the electricity production from traditional plants is function of the three levels of electricity production from RES. Therefore, the higher the RES production, the lower the synchronous generators production.

Calculations carried out by using equation 94 show the levels of RES production and is shown in figure 159.
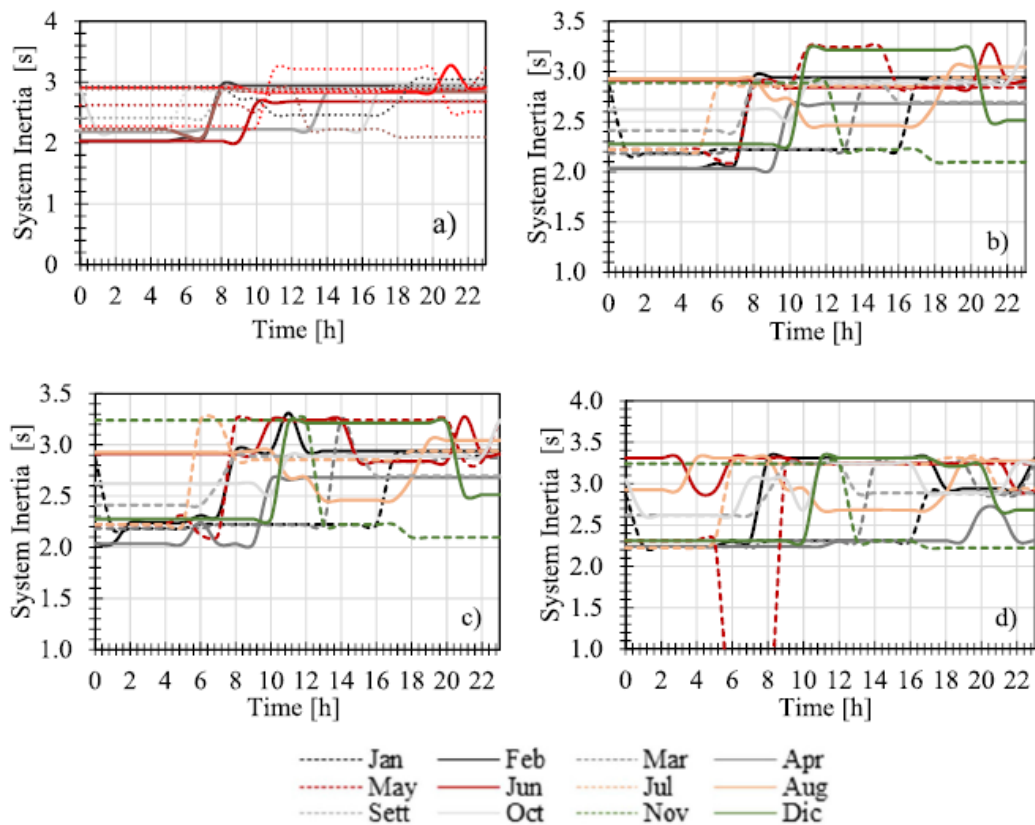
Figure 159. Inertia in cases with and without RES generation. a) No RES, b) minimum RES, c) average RES, d) maximum RES

It can be noticed how the introduction of RES-based generators, interfaced by static converters to the grid, sensibly reduces the system inertia especially when the production of these system is at its maximum. This implies that also the maximum imbalance allowed in the grid is reduced in Case with RES with respect to Case

without RES. The maximum unbalance allowed for the island is calculated by Equation 97

$$\Delta P_{imbalance} = \frac{\Delta f_{max} D}{(e^{\frac{DTd}{2Hsys}} - 1)} \tag{97}$$

where, Td = 2.7s is the response time of the diesel generator =1% represents the load frequency dependence, Δf_{min} is the maximum frequency deviation assumed equal to 2.5 Hz (frequency nadir for the island 47.5 Hz. The inertia varying from 2s in minimum configuration to 3.28s and with maximum RES sharing decrease to 1.91s. The inertia can be improved by using BESS suitably interfaced to the grid by static converters[100]. Following the above-described procedure, the BESS size is calculated for the case of maximum renewable production. assuming H_{target} =4.05s according to Equation 95. HBESS is assumed variable between 6s and 20s and the sum of the rated powers of all the generators is 2.9 MVA.

The results of the calculations show that it is preferable to impose that the synthetic inertia of the BESS is not lower than 10 s in order to maintain the size of the storage system around 2MW for the target 4.05s. In this way, the single units that form the BESS will be easily connectable to the 10 kV grid of the island and will occupy a limited area around 50 and 100 m^2[103–105].

The BESS sized above it is not sufficient for the synthetic inertia service. In this case the installed power could be summarized in the following table 23

Table 23. **BESS Size**

H_{bess} [s]	$P_{bess,0,N}$ [MW]	E_{bess} [kWh]
6	6.02	903.46
7	3.98	597.20
10	1.97	296.09
12	1.48	221.60
15	1.07	160.89
18	0.84	126.29
20	0.74	110.45
25	0.56	84.09

In conclusion, the huge amount of renewable energy production compromises the rotational inertia of the system. This led to excessive frequency deviations during power imbalances that must be solved using suitable methods like the provision of synthetic inertia by BESS. Considering this last aspect, it is reasonable to ask what is the maximum percentage of renewable energy that can be accepted on a small island for the electricity system to function in a secure way. It is not easy to reply to this question since a secure operation of a small island's power system depends on several factors: the inertia of the diesel groups and the maximum disturbance that can occur in the grid. It must be considered that in a wide interconnected power system, like that of Continental Europe Area, the maximum unbalance is conventionally established equal to 3000 MW (reference incident) and it is about 2% of the maximum load of the area. In a small island, presenting only one main supply node and generally from two to five MV lines and from three to four diesel generators sharing the load, it is reasonable to assume a higher reference incident for sizing the system frequency containment reserve and inertia. Nevertheless, this operation must be defined case by case and from it the maximum inertia reduction and therefore the maximum percentage of converter interfaced RES plants depend.

5.6 Case Study in Vietnam small island

The energy demand in Vietnam increasing in the ultimate 20 years because the global domestic product raised up from 7.99 USD billion in 1989 to 406 USD billion in 2022, estimating in 2028 725 USD billion, see figure 160 [106].
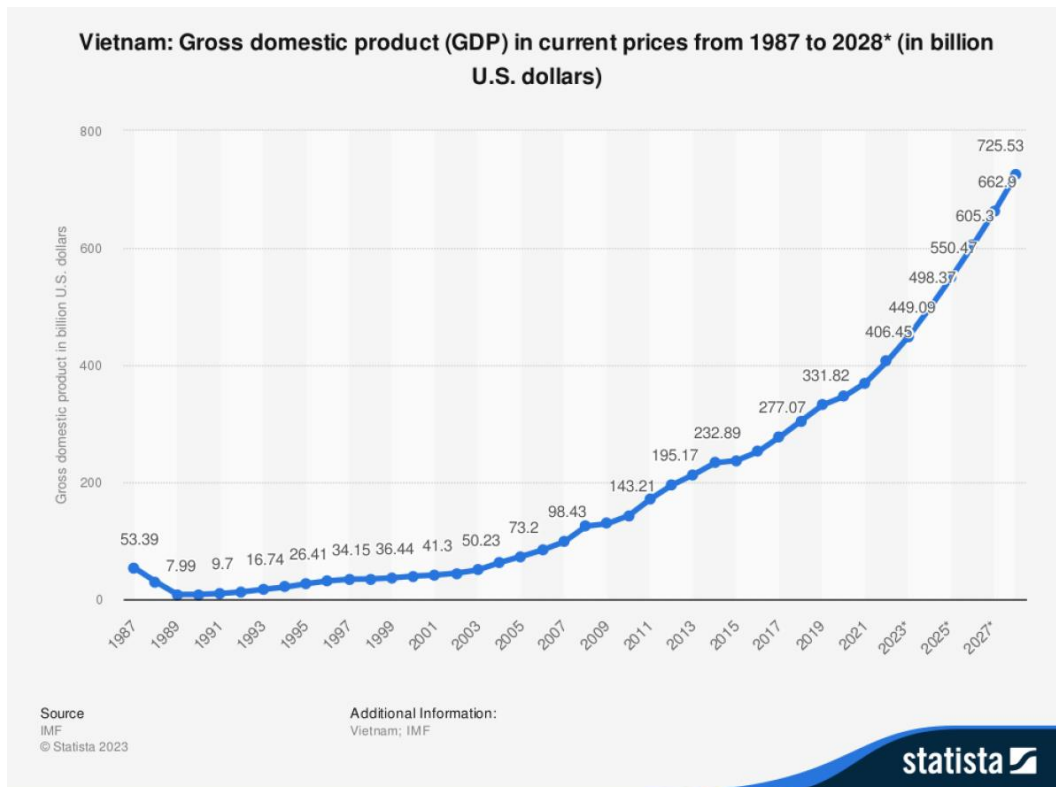
Figure 160. Vietnam GDP evolution

This increase in production has seen an increase in the development of renewable sources. Green production is important in order to counteract the high demand for energy that leads to large consumption and much pollution. To promote the RES installation various incentives have been used by the government[107]. However, the installation of these technologies could be not feasible in small islands, especially if they are located inside reserved areas. A possible solution is represented by sea wave, thanks to the limited environmental impacts. The case study was carried out in small island of An Binh located in south China, see figure 161[108].
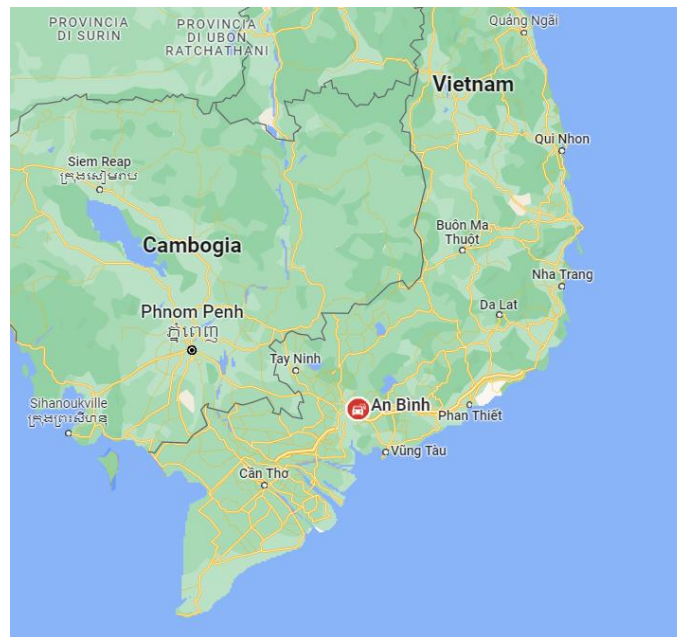
Figure 161. Case study site

Existing low-voltage network is shown in figure 162, The island's generation fleet consists of two 110 kVA diesel generators and a 96 kWp photovoltaic generator connected to the grid with a 100 kW inverter. There is also a 9600 Ah gel storage system at 48 V voltage, connected to the grid via a dedicated 72 kW inverter. The three systems are interfaced to each other and the grid by a multicluster cabinet. The low voltage network (total length 2734,5 m) is radial and has two main branches, XT1 (1527,5 m) and XT2 (1207 m). The flowchart describing the connection between component is reported in figure 163.

Figure 162. Low voltage grid map
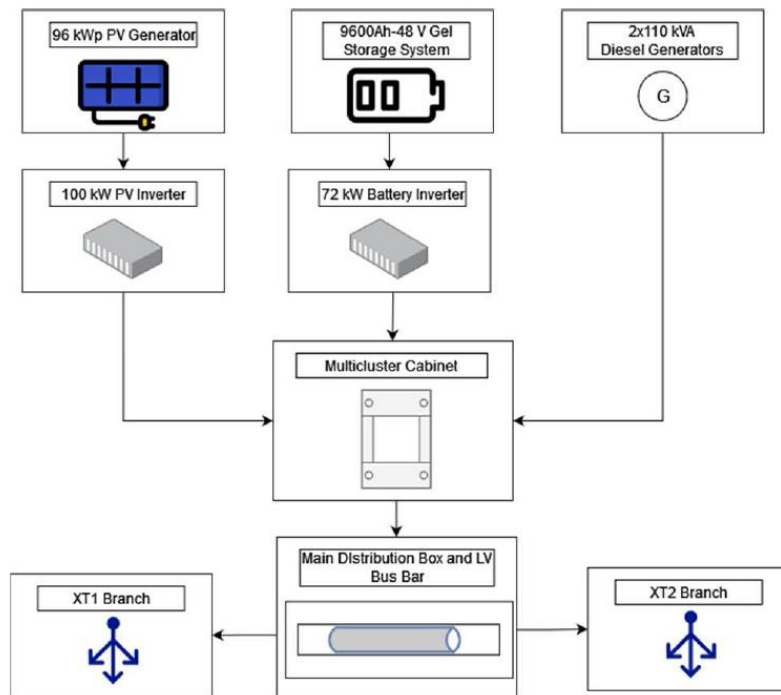
Figure 163. Low voltage grid map flowchart

To produce energy exploiting sea energy was simulated a 50 kWp wave energy converter producing around 65 MWh/y. The generator will be installed on the northwest coast of the island and will be connected to the existing grid through newly constructed dedicated lines (total length = 850 m), as shown in figure 164.

Figure 164. WEC site installation with new electrical grid connection

Grid stability analysis was performed simulating two scenarios: "baseline scenario", considering the current energy mix, and "project scenario", considering the WEC plant production.

Two different simulations are also conducted for each of the two scenarios. In the first case, the assumption that the load can be fully supplied with renewable energy when it is available is made, i.e., assuming the possibility of 100% renewable power supply moments. This possibility, however, is not representative of the real operation of the grid, as the total lack of diesel generation means there is no inertia in the system resulting in the risk of instability. In order to best simulate the actual operation of a grid with a high percentage of renewables, simulations were conducted in which a maximum cap of 85% on load supply from renewables is set, resulting in a minimum feeding from diesel generation of 15%. Firstly, the load and production data were studied during October to December in winter and from May

to July in summer. From the daily consumption and production data, typical daily profiles were derived for each of the simulated months. Figure 165 shows the daily load profile for the above cited months.
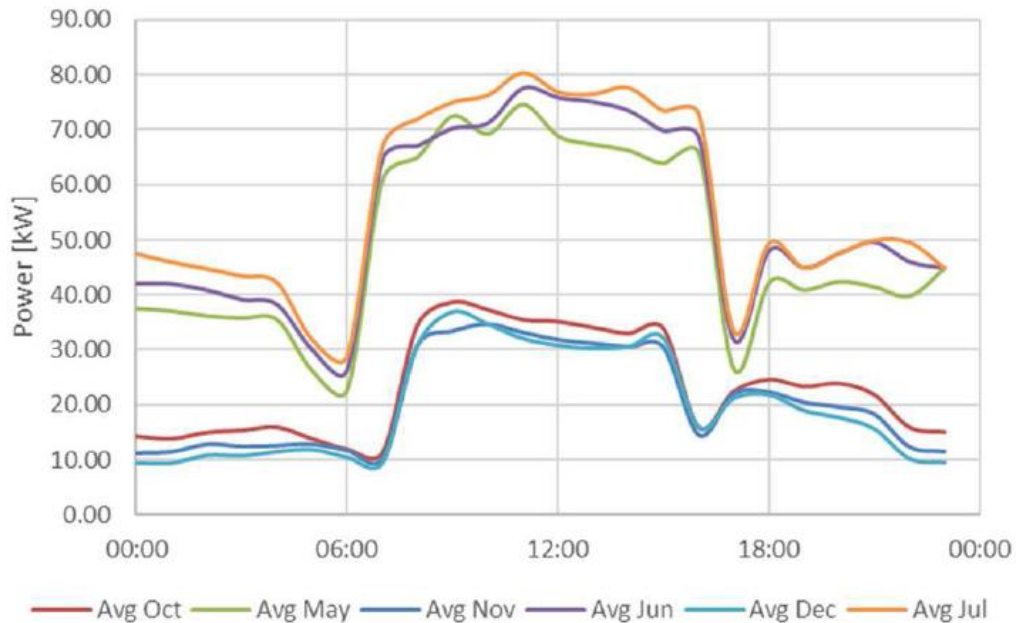
Figure 165. Average daily load profiles

Obviously, there are several differences between summer and winter load demand, especially because in summer the presence of tourists increases the loads. The difference in demand is very high, with hourly differences in summer ranging from +40% during low-load hours to +250% during high-load hours. The electrical peak in summer is around 80 kW and in winter only 35 kW, instead the minimum request in summer is around 25 kW and winter around 10 kW.

In the base scenario for the months investigated, hourly PV generator output was evaluated through the use of PVGIS software. Combining the production curve with the demand curve leads to a graph representing the imbalance between solar energy production and demand, see figure 166.
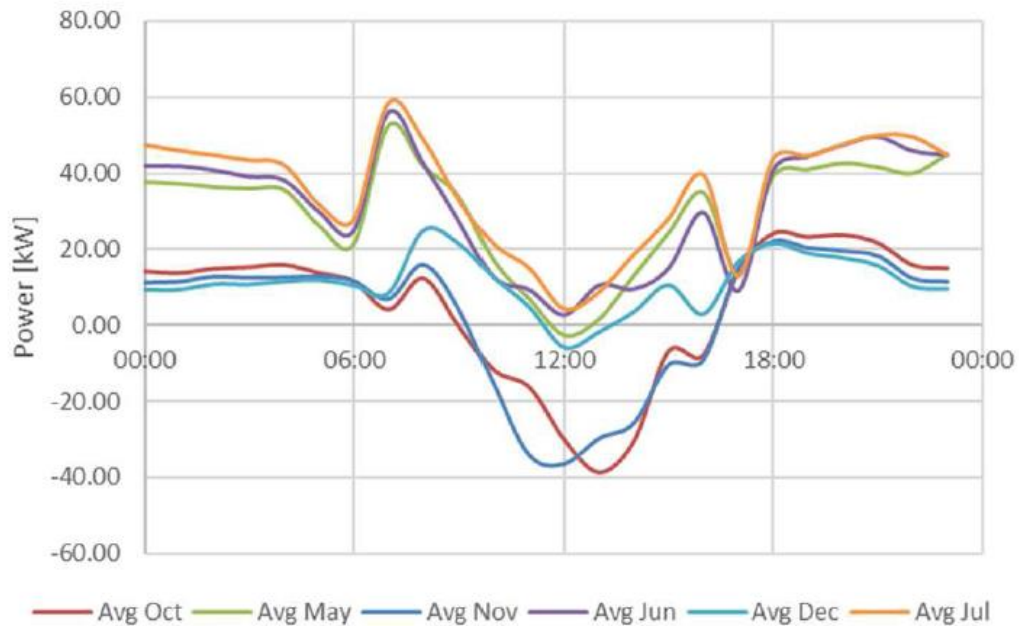
Figure 166. Energy balance between PV solar production and load

A positive value of the imbalance corresponds to a minor PV production with respect to the load and to equivalent energy production by the diesel generators, while a negative value indicates overproduction of solar energy and subsequent accumulation in the storage system. If the storage system is saturated, the overproduction implies curtailment of energy. The photovoltaic generator produces energy from 6 a.m. until 6 p.m./7 p.m., with a peak of 73 kW recorded around 12 a.m. During the summer, no significant curtailment events occur, with production approaching 100 percent of the demand only during a few hours of the day. In the winter months, the curtailment of energy is significant: during daylight hours, at solar production, the energy produced by PV exceeds demand by several kW (39 kW peak). The system inertia is evaluated with the following equation 98, in accordance to ENTSO-E guidelines[109].

$$H_{sys} = \frac{\sum H_i S_{g,i}}{P_{load}} \qquad (98)$$

Where H_{sys} is the total inertia of the system, H_i the inertia of the i-th generator, $S_{g,I}$ the apparent power of the i-th generator ad P_{load} the total load. The diesel generator inertia is assumed equal to 2 seconds[110]. The inertia assumed for Inverter based resource i.e. PV solar plant the inertia is equal to 0 second. This results in an overall lowering of system inertia and increased risk of instability. The calculation is performed on an hourly basis in all cases described in figures 167, 168.
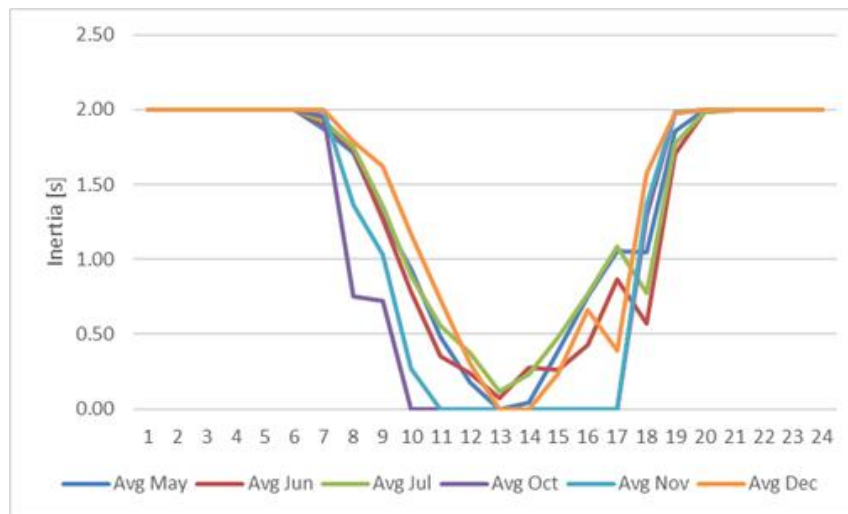
Figure 167. Average daily inertia, baseline scenario, no limit to RES supply
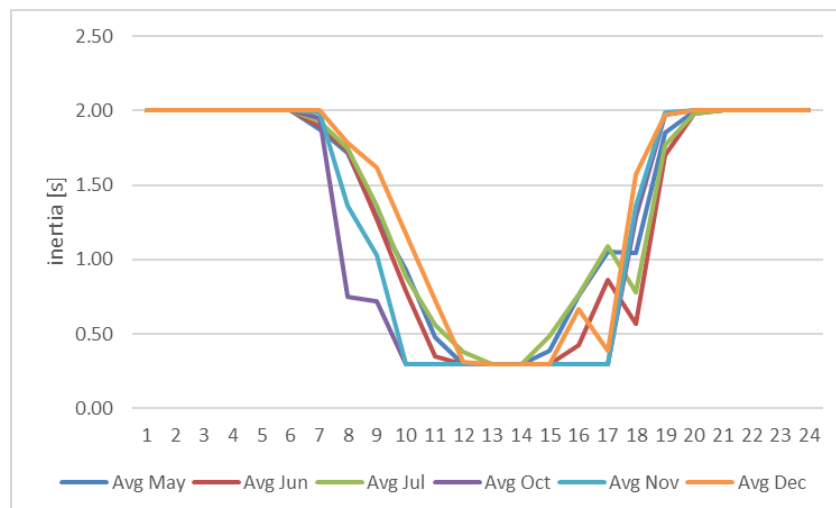
Figure 168. Average daily inertia, baseline scenario, max 85% RES supply

The electrical system under consideration already goes through stability-challenging instants in the current situation. Although there are some periods when

the percentage of renewable totally covers the demand (around 8 hours of 100% RES supply in October and November), such operation is only theoretical because the inverter technology for the PV interface needs a voltage and frequency reference. As a result, the diesel generators turn out to be always operational, which results in increased curtailment of PV energy.

The future scenario, considering the WEC plant production, supposes that the interface between power plant and electrical grid is operated using an inverter. In these conditions, the inertia is once again equal to zero.

Wave energy production remains almost constant during the day for most of the months analysed, with the exceptions of May and November. Average power values are between 5 and 10 kW with maximum peaks of 26-27 kW in the before mentioned exceptional months. As in the previous case, the imbalance between renewable generation and load is analysed, see figure 169.
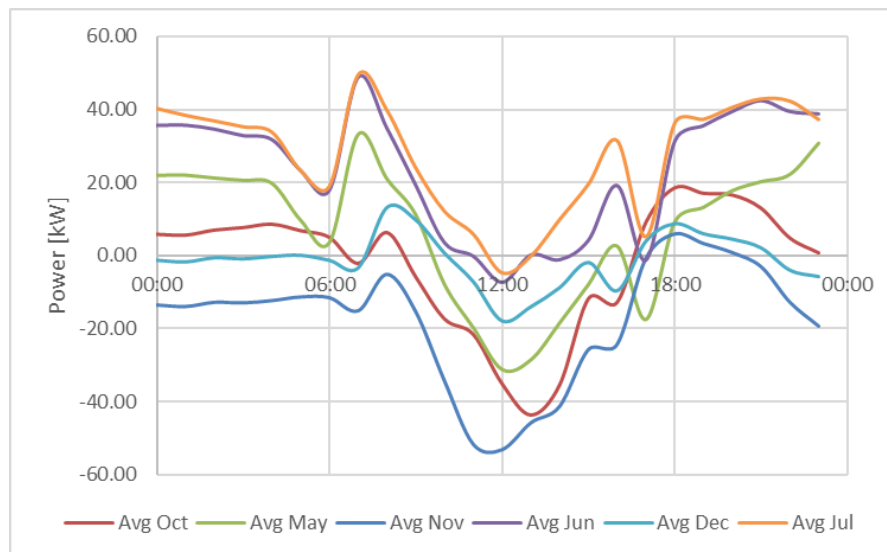
Figure 169. Energy balance between renewable production and load

In the simulations with the simultaneous presence of PV and WPP, the imbalance between energy demand and production becomes more pronounced, especially in the winter months. The summer months still require production from diesel generators, but only at night and generally at times of high load, as 100 percent renewable in the hours near noon is achieved. From a pure energy point of view,

the demand for the winter months is entirely covered by renewable sources, with the month of November in which there is overproduction even at night. As is the case for the previous scenario, figures 170 and 171 show the trend of inertia.
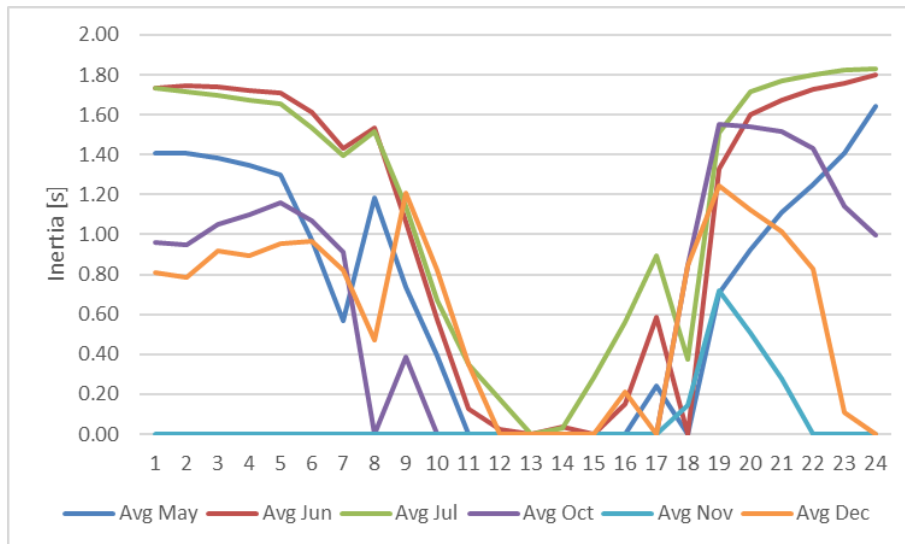
Figure 170. Average daily inertia, baseline scenario, no limit to RES supply
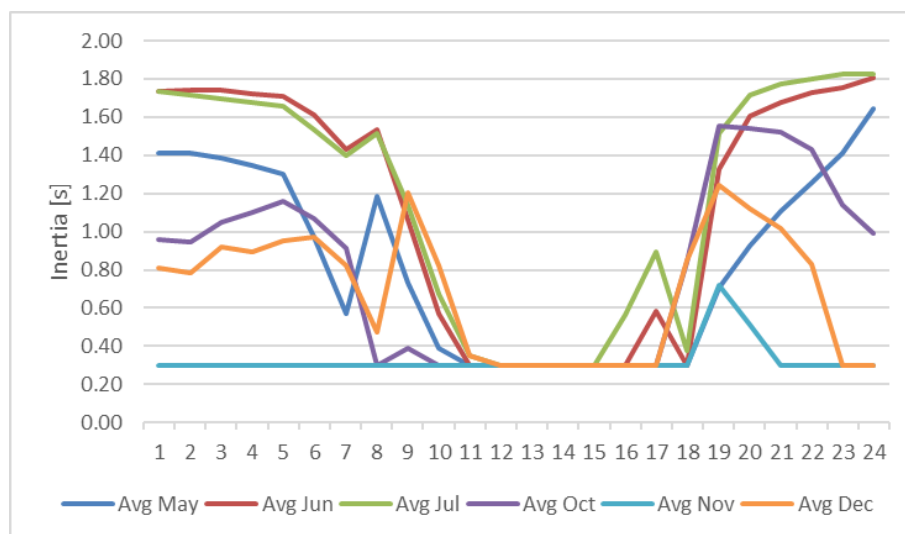
Figure 171. Average daily inertia, baseline scenario, max 85% RES supply

The results of these two scenarios are summarized in the following tables 24 and 25.

Table 24.   Results summary in summer

May-Jun-July	Max imbalance [kW]	Zero hours	Inertia	Average RES curtailment [kWh/day]
Baseline Scenario				
Max 100% RES	2.79	1-3		3 - 9
Max 85% RES	2.79	0		9 - 27
Future Scenario				
Max 100% RES	31.26	2-7		10 - 100
Max 85% RES	31.26	0		30 - 170

Table 25.   Results summary in winter

May-Jun-July	Max imbalance [kW]	Zero hours	Inertia	Average RES curtailment [kWh/day]
Baseline Scenario				
Max 100% RES				
Max 85% RES	38.50	2-8		15 - 160
Future Scenario	38.50	0		20-190
Max 100% RES				
Max 85% RES	53.30	5-20		30 - 370

The conducted analysis highlights a high degree of overproduction in the case of simultaneous operation of photovoltaic generator and wave generator. There are many theoretically 100% renewable hours, but this behaviour is impractical because the grid always needs a rotating component to ensure the stability of the electrical system. By always keeping a minimal rotating generation component active, 0-inertia hours are eliminated but renewable energy curtailment increases. The inertia of the system is an important parameter to evaluate the behavior of the system during a power transient. In the same way of Pantelleria island, this case study shows the RoCoF (Rate of Change of Frequency) index, equation 99. The initial value of the df/dt is the instantaneous RoCoF just after an imbalance of power in

the electrical power system (i.e., disconnection of a generator/load tripping), before the action of any control.

$$RoCoF_{t=0} = \frac{\Delta P_{imbalance}}{P_{load}} \cdot \frac{f_0}{2 \cdot H} \tag{99}$$

The lower the system inertia, the higher the initial RoCoF. If the frequency changes too quickly, the system has not enough time to respond to the imbalance: this can lead to lower/higher frequency peaks that can cause the tripping of under/over frequency protection and lead to a disconnection of the generators with a possible consequent black-out. For this reason, a 100% renewable supply is not possible with the classical inverter interface technology.

6.   Monitoring system

In order to correctly size a wave energy converter (WEC), it is necessary to carry out a series of environmental assessments that provide for the study of wave characteristics. To this end, several approaches are currently available:

- Buoy-mounted or deep-sea sensors to determine ocean characteristics.

- Extrapolation of information from space sensors considering the electromagnetic spectrum due to the reflection of visible sunlight on the waves.

The first technique, the most accurate, requires the installation of sensors directly on site. Meteorological buoys are devices designed to collect meteorological and oceanic data.

They can measure different parameters related to air such as temperature, atmospheric pressure, wind speed and its direction. They also measure sea wave parameters such as water temperature, height, and wave period.

The raw data can be processed and recorded on board the buoy and then transmitted via radio, cellular or satellite communications to meteorological centers for use in weather forecasting and climate study, necessary to carry out studies of an engineering nature and research programs.

In our laboratory of marine technology, a low-cost buoy was built and tested to solve this aim, see figure 172.
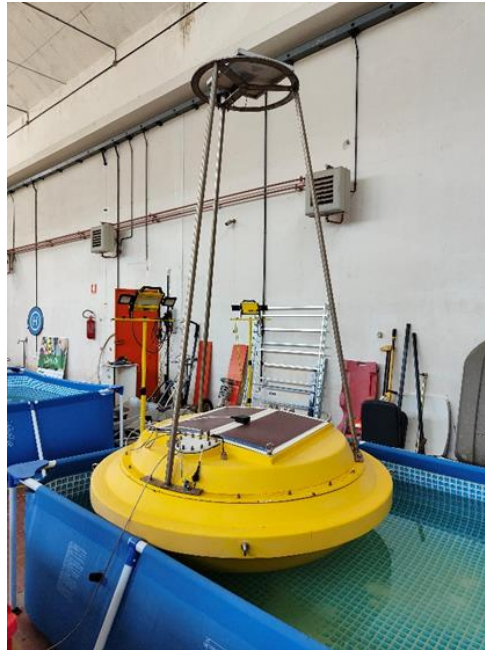
Figure 172. Monitoring buoy

The buoy was built a few years ago and optimized subsequently. An important improvement was introduced during my PhD, related to the introduction of certified components to achieve more reliable measurements. In particular, the main components are the IMU LSM9DS1 iNEMO STMicroelectronic module, and the SIMATIC IOT2000 controller.

The iNEMO STMicroelectronics LSM9DS1 inertial module is an integrated system that features a linear acceleration 3D digital sensor, a 3D digital angular velocity sensor, and a 3D digital magnetic sensor. The LSM9DS1 has a full scale for linear acceleration of ±2 g/±4 g/±8 g, a full scale for the magnetic field of $\pm4/\pm8/\pm12/\pm16$ gauss and for the angular velocity of $\pm245/\pm500/\pm2000$ dps. The LSM9DS1 includes an I2C serial bus interface that supports standard and fast modes (100 kHz and 400 kHz) and a standard serial SPI interface. Magnetic sensing, accelerometer and gyroscope can be enabled or set to shutdown mode for intelligent energy management. The LSM9DS1 is available in an integrated plastic land grid array (LGA), guaranteed to work in a wide temperature range from -40 ° C to +85 ° C. The following figure 173 shows the IMU block diagram.
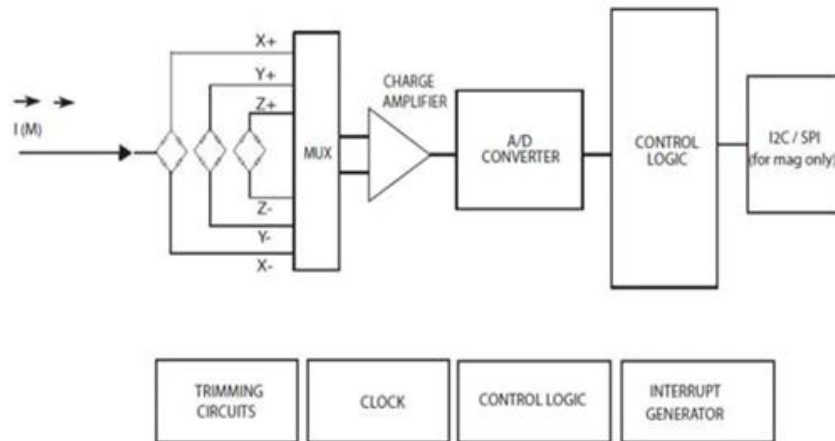
Figure 173. IMU block diagram

The Siemens SIMATIC IOT2000 gateway enables the connection of additional digital and analog inputs/outputs (I/O) in an industrial environment to IT or the cloud. It is compatible with open-source software such as arduino IDE and Yocto Linux, and uses high-level programming languages such as Java, C++ and JSON. It allows the collection, processing, and transmission of data directly into the production environment. The system supports numerous protocols (S7 protocol, OPC UA, Modbus TCP, TCP/IP, etc.) via various interfaces, including RS232/422/485, USB serial interface, Ethernet or Wifi via mPCIe. Connectable through GPIO and programmable, the robust shield is equipped with CE and UL certifications and is able to work in industrial environments 24 hours a day, 7 days a week.

To complete the measurement and data collection system, there is the ethernet card of the PC and an internet switch, to allow you to release the connection. All placed away from the buoy and controllable remotely. In addition, it is possible to store data via μSD, in such a way that you have an emergency backup in case of malfunction or interruption of the transmission. The measurements carried out in a little swimming pool tested the effective work of the installed sensors. The installed motion sensor which, includes an accelerometer, a gyroscope and a magneto-compass, all triaxial, has been tested together with the data transmission system in such a way as to verify the right functioning and carry out a pre-processing of data

directly on board the buoy, in order to limit the amount of information to be sent to the control center. Thanks to this application, it is possible to receive the necessary information in real time with great precision and sensitivity even to the smallest movements of the buoy. The whole thing is easily removable on a CSV basis for later processing.

Below are examples of data collection carried out in the laboratory over a period of one minute. It is possible to notice the great sensitivity of the sensor, which allows you to study even the smallest oscillations of the parameters under examination. The developed software allows the real-time study of the 3D movements provided by the IMU sensor and in particular returns the values of linear acceleration in g, angular velocity in dps and magnetic field in gauss, see figures 174, 175, 176.
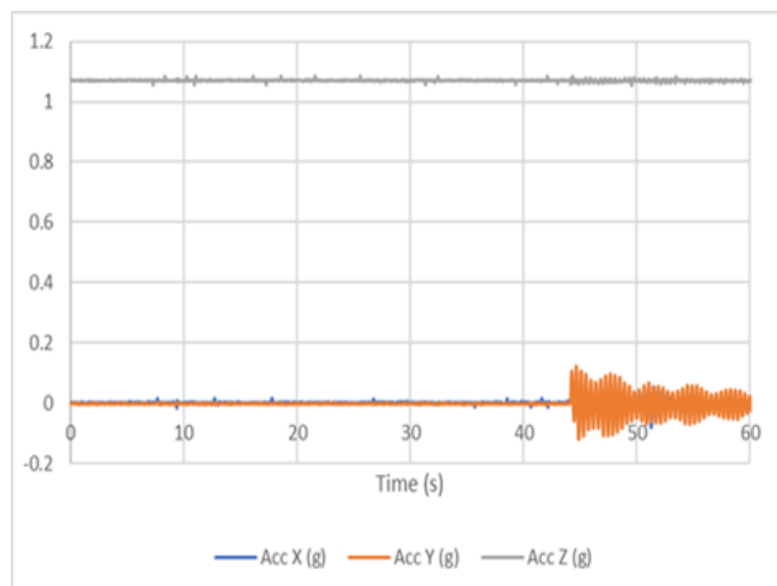
Figure 174. Tri-axial acceleration measurement
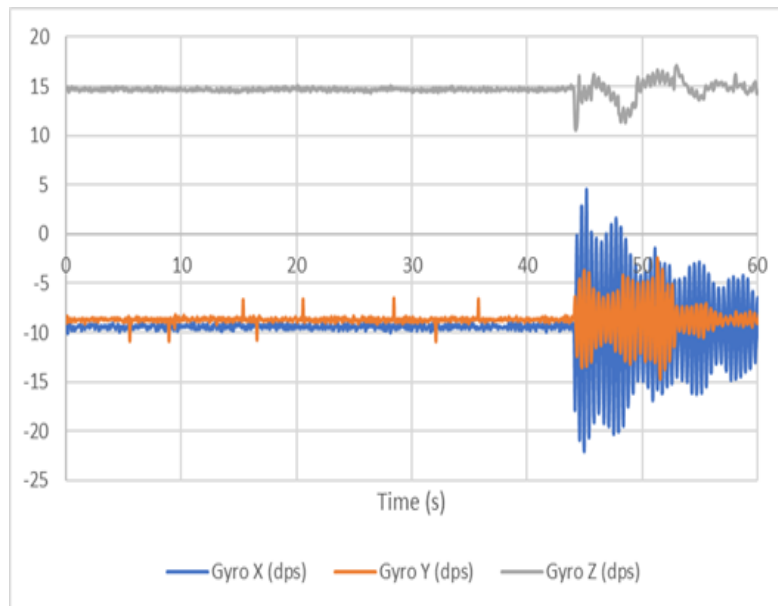
Figure 175. Tri-axial angular velocity measurement
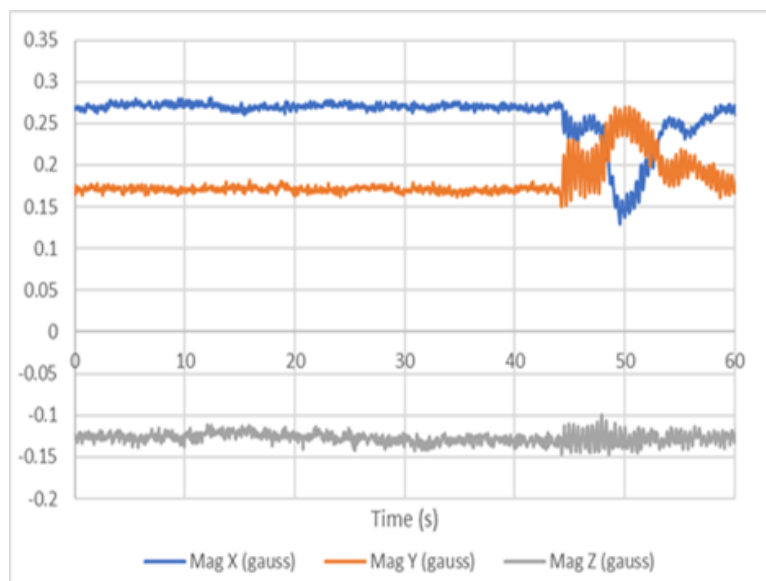
Figure 176. Tri-axial magnetic field measurement

The buoy guarantees the follow advantages:

- Low cost.

- Easy assembly and installation.

- Data transmission online.

- Solar panel for power on-board systems.

As above described this kind of technology could work coupled with wave energy converter to produce electrical energy with maximum efficiency. The system could be composed by electronic power controls that manage the producibility measuring the wave energy potential at buoy point and then preparing the PTO to work at maximum power point. The following flowchart explains this electronic and mechanical connection.

Figure 177. WEC flowchart

Conclusion

This thesis work was carried out by following the topics on which the research project was based over the three years. The results obtained make it possible to expand the literature to date with data obtained by means of mechanical and electrical simulations to be used in order to have terms of comparison for other devices that might also be made. The results show that linear generators can be used in both onshore and offshore systems with the need to increase efficiency and the ability to extract energy from the sea. The caption system, usually buoy, is the part of the system that can make the difference because it is the first step in transmitting energy up to the generator. The best result achieved during the three years is definitely the confirmation that different kinds of generation systems can be designed and sized that could be the beginning of a new technology to be optimized to industrialization.

The first year of the PhD focusses the tidal systems and the Italian wave network. For these reasons during the first months a deep study made it possible to recognize and distinguish the various technologies present in the state of the art. After a general study of the technologies, i went into detail by studying their operating principle. Each WEC was studied in order to distinguish its operating principle and its components. A focus was made on the catchment system, generally the buoys, and the system for converting mechanical energy into electricity, the power take-off (PTO). In addition to the theoretical part several case study and laboratory simulation tests were carried out. In particular during the first year, it was possible to put into practice what had been studied by perfecting a PTO built to scale in the marine technology laboratory (paragraph 4.1). This device makes it possible to extract electrical energy by exploiting wave motion captured from the land. It uses a rod to convert mechanical energy from the sea into electrical energy by rotating an alternator attached to it. Once completed, the device was measured in the laboratory in order to study its behaviors. As described, the PTO is composed by wood and steel, and to estimate its environmental impact a preliminary LCA studies

were performed. Firstly, considering as functional unit itself, essentially the impact related to its assembly and then using 1 kWh of electrical energy production. During the first year also the monitoring system is used to characterize a wave system. The theoretical part was studied and then a buoy capable of carrying out these measurements was also tested in the marine technology laboratory. Using accelerometers and gyroscopes, it can measure the accelerations to which it is subjected and display them in real time remotely on a computer.

Completed the literature research, several experimentations were conducted on the linear generators made of ferromagnetic material and an ironless one. As linear generators are among the technologies used to produce electricity in the wave industry, it is necessary to understand whether weight and electrical losses can be optimized. To do this, identical load tests were carried out to measure the voltage, current, resistance and power values generated in both generators. The big difference noticed immediately during the tests is the different cogging force which characterizes the iron generator, and which is not present in the ironless one. In the same way of the on-shore WEC the LCA studies were conducted. The second year started with the refinement of mechanical and electrical tests on the three generators. Especially, to reduce the cogging force in iron generator it was disassembled and reassembled, in order to modify the electrical wiring. After the two phases theory and laboratory tests several simulations was performed. In order to characterize the operation of the linear generator, hydrodynamic simulations were carried out using the "ansys aqwa" software. The results obtained are based on energy producibility studied as if the device were installed in the Mediterranean Sea and in small island also out of the Europe. The most simulations have been carried out in small island, sensitive sites related to the instability of the grid to resist production from RES.

After the technical analysis to compare the technologies, some economic evaluations were considered in term of LCOE. The case under consideration is the same as that described in paragraph 4.5, i.e. buoy, ropes, pulleys, mechanical gears and linear generator.

As shown state of art paragraph in this work, the electrical production from RES could be used to power electrolysers capable to produce hydrogen. In this way a review of the common technology was performed highlighting the advantages and disadvantages of each one. This solution represents a very green environmental technology to produce fuel, H_2, without traditional oil or gases plant. The system composed by WEC and electrolysers could be considered a power reserve capable of help electrical grid from over renewable energy production when does not is required.

In the ultimate semester the battery technologies have been studied. The concept of energy storage has developed greatly. Since renewables technology have taken a large share of the electricity market, it has become necessary to manage the feed in. Storage systems play a key role in this field. They can improve the stability of the electric grid by balancing the generation of energy from nonprogrammable renewable sources and the much-distributed generation due to domestic systems. The classic balancing system between power fed into the grid and consumed involves the use of active systems that control grid frequency and voltage. The use of batteries, on the other hand, involves the possibility of regulation with static systems. In general, this approach could be a solution for balancing demand and production in small islands or all those stand-alone utilities. To complete the battery energy scenario two case study in Pantelleria island and Vietnam were performed. During the three years of PhD course several transversal activities were conducted. In this way the engineering education was optimized in a multidisciplinary orientation. The acoustic topic was performed during the course studying the rules of indoor and outdoor conditions. A great experience was the acoustic optimization of the "Sala d'Ercole" in the Palazzo dei Normanni in Palermo. The subject of the work carried out is the definition of the reverberation time of sounds and the assessment of the intelligibility of speech in the hall, in its current state and with the audio systems in operation. This check allows to optimize the functionality of the room system before and after optimization.

In addition to this research topic, at the beginning of 2023, the new university energy management team had to counter the sharp increase in the price of electricity and gas due to the geopolitical conflicts that occurred. I had the chance to join the team trying to solve the energy problem. Evaluations are made of photovoltaic installation, replacement of old gas systems with new heat pump ones and home automation systems to control operating times. Many of these models were performed with the help of graduate students who had the pleasure of carrying out numerous energy analyses. Another very interesting activity was being able to carry out energy requalification interventions on some plants on the Egadi islands, as part of the European "Green Islands" project it was possible to study possible energy retrofits of municipal buildings (for example the Tonnara Florio in Favignana) and lighting systems.

References

1. Saquib Maqsood, M.; Prasad Padhi, B. Ocean Energy: An Insight. *Int. J. Eng. Manag. Res.* **2017**, 59–64.

2. World Energy Council *World Energy Resources*; London, 2016; Vol. 1;.

3. Cascajo, R.; García, E.; Quiles, E.; Correcher, A.; Morant, F. Integration of marine wave energy converters into seaports: A case study in the port of Valencia. *Energies* **2019**, *12*, doi:10.3390/en12050787.

4. Barstow, S.; Mørk, G.; Mollison, D.; Cruz, J. The Wave Energy Resource. In *Ocean Wave Energy*; Springer Berlin Heidelberg: Berlin, Heidelberg, 2008; pp. 93–132 ISBN 978-3-540-74894-6, 978-3-540-74895-3.

5. Neill, S.P.; Angeloudis, A.; Robins, P.E.; Walkington, I.; Ward, S.L.; Masters, I.; Lewis, M.J.; Piano, M.; Avdis, A.; Piggott, M.D.; et al. Tidal range energy resource and optimization – Past perspectives and future challenges. *Renew. Energy* **2018**, *127*, 763–778, doi:10.1016/j.renene.2018.05.007.

6. Yang, X.; Haas, K.A.; Fritz, H.M. Evaluating the potential for energy extraction from turbines in the gulf stream system. *Renew. Energy* **2014**, *72*, 12–21, doi:10.1016/j.renene.2014.06.039.

7. Guo, J.; Zhang, Z.; Xia, C.; Guo, B.; Yuan, Y. Topographic–baroclinic instability and formation of Kuroshio current loop. *Dyn. Atmos. Ocean.* **2018**, *81*, 15–29, doi:10.1016/j.dynatmoce.2017.11.002.

8. Krug, M.; Schilperoort, D.; Collard, F.; Hansen, M.W.; Rouault, M. Signature of the Agulhas Current in high resolution satellite derived wind fields. *Remote Sens. Environ.* **2018**, *217*, 340–351, doi:10.1016/j.rse.2018.08.016.

9. Tinaikar, A.; Padate, A.; Jain, J. Ocean Thermal Energy Conversion. *Int. J. Energy Power Eng.* **2013**, *2*, 143–146, doi:10.11648/j.ijepe.20130204.11.

10. World Energy Council World Energy Resources: Marine Energy 2016. **2016**, 79, doi:http://www.worldenergy.org/wp-

content/uploads/2013/09/Complete_WER_2013_Survey.pdf.

11.   Asian Development Bank *Wave Energy Conversion and Ocean Thermal Energy Conversion Potential in Developing Member Countries*; Asian Development Bank: Mandaluyong City, Philippines, 2014; ISBN 978-92-9254-530-7.

12.   Helfer, F.; Lemckert, C.; Anissimov, Y.G. Osmotic power with Pressure Retarded Osmosis: Theory, performance and trends - A review. *J. Memb. Sci.* **2014**, *453*, 337–358, doi:10.1016/j.memsci.2013.10.053.

13.   Curto, D.; Franzitta, V.; Guercio, A. A review of the water desalination technologies. *Appl. Sci.* **2021**, *11*, 1–36, doi:10.3390/app11020670.

14.   Laing, A.; Gemmill, W.; Magnusson, A.; Burroughs, L.; Reistad, M.; Khandekar, M.; Holthuijsen, L.; Ewing, J.; Carter, D. *Guide to wave analysis and forecasting*; World Meteorological Organization: Geneva, Switzerland, 1998; Vol. 1998; ISBN 9263127026.

15.   Igwe Chijindu Ikechukwu, Chinonso Hubert Achebe, A.C. Review of Alternative Energy Production Methods by Oxidation of Electrolysed Hydrogen in a Hydrogen Fuel Cell. *Glob. Sci. J.* **2022**, *10*, 24.

16.   Simon Flowers www.woodmac.com/Future energy – green hydrogen Available online: https://www.woodmac.com/news/the-edge/future-energy-green-hydrogen/ (accessed on Sep 5, 2022).

17.   hydrogen-transports @ www.eni.com Available online: https://www.eni.com/en-IT/sustainable-mobility/hydrogen-transports.html (accessed on Sep 7, 2022).

18.   zeroe @ www.airbus.com Available online: https://www.airbus.com/en/innovation/zero-emission/hydrogen/zeroe (accessed on Sep 7, 2022).

19.   Coradia iLint @ www.alstom.com Available online: https://www.alstom.com/solutions/rolling-stock/coradia-ilinttm-worlds-1st-hydrogen-powered-train (accessed on Sep 7, 2022).

20.   mirai @ www.toyota.it Available online:

https://www.toyota.it/gamma/nuova-mirai (accessed on Sep 7, 2022).

21.   global-primary-energy   @   ourworldindata.org   Available   online:
      https://ourworldindata.org/grapher/global-primary-energy (accessed on Sep
      13, 2022).

22.   electricity-prod-source-stacked @ ourworldindata.org Available online:
      https://ourworldindata.org/grapher/electricity-prod-source-stacked
      (accessed on Sep 13, 2022).

23.   IEA *World Energy Outlook 2021*; 2021;

24.   International Renewable Energy Agency *Renewable Capacity Highlights*;
      2021;

25.   IEA *World Energy Investment 2019*; 2019;

26.   Sørensen, B. *Renewable Energy, its physics engineering, use, environmental
      impacts, economy and planning aspects*; Third.; 2004; ISBN 0126561532.

27.   Soromotin, A. V. Ecological consequences of different stages of the
      development of oil and gas deposits in the taiga zone of the Tyumen' oblast.
      Contemp. Probl. Ecol. **2011**, *4*, 600–607, doi:10.1134/S1995425511060063.

28.   Beccali, M.; Cellura, M.; Mistretta, M. Environmental effects of energy
      policy in Sicily: The role of renewable energy. *Renew. Sustain. Energy Rev.*
      2007, *11*, 282–298, doi:10.1016/j.rser.2005.02.001.

29.   Rogelj, J.; Schaeffer, M.; Meinshausen, M.; Knutti, R.; Alcamo, J.; Riahi,
      K.; Hare, W. Zero emission targets as long-term global goals for climate
      protection. *Environ. Res. Lett.* **2015**, *10*, 105007, doi:10.1088/1748-
      9326/10/10/105007.

30.   Meinshausen, M.; Meinshausen, N.; Hare, W.; Raper, S.C.B.; Frieler, K.;
      Knutti, R.; Frame, D.J.; Allen, M.R. Greenhouse-gas emission targets for
      limiting global warming to 2 °C. *Nature* **2009**, *458*, 1158–1162,
      doi:10.1038/nature08017.

31.   United Nations *Kyoto Protocol to the United Nations Framework –
      Convention on Climate Change*; United Nations, 1998;

32.   United Nations Climate Change *Paris Agreement*; 2015;

33.   Curto, D.; Viola, A.; Franzitta, V.; Trapanese, M.; Cardona, F. A New Solution for Sea Wave Energy Harvesting, the Proposal of an Ironless Linear Generator. *J. Mar. Sci. Eng.* **2020**, *8*, 93, doi:10.3390/jmse8020093.

34.   Liberti, L.; Carillo, A.; Sannino, G. Wave energy resource assessment in the Mediterranean, the Italian perspective. *Renew. Energy* **2013**, *50*, 938–949, doi:10.1016/j.renene.2012.08.023.

35.   Falcão, A.F. de O. Wave energy utilization: A review of the technologies. *Renew. Sustain. Energy Rev.* **2010**, *14*, 899–918, doi:10.1016/j.rser.2009.11.003.

36.   Curto, D.; Franzitta, V.; Guercio, A.; Trapanese, M. Testing a linear ironless generator for the sea wave energy harvesting. *Ocean. Conf. Rec.* **2022**, 5, doi:10.1109/OCEANSChennai45887.2022.9775494.

37.   Zhao, X.L.; Ning, D.Z.; Zou, Q.P.; Qiao, D.S.; Cai, S.Q. Hybrid floating breakwater-WEC system: A review. *Ocean Eng.* **2019**, *186*, doi:10.1016/j.oceaneng.2019.106126.

38.   Aderinto, T.; Li, H. Ocean Wave energy converters: Status and challenges. *Energies* **2018**, *11*, 1–26, doi:10.3390/en11051250.

39.   Bhattacharyya, R.; McCormick, M.E. Wave Power Activities in Northern Europe. In *Wave Energy Conversion*; Elsevier Science, 2003; pp. 95–123.

40.   Malmo, O.; Reitan, A. Development of the Kvaerner Multiresonant OWC. In *Hydrodynamics of Ocean Wave-Energy Utilization*; Springer Berlin Heidelberg: Berlin, Heidelberg, 1986; pp. 57–67 ISBN 978-3-642-82668-9.

41.   Maurya, A.K.; Singh, S.P. Assessment of Ocean Wave Energy Converters for Indian Coastal Region. *IETE Tech. Rev.* **2020**, *37*, 476–488, doi:10.1080/02564602.2019.1659189.

42.   Ravindran, M.; Koola, P.M. Energy from sea waves — the Indian wave energy programme. *Curr. Sci.* **1991**, *60*, 676–680.

43.   Khan, J.; Bhuyan, G.S. *Ocean Energy: Global Technology Development Status*; 2009;

44.   Agence Française De Développement; Indian Renewable Energy

Development Agency Limited *Study on Tidal & Waves Energy in India: Survey on the Potential & Proposition of a Roadmap*; 2014;

45. Whittaker, T.J.T.; Beattie, W.; Folley, M.; Boake, C.; Wright, A.; Osterried, M. The Limpet Wave Power Project – The First Years Of Operation. *Renew. Energy - Whittaker* **2004**, 1–8.

46. Tethys Pico Oscillating Water Column Available online: https://tethys.pnnl.gov/annex-iv-sites/pico-oscillating-water-column (accessed on Aug 30, 2021).

47. Tethys Mutriku Wave Power Plant Available online: https://tethys.pnnl.gov/annex-iv-sites/mutriku-wave-power-plant (accessed on Aug 30, 2021).

48. Mouffe, L.; De Rouck, J.; Verbrugghe, T.; Ranjitkar, G.; Obermann, E.; Wei, P.; Nielsen, K.; Magagna, D.; Soede, M.; De Roeck, Y.-H.; et al. *Annual report. An Overview of Ocean Energy Activities in 2017*; 2017;

49. Vicinanza, D.; Margheritini, L.; Kofoed, J.P.; Buccino, M. The SSG Wave Energy Converter: Performance, Status and Recent Developments. *Energies* **2012**, *5*, 193–226, doi:10.3390/en5020193.

50. Yemm, R.; Pizer, D.; Retzler, C.; Henderson, R. Pelamis: experience from concept to connection. *Philos. Trans. R. Soc. A Math. Phys. Eng. Sci.* **2012**, *370*, 365–380, doi:10.1098/rsta.2011.0312.

51. Poullikkas, A. Technology Prospects of Wave Power Systems. *Electron. J. Energy Environ.* **2014**, *2*, 47–69, doi:10.7770/ejee-V2N1-art662.

52. Tarrant, K.; Meskell, C. Investigation on parametrically excited motions of point absorbers in regular waves. *Ocean Eng.* **2016**, *111*, 67–81, doi:10.1016/j.oceaneng.2015.10.041.

53. Blackledge, J.; Coyle, E.; Kearney, D.; McGuirk, R.; Norton, B. Estimation of wave energy from wind velocity. *Eng. Lett.* **2013**, *21*, 158–170, doi:10.21427/D71P6P.

54. Alfarsi, H. CETO System: Clean Electricity and Water Desalination Using Ocean Waves. *Profolus* 2021.

55. Thomson, R.C.; Chick, J.P.; Harrison, G.P. An LCA of the Pelamis wave energy converter. *Int. J. Life Cycle Assess.* **2019**, *24*, 51–63, doi:10.1007/s11367-018-1504-2.

56. Wikipedia Pelamis Wave Energy Converter Available online: https://en.wikipedia.org/wiki/Pelamis_Wave_Energy_Converter (accessed on Aug 30, 2021).

57. EMEC Pelamis Available online: http://www.emec.org.uk/about-us/wave-clients/pelamis-wave-power/.

58. Evans, P. Oyster ocean power system to provide 1 GW by 2020 Available online: https://newatlas.com/oyster-ocean-power-system/11180/.

59. EMEC AQUAMARINE POWER Available online: http://www.emec.org.uk/about-us/wave-clients/aquamarine-power/ (accessed on Aug 30, 2021).

60. AW Energy WAVEROLLER Available online: https://aw-energy.com/waveroller/ (accessed on Aug 30, 2021).

61. Energy Innovation Cluster WAVESTAR Available online: https://wavepartnership.dk/wavestar-0 (accessed on Aug 30, 2021).

62. Jordan wavestar-002 Available online: https://www.neozone.org/ecologie-planete/wavestar-la-centrale-electrique-qui-utilise-la-houle-pour-produire-de-lenergie/attachment/wavestar-002/ (accessed on Aug 30, 2021).

63. Eco Wave Power Photos Available online: https://www.ecowavepower.com/gallery/photos/ (accessed on Aug 30, 2021).

64. Ecthelion Norwave Wave Power Plant Available online: https://sketchfab.com/3d-models/norwave-wave-power-plant-482851fc4c8041d99d456289c01dc764.

65. Bak, P.; Peter, J.; Peter Frigaard; Jens Peter Kofoed1 & Wilfried Knapp2; University;, 1Dept. Civil Engineering; Aalborg; Munich, T.U. of Wave Dragon: wave power plant using low-head turbines. In Proceedings of the Hidroenergia 04: International Conference and Exhibition on Small

Hydropower General; Falkenberg, 2004.

66. Tedd, J.; Peter Kofoed, J. Measurements of overtopping flow time series on the Wave Dragon, wave energy converter. *Renew. Energy* **2009**, *34*, 711–717, doi:10.1016/j.renene.2008.04.036.

67. Buccino, M.; Banfi, D.; Vicinanza, D.; Calabrese, M.; Del Giudice, G.; Carravetta, A. Non breaking wave forces at the front face of Seawave Slotcone Generators. *Energies* **2012**, *5*, 4779–4803, doi:10.3390/en5114779.

68. Ahamed, R.; McKee, K.; Howard, I. Advancements of wave energy converters based on power take off (PTO) systems: A review. *Ocean Eng.* **2020**, *204*, 107248, doi:10.1016/j.oceaneng.2020.107248.

69. Pecher, A.; Kofoed, J.P. *Handbook of Ocean Wave Energy- Wave-to-Wire Modelling of WECs*; 2017; ISBN 978-3-319-39889-1.

70. Falcão, A.F.O.; Henriques, J.C.C. Oscillating-water-column wave energy converters and air turbines: A review. *Renew. Energy* **2016**, *85*, 1391–1424, doi:10.1016/j.renene.2015.07.086.

71. Xu, J.; Yang, Y.; Hu, Y.; Xu, T.; Zhan, Y. MPPT control of hydraulic power take-off for wave energy converter on artificial breakwater. *J. Mar. Sci. Eng.* **2020**, *8*, 1–20, doi:10.3390/JMSE8050304.

72. Falcão, A.F. d. O. Wave energy utilization: A review of the technologies. *Renew. Sustain. Energy Rev.* **2010**, *14*, 899–918, doi:10.1016/j.rser.2009.11.003.

73. Jain, K.; Jain, K. Hydrogen Fuel Cell: A Review of different types of fuel Cells with Emphasis on PEM fuel cells and Catalysts used in the PEM fuel cell. *Int. J. All Res. Educ. Sci. Methods* **2021**, *9*, 1012–1025.

74. IRENA Innovation trends in electrolysers for hydrogen production. **2021**, 37.

75. Kalamaras, C.M.; Efstathiou, A.M. Hydrogen Production Technologies: Current State and Future Developments. In Proceedings of the Conference Papers in Energy; 2013; Vol. 2013, pp. 1–9.

76. Peng, X.; Deng, Z.; Zhao, X.; Li, G.; Song, J.; Liang, D.; Sun, X.; Xu, G.; Kang, W.; Liu, M. Experimental and Analytical Study of a Proton Exchange

Membrane Electrolyser Integrated with Thermal Energy Storage for Performance Enhancement. *Int. J. Photoenergy* **2022**, *2022*, 1–9, doi:10.1155/2022/7543121.

77. Pecher, A.; Kofoed, J.P. *Handbook of Ocean Wave Energy*; Pecher, A., Kofoed, J.P., Eds.; Ocean Engineering & Oceanography; Springer International Publishing: Cham, 2017; Vol. 7; ISBN 978-3-319-39888-4.

78. Curto, D.; Franzitta, V.; Guercio, A. Sea Wave Energy. A Review of the Current Technologies and Perspectives. *Energies* **2021**, *14*, 6604, doi:10.3390/en14206604.

79. Curto, D.; Franzitta, V.; Guercio, A.; Napoli, G. First analyses on a mechanical motion converter to produce electrical energy from sea wave. In Proceedings of the Global Oceans 2020: Singapore – U.S. Gulf Coast; IEEE, 2020; pp. 1–7.

80. Franzitta, V.; Viola, A.; Trapanese, M. Design of a transverse flux machine for power generation from seawaves. *J. Appl. Phys.* **2014**, *115*, 17E712, doi:10.1063/1.4865883.

81. Boscaino, V.; Cipriani, G.; Di Dio, V.; Corpora, M.; Curto, D.; Franzitta, V.; Trapanese, M. Experimental validation of a distribution theory based analysis of the effect of manufacturing tolerances on permanent magnet synchronous machines. *AIP Adv.* **2017**, *7*, 056650, doi:10.1063/1.4975994.

82. Penalba, M.; Ringwood, J. V. A review of wave-to-wire models for wave energy converters. *Energies* **2016**, *9*, doi:10.3390/en9070506.

83. Li, W.; Isberg, J.; Engström, J.; Waters, R.; Leijon, M. Optimization of the power absorption for a linear generator wave energy converter. *Twenty Fitfth Int. Offshore Polar Eng. Conf.* **2015**, 857–861.

84. Drew, B.; Plummer, A.R.; Sahinkaya, M.N. A review of wave energy converter technology. *Proc. Inst. Mech. Eng. Part A J. Power Energy* **2009**, *223*, 887–902, doi:10.1243/09576509JPE782.

85. Franzitta, V.; Curto, D.; Milone, D.; Trapanese, M. Energy Saving in Public Transport Using Renewable Energy. *Sustainability* **2017**, *9*, 106,

doi:10.3390/su9010106.

86.   IRENA *Renewable Power Generation Costs in 2021*; 2022; ISBN 978-92-9260-244-4.

87.   Carballo, R.; Iglesias, G. Wave farm impact based on realistic wave-WEC interaction. *Energy* **2013**, *51*, 216–229, doi:10.1016/j.energy.2012.12.040.

88.   Leijon, M.; Boström, C.; Danielsson, O.; Gustafsson, S.; Haikonen, K.; Langhamer, O.; Strömstedt, E.; Stålberg, M.; Sundberg, J.; Svensson, O.; et al. Wave energy from the north sea: Experiences from the lysekil research site. *Surv. Geophys.* **2008**, *29*, 221–240, doi:10.1007/s10712-008-9047-x.

89.   Legambiente *Isole sostenibili. Osservatorio sulle isole minori. Le sfide per le isole minori italiane e le buone pratiche nel mondo*; 2019;

90.   Krichen, M.; Basheer, Y.; Qaisar, S.M.; Waqar, A. A Survey on Energy Storage: Techniques and Challenges. *Energies* **2023**, *16*, doi:10.3390/en16052271.

91.   Cronk, P.; Van de Ven, J.; Strohmaier, K. Design optimization, construction, and testing of a hydraulic flywheel accumulator. *J. Energy Storage* **2021**, *44*, 103281, doi:10.1016/j.est.2021.103281.

92.   Kuang, Y.; Zhang, Y.; Zhou, B.; Li, C.; Cao, Y.; Li, L.; Zeng, L. A review of renewable energy utilization in islands. *Renew. Sustain. Energy Rev.* **2016**, *59*, 504–513, doi:10.1016/j.rser.2016.01.014.

93.   Zhang, J.; Gu, M.; Chen, X. Micro and Nano Engineering Supercapacitors for renewable energy applications : A review. *Micro Nano Eng.* **2023**, *21*, 100229, doi:10.1016/j.mne.2023.100229.

94.   Rodríguez-rego, J.M.; Macías-garcía, A.; Mendoza-cerezo, L.; Díaz-parralejo, A.; Carrasco-amador, J.P. Design , machining and characterization of the components required for the manufacture of a supercapacitor. *J. Energy Storage* **2023**, *73*, 109110, doi:10.1016/j.est.2023.109110.

95.   Brenna, M.; Foiadelli, F.; Tironi, E.; Zaninelli, D. Ultracapacitors application for energy saving in subway transportation systems. *2007 Int. Conf. Clean Electr. Power, ICCEP '07* **2007**, 69–73, doi:10.1109/ICCEP.2007.384188.

96. Curto, D.; Favuzza, S.; Franzitta, V.; Guercio, A.; Amparo Navarro Navia, M.; Telaretti, E.; Zizzo, G. Grid Stability Improvement Using Synthetic Inertia by Battery Energy Storage Systems in Small Islands. *Energy* **2022**, *254*, 124456, doi:10.1016/j.energy.2022.124456.

97. Ullah, N.R.; Thiringer, T.; Karlsson, D. Temporary primary frequency control support by variable speed wind turbines - Potential and applications. *IEEE Trans. Power Syst.* **2008**, *23*, 601–612, doi:10.1109/TPWRS.2008.920076.

98. Nguyen, H.T.; Yang, G.; Nielsen, A.H.; Jensen, P.H. Frequency stability enhancement for low inertia systems using synthetic inertia of wind power. *IEEE Power Energy Soc. Gen. Meet.* **2018**, *2018-Janua*, 1–5, doi:10.1109/PESGM.2017.8274566.

99. Wang, Z.; Zhuo, F.; Wu, J.; Yi, H.; Zhai, H.; Zeng, Z. Inertia time constant design in microgrids with multiple paralleled virtual synchronous generators. *2017 19th Eur. Conf. Power Electron. Appl. EPE 2017 ECCE Eur.* **2017**, *2017-Janua*, 1–9, doi:10.23919/EPE17ECCEEurope.2017.8099273.

100. Sa'ed, J.A.; Curto, D.; Favuzza, S.; Musca, R.; Navia, M.N.; Zizzo, G. A Simulation Analysis of VSM Control for RES plants in a Small Mediterranean Island. *Proc. - 2020 IEEE Int. Conf. Environ. Electr. Eng. 2020 IEEE Ind. Commer. Power Syst. Eur. EEEIC / I CPS Eur. 2020* **2020**, doi:10.1109/EEEIC/ICPSEurope49358.2020.9160501.

101. Ministero dell'ambiente e della sicurezza energetica Prezzi medi mensili dei carburanti e combustibili Available online: https://dgsaie.mise.gov.it/prezzi-mensili-carburanti?pid=3.

102. Caporale, G.M.; Gil-Alana, L.A. Long-term interest rates in Europe: A fractional cointegration analysis. *Int. Rev. Econ. Financ.* **2019**, *61*, 170–178, doi:10.1016/j.iref.2019.02.004.

103. Menezes, A.C.; Cripps, A.; Buswell, R.A.; Wright, J.; Bouchlaghem, D. Estimating the energy consumption and power demand of small power equipment in office buildings. *Energy Build.* **2014**, *75*, 199–209,

doi:10.1016/j.enbuild.2014.02.011.

104. Franzitta, V.; Curto, D.; Rao, D. Energetic Sustainability Using Renewable Energies in the Mediterranean Sea. *Sustainability* **2016**, *8*, 1164, doi:10.3390/su8111164.

105. Benato, R.; Bruno, G.; Palone, F.; Polito, R.M.; Rebolini, M. Large-scale electrochemical energy storage in high voltage grids: Overview of the Italian experience. *Energies* **2017**, *10*, doi:10.3390/en10010108.

106. Statista *statistic_domestic-product-gdp-in-vietnam-toward 2028*; Amburgo, Germaany;

107. Curto, D.; Doan, B. Van; Franzitta, V.; Montana, F.; Nguyen, N.Q.; Riva Sanseverino, E. Wave and Wind Energy Systems Integration in Vietnam : Analysis of Energy Potential and Economic Feasibility. In Proceedings of the 2020 IEEE International Conference on Environment and Electrical Engineering and 2020 IEEE Industrial and Commercial Power Systems Europe (EEEIC / I&CPS Europe); 2020; pp. 1–6.

108. Curto, D.; Franzitta, V.; Guercio, A.; Musca, R.; Vasile, A.; Zizzo, G. Stability Analysis in a Vietnam Small Island for the Deployment of a Nearshore Wave Power Plant. *2022 Work. Blockchain Renewables Integr. BLORIN 2022* **2022**, 236–241, doi:10.1109/BLORIN54731.2022.10028639.

109. Rate of Change of Frequency (ROCOF) withstand capability 2017.

110. Ódor, G.; Hartmann, B. Power-law distributions of dynamic cascade failures in power-grid models. *Entropy* **2020**, *22*, doi:10.3390/E22060666.